CONSOLIDATION OF GEOLOGIC STUDIES OF GEOPRESSURED GEOTHERMAL RESOURCES IN TEXAS

1989 Annual Report

C. W. Kreitler (Project Director), R. M. Capuano (Principal Scientist)
M. S. Akhter, H. S. Hamlin, M. E. Erwin, and T. G. Walter

Prepared for the U.S. Department of Energy
Advanced Technologies Division
under Cooperative Agreement No. DE-FC07-85NV10412

Bureau of Economic Geology
W. L. Fisher, Director
The University of Texas at Austin
Austin, Texas 78713

May 1990

CONTENTS

Figures in Section I

Table in Section I

Appendix Figures in Section I

Appendix Table in Section I

SECTION II: HYDROCHEMICAL STUDIES FOR LONG-TERM-FLOW TESTING OF PLEASANT BAYOU GEOPRESSURED GEOTHERMAL WELL NO. 2

By Regina M. Capuano and Mark E. Erwin

Figures in Section II

Tables in Section II

SECTION III: CO-LOCATION OF HEAVY OIL AND GEOPRESSURED GEOTHERMAL BRINE RESOURCES, EXAMPLES FROM SOUTH TEXAS AND SOUTHERN CALIFORNIA

By H. Scott Hamlin, Timothy G. Walter, and Charles W. Kreitler

Figures in Section III

Tables in Section III

SECTION I: HYDROGEOLOGIC STUDIES OF THE PLEASANT BAYOU GEOPRESSURED GEOTHERMAL RESERVOIR

M. Saleem Akhter and Charles W. Kreitler

assisted by Vichai Maroongroge and Timothy G. Walter

ABSTRACT

The objective of the current studies at the Pleasant Bayou geopressured geothermal reservoir in Brazoria County, Texas, was to evaluate the resource base and long-term performance. The approach was to develop an integrated understanding of the hydrogeology of the reservoir and the hydrochemistry of the produced brine. Such an understanding would allow determination of the extent of lateral and vertical hydrologic continuity of the target zone and to identify the sources of brine being produced from the geopressured reservoir.

The current phase of long-term production testing of the Frio C-zone at Pleasant Bayou Well No. 2 began in May 1988. During the past 16 months of production nearly 6.8 million barrels of brine and 162.2 million cubic feet of gas have been produced and a relatively small (less than 300 psi) drop in bottom-hole pressure has been observed at sustained producing rates of between 15,000 and 20,000 barrels per day. Earlier geologic studies have estimated the effective pore volume of the C-zone in the neighborhood of 6.2 to 6.6 billion barrels. Analysis of pressure and production data from current testing indicates that the limits of the geopressured reservoir at Pleasant Bayou have not been reached, that is, either the size of the reservoir could be larger than anticipated or there could be a continuous influx of waters from other geopressured sources that sustains the reservoir energy at Pleasant Bayou. Geochemical testing has proved inconclusive in identifying other sources of water partly because of the variability of chemical composition within the produced zone.

Evaluation of reservoir performance at active oil and gas fields in the immediate vicinity of the Pleasant Bayou fault block has not provided evidence of direct hydrologic communication between the geopressured aquifer and the overlying hydrocarbon reservoirs. The pattern of depletion in these oil and gas fields reflects some characteristic features that may become evident in Pleasant Bayou over a long period of production. Moreover, additional refinement of the integrated hydrogeologic-hydrochemical model is possible either through prolonged testing at Pleasant Bayou No. 2 well or through drilling and testing of additional wells in the Pleasant Bayou fault block. Determining the nature of bounding faults around the test well will require additional seismic data as well as multiwell testing of the reservoir.

INTRODUCTION

The Bureau of Economic Geology has been involved in the evaluation of the geopressured geothermal energy resources in Texas since the 1970's. The structural geology, development of geopressures along the Texas Gulf Coast, stratigraphic framework, depositional setting, reservoir composition and diagenesis, and fluid composition have all been investigated in the geopressured reservoirs. During FY 1988 the focus was on geologic description, whereby sandstone geometry, dimensions, internal heterogeneities and interconnectedness were evaluated. The annual report by Hamlin and Tyler (1988) details the geologic studies. The geologic model developed at this stage was used by S-Cubed (Riney, 1988) in numerical simulations to model the pressure drawdown and buildup tests conducted at Pleasant Bayou No. 2 (fig. 1) and to refine the locations of the internal faults within the main Pleasant Bayou fault block (fig. 2).

The FY 1989 hydrogeologic investigations at Pleasant Bayou were concentrated on the following aspects:

1. Evaluation of pressure-production data from nearby oil and gas fields for mapping pressure distribution and identification of depletion, if any, from original conditions.

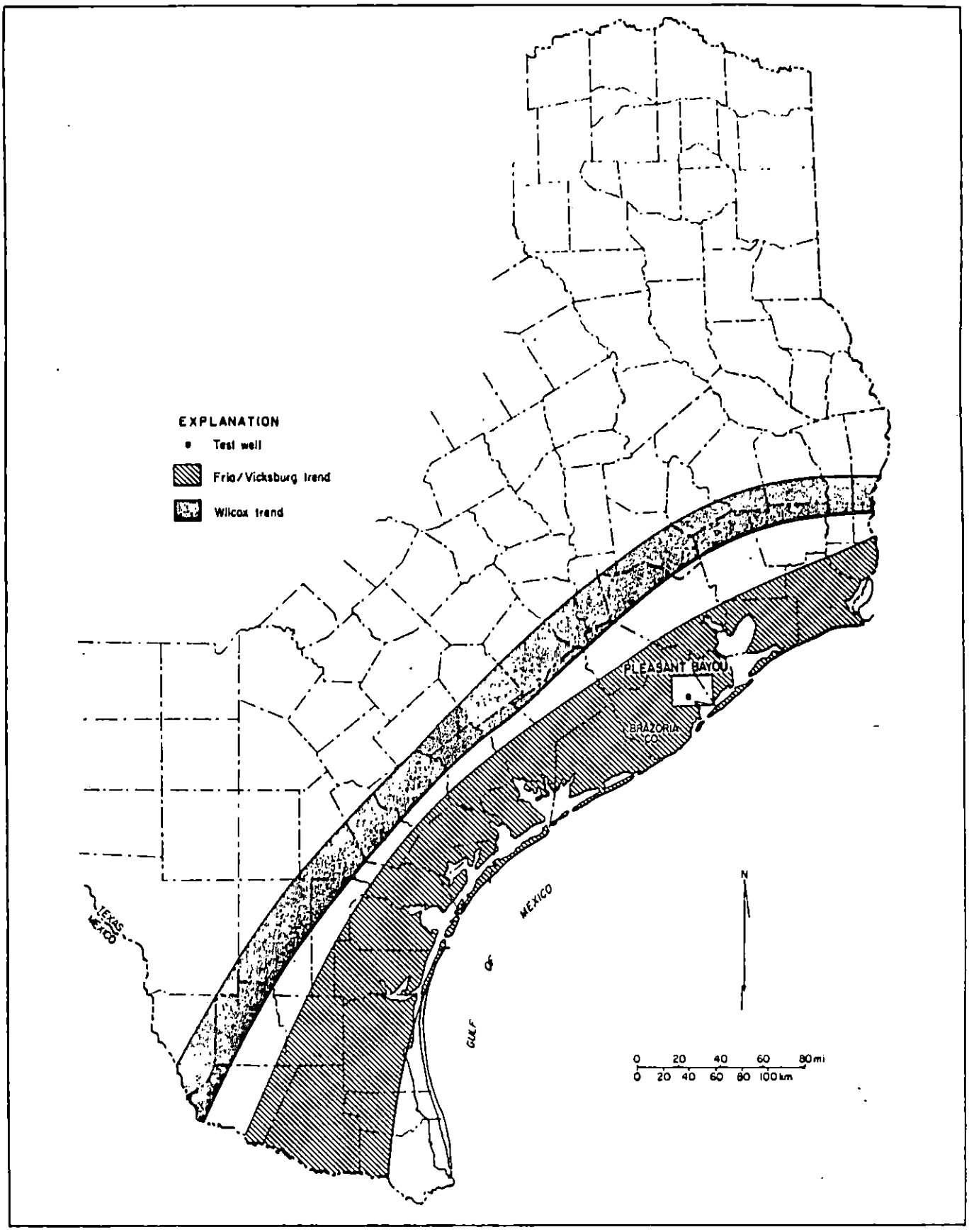

Figure 1. Location map of Pleasant Bayou No. 2 test well and major geothermal exploration trends, Texas Gulf Coast. Modified from Winker and others (1983).

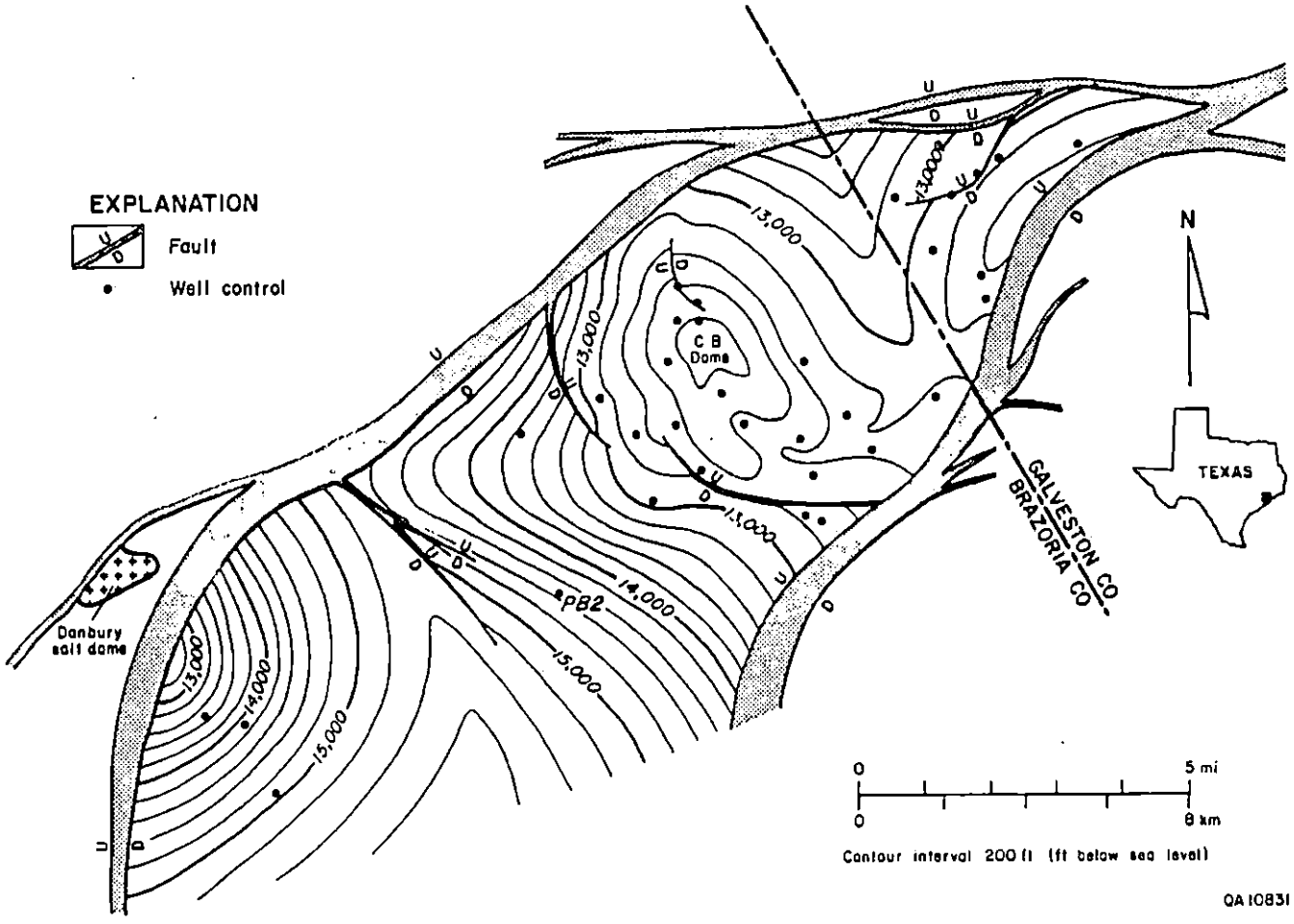

Figure 2. Structure map contoured on top of the C-zone. Revised from Winker and others (1983) and Ewing and others (1984).

2. Assessment of reservoir properties and hydrodynamics from production testing at Pleasant Bayou No. 2.
3. Identification of reservoir-drive mechanisms and estimation of geopressured brine reserves.
4. Integration of geologic, hydrogeologic and hydrochemical description of the Pleasant Bayou reservoir.

The concept of geopressured-geothermal well performance broadly includes evaluation of changes in reservoir flow properties and formation mechanical properties as a function of pressure depletion, subsurface subsidence, changes in composition of produced fluids, and mobilization of fluids in adjacent formations. The description of current pressure distribution in the Frio and equivalent formations at Pleasant Bayou provides an estimate of the pressure depletion as well as the potential for fluid migration. The geologic description identifies the barriers and conduits (faults and interconnected sands) available for the fluid flow. The hydrochemical investigation of fluid properties can provide evidence of ongoing fluid comingling and cross-formation flow.

RESERVOIR DESCRIPTION—PLEASANT BAYOU FAULT BLOCK

Geology

Depositional Framework and Structure

In the Brazoria Fairway, located in Brazoria and Galveston Counties, contemporaneous deltaic sedimentation, movement along growth faults, and mobilization of deep salt into domes resulted in the accumulation of several hundred feet of sandstone having fluid temperatures greater than 149 °C (300 °F) (Bebout and others, 1978). Permeabilities within these reservoirs

are greater than 20 md. This high permeability is related to secondary leached porosity, which developed in the moderate to deep subsurface.

The Pleasant Bayou No. 2 well currently produces from perforations ranging from 4,463 to 4,482 m (14,644 to 14,704 ft) (fig. 3). This interval is in the middle sandstone unit of the C-zone of the Frio T5 unit in the Brazoria Fairway. The sandstone-shale section within Pleasant Bayou is represented by seven progradational depositional sequences (Bebout and others, 1978). Each sequence is composed of a gradational vertical succession, characterized by low-porosity prodelta and distal delta-front shale and sandstone at the base, to porous distributary-mouth-bar and delta-plain sandstone and shale at the top. The older depositional sequences represent the distal half of a lobate delta, and the later events represent the entire deltaic complex. The C-zone is laterally bounded by large growth faults creating the Pleasant Bayou fault block. The fault block covers an area of about 223 km^2 (87 mi^2) to a depth greater than 4,573 m (15,000 ft). The fault block was defined from stratigraphic correlations picked on SP and resistivity logs, from seismic reflection data, and from distribution of benthic foraminifera (Bebout and others, 1978; Morton and others, 1983; Winker and others, 1983; Ewing and others, 1984; Hamlin and Tyler, 1988). The major structural faults around the Pleasant Bayou No. 2 well are two large growth faults, Danbury salt dome and salt-withdrawal basin, and Chocolate Bayou dome (fig. 4). The T3 and T4 sandstones are thick and display good lateral continuity throughout the Pleasant Bayou area. The T3 sandstone unit approximately corresponds to the boundary between normally pressured and geopressured sandstones (Morton and others, 1983). In the T5 sandstone unit at the level of the C-zone, displacements across the large growth faults range from 152 to 304 m (500 to 1,000 ft) and are accompanied by pronounced stratigraphic changes (Hamlin and Tyler, 1988).

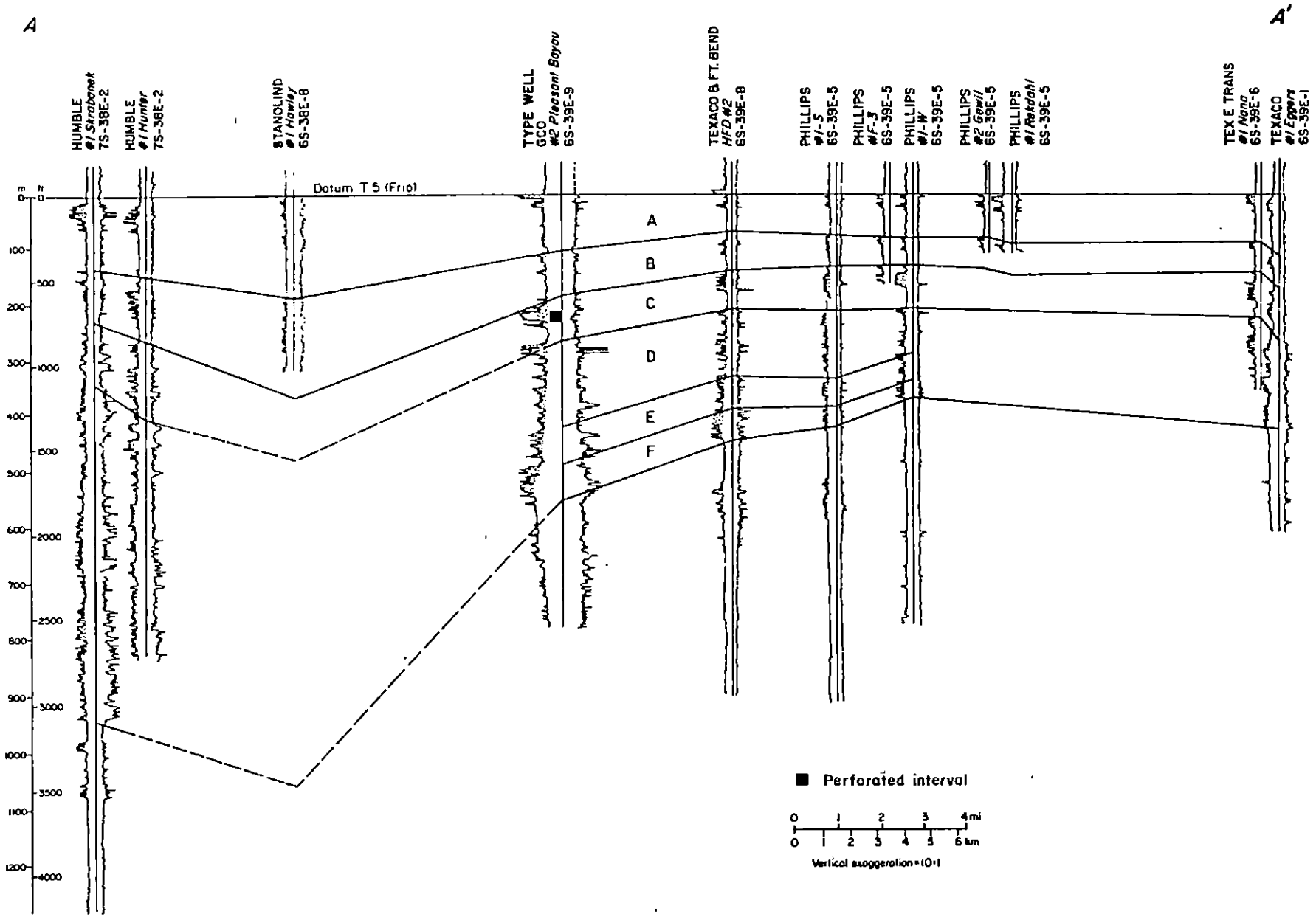

Figure 3. West-east electric-log cross section A–A′ of the lower Frio Formation, showing the main geopressured correlation intervals in the Pleasant Bayou fault block and the perforated interval in the test well. Line of section shown in figure 4. Modified from Winker and others (1983).

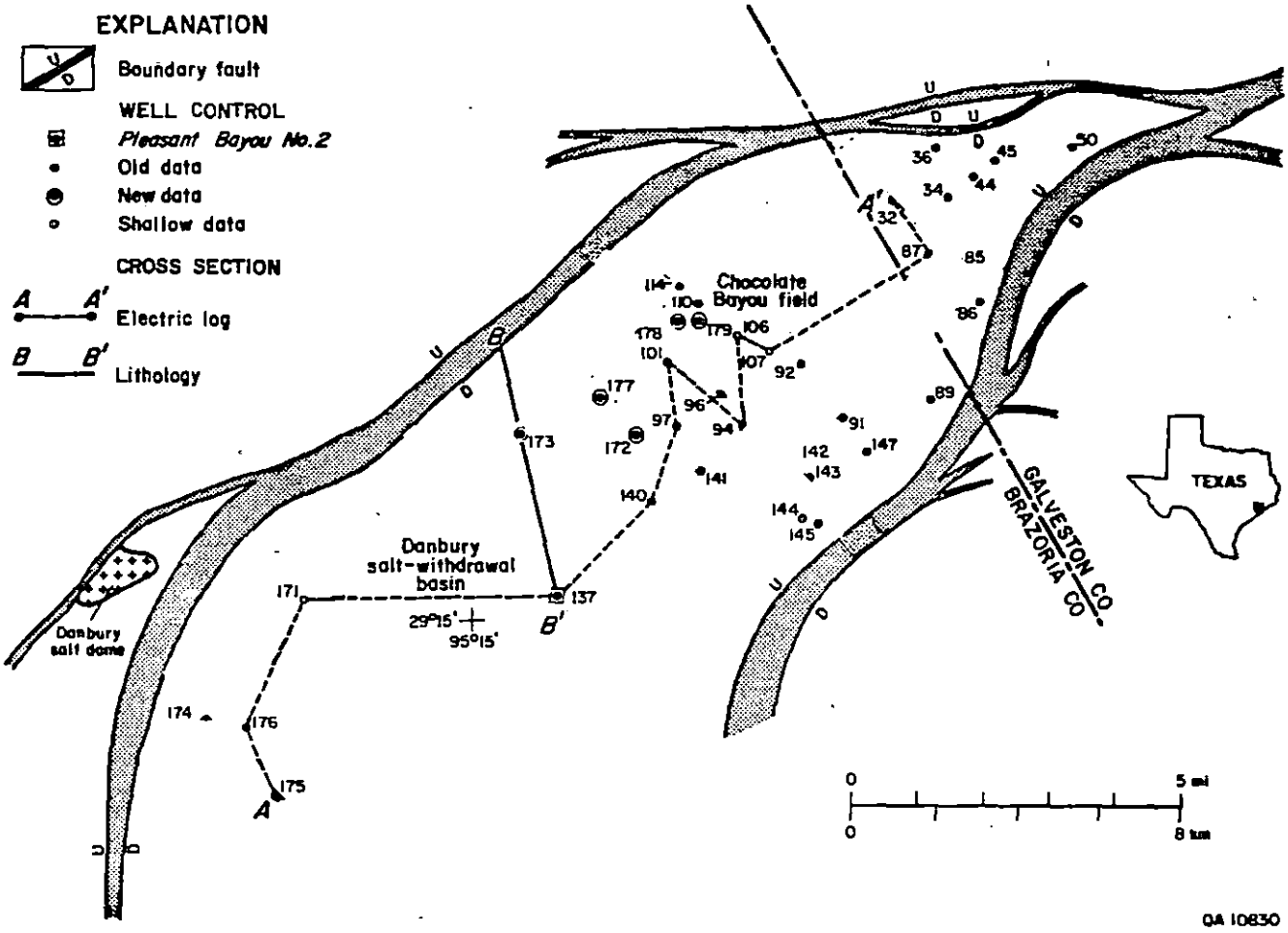

Figure 4. Index map of the Pleasant Bayou fault block showing well control and cross section lines. Cross section A–A′ shown in figure 3; cross section B–B′ shown in figure 5.

Reservoir Continuity

Hamlin and Tyler (1988) traced lateral continuity of the productive C-zone in the test well with other sandstone units by correlating interbedded mudstones. A mudstone continuous throughout the fault block and having a minimum thickness of 3 m (10 ft) was thus considered capable of isolating the sandstones above from those below it. Only two mudstones in the C-zone, the upper and basal mudstones, were found to be continuous throughout the fault block, (fig. 5). Numerous other discontinuous mudstones in the reservoir allowed local communication between the other sandstone units. As part of the FY89 effort to analyze structural and stratigraphic features, well log data were reexamined within the Pleasant Bayou and adjacent fault blocks. Main structural features of the fault block include two large, northeast-trending, boundary-forming growth faults. The more northerly fault transects Danbury salt dome to the west and defines the northern edge of the Chocolate Bayou dome in the central portion of the block. Pleasant Bayou No. 2 is southwest of Chocolate Bayou dome within the salt-withdrawal basin. Four additional dip-oriented cross sections and one strike-oriented one were constructed for this study (fig. 6). The well numbers referenced in the geologic cross sections correspond to wells included in table A-1 in the appendix.

Pleasant Bayou Fault Block

Lower Frio correlation units (T3–T5) within the Pleasant Bayou fault block display lateral variability in thickness and shale interbedding (figs. 7 through 11). Within the block the T3 unit is about 213 m (700 ft) thick, consisting of thin sandstones separated by thick shales (fig. 7). Sandstones are typically 6 to 9 m (20 to 30 ft) thick separated by 24- to 46-m (80- to 150-ft) thick shales. Expansion is most evident in the T4 and T5 units, with only slight thinning over Chocolate Bayou dome. The T4 unit thicknesses range from 488 m (1,600 ft) in the withdrawal

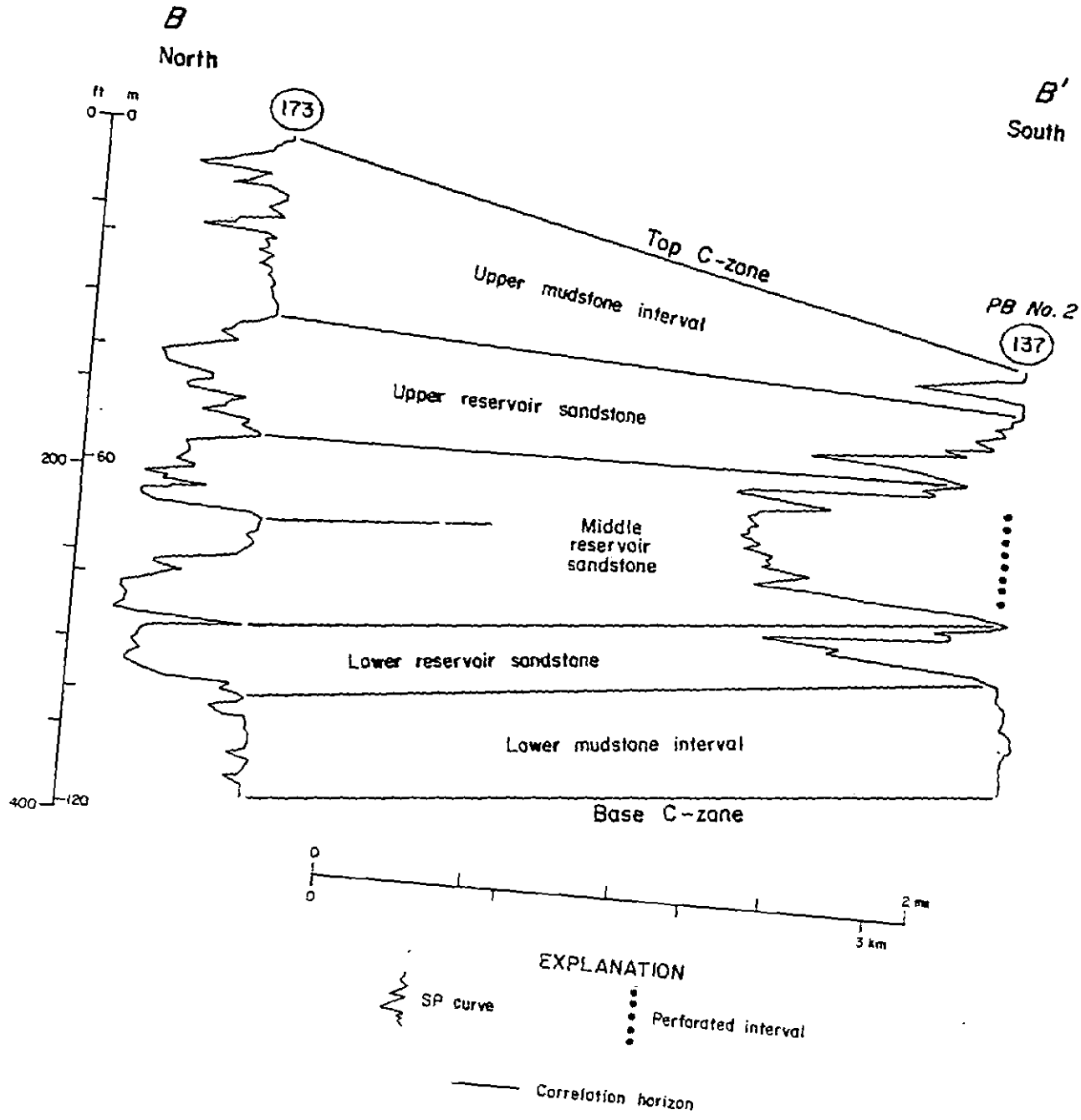

Figure 5. North-south cross section B–B′ showing major sandstone and mudstone intervals, key correlation horizons, and typical SP patterns of the C-zone. Line of section shown in figure 4.

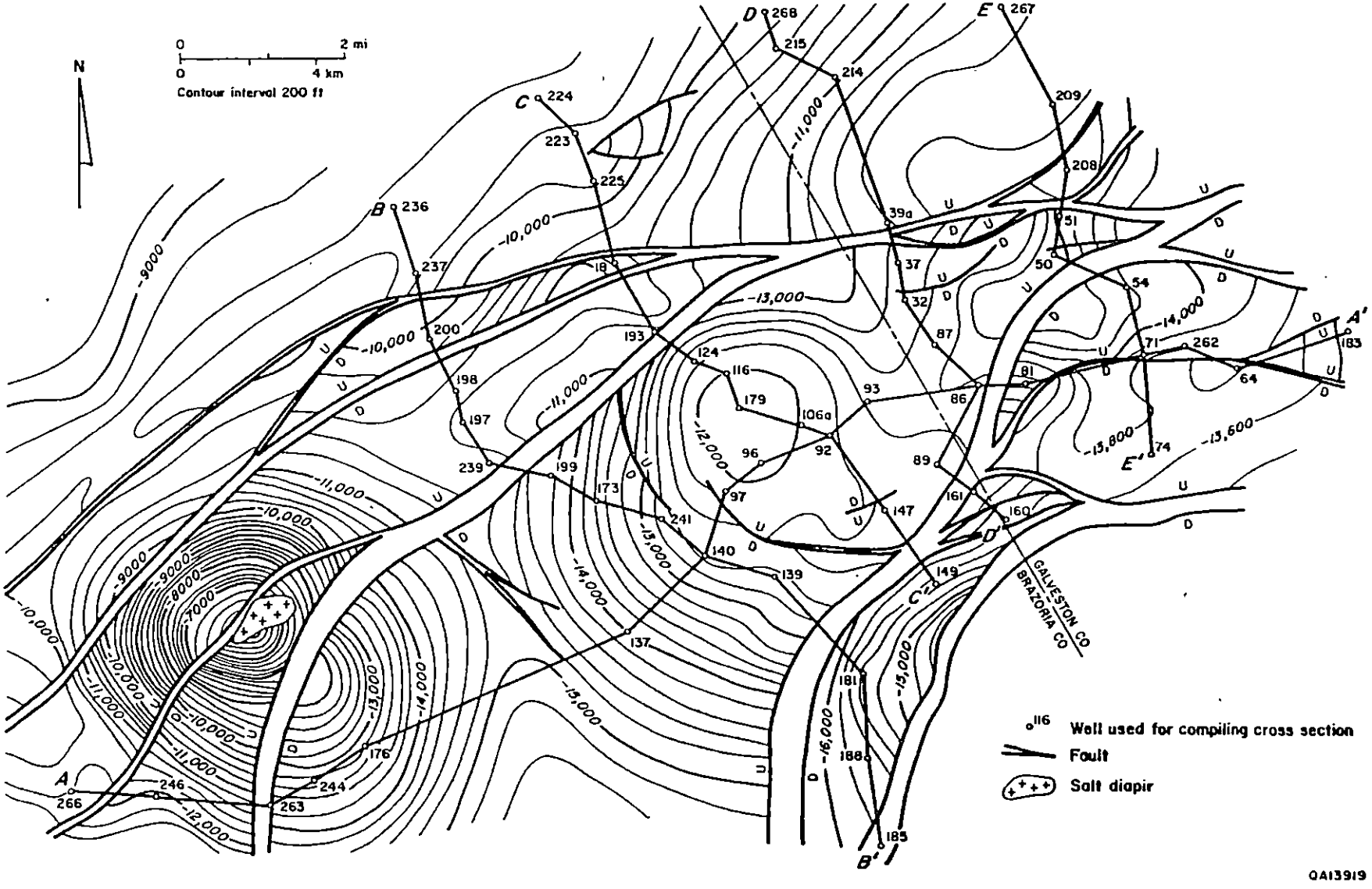

Figure 6. Location of cross sections A–A′ through E–E′ in Pleasant Bayou fault-block area. Cross section A–A′ shown in figure 7; cross section B–B′ shown in figure 8; cross section C–C′ shown in figure 9; cross section D–D′ shown in figure 10; cross section E–E′ shown in figure 11.

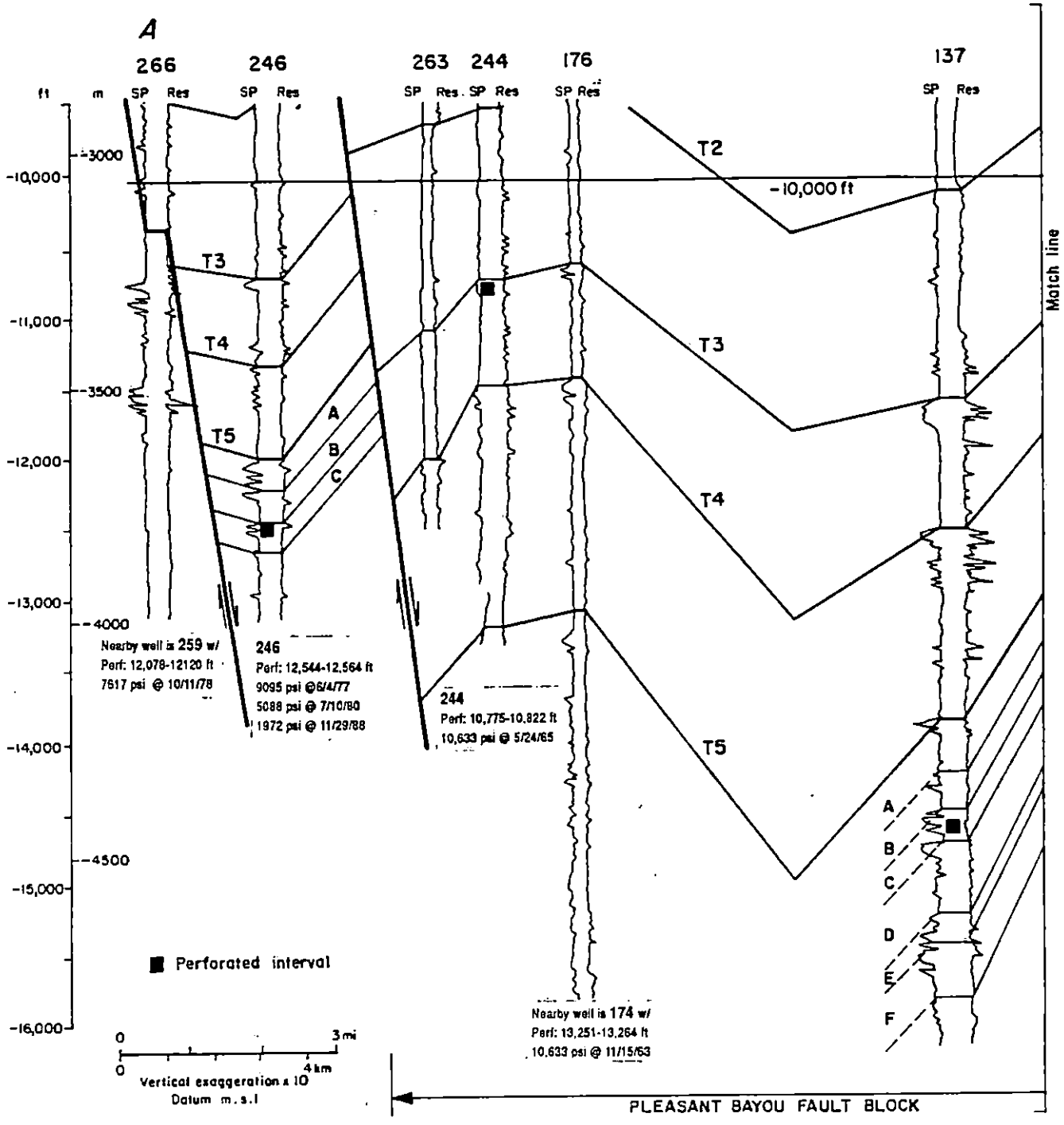

Figure 7. West-east strike-oriented cross section A–A′ of Pleasant Bayou fault-block area. Line of section shown in figure 6. Sea level datum.

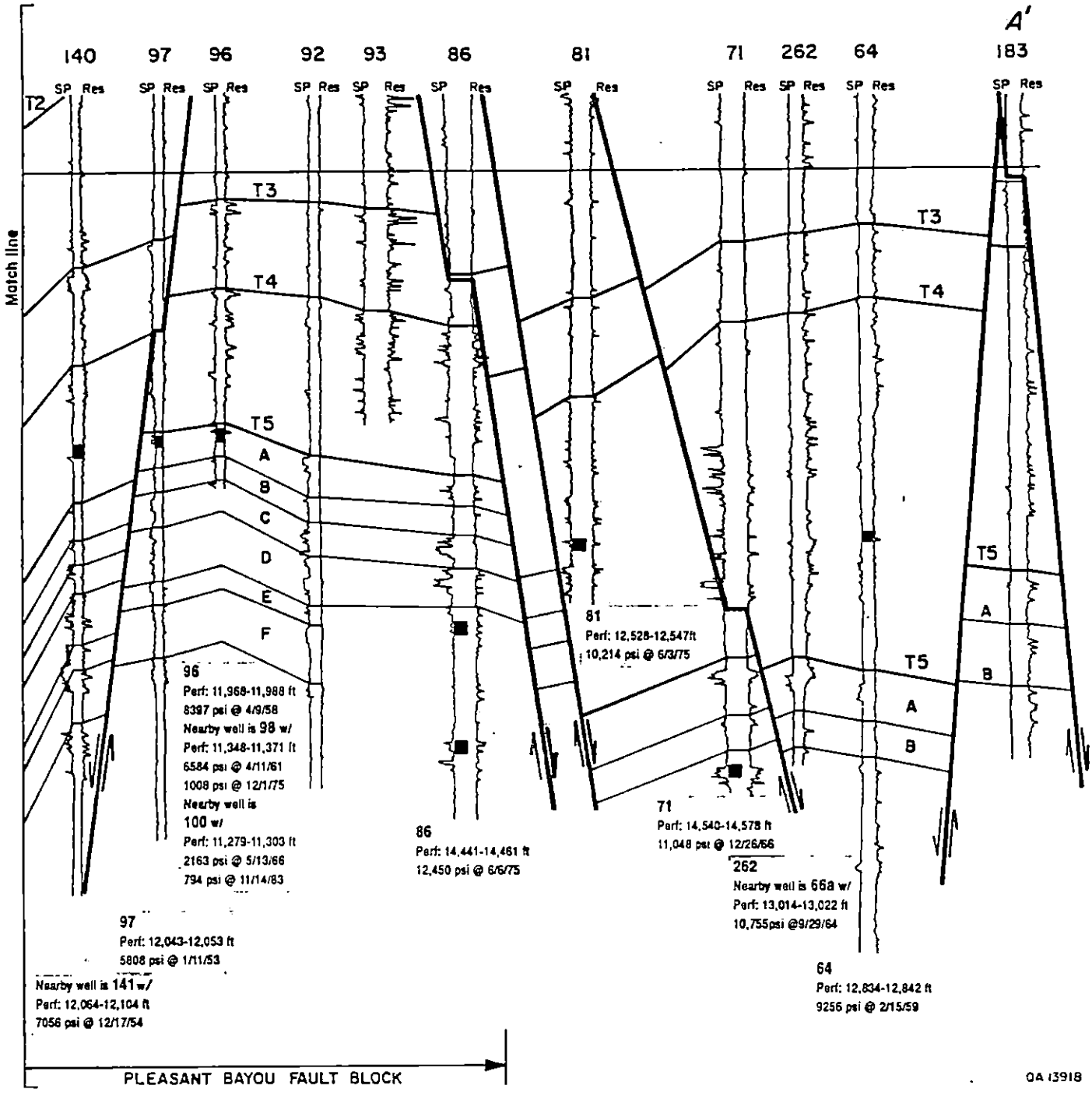
A'
140
97
96
92
93
86
81
71
262
64
183
SP Res
T2
T3
T4
T5
A
B
C
D
E
F
Match line
96
Perf: 11,968-11,988 ft
8397 psi @ 4/9/58
Nearby well is 98 w/
Perf: 11,348-11,371 ft
6584 psi @ 4/11/61
1008 psi @ 12/1/75
Nearby well is
100 w/
Perf: 11,279-11,303 ft
2163 psi @ 5/13/66
794 psi @ 11/14/83
97
Perf: 12,043-12,053 ft
5808 psi @ 1/11/53
Nearby well is 141 w/
Perf: 12,064-12,104 ft
7056 psi @ 12/17/54
86
Perf: 14,441-14,461 ft
12,450 psi @ 6/6/75
81
Perf: 12,528-12,547ft
10,214 psi @ 6/3/75
71
Perf: 14,540-14,578 ft
11,048 psi @ 12/26/66
262
Nearby well is 66a w/
Perf: 13,014-13,022 ft
10,755psi @9/29/64
64
Perf: 12,834-12,842 ft
9256 psi @ 2/15/59
PLEASANT BAYOU FAULT BLOCK
OA 13918

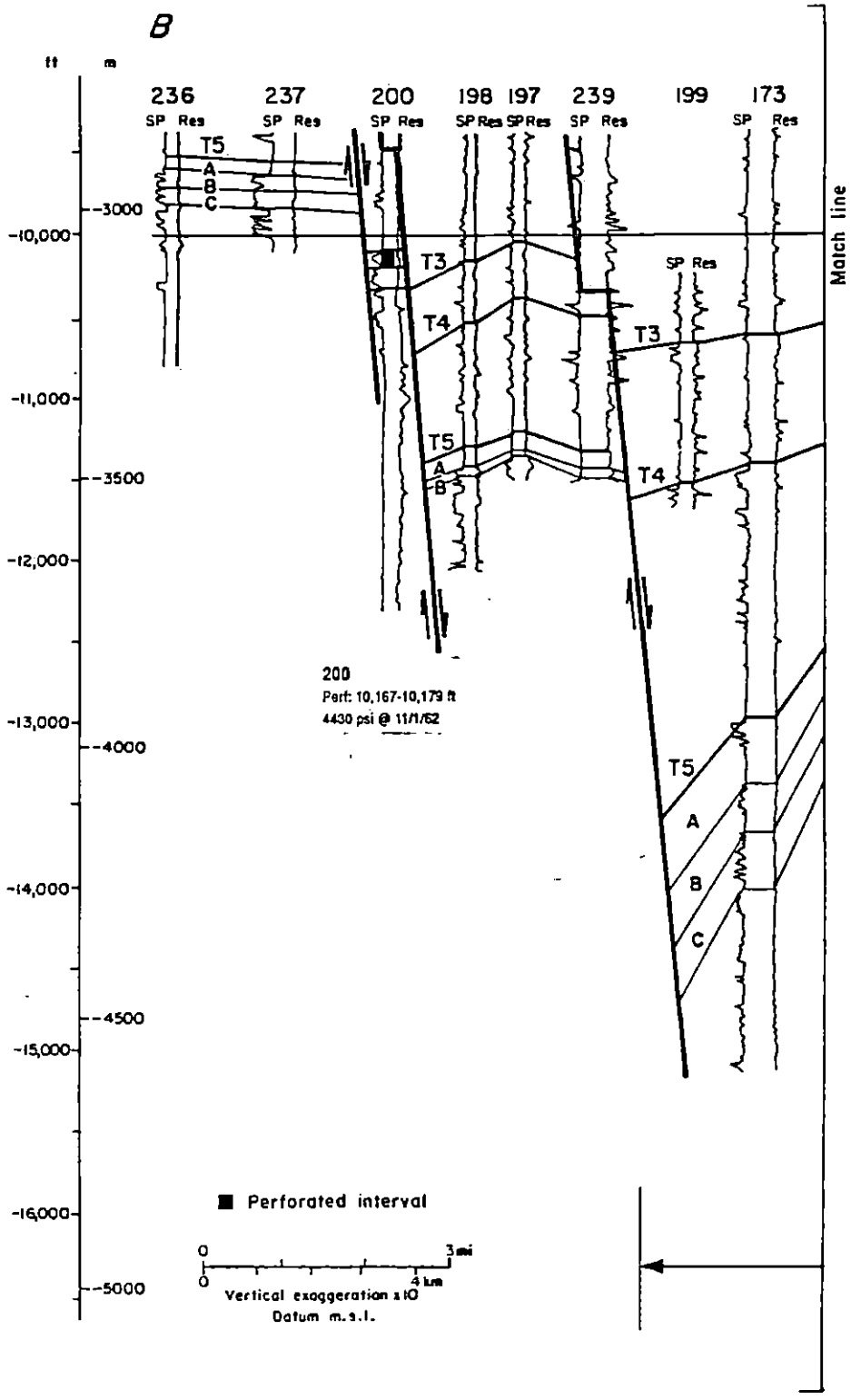

Figure 8. North-south dip-oriented cross section B–B′ of Pleasant Bayou fault-block area. Line of section shown in figure 6. Sea level datum.

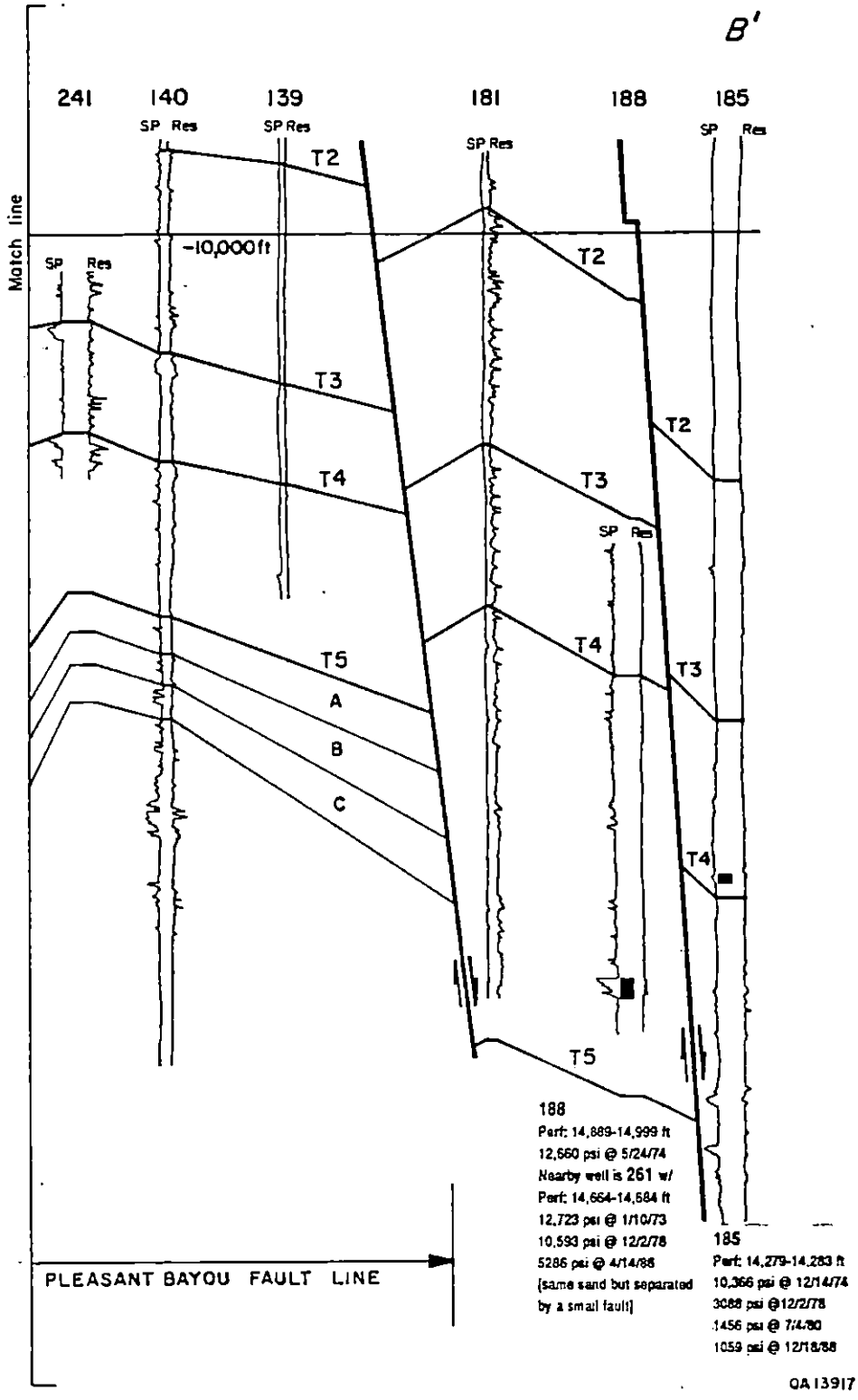
B'
241
140
139
181
188
185
SP Res
T2
T3
T4
T5
A
B
C
-10,000ft
Match line
PLEASANT BAYOU FAULT LINE
188
Perf: 14,889-14,999 ft
12,660 psi @ 5/24/74
Nearby well is 261 w/
Perf: 14,664-14,584 ft
12,723 psi @ 1/10/73
10,593 psi @ 12/2/78
5286 psi @ 4/14/86
(same sand but separated by a small fault)
185
Perf: 14,279-14,283 ft
10,366 psi @ 12/14/74
3088 psi @12/2/78
1456 psi @ 7/4/80
1059 psi @ 12/18/88
QA13917

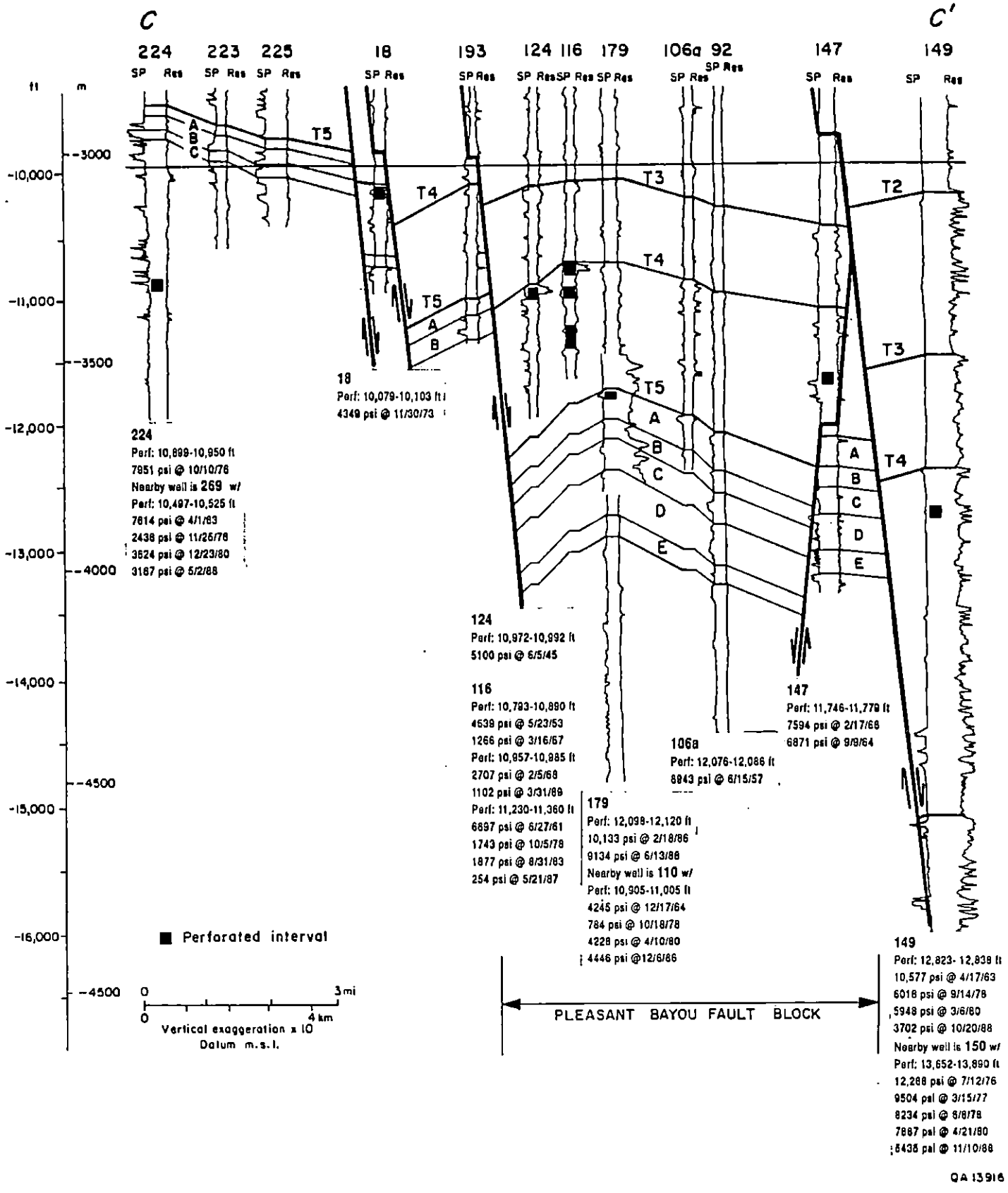

Figure 9. North-south dip-oriented cross section C–C′ of Pleasant Bayou fault-block area. Line of section shown in figure 6. Sea level datum.

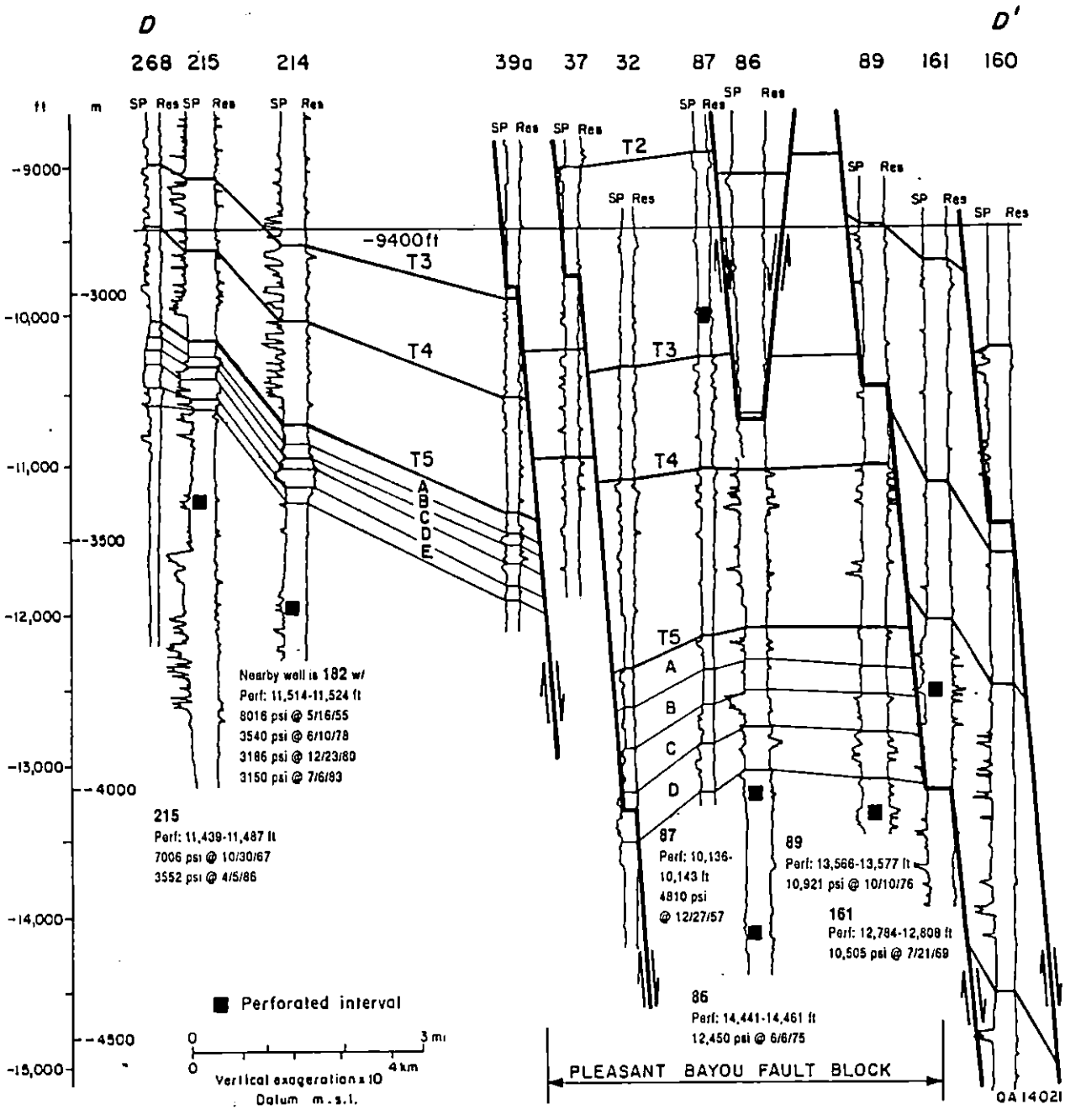

Figure 10. North-south dip-oriented cross section D–D′ of Pleasant Bayou fault-block area. Line of section shown in figure 6. Sea level datum.

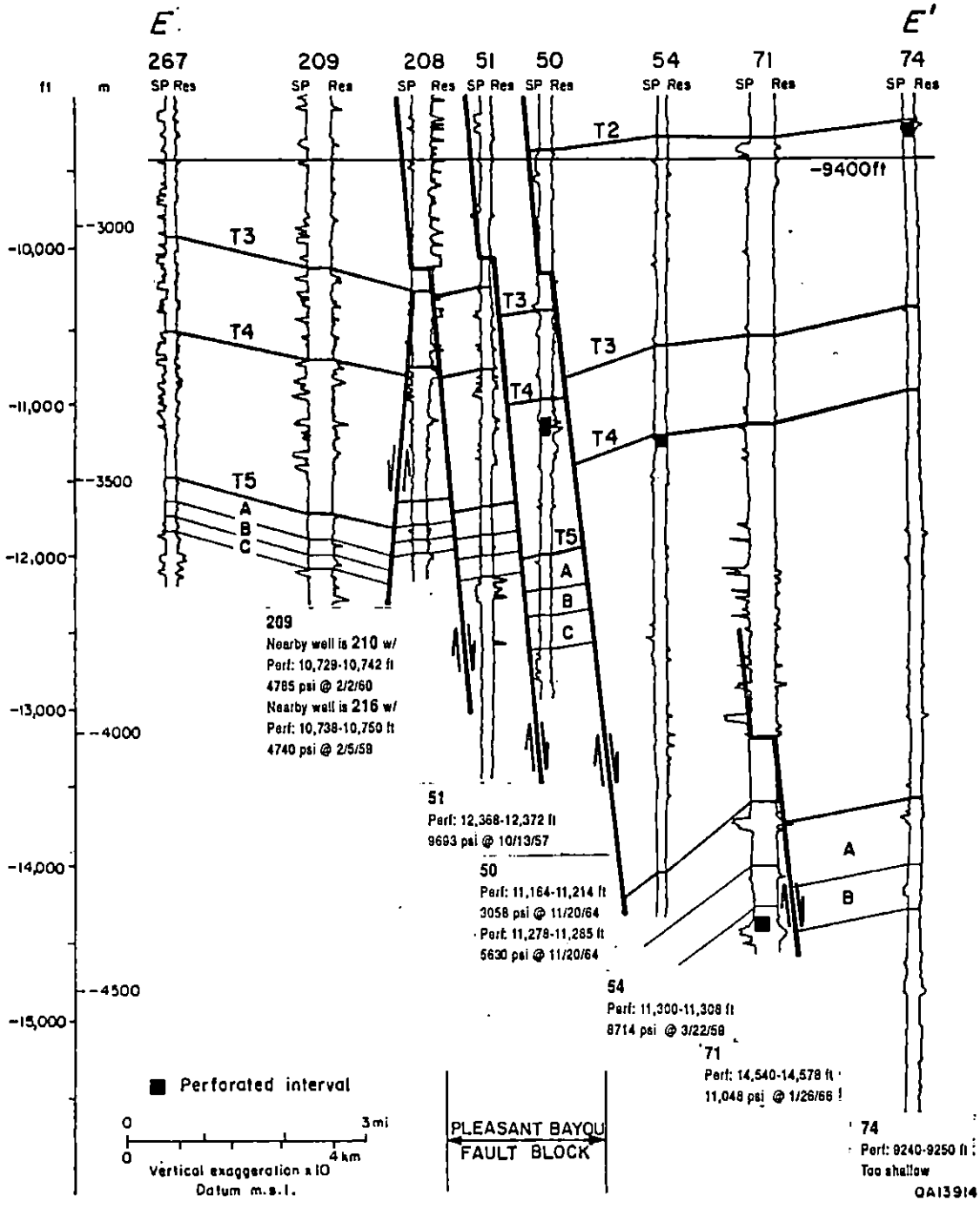

Figure 11. North-south dip-oriented cross section E–E′ of Pleasant Bayou fault-block area. Line of section shown in figure 6. Sea level datum.

basin to 274 m (900 ft) in the apex of the block. This unit generally thins southward as well, to about 305 m (1,000 ft) near the southern boundary fault. T4 unit sandstones range in thickness from 9 to 30 m (30 to 100 ft) in the withdrawal basin to 4.5 to 9 m (15 to 30 ft) in the central and apex areas. Shales 30- to 61-m (100- to 200-ft) thick separate the sandstones. A through F sandstones of the T5 unit within the block vary with position laterally and downdip. The A sandstone varies from approximately 61 m (200 ft) in thickness in the apex area to nearly 122 m (400 ft) in the withdrawal basin. Sandstones vary in thickness from virtual absence in the apex area to 15 m (50 ft) or more in the withdrawal basin. Most shales in the A sandstone are at least 46 m (150 ft) thick.

The B sandstone within the block shows similar variability exhibiting a range of thickness from 46 to 92 m (150 to 300 ft). Sandstones vary in thickness from 3 to 9 m (10 to 30 ft), separated by shales 12 to 21 m (40 to 70 ft) thick. The main C sandstone reservoir exhibits a relatively uniform increase in thickness from 46 m (150 ft) in the apex area southwestward to 107 m (350 ft) in the withdrawal basin. Sandstone-body thicknesses range from 6 to 21 m (20 to 70 ft), separated by 9- to 46-m (30- to 150-ft) shales (Hamlin and Tyler, 1988). The D and E sandstones typically are 107 m and 46 m (350 and 150 ft) thick, respectively. The D sandstones range from 3 to 15 m (10 to 50 ft) in thickness and contain 6- to 18-m (20- to 60-ft) shales. E sandstones are thin and spiky and have a maximum thickness of about 6 m (20 ft).

North Area

The T5 unit sandstones correlated north of the Pleasant Bayou fault block typically consist of massive sandstones 15 to 46 m (50 to 150 ft) or more thick interspersed with small shale units usually less than 9 m (30 ft) thick. The B- and C-zones are particularly massive in the central and western portion of the area to the north. The A-zone sandstones have largely disappeared throughout the area north of the block, and the D-zone consistently shows a shale unit in the lower half of the zone that has a thickness in excess of 9 m (30 ft).

The main sandstones of the T correlation units coalesce to the north of the Pleasant Bayou fault block as a result of interbedded shales thinning and pinching out northward. Stratigraphic correlations have been made within these sandstones. Rapid expansion of the shales is observed southward as the growth faults are successively crossed. Expansion is readily observed in section A–A′ (fig. 8) and section B–B′ (fig. 9) as the units are followed into the deep withdrawal basin in the southwest portion of the block.

South Area

To the south and southeast of the Pleasant Bayou block, extensive expansion of the T4 and T5 units is observed as reflected in cross sections A–A′ to E–E′ (figs. 7 to 11). The T4 unit exceeds 793 m (2,600 ft) in thickness, most of the expansion occurring within the shales. T5 unit thickness is unknown. The A and B sandstone thicknesses are in excess of 122 m (400 ft) in the south and southeast. Where observed, sandstone thicknesses do not vary appreciably from that of corresponding zones within the block, but thin sandstones distinguishable within the block are less apparent southward. Only the larger sandstones exist on the downdip side of the south fault. For instance, in figure 10 (section D–D′) the A sandstone exhibits a persistent 18-m (60-ft) blocky sandstone near the top of the zone in well no. 160, but no other A sandstone is observed even though the A sandstone on the immediate updip side has a number of small sands.

Geologic evidence suggests an absence of sandstone continuity across major faults. This absence is readily seen in the central, western, and southern portions of the area, but is less apparent across the northeast apex of the Pleasant Bayou fault block. Figure 8 (section B–B′) illustrates this lack of sand continuity, where the thick C sandstone in well no. 140 coincides across the boundary fault with a shaly section in the T4 unit in well no. 181. The same is true of the relatively thick sandstones at the tops of the T3 and T4 units in the same wells. Even when sandstones appear to align with sandier zones across the fault, such as the C sandstone in figure

11 (section E–E'), well nos. 50 and 54, offset is still such that co-occurrence across the fault results in poor sandstone-sandstone continuity.

Comparison of average fault offset to average sandstone thickness offers the most direct evidence for lack of continuity. Offset shown on the dip sections is generally an order of magnitude or more thicker than average sandstone bodies. This difference may be seen, for instance, in figure 10 (section D–D'), well nos. 160 and 161, where the A sandstone averages just 3 m (10 ft) in thickness inside the block, but offset across the fault is at least 640 m (2,100 ft) because of shale expansion. Shales on the downdip side (well no. 160) average greater than 30 m (100 ft) in thickness. Total shale thicknesses are several times those of the sandstone, and with few exceptions, coincidence of any two sand bodies will rarely occur across the boundary-forming faults.

One of these exceptions may occur in the extreme northeast apex of the fault block. Correlations on figure 11 (section E–E') indicate that fault offsets are found much less frequently across the north boundary fault. This fault cuts between wells 208 and 51 and shows perhaps only 30.5 m (100 ft) of displacement at T5. Although the T5 unit contains little sandstone in the east, coincidence of sandstone bodies is more probable, at least for the T4 correlation package.

Hamlin and Tyler (1988) noted that fault gouge within the fault planes of the internal and boundary-forming faults may act as a potential barrier to fluid flow across the faults even if adjacent sandstones occur across the faults. It is impossible to resolve from well log examination alone whether permeability barriers exist.

Hydrogeology

Pressure Regimes and Hydrodynamics

Pressure-depth profiles and potentiometric surfaces constructed from reservoir-pressure data in the Texas Gulf Coast Frio Formation reflect existence of three hydrologic regimes: a shallow, fresh to moderately saline water section in the upper 915 to 1,220 m (3,000 to 4,000 ft), an underlying 1,220- to 1,524-m (4,000- to 5,000-ft) thick, essentially saline hydrostatic section, and a deeper geopressured section having moderate to high salinities (figs. 12 and 13) (Kreitler and others, 1988). A pressure-depth profile in Brazoria and Galveston Counties reflects a similar trend (fig. 14) wherein the 10.5-kPa/m (0.465-psi/ft) gradient line distinguishes the hydrostatic pressures from the geopressures. The 10.5-kPa/m (0.465-psi/ft) gradient identifies a density of a predominantly 100,000-ppm salinity brine. The transition from a normally pressured to a geopressured hydrologic environment could either be abrupt where the vertical geopressure gradient changes abruptly, or it could be gradual where the presence of interbedded sandstones and clays results in a gradual, stepwise transition. In the absence of pressure-depth profiles within the same well that could be correlated across many wells and specific hydrologic units, it is hard to identify the nature of transition from hydrostatic pressure to geopressures. Fluid pressures in sediments are dominated by two factors, the compression due to burial and compaction on the one hand, and the resistance to leakage on the other (Dickinson, 1953). A reduction of porosity and permeability is observed with compaction. Within which of the areas between the 10.5-kPa/m (0.465-psi/ft) line and the lithostatic load line of 22.6 kPa/m (1.0 psi/ft)(fig. 14) the sediments lie depends on the state of equilibrium reached between the weight of the overburden and the load-bearing strength of the sediments under varying degrees of fluid leakage. Ewing and others (1984) provided the following description of pressure regimes in the Pleasant Bayou area: (1) an upper zone of normally

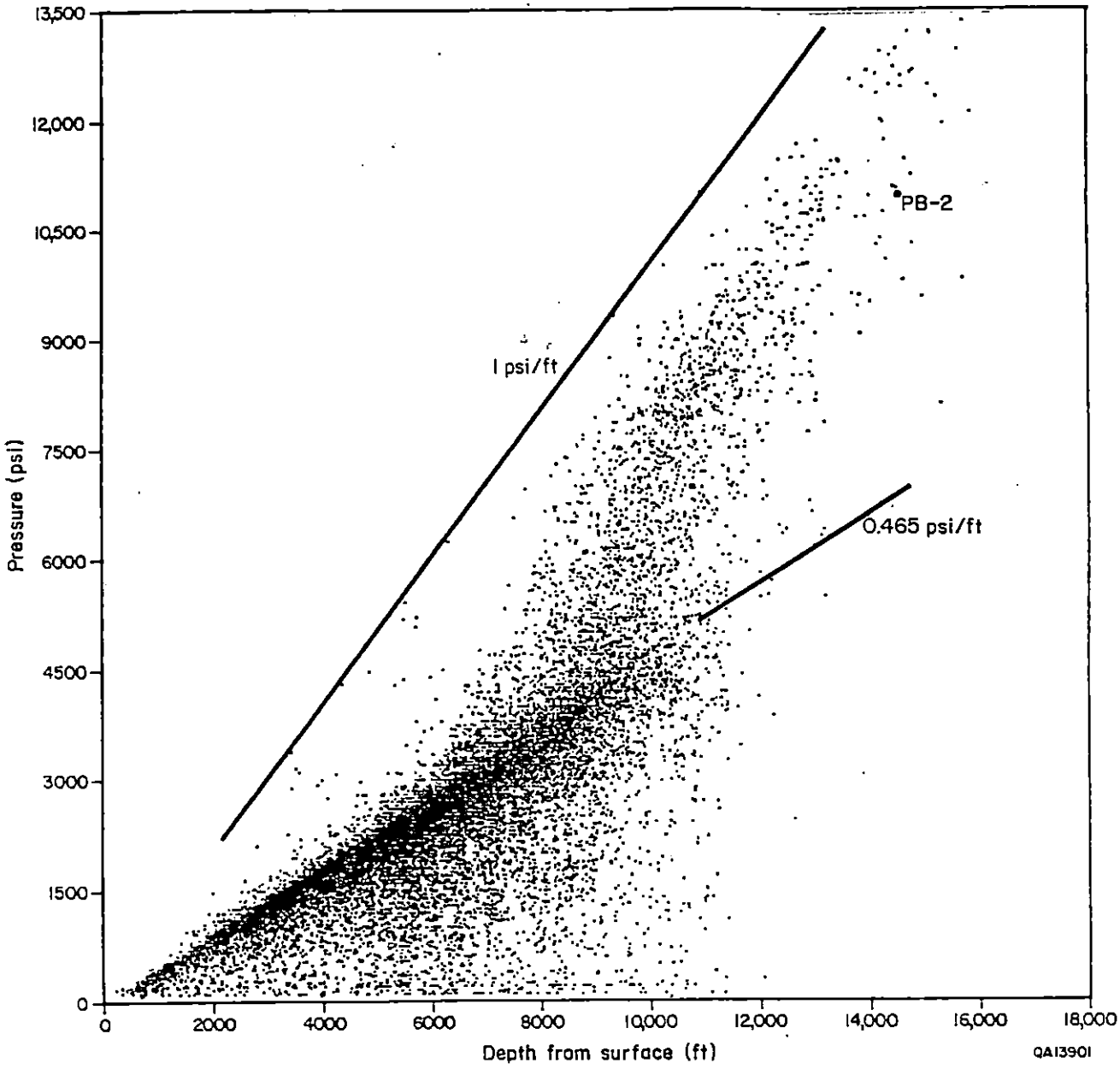

Figure 12. Pressure-depth diagram for Frio in Texas Gulf Coast. Onshore data from drill-stem tests and bottom-hole-pressure measurements.

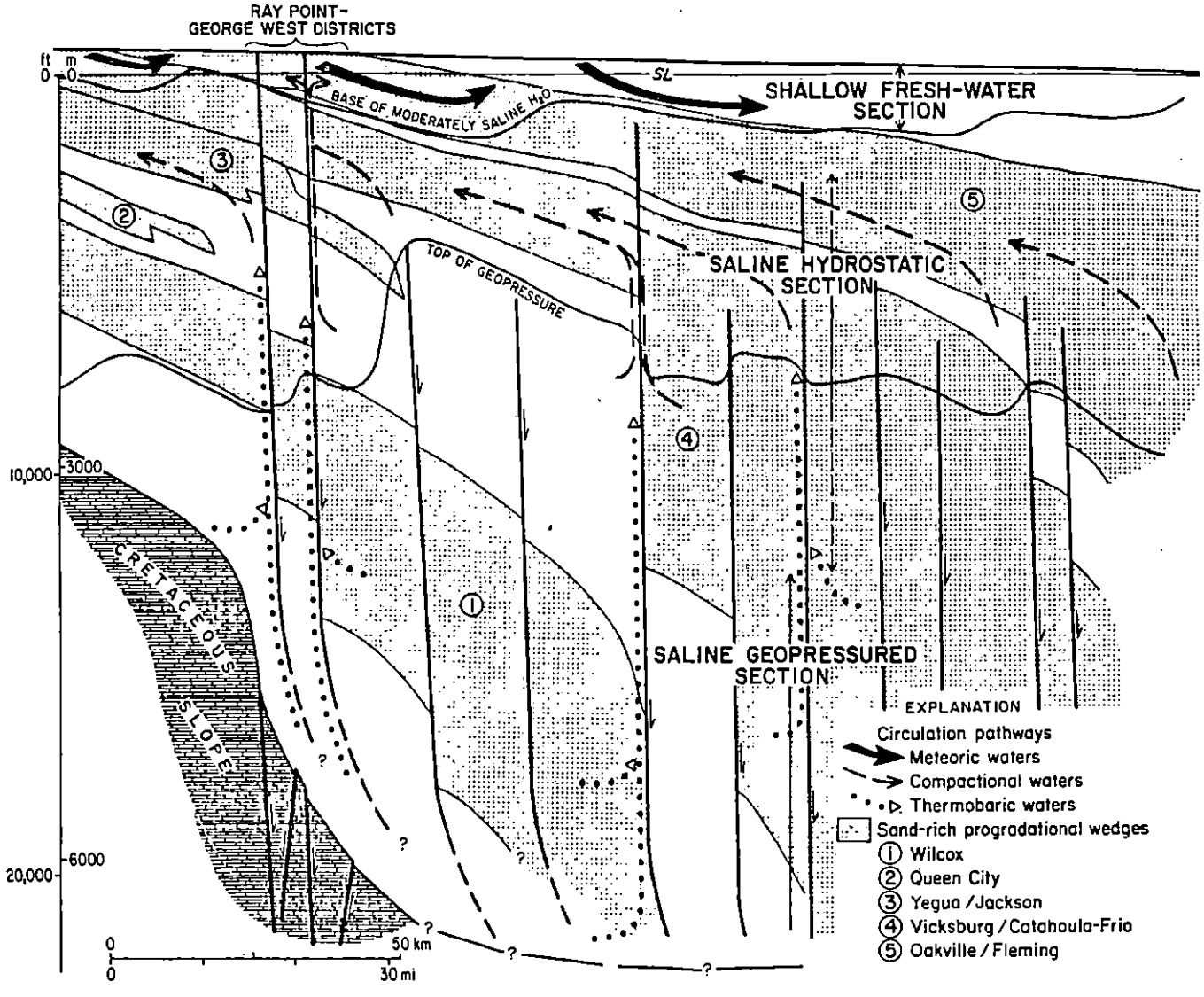

Figure 13. Ground-water regimes and circulation pathways within the Tertiary basin fill of the northwestern Gulf Coast Basin. Modified from Galloway and others (1982).

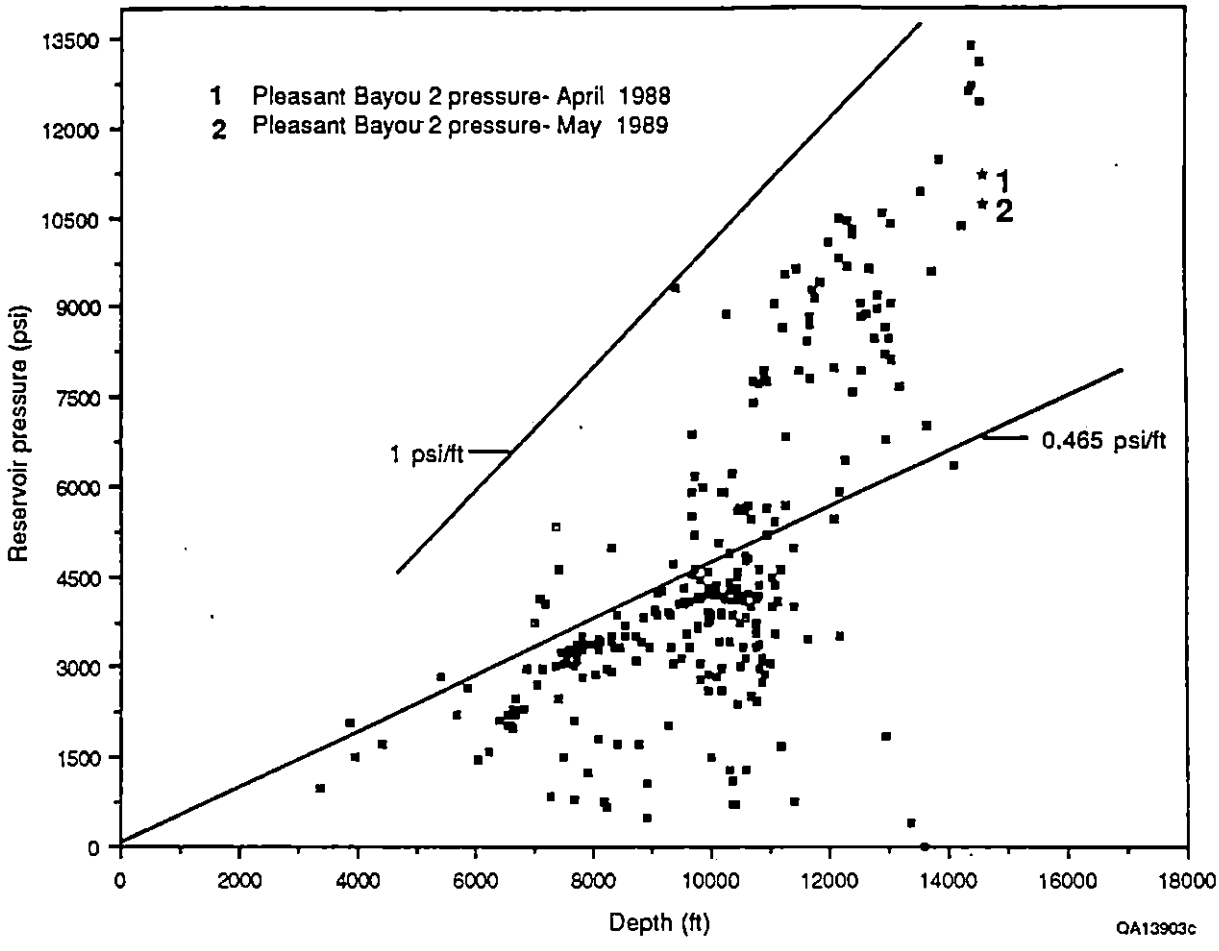

Figure 14. Pressure-depth diagram for Frio in Brazoria and Galveston Counties. Pressures from drill-stem tests, bottom-hole measurements and estimated from shut-in wellhead pressures.

pressured sandstones and shales, (2) a zone of normally pressured sandstones and overpressured shales, (3) a zone of moderately overpressured sandstones and more greatly overpressured shales, and deepest, (4) a zone of highly overpressured sandstones and shales. The normally pressured sandstones of zones 1 and 2 exhibit high permeability and continuity across the growth faults, whereas the sandstones of zones 3 and 4 possess generally lower porosity and permeability and greater lateral discontinuity. Within zone 4, the variation in brine salinities, formation porosities, and permeabilities observed in the geopressured C-zone at Pleasant Bayou and equivalent productive horizons in the nearby oil and gas fields precludes accurate quantitative determination of the degree of geopressuring.

Geothermal Environment

The geothermal regime is relevant for the occurrence of geopressures because mobile water is the most important factor in terrestrial heat flow in sedimentary basins (Bogomolov, 1967). Clay beds act as barriers to upward flow of water, greatly reducing the rate of upward flow of heat, and geopressured reservoirs become overheated. Convective distribution of heat occurs in the reservoirs but not in the clay beds overlying them; thus, the geothermal gradient is steepest in that part of the clay beds that immediately overlie geopressured aquifers. A temperature-depth profile for the northern Texas Gulf Coast was plotted on the basis of measured and estimated bottom-hole temperatures from oil and gas wells during drilling and completion (fig. 15). This plot does not reflect a sharp break in the temperature gradient. The trends in the temperature-depth plot for Brazoria and Galveston Counties are similar (fig. 16). The reliability of these temperature data as reported in the Railroad Commission of Texas data base (1989) cannot be confirmed because the measurement procedure and equilibration times are hard to verify. If the bottom-hole thermometer is not allowed to equilibrate for an adequate period before production of a well, it will read an incorrect measurement. The temperature data gathered for this report reflect a geothermal gradient of about 1.7°F per 100 ft, similar to the

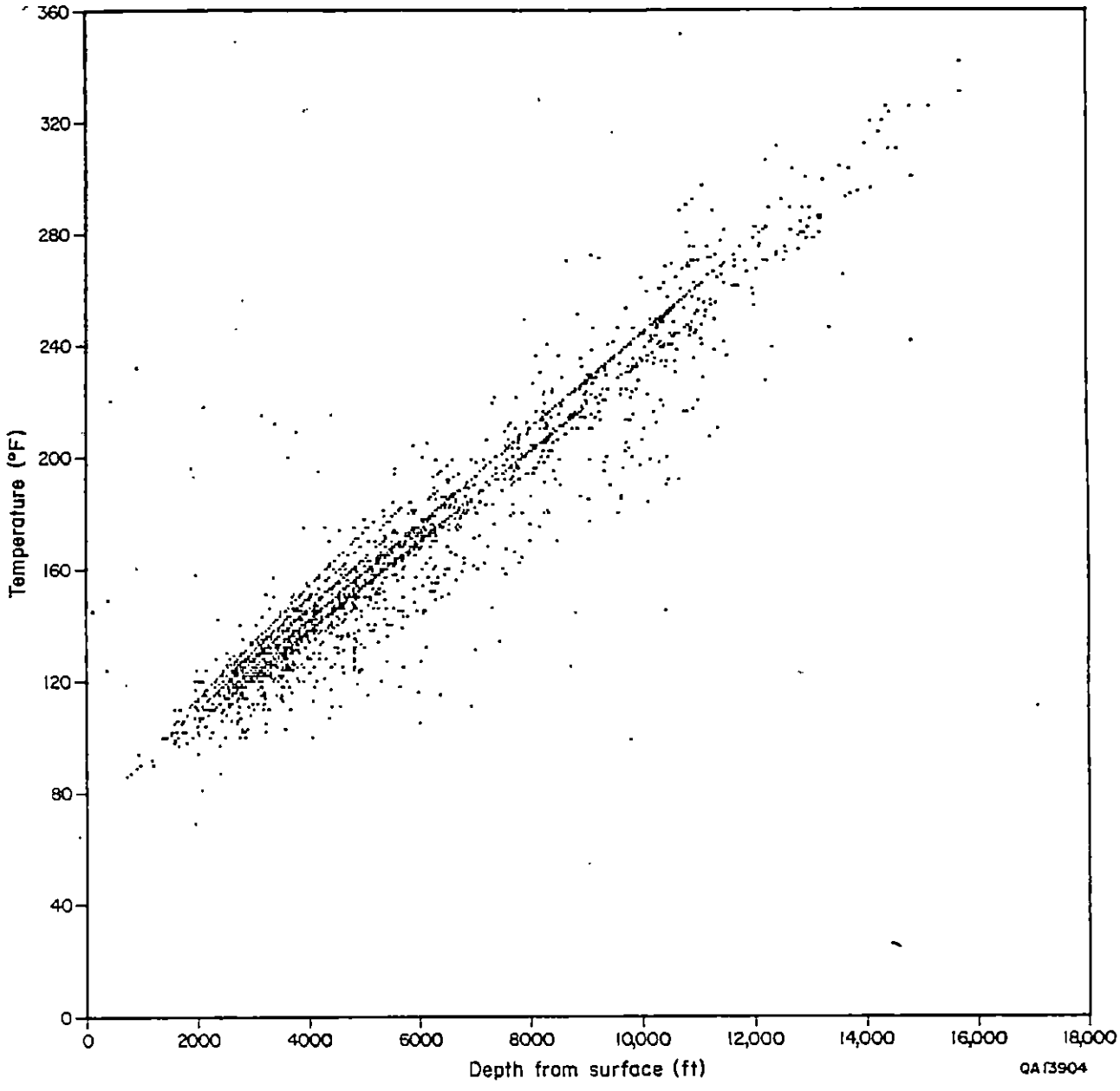

Figure 15. Temperature-depth plot for Texas central Gulf Coast region.

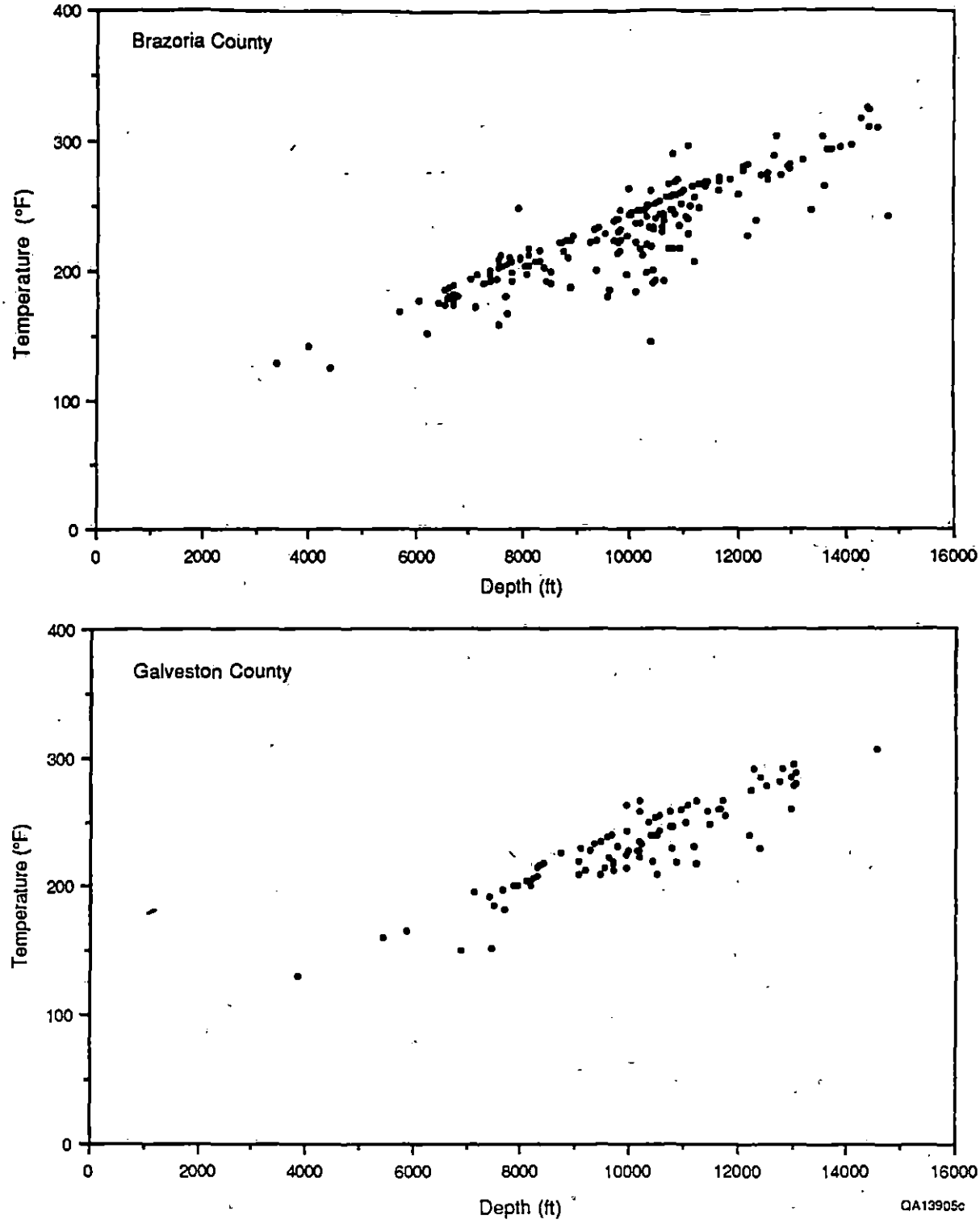

Figure 16. Temperature-depth plot for oil and gas wells in Pleasant Bayou fault-block area.

value measured in Pleasant Bayou Test Well No. 2 (307°F at 14,674 ft). Bebout and others (1978) reported an average geothermal gradient of 1.8°F per 100 ft for measured bottom-hole temperatures in the Pleasant Bayou area. Although the temperature-depth profile for the Pleasant Bayou area does not exhibit a sharp discontinuity related to any overlying shale seal, the geothermal gradient value compares well with the value estimated for this environment.

Reservoir Model

Earlier data on pressure and fluid composition from sandstone units across the major growth faults bounding the Pleasant Bayou fault block indicate that the aquifer within the fault block is hydrologically isolated (Hamlin and Tyler, 1988). Displacements across internal faults may reach 122 m (400 ft) but are more typically less than 61 m (200 ft). Analysis of early production tests indicated that internal faults may have formed partial barriers to flow (Garg and others, 1981). The most significant internal faults lie between the test well and Chocolate Bayou field. Variable displacement along the length of internal faults may cause permeable sandstone units to be displaced either totally or only partially against other permeable units. When the displacement is partial, reservoir continuity exists; otherwise the fault may act as a barrier to fluid flow. Hamlin and Tyler (1988) discussed in detail the possible configuration of permeable units in the C-zone at the internal fault planes in the Pleasant Bayou fault block. These considerations formed the basis of the geologic reservoir model developed by Hamlin and Tyler (1988). Riney (1989) at S-Cubed incorporated these fault emplacements in the numerical model designed to describe the production characteristics at Pleasant Bayou.

Results of Current Production Test

The current phase of production testing at Pleasant Bayou No. 2 began on May 28, 1988. Since then the well has produced from the C-zone through perforations between depths of

4,463 and 4,482 m (14,644 and 14,704 ft). Production rate has been maintained between 15,000 and 20,000 barrels per day (bpd), and during this 16-mo period nearly 7.2 million stock tank barrels (MMstb) of brine and 172.9 million standard ft^3 (MMscf) of gas has been produced. The well has been in production more than 95 percent of the time. A decline of about 2,067 kPa (300 psi) has been observed in the flowing bottom-hole pressure that is calculated from the wellhead flowing pressure by S-Cubed (Riney, 1989). The static reservoir pressure at the beginning of the current phase of testing at the 4,450 m (14,600 ft) datum was 75.4×10^3 kPa (10,944 psi) and was calculated to be about 73.4×10^3 kPa (10,650 psi) at the same datum during the 65-hr pressure-buildup test conducted from May 14 through 18, 1989 (Riney, 1989). An earlier reservoir pressure recorded in 1979 during a drill-stem test in the test interval 4,463 to 4,482 m (14,644 to 14,704 ft) was 78.5×10^3 kPa (11,400 psi) (Gregory and Backus, 1979). Riney and others (1985) estimated an initial reservoir pressure of 76.9×10^3 kPa (11,168 psi) at 4,474 m (14,674 ft).

Figure 17 reflects the cumulative brine and gas production, and figure 18 is the change in bottom-hole and wellhead flowing pressures with time. The brine production rate and gas/brine ratio are plotted in figure 19. The short spikes on the plots for the well rate and bottom-hole pressure reflect changes in operating conditions, for example, downtime for repairs. No significant change in the gas/brine ratio has been observed during the test period, indicating that no free gas is being formed in the reservoir and that the reservoir pressure is above saturation pressure. The plots of flowing bottom-hole pressure versus cumulative brine and gas production are shown in figures 20 and 21. Also plotted in figures 20 and 21 are the two values of estimated average reservoir pressures. This decline in pressures is small and conforms to the characteristic of early time performance from a geopressured reservoir. The Pleasant Bayou reservoir is still in an early stage of depletion, and after a longer production period this decline may accelerate.

Earlier, Randolph (1985) looked at gas deliverability from Pleasant Bayou No. 2 and estimated that the well was capable of producing in excess of 150 Mcf/d down to a bottom-hole

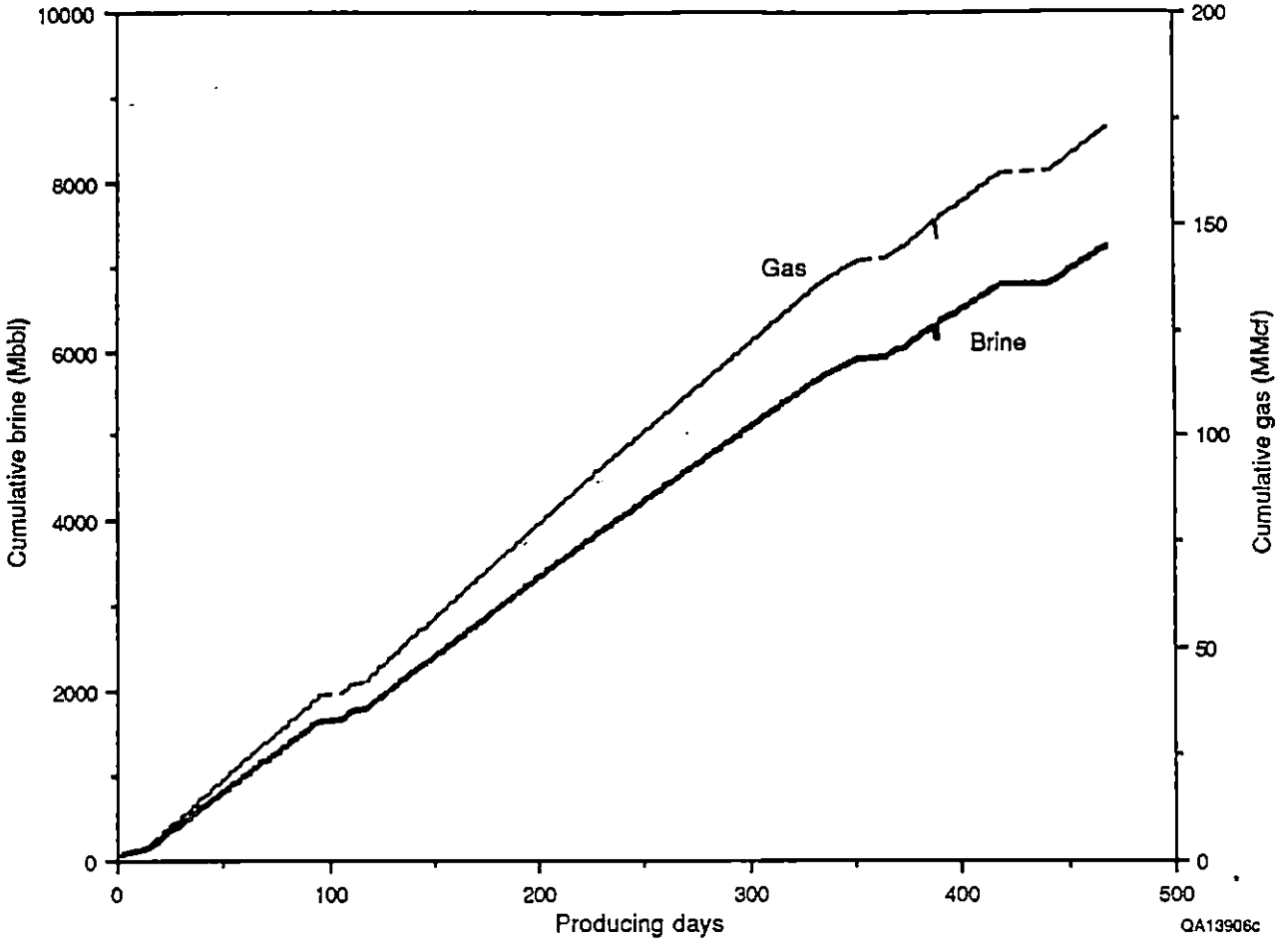

Figure 17. Cumulative brine and gas production from Pleasant Bayou Test Well No. 2 during current long-term production test.

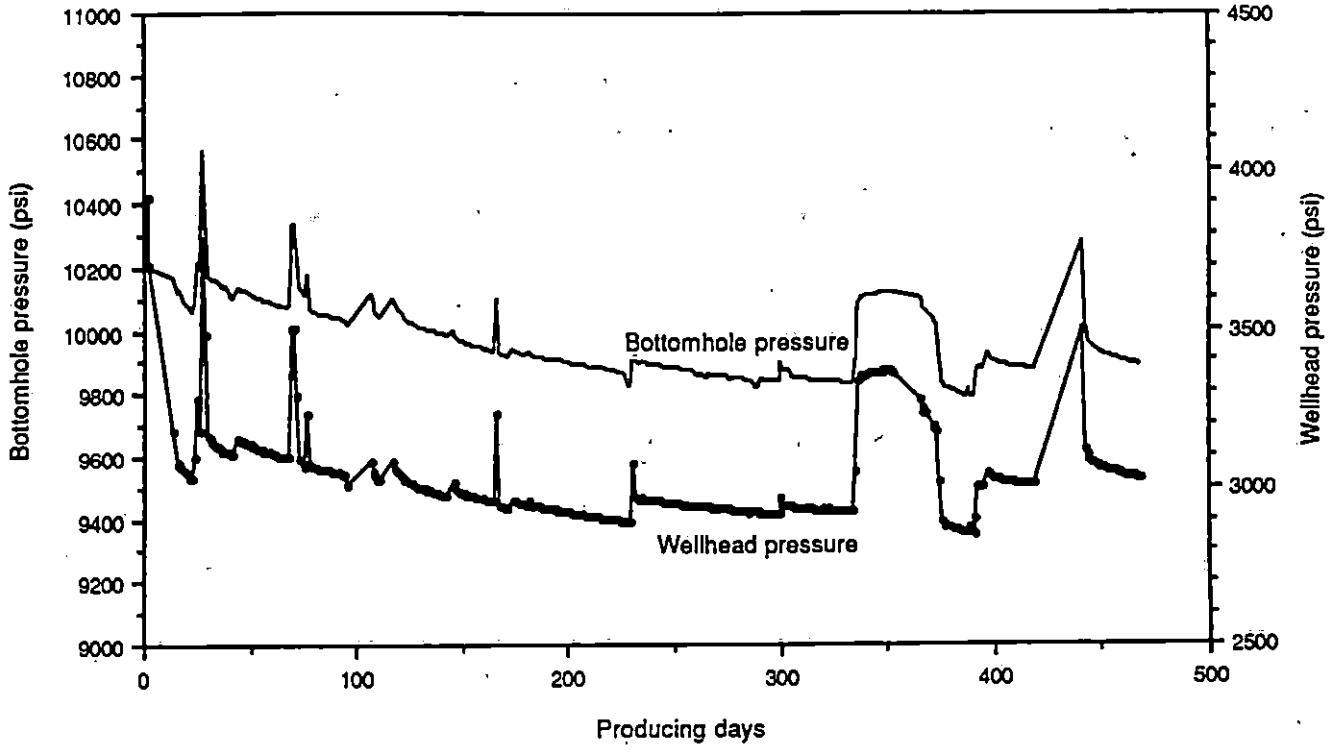

Figure 18. Trend in flowing wellhead pressure and calculated bottom-hole pressure at Pleasant Bayou No. 2 during current long-term testing.

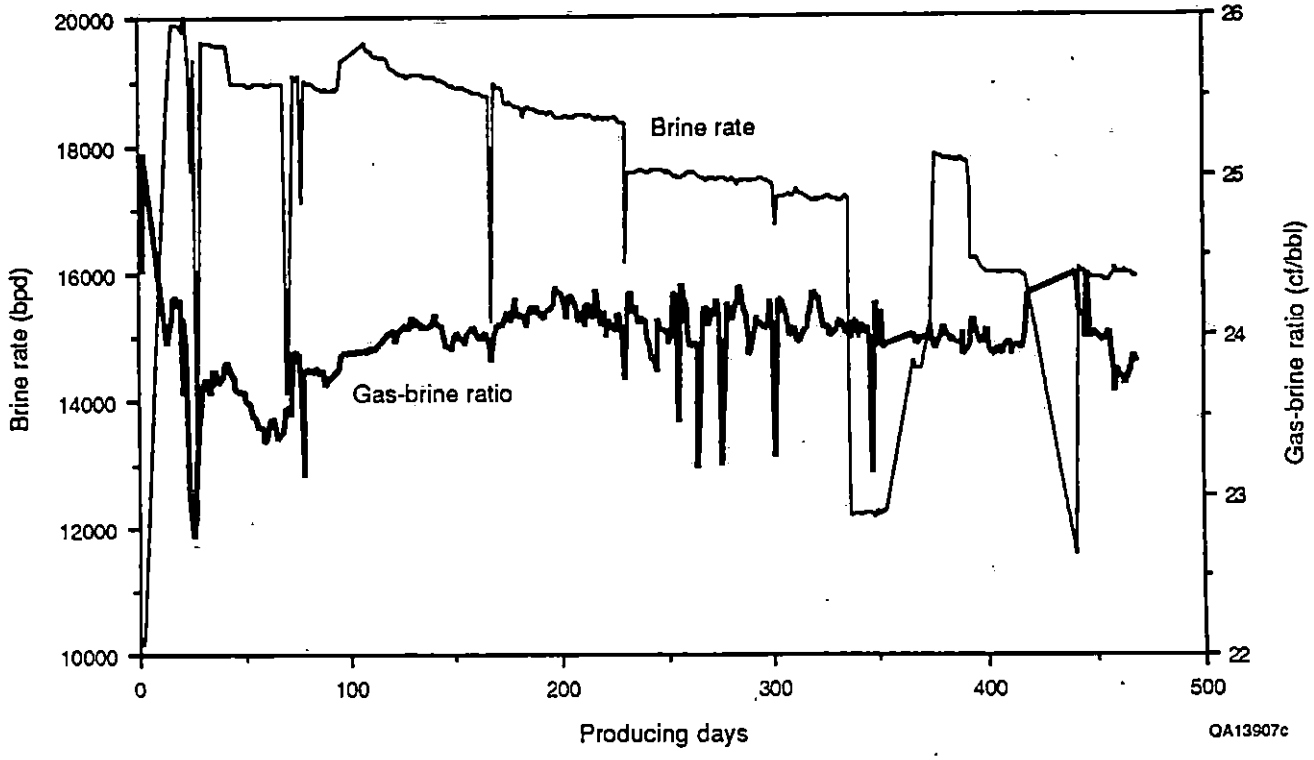

Figure 19. Brine production rate and gas/brine ratio during current long-term testing at Pleasant Bayou No. 2.

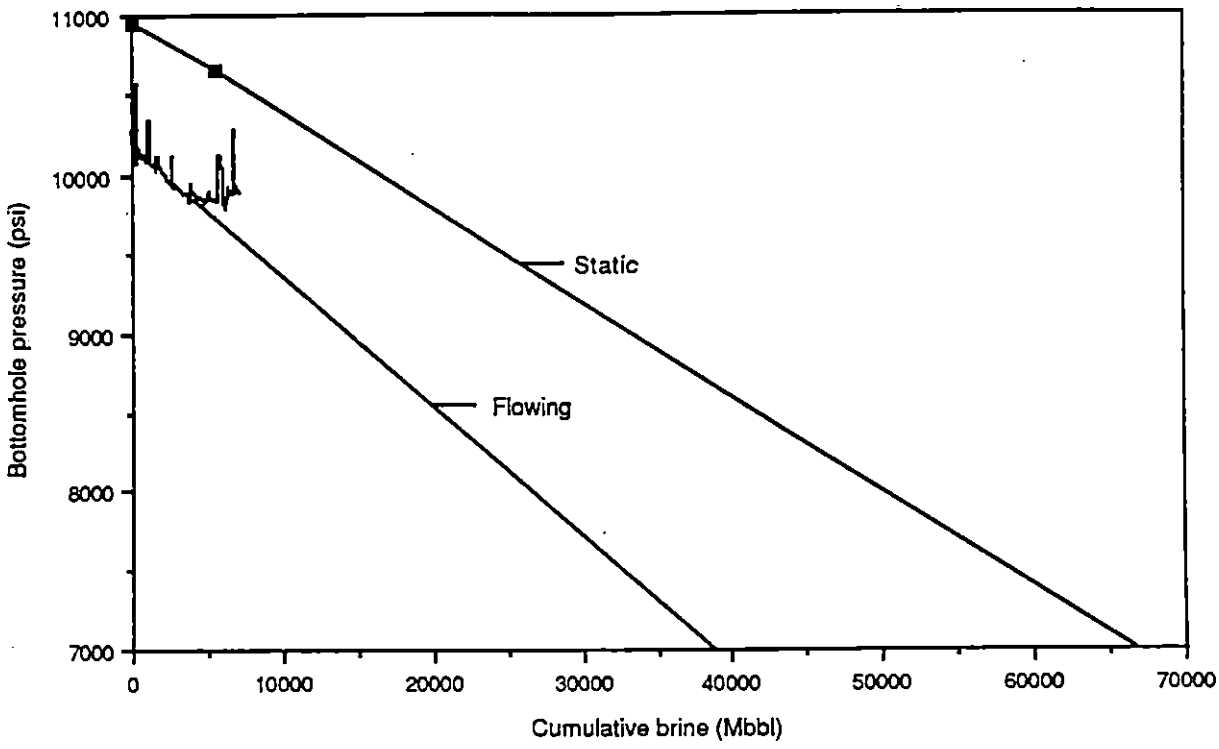

Figure 20. Bottom-hole pressure versus cumulative brine production at Pleasant Bayou No. 2.

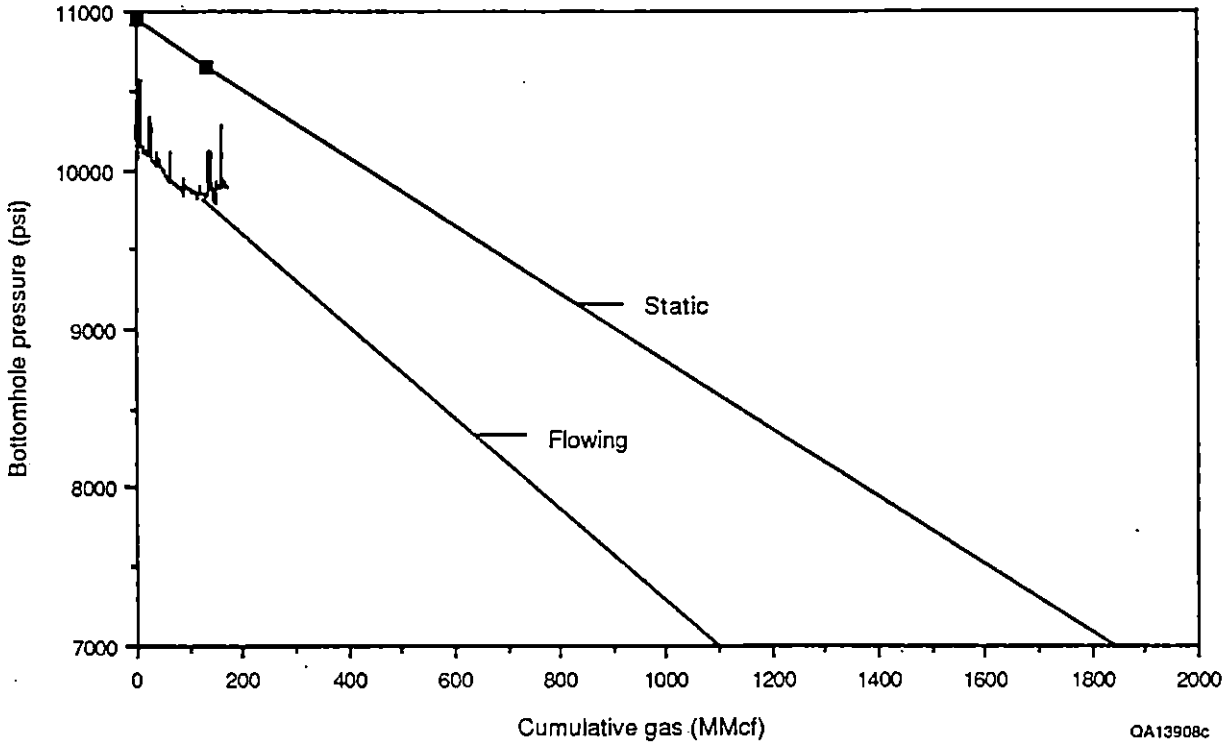

Figure 21. Bottom-hole pressure versus cumulative gas production at Pleasant Bayou No. 2.

flowing pressure of about 45.5×10^3 kPa (6,600 psi). Lowering reservoir pressure below the bubble-point pressure will also generate free gas in the reservoir, and mobilization of this free gas will provide adequate gas lift energy for coproduction of gas and brine. For a brine in-place volume of 6 billion barrels (Bbbl) and a gas/brine ratio of about 24 scf/stb, the gas in-place volume would be 144 bcf. In figures 20 and 21 a straight line extrapolation of the flowing bottom-hole pressure to a value of 48.2×10^3 kPa (7,000 psi) shows that 38 million stb of brine and 1.1 billion scf of gas will be recovered by that time. This would reflect a less-than-1-percent brine and gas recovery. The other factors that will influence ultimate fluid recovery from the reservoirs include the effects of additional aquifer recharge, change in formation and fluid compressibility with reduction in pressure, free gas movement, and shale dewatering. Reduction of reservoir pressure below the saturation pressure would result in free gas coming out of the solution, and buildup of this free gas around the well bore would reduce its relative permeability to water and cause a reduction in reservoir productivity. This permeability reduction is a function of production rate, which itself influences the overall pressure drawdown.

Garg (1979) estimated a recovery factor of 4 to 12 percent from the Pleasant Bayou reservoir on the basis of primary pressure depletion. A similar exercise can be performed here:

$$\text{Fraction of total fluid recovered, } V_{pf} = C_t (P_i - P_{wf}) \quad (1)$$

and

$$C_t = C_m(1 - \phi)/\phi + C_f \quad (2)$$

where

C_t = total compressibility;

C_m = uniaxial formation compressibility (10^{-6} to 5×10^{-6} psi^{-1});

C_f = fluid (water + brine) compressibility (4×10^{-6} psi^{-1});

ϕ = formation porosity (0.2);

P_i = initial reservoir pressure (10,944 psi);

P_{wf} = bottom-hole flowing pressure (7,000 psi).

Then

$C_t = 8 \times 10^{-6}$ to 24×10^{-6} psi^{-1},

and

V_{pf} = 3 to 9 percent.

These calculations show that the energy recoverable by primary pressure depletion is a small fraction of the total energy contained in the reservoir. Arguments for reinjection of the produced brine to maintain reservoir pressure and enhance the ultimate recovery have been presented before (Garg, 1979). Reinjection of the processed brine into the producing reservoir will maintain the pore pressure and enhance total recoverable energy. The computer simulation performed for the brine-reinjection case (Garg, 1979) assumed a dissolved-gas content 50 percent higher than what is shown from the production test. These simulations showed that significantly higher methane recovery was possible under brine reinjection, as well as that the production rates could be maintained at a much higher level for longer periods. However, considerable uncertainties are involved in the reinjection case. First, reinjection can only be initiated after the reservoir pressure has significantly declined (to about 8,000 psi); otherwise considerable energy will be expended in reinjecting high volumes into a high pressured reservoir, involving the potential for formation fracture. Second, reservoir-pressure depletion causes compaction and reduction in formation permeability. Injection of a cooler brine into this lower permeability reservoir also enhances the pumping energy requirements. Multiple wells may be required for reinjection operations. Thus, reinjection may be a practical option, but its economics needs to be carefully evaluated.

The reservoir pore volume that has contributed to production during the current production test was estimated by using the following equation (Dake, 1978):

$$V_p = \pi r^2 h \phi \tag{3}$$

where

r = reservoir radius produced,

h = reservoir thickness,

ϕ = formation porosity,

V_p = total production during current testing (7.23×10^6 bbl = 40.6×10^6 ft^3).

Then

$r^2 = V_p/(h\phi)$

$= 40.6 \times 10^6/[(60)(0.19)]$

$= 3.56 \times 10^6$ ft^2.

Hence

r = 1,887 ft.

This result implies that in theory the 60-ft (18-m) thick reservoir would be totally depleted to a radius of 1,887 ft (575 m) were a 7.23-MMbbl brine production to occur. This is a volumetric calculation based on assumptions of a homogeneous, isotropic reservoir having no vertical leakage and experiencing radial flow. However, the small pressure depletion at Pleasant Bayou is indicative of a larger area around the well bore contributing to flow. The size of this area of influence depends on the cone of depression generated at the well bore and how far out in the reservoir the transient-pressure effect has spread since the beginning of the current long-term production test on May 27, 1988. The radius of investigation influenced by the current production test is determined by the following correlation (Dake, 1978):

$$Q = [kh(P_r - P_{wf})]/[141.2\mu B(\ln r_e/r_w - 0.75 + s] \quad (4)$$

or

$$\ln r_e/r_w = [kh(P_r - P_{wf})]/[141.2Q\mu B] + 0.75 - s \quad (5)$$

where

Q = production rate (STB/D),

P_r = reservoir static pressure (psi),

P_{wf} = flowing bottom-hole pressure (psi),

μ = fluid viscosity (centipoise),

B = reservoir volume factor (bbl/bbl),

kh = permeability thickness (md-ft),

s = skin factor,

r_w = well-bore radius (ft),

r_e = reservoir radius of investigation (ft).

Using the values from the S-Cubed report of July 12, 1989 (Riney, 1989), the following parameters were calculated:

skin factor $s = -1.02 + 3.9 \times 10^{-4} Q$

$= -1.02 + (3.9 \times 10^{-4})\ (18{,}000)$

$= 6$

and

kh = 12,092,

P_r = 10,650 psi,

P_{wf} = 9,800 psi,

B = 1.05,

μ = 0.27

then

r_e = 4,092 ft.

The calculation of radius of investigation r_e also assumes radial flow in a homogeneous isotropic reservoir and represents the distance to which pressure has been affected under steady-state flow conditions. The depleted radius, 1,877 ft (575 m), and the radius of investigation, 4,092 ft (1,248 m), represent the range between which reservoir depletion and pressure alteration has occurred. These calculations indicate that the area of drained reservoir has not expanded far enough laterally to intersect a major fault that could act as a hydrologic conduit. Although under conditions of reservoir heterogeneities and preferential fluid flow paths a larger area may be influenced, evidence of flow encompassing a large area is insufficient. The chemical composition of produced brine showed no significant changes. Waters from a leaking fault have yet to be drawn to the Pleasant Bayou test well.

Reservoir Mechanism, Reserves, and Reservoir Performance

Geopressured reservoirs are, theoretically, closed compartments having a fixed volume. Production of substantial quantities of fluids (oil, gas, condensate, and water) from these would result in a large depletion of the reservoir pressure. A reliable estimate of the resource base is essential for efficient development and operation of the geopressured geothermal reservoir. Moreover, long-term recovery from the reservoir, as a function of pressure and time, will depend on the sources of energy and the drive mechanism. The sources of reservoir energy controlling fluid production are one or a combination of the following factors: (1) expansion of the overpressured brine in the aquifer, (2) expansion of the hydrocarbons associated or dissolved in the brine, and (3) compaction of the aquifer rock. Additionally, release of liquids from low-permeability zones due to the reduction of reservoir pressures may contribute to fluid production. The primary source of energy in Pleasant Bayou field is probably the expansion of the overpressured brine and dissolved gas. Because the reservoir pressure is above the bubble-point pressure, no free gas cap is present, and gas-cap expansion is currently not contributing to the reservoir energy. Water influx from contiguous aquifers is a topic of considerable discussion in the hydrochemical study in this report (Capuano and Erwin, 1990), but no conclusive evidence is available.

In geopressured reservoirs the decline of pressure with production is hard to predict and should be used with care in analyzing reservoir mechanics and in estimating reserves. This exercise is complicated because of the special hydrodynamics of geopressures and factors that are usually not incorporated in the traditional reservoir analysis. Factors such as change in reservoir compressibility are not included in the traditional material balance, volumetric calculations, and decline-curve analysis. Bearing this in mind, we adopted comparison with surrounding oil and gas fields as an alternative approach for estimating the brine reserves in place at Pleasant Bayou. Thus, volumetric estimates and decline-curve analysis of fields in the

vicinity of the Pleasant Bayou fault block were performed. Certain shortcomings in this method were evident: (1) the pressure data reported for the gas fields are not always reliable, either because of inadequate shut-in times for wells in low-permeability reservoirs or because of the averaging of pressures for multiwell fields, and (2) the fluid production reported for these fields does not always include an accurate accounting of the water and condensate production, which has a bearing on correlating cumulative production to pressure decline. Data from the fields reviewed for reserve estimation and pressure analysis were screened to identify the problems mentioned earlier.

Hydrogeologic Correlation with Nearby Fields

Hydrologic continuity within the Pleasant Bayou fault block and across its boundaries can be evaluated by correlating the pressures in the C-zone or closely associated reservoirs. Hydrocarbon production in the nearby geopressured oil and gas fields and brine production from the test well have the potential of influencing pressures in the respective reservoirs. Thus, reservoir pressures in the Pleasant Bayou and nearby fields were used to generate potentiometric surfaces and to determine the relative depletion rates of these reservoirs. The idea was to compare and correlate pressure changes and to infer mutual influence of depletion.

No commercial production has been reported in the Pleasant Bayou fault block from the C-zone, although the zone has been productive in Alta Loma and Algoa Orchards fields located north, and Martin Ranch and Chocolate Bayou South fields located southeast of the fault block. Figure 22 shows the location of the fields and wells in the vicinity of the fault block for which pressure-production data were evaluated to correlate with the Pleasant Bayou test well. Table A-1 in the appendix lists the well data base containing the location, production, and average reservoir properties for these and other wells that have been used for compiling the geologic and hydrologic cross sections in this area. The well numbers in figure 22 correspond to the well log numbers in table A-1 in the appendix.

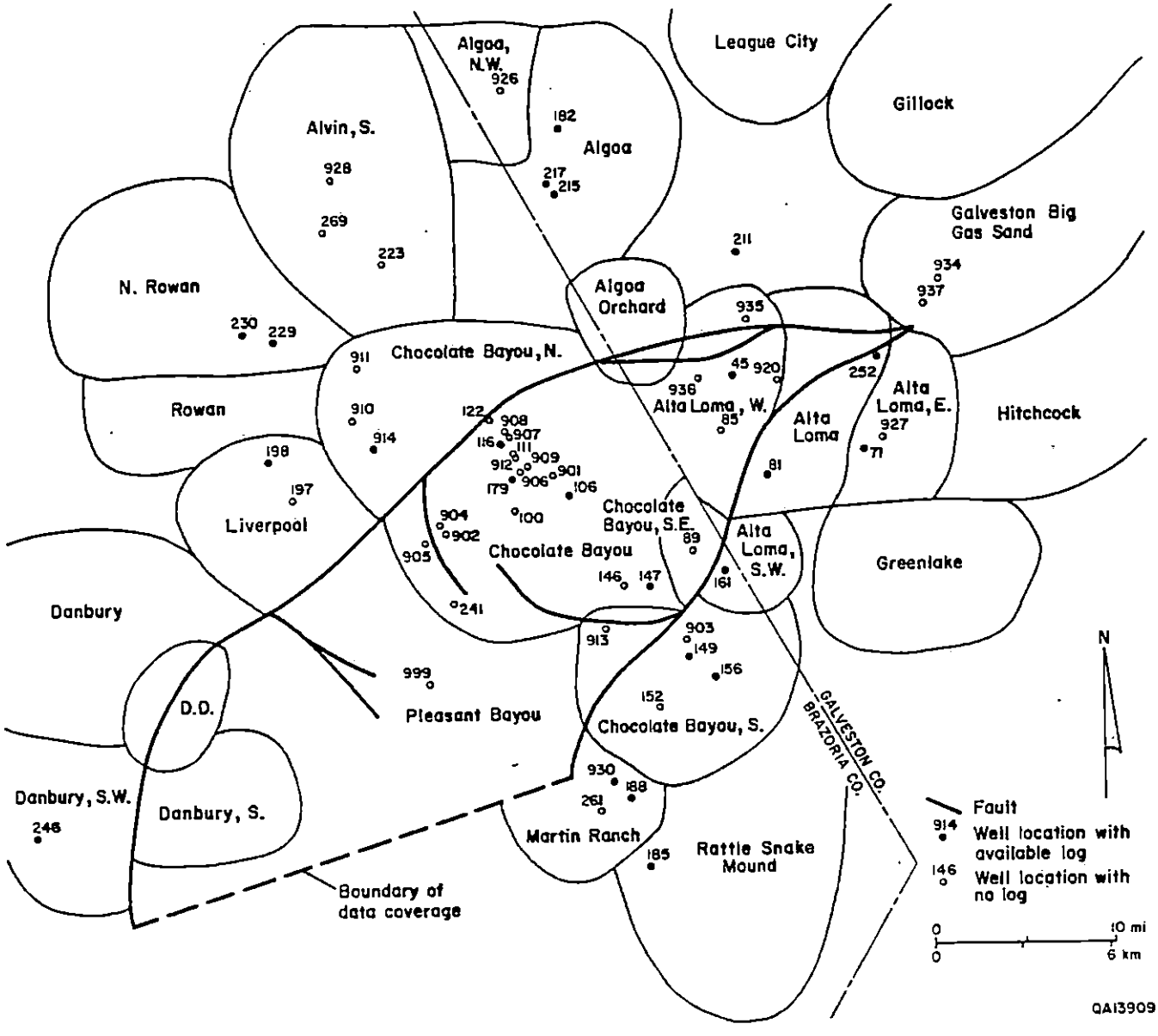

Figure 22. Location of oil and gas fields and well control in vicinity of Pleasant Bayou fault block.

Reservoir Properties, Pressure Decline, and Production in Nearby Fields

Nearly all the oil and gas wells producing from deep Frio Formation in the Pleasant Bayou fault block vicinity are completed in sand units above the Frio C-zone. Average porosities in these producing intervals are in the 15- to 30-percent range and permeabilities in the 200- to 1,500-md range. Productive sands are from 9.1 to 45.7 m (30 to 150 ft) thick. Production and pressure data from nearly 200 wells were downloaded from Dwight's Energydata, Inc. (1989), data base and integrated with data available from other sources for compilation of potentiometric surfaces as well as for evaluation of depletion in the various producing fields. The appendix contains the plots for p/z (reservoir pressure/compressibility factor) and trends in pressure and production rate with time for 20 wells in the geopressured gas fields in the vicinity of Pleasant Bayou fault block. These pressure-decline plots are commonly used in the material-balance analysis for estimation of initial gas reserves in place, and for determination of the reservoir-drive mechanisms. This method was employed to compare the depletion of energy in the gas fields to the depletion observed in the Pleasant Bayou geopressured aquifer in order to draw conclusions about the future-production potential at Pleasant Bayou. In figure 23 are idealized p/z plots for geopressured reservoirs producing under natural depletion and aquifer support. Also shown is the linear extrapolation from early-life production data. Since most geopressured reservoirs deviate from an ideal performance, the linear extrapolation results in incorrect estimation of reserves. The p/z curves for fields in the vicinity of Pleasant Bayou showed various combinations of the plots in figure 23. These productive fields were selected in the depth interval of 3,354 to 4,573 m (11,000 to 15,000 ft) below sea level. Most wells are gas and condensate wells; a few produce oil. The following observations are pertinent from the evaluation of the gas fields:

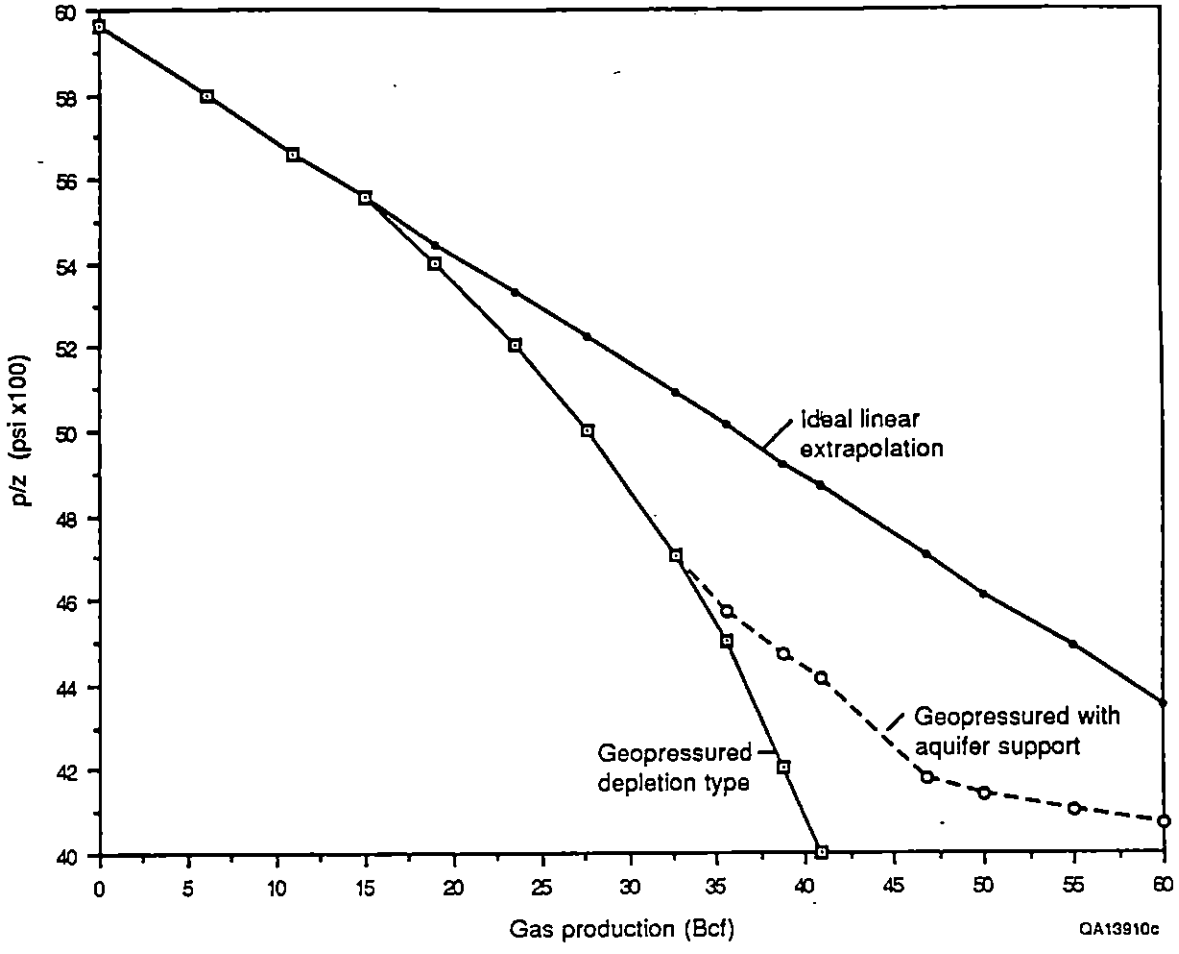

Figure 23. Idealized p/z plots for geopressured reservoirs. Included are depletion type, aquifer support, and linear extrapolation curves.

1. Deliverability from these fields is high in early life, then drops sharply as reservoir pressures decline, although many wells continue to produce for many years after pressures have declined to hydrostatic levels.
2. Most geopressured reservoirs exhibit a nonlinear p/z decline. This nonlinearity is enhanced if the coproduction of water or condensate, or both, is high. The initial slope of the p/z curve is the result of gas expansion and significant pressure maintenance resulting from formation compaction and water expansion.
3. After the geopressured reservoir has declined to hydrostatic pressure, the formation compaction is essentially complete, and the reservoir behaves like a normal gas expansion reservoir. Nearing final depletion, the pressure decline often flattens as production of water increases. This flattening indicates a water drive from a communicating aquifer.
4. The hydrocarbon recovery factor (as a function of initial gas in place) is frequently high, in the 70- to 98-percent range. One possibility for high recoveries could be a systematic underestimation of reserves using the material-balance method. Faulting in the Frio Formation could result in isolation of individual plays within separate compartments. This compartmentalization can prevent the pressures in the producing zone from reflecting the average pressure of the whole reservoir. Thus, the pressure-production data are representative of only a small section of the reservoir, and the estimated gas reserves are closer to recoverable reserves than they are to the initial gas in place. Leakage across faults in the later life of the reservoir can increase total production, reflected in the high recovery factors.

Potentiometric Surface, Pleasant Bayou Fault Block

Potentiometric surfaces based on bottom-hole reservoir pressures in the Pleasant Bayou fault block area in Brazoria and Galveston Counties were constructed. These potentiometric

surfaces were contoured for two time intervals, one for pre-1979 data (when no production was reported at Pleasant Bayou), and the other for post-1979 data (including the most recently reported pressures at Pleasant Bayou). Pressure data in the 3,050- to 4,575-m (10,000- to 15,000-ft) subsea depth interval were selected for this analysis. The objective of this exercise was to map the preproduction pressure distribution and then compare it with the postproduction map for identifying depletion trends in the oil and gas fields near Pleasant Bayou, as well as their possible interaction with the depletion at Pleasant Bayou. Such a comparison would help in drawing inferences about hydrologic continuity within the fault block and across the confining faults. An equivalent salt-water gradient of 10.5 kPa/m (0.465 psi/ft) was used for conversion of the highest available shut-in pressures. Figure 24 shows the location and head elevation, and figure 25 shows the corresponding potentiometric surface for the pre-1979 pressures. Figures 26 and 27 show the (1) location and head elevation and (2) potentiometric surface for the post-1979 data, respectively.

The potentiometric surfaces contain several localized highs and lows (bull's-eyes) resulting from nonuniform depletion in the productive reservoirs. This reflects complex variations in flow trends. Comparison of the surfaces in figures 25 and 27 shows the result of depletion to be more pronounced for Chocolate Bayou field in the center and northwest section of the fault block. The pressure decline at Pleasant Bayou between 1979 and 1989 is small and does not alter the surface appreciably. Potentiometric contours have declined in the Alta Loma field area inside the fault block (figs. 22, 25, and 27). Absence of pressure data to the south of Pleasant Bayou and to the immediate north across the boundary fault prevents determination of hydrologic continuity in that area.

The potentiometric surfaces were also evaluated in conjunction with the geologic cross sections compiled for the Pleasant Bayou fault block. Cross sections A–A′ through E–E′ shown in figures 7 through 11 include available values of reservoir pressures in the corresponding well-completion zones. Conclusions regarding lateral continuity of sand units within the Pleasant Bayou fault block, as well as across the boundary faults, can be drawn from these cross sections.

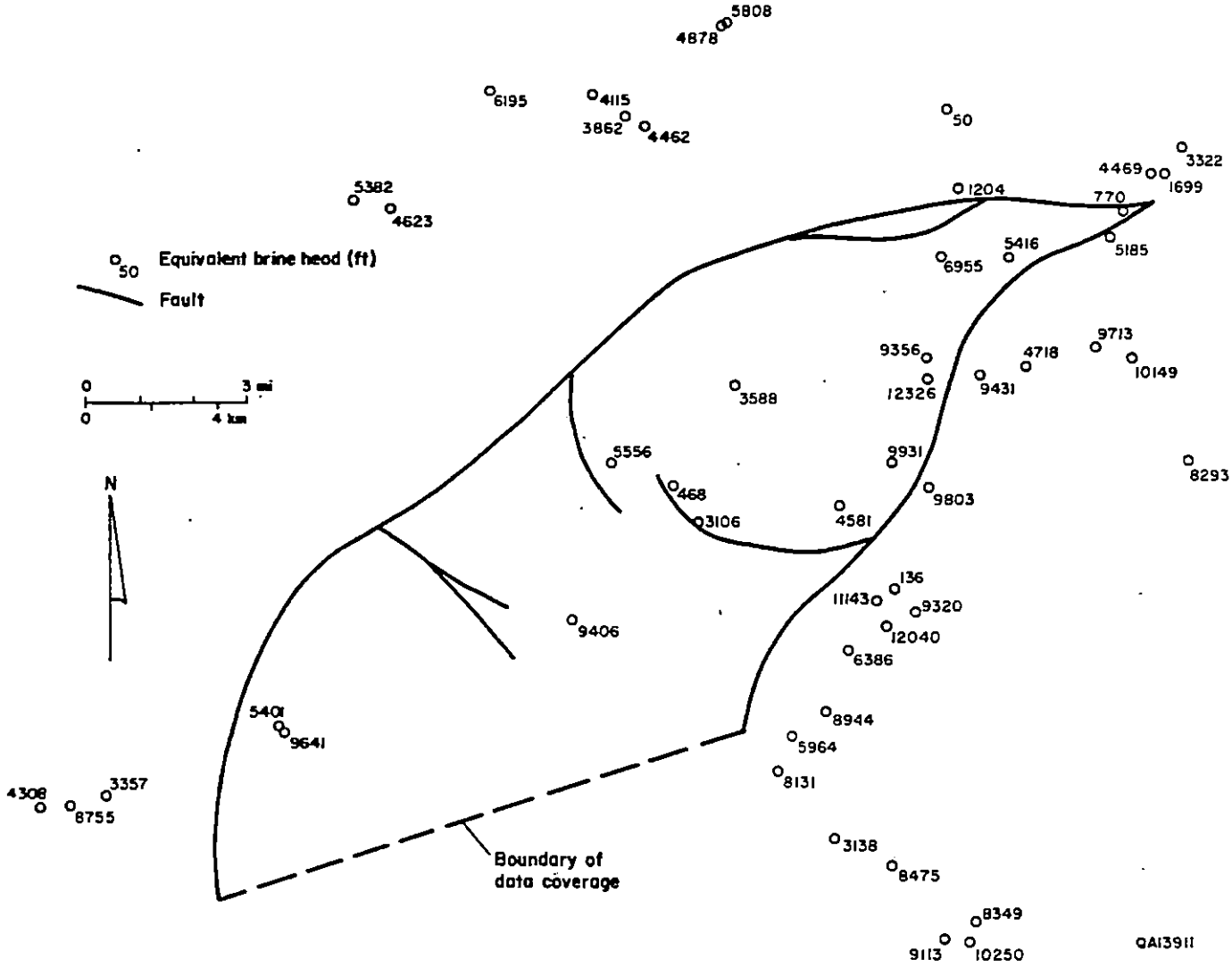

Figure 24. Posted values for equivalent brine heads in vicinity of Pleasant Bayou fault block. Pre-1979 pressures in 11,000–15,000-ft-depth interval. Gradient of 0.465 psi/ft used for conversion of bottom-hole pressures to heads.

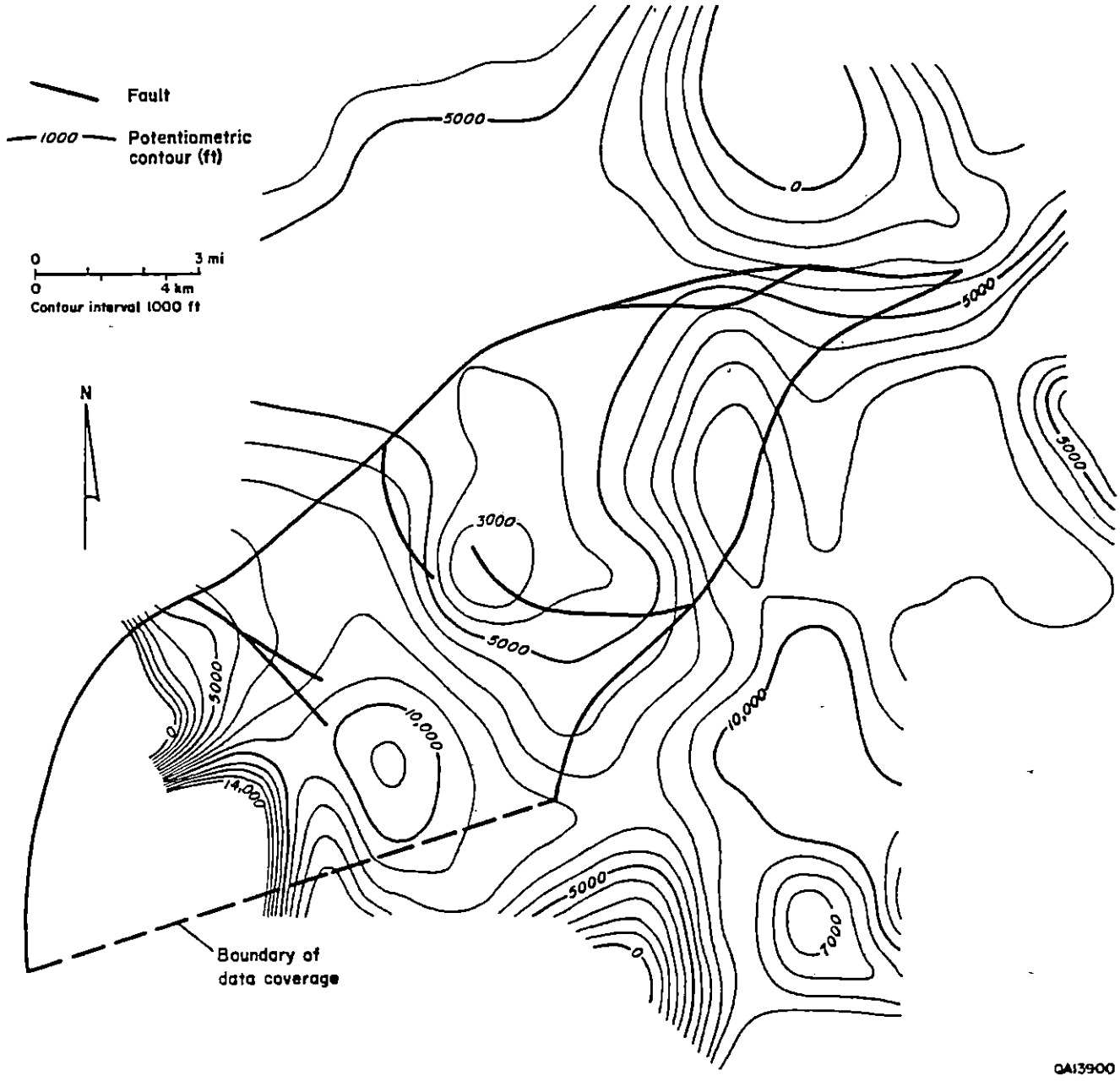

Figure 25. Potentiometric surface based on equivalent brine heads in vicinity of Pleasant Bayou fault block. Pre-1979 pressures in 11,000–15,000-ft-depth interval. Gradient of 0.465 psi/ft used for conversion of bottom-hole pressures to heads.

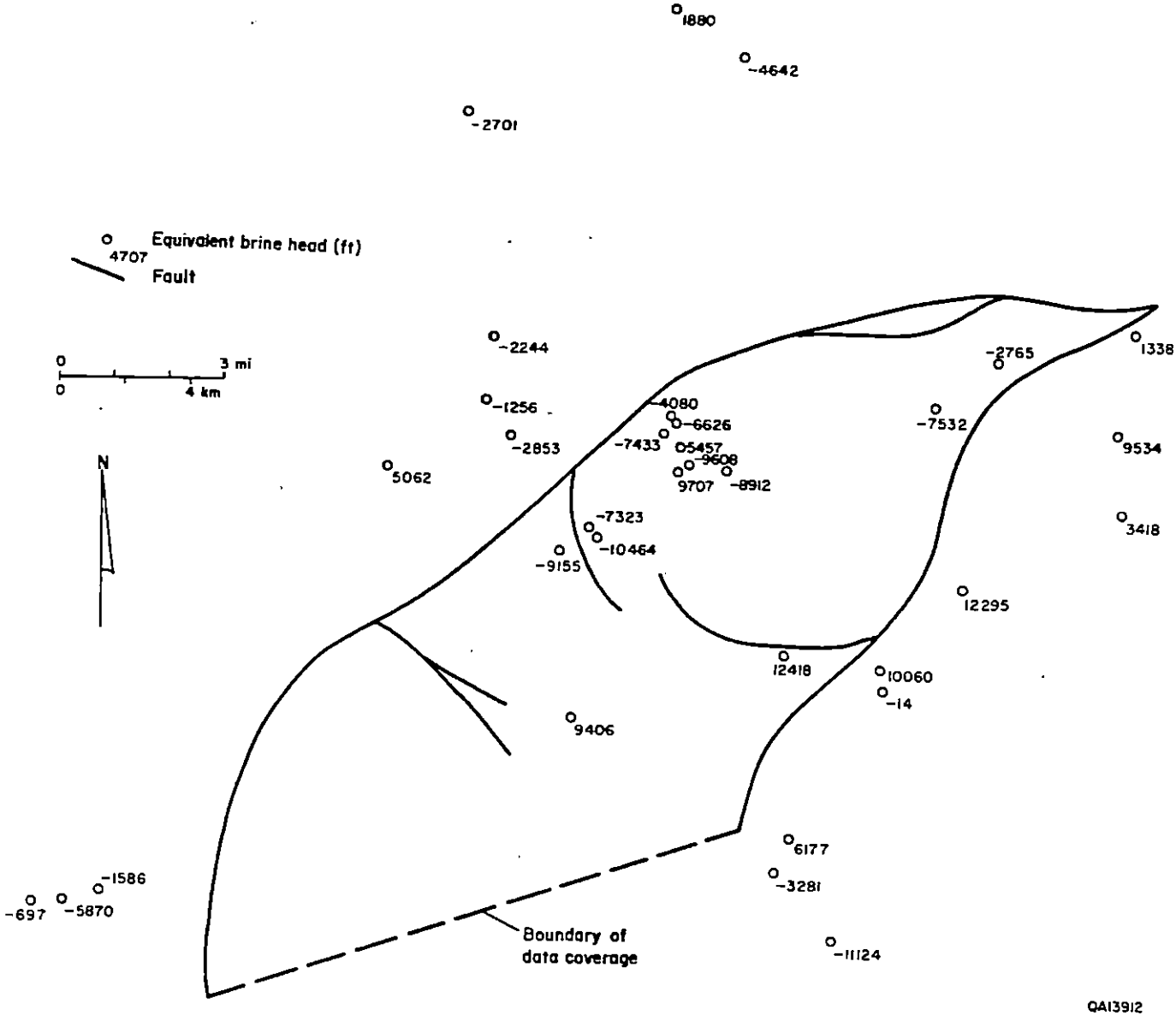

Figure 26. Posted values for equivalent brine heads in vicinity of Pleasant Bayou fault block. Post-1979 pressures in 11,000–15,000-ft-depth interval. Gradient of 0.465 psi/ft used for conversion of bottom-hole pressures to heads.

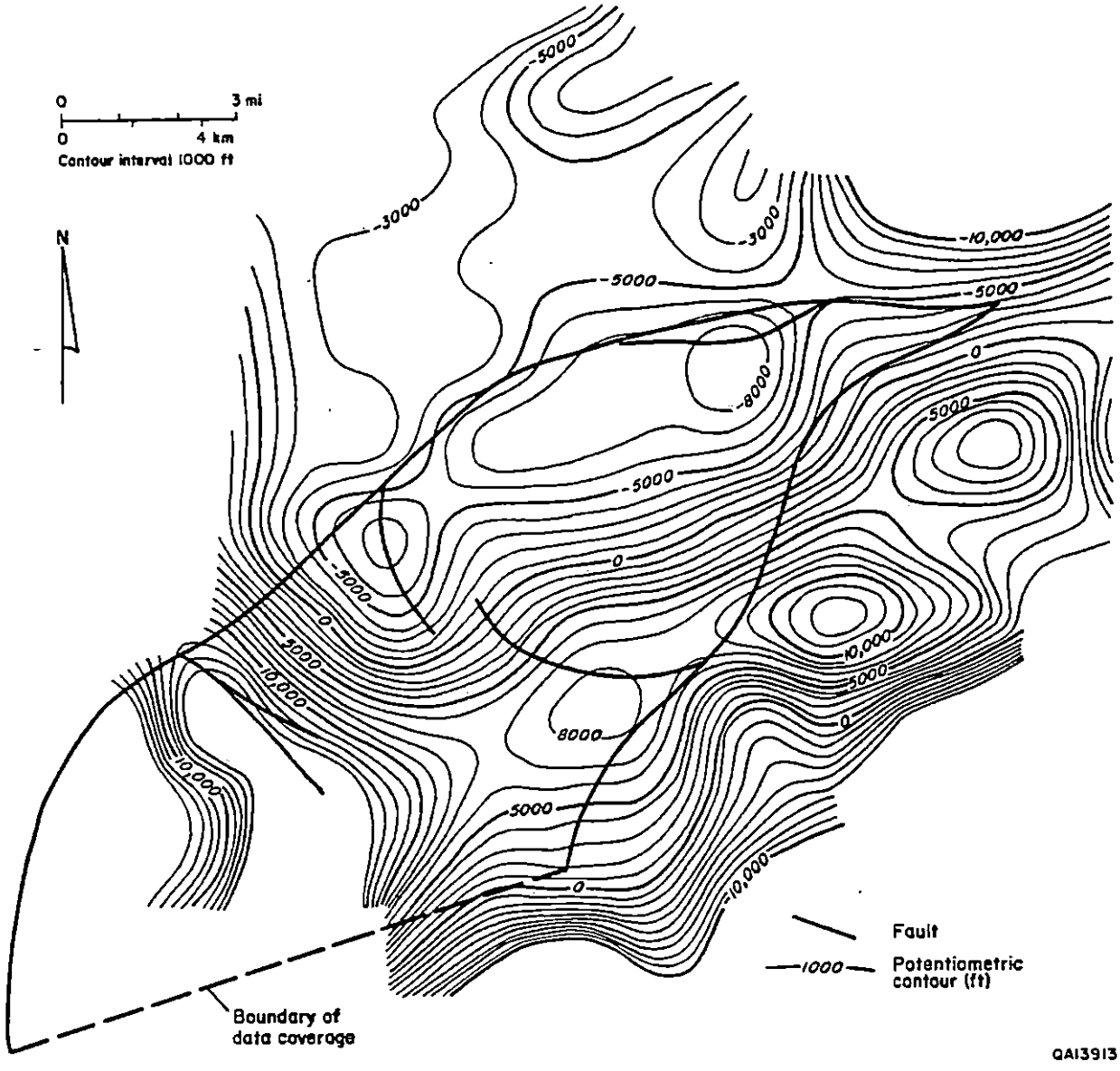

Figure 27. Potentiometric surface based on equivalent brine heads in vicinity of Pleasant Bayou fault block. Post-1979 pressures in 11,000–15,000-ft-depth interval. Gradient of 0.465 psi/ft used for conversion of bottom-hole pressures to heads.

Sparse pressure data in continuous sand units and large variability of these pressures provide no conclusive evidence of hydrologic continuity. Some general trends are observed. Pressures in Alta Loma field in the northeast part of the Pleasant Bayou fault block have uniformly declined in the TS unit inside the fault block, reflecting continuity in that unit. Chocolate Bayou field has exhibited sharp depletion inside the fault block in sand units overlying the C-zone. However, this depletion cannot be correlated with the depletion occurring at Pleasant Bayou as a result of inadequate well control.

Evaluation of post-1979 pressure data from Alta Loma field (°12,800 ft) indicates that negative head values from 1980 to 1982 (fig. 25) inside the Pleasant Bayou fault block reflect reservoir depletion. However, the positive head values in a well (°14,300 ft) 5,000 m (16,400 ft) across the fault show that its productive reservoir has not been affected by depletion inside the fault block. Geologic cross sections A–A′ and E–E′ (figs. 7 and 11) suggest that the productive intervals in these two wells are separated by about 1,500 ft of sands and shales. Any inference of hydrologic continuity over such distance and high reservoir offset is difficult to make.

Drainage radii of wells were calculated from pressure and production data in the Alta Loma field and two possibilities were evaluated:

1. The drainage radius of a well is small enough to confine its drainage area to within the fault block.
2. The drainage radius of a well is large and either reflects a drainage area extending across the fault outside the block or its communication with, and drainage from, the Chocolate Bayou reservoir.

Similar calculations were performed to determine the drainage radii in Chocolate Bayou field. The following correlation (Dake, 1978) for volumetric calculations was used for determining the reservoir drainage radius:

$$V_p = \pi r^2 \, h \, \phi \, (1-S_w), \tag{6}$$

where

r = reservoir radius produced,

h = reservoir thickness,

ϕ = formation porosity,

and

S_w = reservoir water saturation (about 25 percent).

The following steady-state gas-flow equation was used for calculating the drainage radius:

$$\ln(r_e/r_w) = 703 \times 10^{-6}\, k\, h(P_e^2 - P_w^2) / [T\, \mu\, Z\, q_{sc}] \qquad (7)$$

where

r_e = reservoir drainage radius (ft),

r_w = well-bore radius (ft),

kh = permeability thickness product (ft),

P_e = initial reservoir pressure (psi),

P_w = flowing bottom-hole well pressure (psi),

T = reservoir temperature (degrees rankin),

μ = viscosity (centipoise),

Z = compressibility factor

and

q_{sc} = total surface production (ft^3).

This equation results in an unreasonably large r_e. Error in this calculation can result from the difference in squares of pressures or from the production rate, q. Another source of error is that the reservoir is more likely to be in a pseudosteady state because pressure has depleted significantly from the initial level. The uncertainty in difference of squared pressures makes the value of r_e meaningless.

Table 1 summarizes the values of drainage radii computed by incorporating the values of reservoir parameters in equation 6. Also listed in table 1 are the volumes of fluids produced from these fields as reported in Dwight's Energydata, Inc. (1989), database.

The volumetric calculations show that drainage radii for most of the gas reservoirs in Chocolate Bayou field are large, whereas the drainage radii for Chocolate Bayou Southeast are

Table 1. Reservoir parameters and calculated drainage radii for producing gas and oil fields in vicinity of Pleasant Bayou fault block (11,000–15,000-ft-depth interval).

Gas Reservoirs:

Field	Reservoir	Depth (ft)	Thickness[1] (ft)	Porosity fraction[2]	Produced gas (MMcf)	Produced condensate (MMcf)	Produced water (bbl)	Total produced volume (MMcf)	Reservoir volume[3] (MMcf)	Drainage radius (ft)
Chocolate Bayou	Banfield	10,873	12.3	0.25	459,328.9	49,000.0	—	508,328.9	1,510.0	13,972
Chocolate Bayou	Weiting Upper	11,351	12.3	0.24	174,520.0	8,260.0	—	182,780.0	527.0	8,428
Chocolate Bayou	Weiting Lower	11,612	12.3	0.29	61,505.0	4,436.0	—	65,941.0	173.1	4,835
Chocolate Bayou	Andrau	11,590	14.2	0.29	584,560.7	40,300.0	—	624,860.7	2,360.0	4,774
Chocolate Bayou	Frio H	11,500	12.3	0.29	2,688.7	156.0	—	2,844.7	10.5	1,197
Chocolate Bayou	Frio P	10,874	12.3	0.29	539.5	45.0	—	584.5	1.2	406
Chocolate Bayou	Frio P West	11,500	12.3	0.29	3,651.1	192.0	—	3,843.1	17.7	1,555
Chocolate Bayou	Mc Kelvy	11,500	12.3	0.25	13,114.5	125.7	—	13,240.2	61.1	3,007
Chocolate Bayou,SE	Mc Ilvane	13,572	12.3	0.25	93.7	20.1	—	113.8	0.2	165
Alta loma	Banfield	11,163	12.3	0.29	3,410.0	302.4	69,050.0	3,738.0	15.9	1,340

Oil Reservoirs:

Field	Reservoir	Depth (ft)	Thickness[1] (ft)	Porosity fraction[2]	Produced oil (stb)	Produced condensate (MMcf)	Produced associated gas (MMcf)	Reservoir volume factor	Oil saturation factor	Drainage radius (ft)
Chocolate Bayou	Alibel	11,200	10.4	0.29	9,949,593	0	0.0	1.5	0.7	3,554
Chocolate Bayou	Grubbs Sand	11,200	5.0	0.31	685,213	0	20.1	1.0	0.7	1,079
Chocolate Bayou, SE	Weiting Lower	11,200	10.4	0.30	210,764	0	0.0	1.4	0.8	460
Alta Loma, West	Schenk	11,200	10.4	0.30	386,985	806	3,257.9	1.0	0.7	1,584

[1] Average productive thickness from Dwight's production data.

[2] Average porosity from Dwight's production data.

[3] Volume at reservoir conditions.

small. These calculations are based on the volume of fluids withdrawn from the reservoirs; the actual radii of influence based on pressure transient effects may be larger. Assuming that the physical properties of the reservoirs are within the range listed in table 1, hydrologic communication possibly exists between reservoirs in Chocolate Bayou field and reservoirs outside the fault block. Another possibility is that hydrocarbon fluids may be draining from sandstones overlying the Pleasant Bayou reservoir in the vicinity of the test well. (The latter possibility is ruled out, however, because these sandstone units, as well as those just southwest of Chocolate Bayou field, were found to be dry during exploration.)

The next issue is whether the Chocolate Bayou Southeast-Lower Weiting field is depleted. If the field is not depleted, no conclusions can be drawn. However, production reports (Dwight's Energydata, Inc., 1989) indicate that reservoir pressure has been depleted to abandonment level. Hydrologic continuity possibly exists between this reservoir and sandstones outside the fault block, but the communicating beds contain no hydrocarbons. The potentiometric surface in figure 26 shows that fields in the vicinity of Chocolate Bayou Southeast outside the fault block have much higher pressures. Thus hydrologic continuity is probably absent between Chocolate Bayou Southeast–Lower Weiting field and other reservoirs surrounding it.

The drainage radius of 483 m (1,584 ft) calculated for the Alta Loma West oil field (table 1) does not provide conclusive evidence of communication outside the fault block. The field is depleted as shown by its pressure data. Potentiometric head values (fig. 25) in this field are significantly lower than others in the vicinity.

DISCUSSION

The relatively small change in the Pleasant Bayou reservoir pressure may not have caused alteration in reservoir-flow properties or in the mechanical properties of the formation as yet. Likewise, no measurable subsurface subsidence would have resulted from brine production so

far. The issue of mobilization of fluids in adjacent formations, including the overlying shales, and changes in produced fluid composition will be addressed in the following section of this report. The current hydrogeologic investigations concentrated on the performance of neighboring geopressured oil and gas fields and attempted to correlate them to what might be anticipated at Pleasant Bayou. Also evaluated here was whether hydrologic communication with these hydrocarbon-bearing formations exists.

Evidence suggesting that direct hydrologic communication exists between the Pleasant Bayou geopressured reservoir and the overlying oil- and gas-bearing formations within the fault block or similar sands outside the fault block is not conclusive. If such communication existed we would have observed either a greater degree of pressure support in the oil and gas fields, which thus slowed down their decline rate, or an increasing gas/brine ratio at the Pleasant Bayou test well. The high production rate at the Pleasant Bayou test well could have resulted in gas coning from a communicating gas reservoir. On the other hand, the volume of brine produced at Pleasant Bayou is very small as a percentage of the estimated reserves and even if the transient pressure effect has travelled a long distance it will take many years of production to observe a direct correlation with pressure-production behavior in surrounding oil and gas fields.

The pressure data used in this study were only available in fields that have been extensively drilled for oil and gas. The southwest section within the Pleasant Bayou fault block has been inadequately drilled and has well control insufficient for reliable interpretation of potentiometric surfaces. The reliability of available pressure data was improved by screening out data which were anomalously high or low relative to neighboring values. Moreover, an attempt was made to select initial pressures before significant depletion from the reservoir. Pressures also were separated in time for evaluating the effect of reservoir depletion. The potentiometric surfaces represent average potentials and are useful in inferring general directional gradients.

The estimation of drainage radii and the inference of hydrologic continuity based on them are at best approximate. The uncertainties in these calculations stem from the

approximate nature of the physical parameters used therein. Greater reliability in estimating reservoir properties (permeability, thickness, porosity) and more pressure data from greater well control would improve the confidence level in these calculations.

CONCLUSIONS

The geologic description of the Pleasant Bayou reservoir is based on earlier seismic, core, and log data primarily from oil and gas wells that are at considerable distance from the test well. Although log and core information is available from the test well, it is difficult to place too much confidence in the reservoir model and mapping of discontinuities in the fault block over long distances. Additional geologic input could considerably refine the geologic model and enhance the predictive capability for estimating the true reserve base. This additional information can be obtained in two ways: (1) collecting three-dimensional seismic data near the test well, which will improve the description of subsurface structural and stratigraphic relationships and the location and extent of the faults, as well as provide help in estimating lithology and porosity variations away from well control, and (2) drilling and testing two or three additional wells (combined with deepening some existing wells) around the existing test well, which would provide better control on reservoir heterogeneities and boundaries from transient-pressure behavior. The integration of 3-D seismic data with logs and multiwell test data will improve description of the compartmentalized nature of the Pleasant Bayou reservoir.

Union Exploration Partners, a Houston-based company, recently drilled and abandoned a deep well close to Pleasant Bayou No. 2. This well did not penetrate the geopressured brine aquifer. Aquisition or leasing of this well and recompletion in the geopressured zone can provide important information for correlation with the test well. Similarly, other existing inactive oil and gas wells near the test wells could be leased, deepened, and tested in the geopressured brine zone. This may be a more productive alternative to long-term single-well testing at Pleasant Bayou No. 2. The economics of these alternatives should be evaluated.

ACKNOWLEDGMENTS

This research was funded by the U.S. Department of Energy, Advanced Technologies Division, under contract no. DE-FC07-NV10412. The manuscript was edited by Lana Dieterich. Word processing was by Melissa Snell. Figures were prepared by Yves Oberlin, Joel Lardon, and Wade Kolb under the direction of Richard L. Dillon. We extend our appreciation to all who contributed to the preparation of this report.

REFERENCES

Bebout, D. G., Loucks, R. G., and Gregory, A. R., 1978, Frio sandstone reservoirs in the deep subsurface along the Texas Gulf Coast, their potential for the production of geopressured geothermal energy: The University of Texas at Austin, Bureau of Economic Geology Report of Investigations No. 91, 92 p.

Bogomolov, Y. G., 1967, Geotemperature regime: Bulletin of International Association of Scientific Hydrology, v. 12, no. 4, p. 86–91.

Capuano, R. M., and Erwin, M. E., 1990, Hydrochemical studies for long-term-flow testing of Pleasant Bayou Geopressured Geothermal Well No. 2, *in* Kreitler, C. W., Capuano, R. M., Akhter, M. S., Hamlin, H. S., Erwin, M. E., and Walter, T. G., Consolidation of geologic studies of geopressured geothermal resources in Texas: The University of Texas at Austin, Bureau of Economic Geology, 1989 annual report prepared for the U.S. Department of Energy, Advanced Technologies Division, under contract no. DE-FC07-85NV10412, p. 89.

Dake, L. P., 1978, Fundamentals of reservoir engineering: Amsterdam, Elsevier, Developments in petroleum science, Book 8, 443 p.

Dickinson, G., 1953, Reservoir pressures in Gulf Coast Louisiana: American Association of Petroleum Geologists Bulletin, v. 37, no. 2, p. 410–432.

Dwight's Energydata, Inc., 1989, Production data for oil and gas fields in Vision electronic database: Richardson, Texas.

Ewing, T. E., Light, M. P. R., Tyler, Noel, 1984, Integrated geologic study of the Pleasant Bayou–Chocolate Bayou area, Brazoria County, Texas—first report, *in* Ewing, T. E., Tyler, Noel, Morton, R. A., and Light, M. P. R., Consolidation of geologic studies of geopressured geothermal resources in Texas: The University of Texas at Austin, Bureau of Economic Geology, 1983 annual report prepared for the U.S. Department of Energy, Division of Geothermal Energy, under contract no. DE-AC08-79ET27111, p. 90–142.

Galloway, W. E., Hobday, D. K., and Magara, Kinji, 1982, Frio Formation of the Texas Gulf Coast Basin—depositional systems, structural framework, and hydrocarbon origin, migration, distribution, and exploration potential: The University of Texas at Austin, Bureau of Economic Geology Report of Investigation No. 122, 78 p.

Garg, S. K., 1979, Reinjection of fluids into a producing geopressured reservoir, 1979, *in* Dorfman, M. H., and Fisher, W. L., eds., Proceedings of the Fourth U.S. Gulf Coast Geopressured-Geothermal Energy Conference: The University of Texas at Austin, Center for Energy Studies, p. 1000–1027.

Garg, S. K., Riney, T. D., and Fwu, J. M., 1981, Analysis of phase I flow data from Pleasant Bayou No. 2 geopressured well, *in* Bebout, D. G., and Bachman, A. L., eds., Proceedings of the Fifth Geopressured-Geothermal Energy Conference: Louisiana State University, p. 97–100.

Gregory, A. R., and Backus, M. M., 1979, Geopressured formation parameters, geothermal well, Brazoria County, *in* Dorfman, M. H., and Fisher, W. L., eds., Proceedings of the Fourth U.S. Gulf Coast Geopressured-Geothermal Energy Conference: The University of Texas at Austin, Center for Energy Studies, p. 235–311.

Hamlin, H. S., and Tyler, Noel, 1988, Consolidation of geologic studies of geopressured-geothermal resources in Texas: The University of Texas at Austin, Bureau of Economic Geology, annual report prepared for the U.S. Department of Energy, Advanced Technologies Division under contract no. DE-FC07-85NV10412, 45 p.

Kreitler, C. W., Akhter, M. S., Donnelly, A. C. A., and Wood, W. T., 1988, Hydrogeology of formations used for deep-well injection, Texas Gulf Coast: The University of Texas at Austin, Bureau of Economic Geology, annual report prepared for the U.S. Environmental Protection Agency under cooperative agreement no. CR812786-01-0, 204 p.

Morton, R. A., Ewing, T. E., and Tyler, Noel, 1983, Continuity and internal properties of Gulf Coast sandstones and their implications for geopressured fluid production: The University of Texas at Austin, Bureau of Economic Geology Report of Investigations No. 132, 70 p.

Railroad Commission of Texas, 1989, Production data files for oil and gas producing properties: Austin, Texas, unpaginated.

Randolph, P. L., 1985, Co-production resource and bottomhole flowing pressure without artificial lift, *in* Dorfman, M. H., and Morton, R. A., eds., Proceedings of the Sixth U.S. Gulf Coast Geopressured-Geothermal Energy Conference, Austin, Texas: New York, Pergamon Press, p. 239–248.

Riney, T. D., 1987, Geopressured-geothermal reservoir data—synthesis and model development—June: San Diego, California, S-Cubed, report prepared for the U.S. Department of Energy and The University of Texas at Austin under cooperative agreement contract no. DE-FC07-85NV10412, 46 p.

———— 1988, Pleasant Bayou and Gladys McCall—December: San Diego, California, S-Cubed, interim report to M. H. Dorfman, prepared for the U.S. Department of Energy and The University of Texas at Austin under cooperative agreement contract no. DE-FC07-85NV10412, 37 p.

———— 1989, Recalibration of the WELBOR model, revised estimates of the bottomhole pressures, analysis of the 65-hour buildup test, and updated simulation of production history—June: San Diego, California, S-Cubed, interim report to M. H. Dorfman, prepared for the U.S. Department of Energy and The University of Texas at Austin under cooperative agreement contract no. DE-FC07-85NV10412, 19 p.

Riney, T. D., Garg, S. K., and Wallace, R. H., 1985, Effect of shale-water recharge on brine and gas recovery from geopressured reservoirs, *in* Dorfman M. H., and Morton, R. A., eds., Proceedings of the Sixth U.S. Gulf Coast Geopressured-Geothermal Energy Conference, Austin, Texas: New York, Pergamon Press, p. 193–202.

Winker, C. D., Morton, R. A., Ewing, T. E., and Garcia, D. D., 1983, Depositional setting, structural style, and sandstone distribution in three geopressured geothermal areas, Texas Gulf Coast: The University of Texas at Austin, Bureau pf Economic Geology Report of Investigations No. 134, 60 p.

APPENDIX

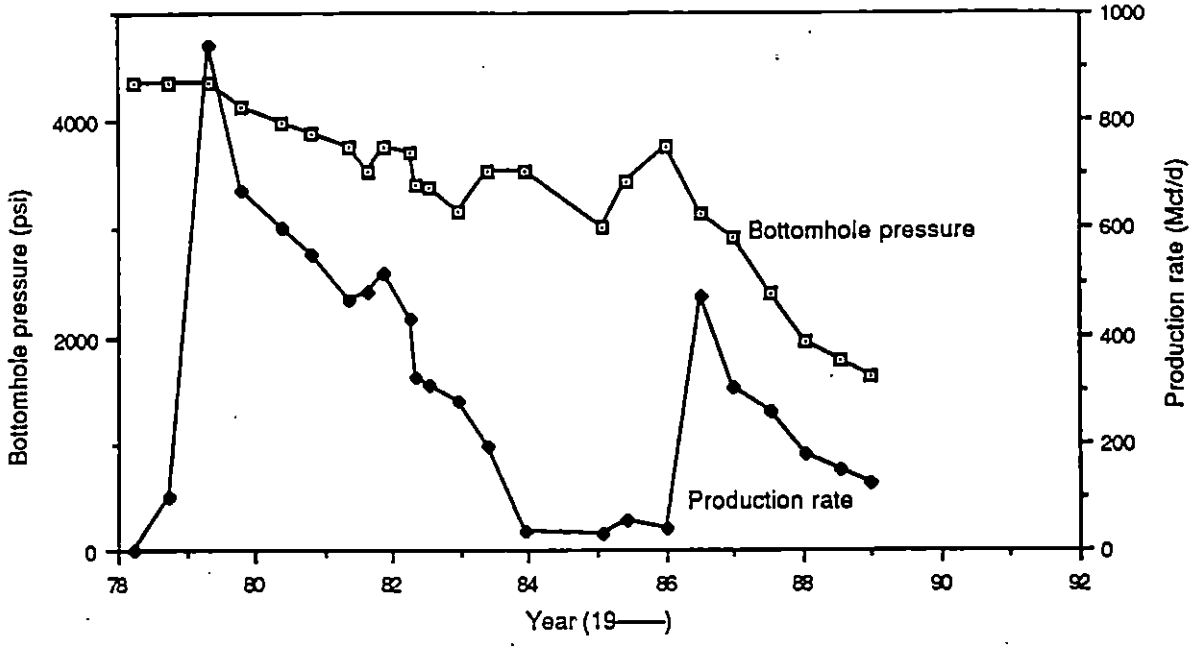

Figure A-1. Plot of bottom-hole pressure versus time for well no. 911, F. B. Lacy No. 1 Bright Gas Unit.

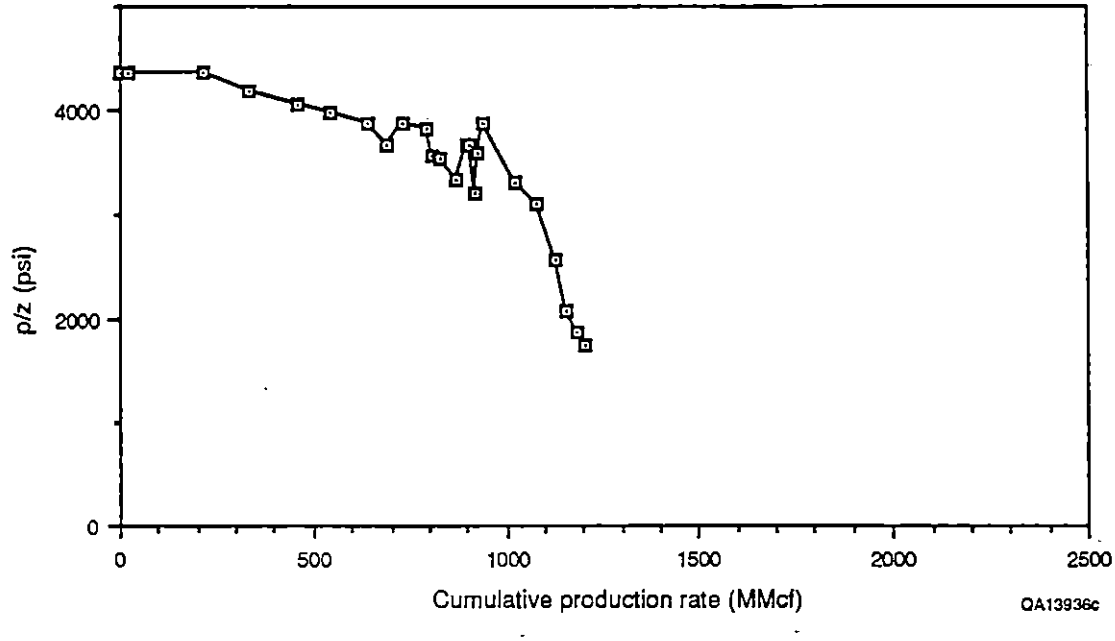

Figure A-2. Plot of p/z versus cumulative production rate for well no. 911, F. B. Lacy No. 1 Bright Gas Unit.

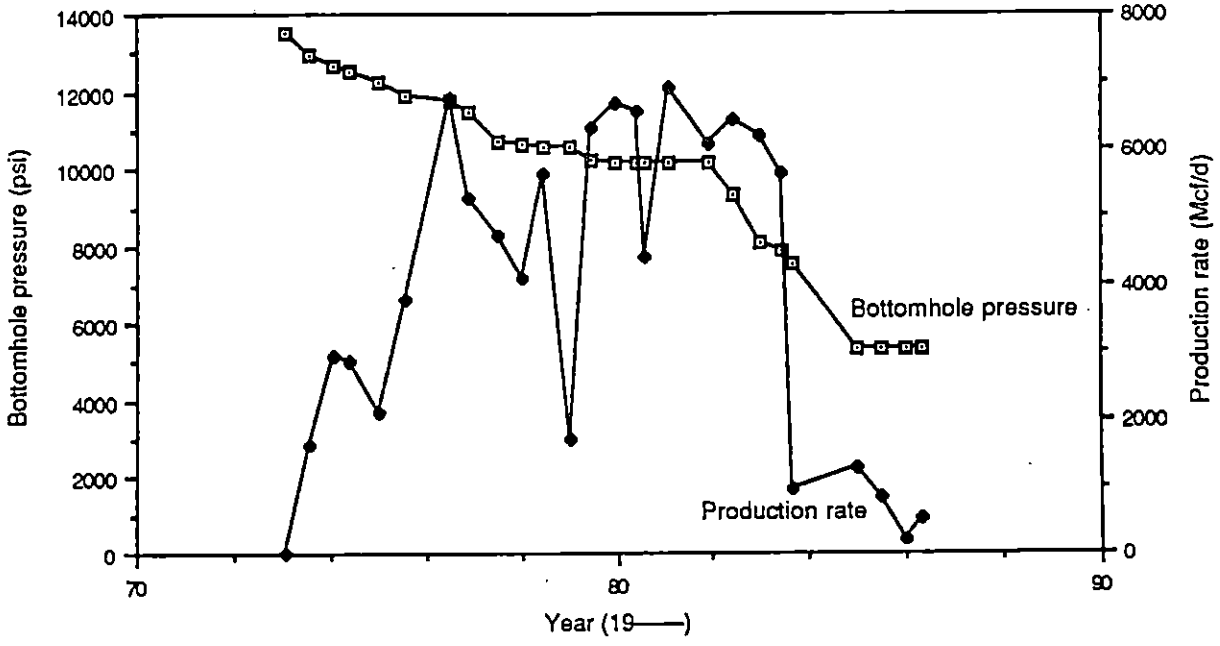

Figure A-3. Plot of bottom-hole pressure versus time for well no. 261, General Crude No. 1 Martin Ranch Fee.

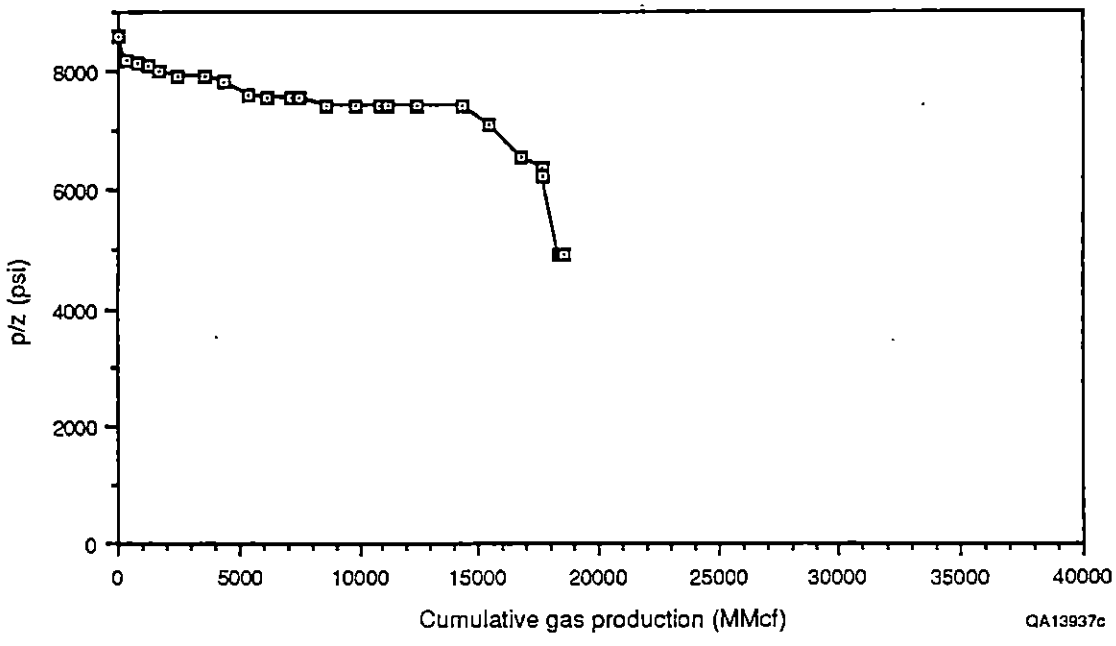

Figure A-4. Plot of p/z versus cumulative production rate for well no. 261, General Crude No. 1 Martin Ranch Fee.

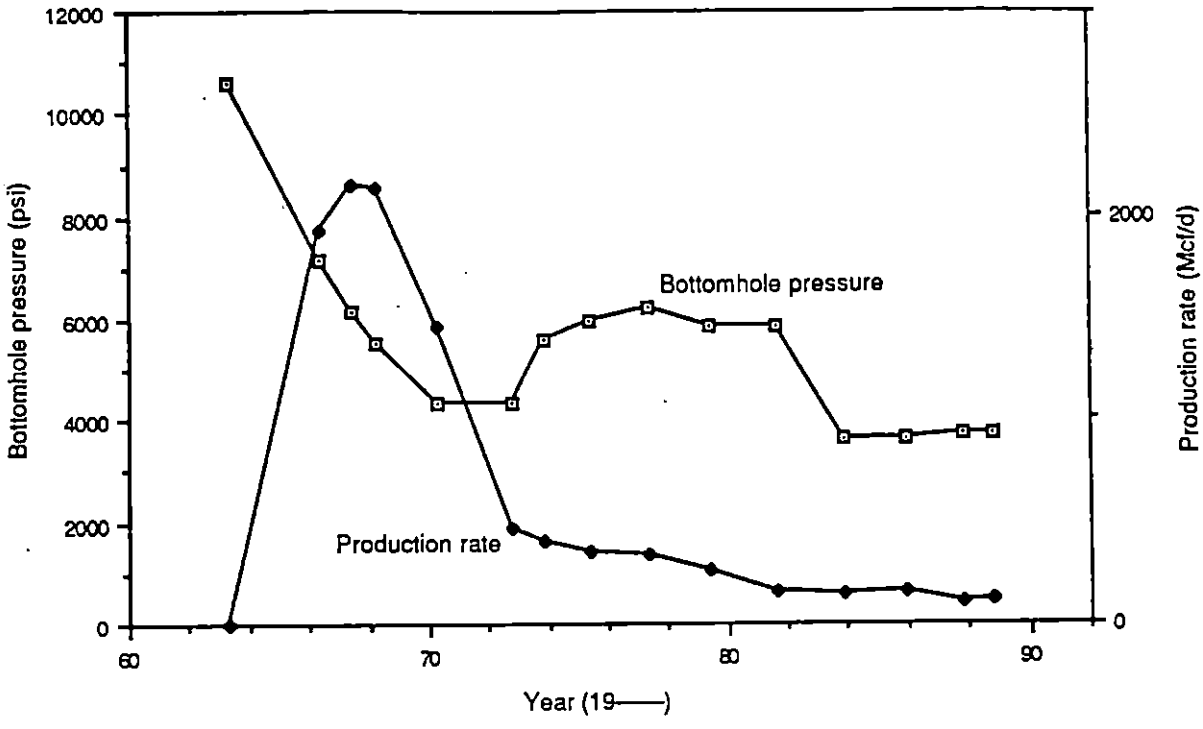

Figure A-5. Plot of bottom-hole pressure versus time for well no. 149, Phillips No. CC-1 Houston Farms.

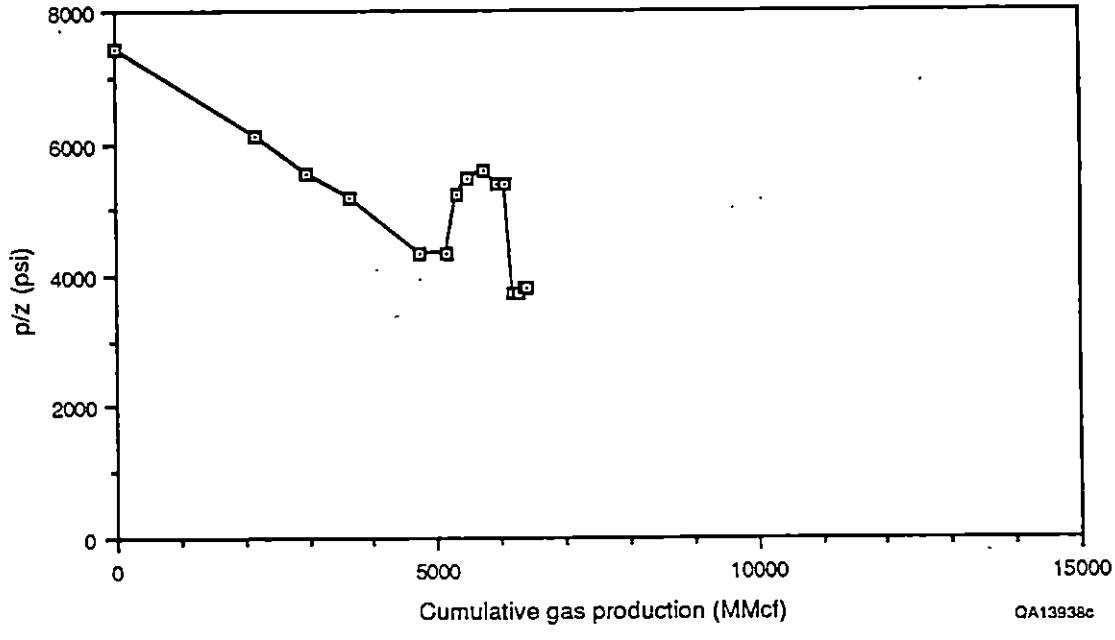

Figure A-6. Plot of p/z versus cumulative production rate for well no. 149, Phillips No. CC-1 Houston Farms.

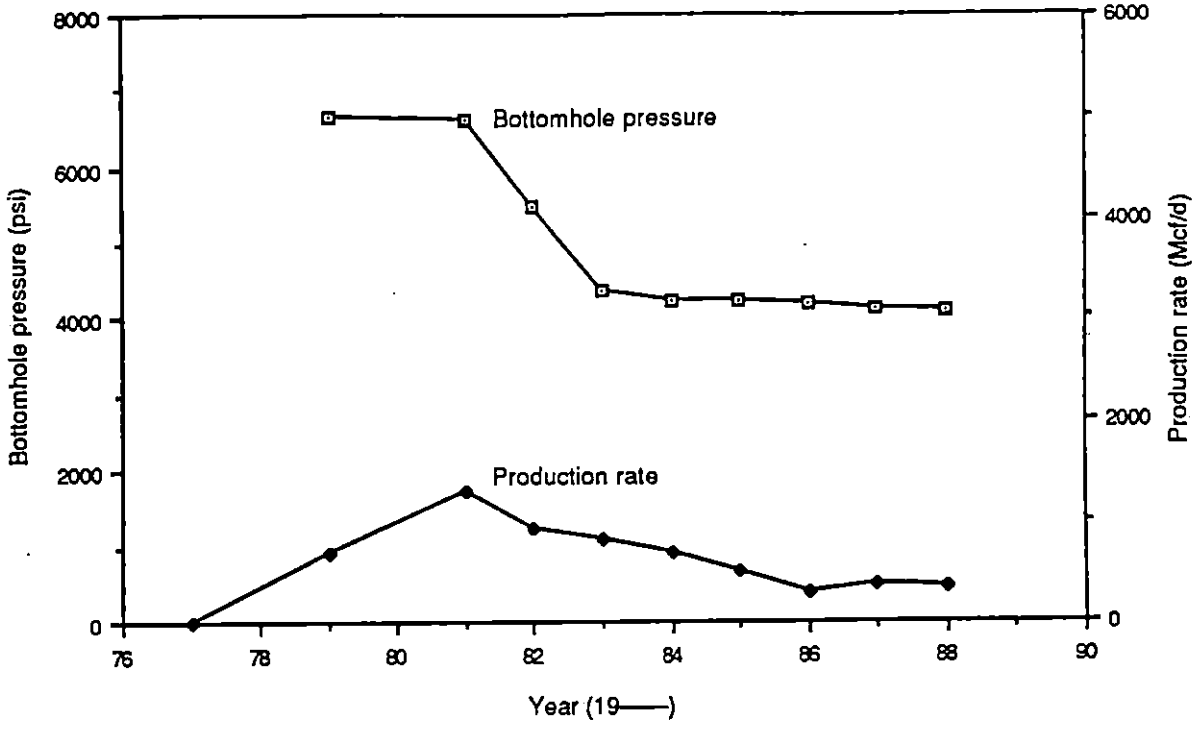

Figure A-7. Plot of bottom-hole pressure versus time for well no. 124, Phillips No. 1 Banfield.

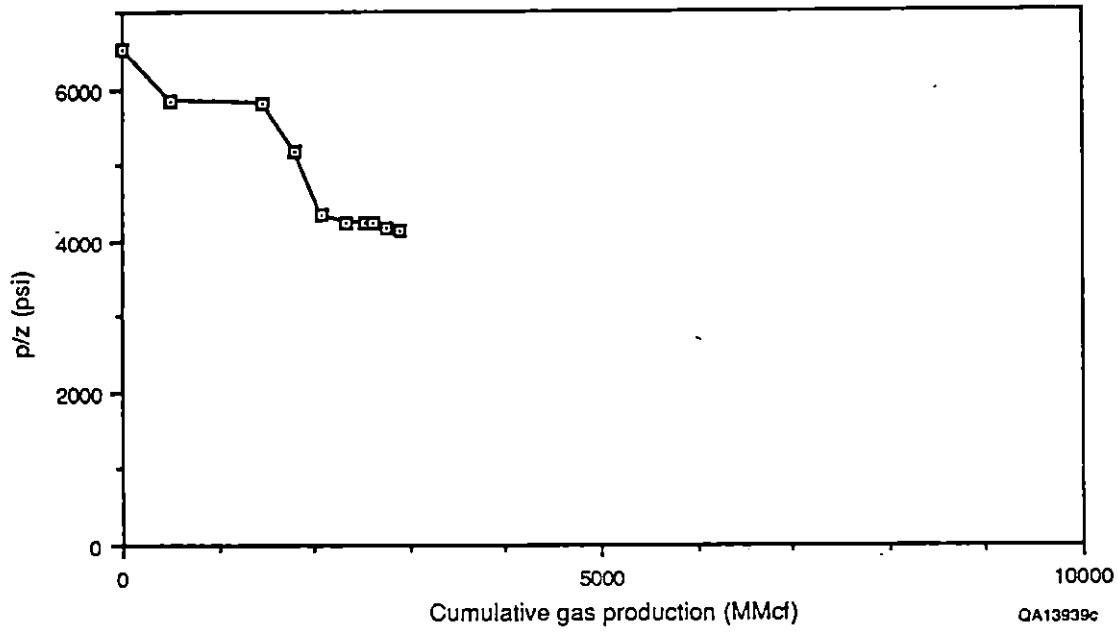

Figure A-8. Plot of p/z versus cumulative production rate for well no. 124, Phillips No. 1 Banfield.

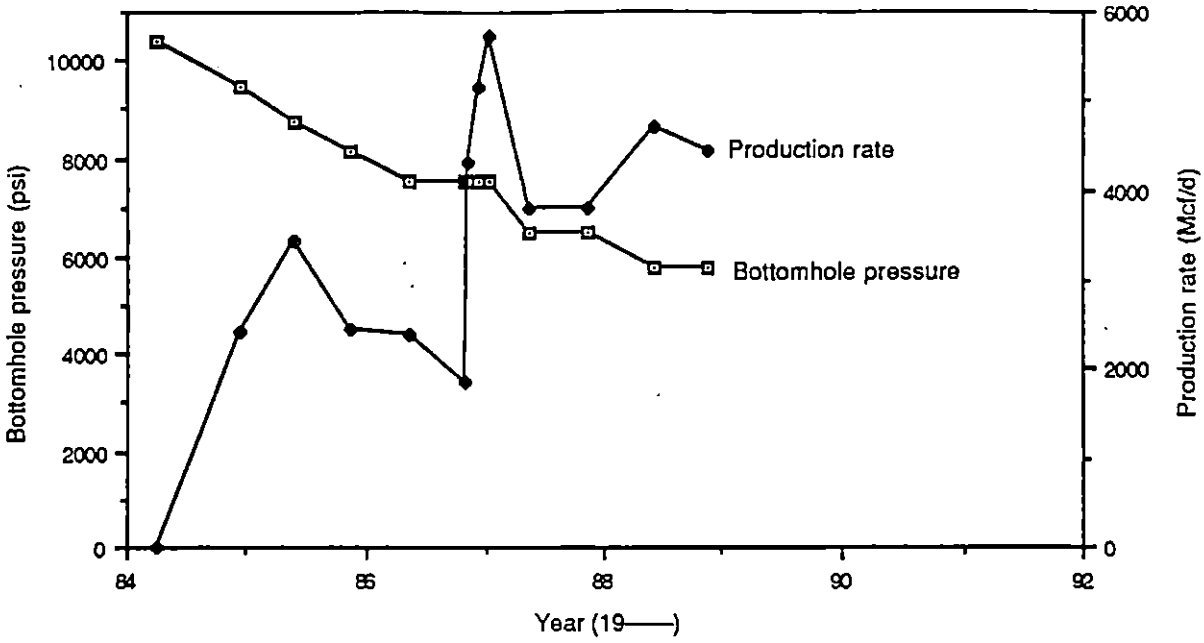

Figure A-9. Plot of bottom-hole pressure versus time for well no. 903, Rutherford No. 2U I. P. Farms.

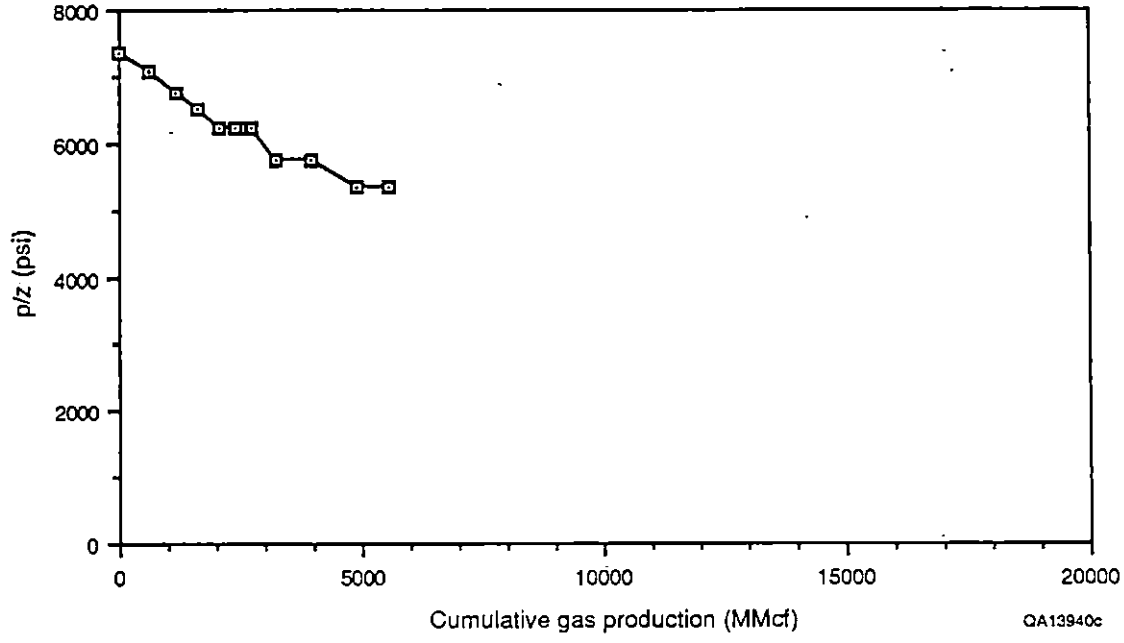

Figure A-10. Plot of p/z versus cumulative production rate for well no. 903, Rutherford No. 2U I. P. Farms.

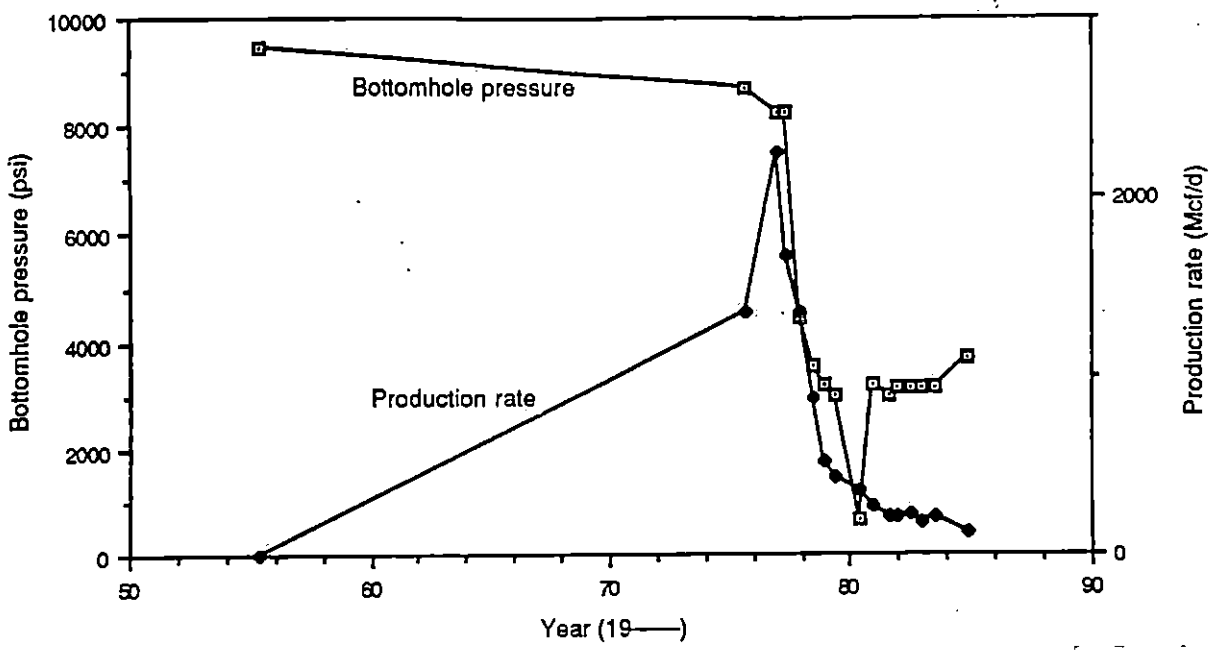

Figure A-11. Plot of bottom-hole pressure versus time for well no. 246, Anschutz No. 1 Peterson.

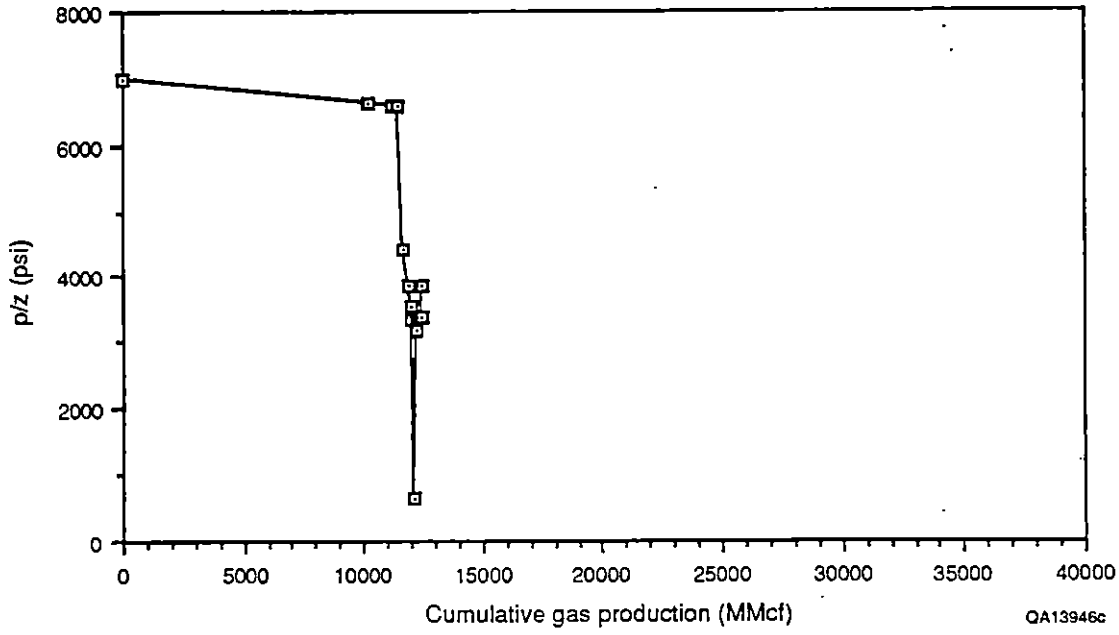

Figure A-12. Plot of p/z versus cumulative production rate for well no. 246, Anschutz No. 1 Peterson.

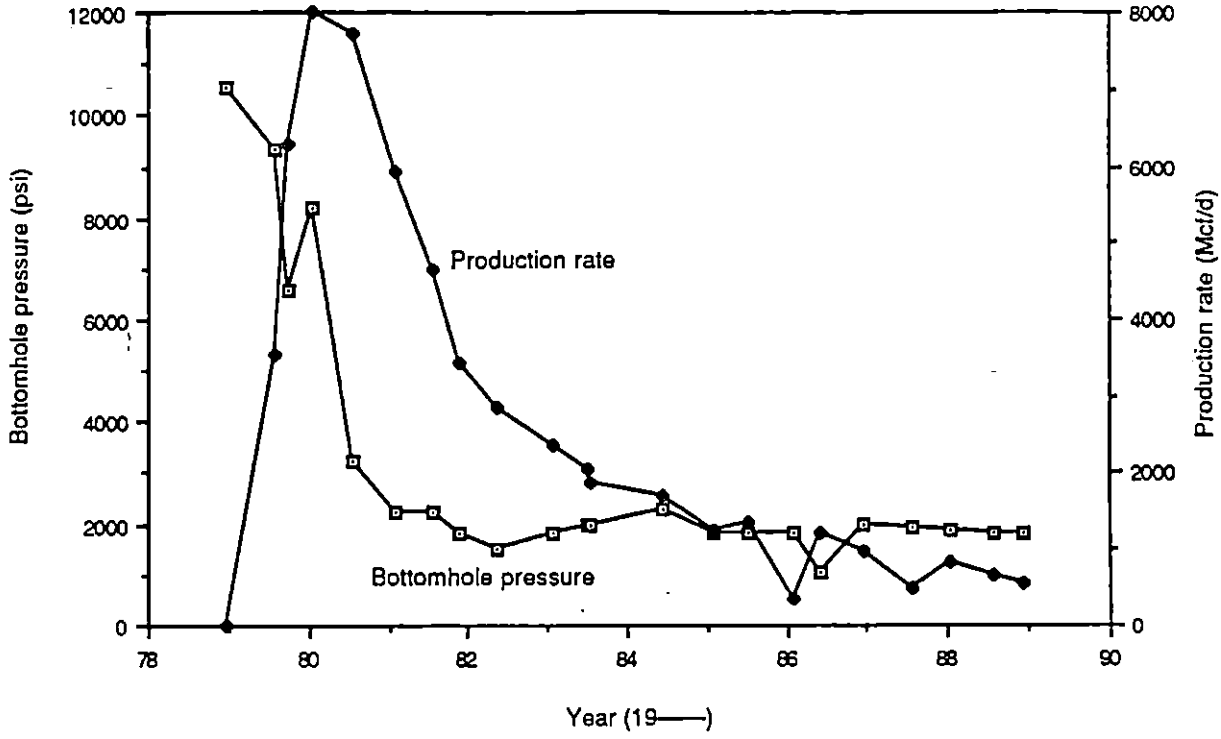

Figure A-13. Plot of bottom-hole pressure versus time for well no. 260, Anschutz No. 1 Renn.

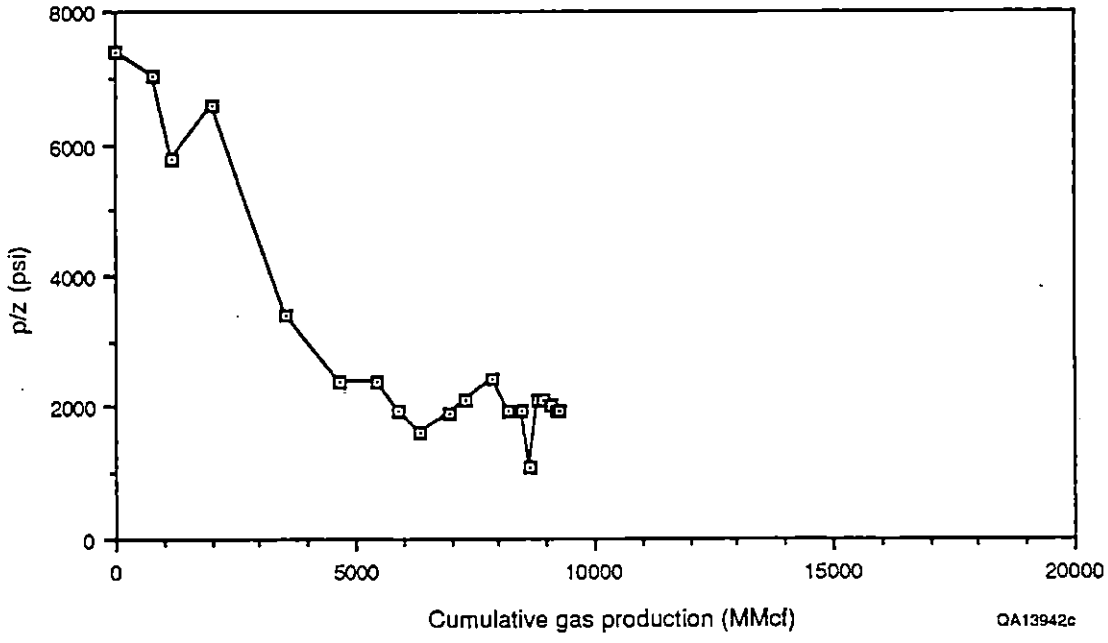

Figure A-14. Plot of p/z versus cumulative production rate for well no. 260, Anschutz No. 1 Renn.

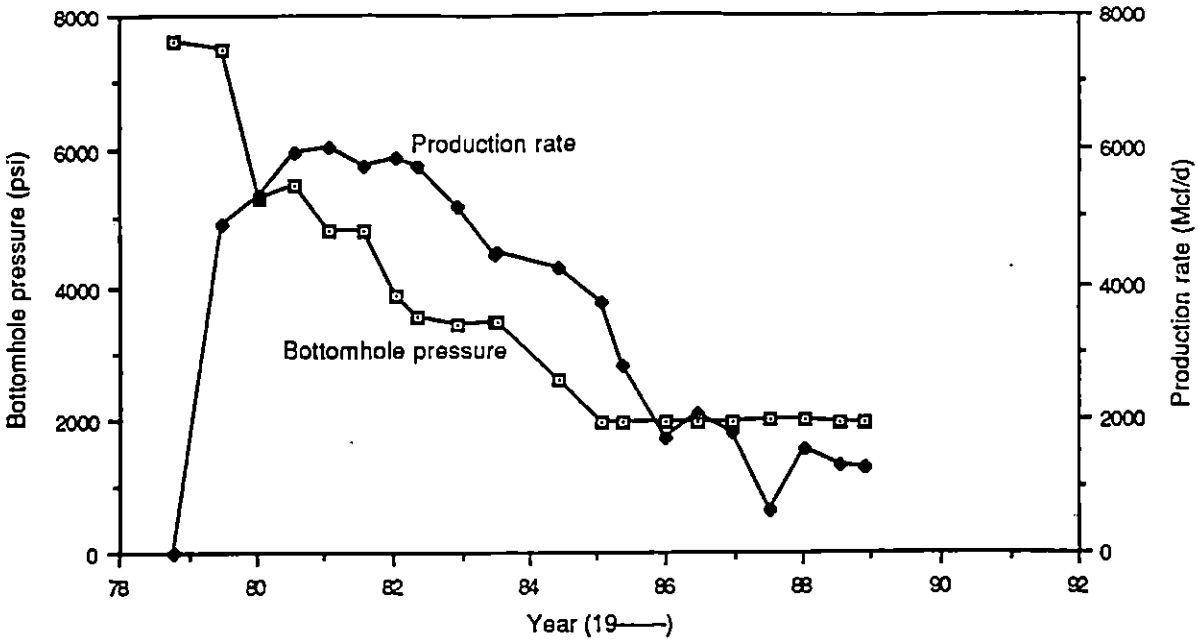

Figure A-15. Plot of bottom-hole pressure versus time for well no. 259, Anschutz No. 1 Marmion.

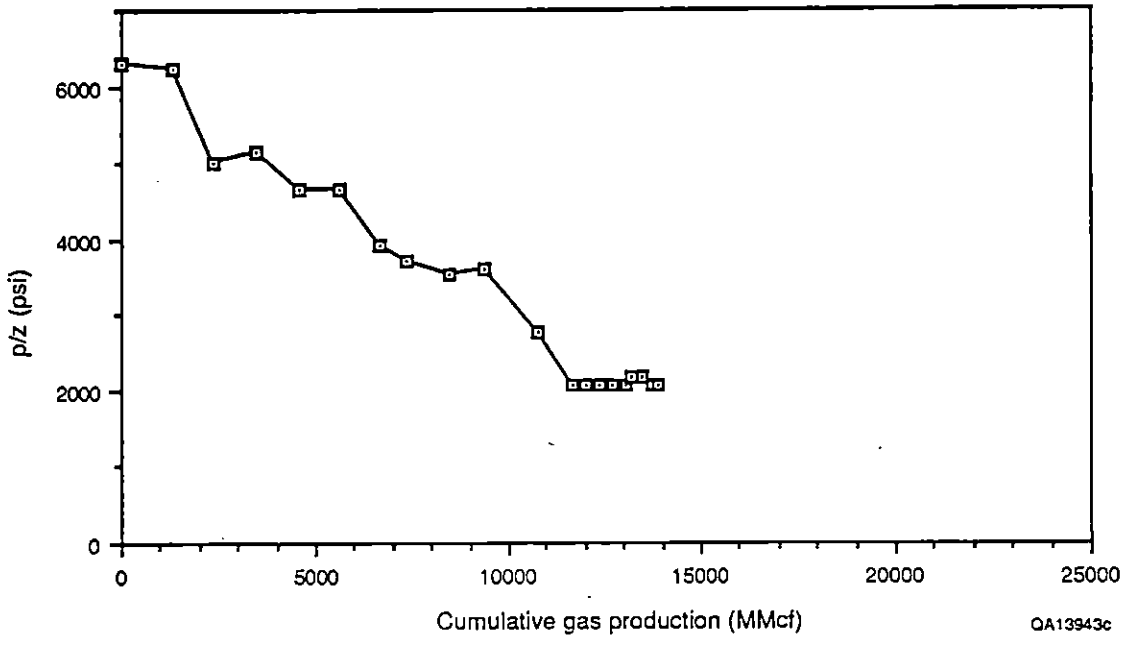

Figure A-16. Plot of p/z versus cumulative production rate for well no. 259, Anschutz No. 1 Marmion.

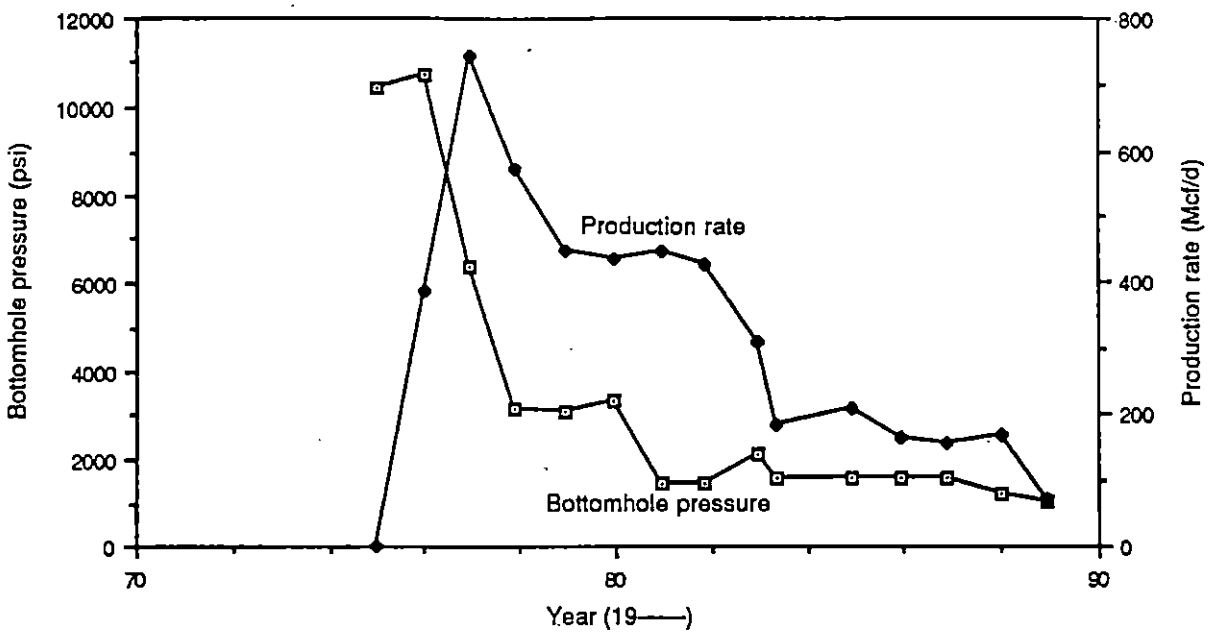

Figure A-17. Plot of bottom-hole pressure versus time for well no. 185, General Crude No. 1 Shell Point.

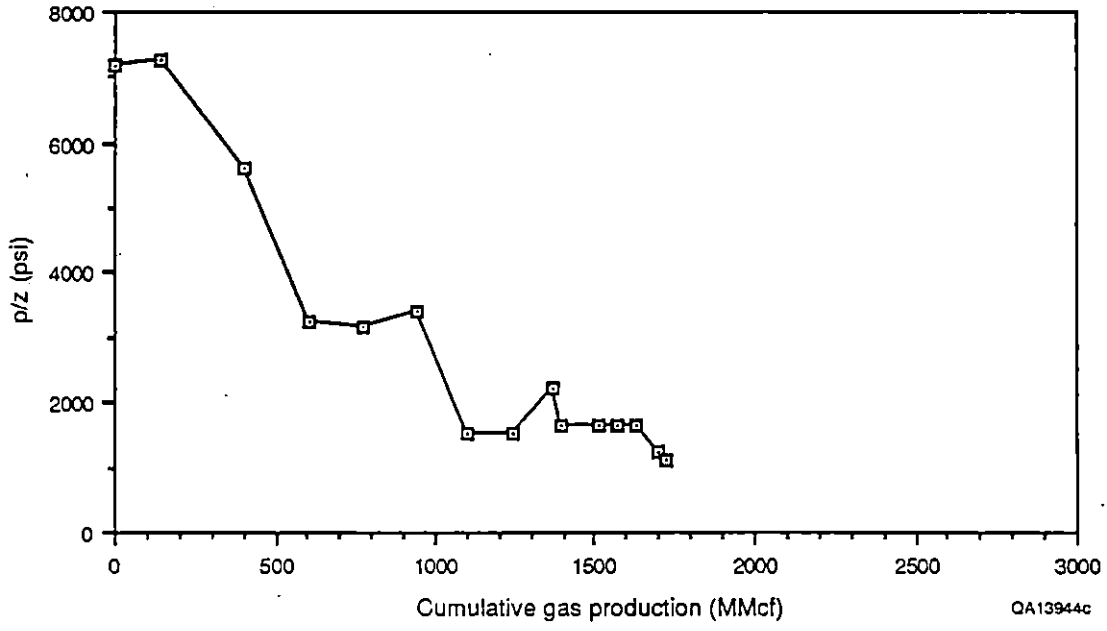

Figure A-18. Plot of p/z versus cumulative production rate for well no. 185, General Crude No. 1 Shell Point.

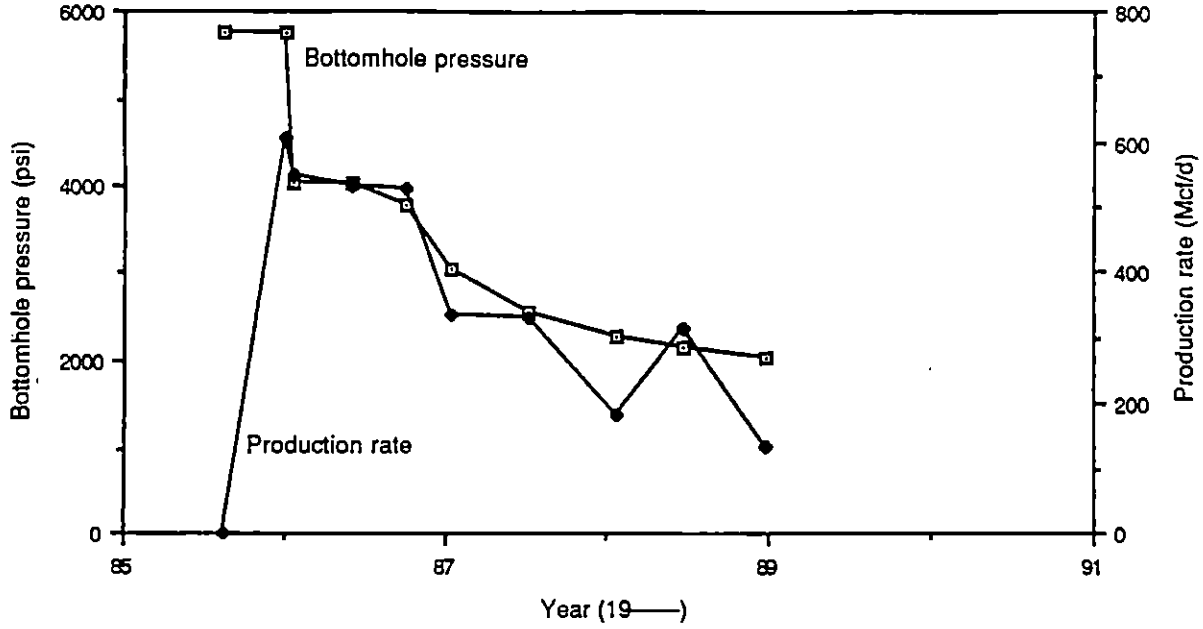

Figure A-19. Plot of bottom-hole pressure versus time for well no. 926, Cockrell No. 1 R. A. Williams.

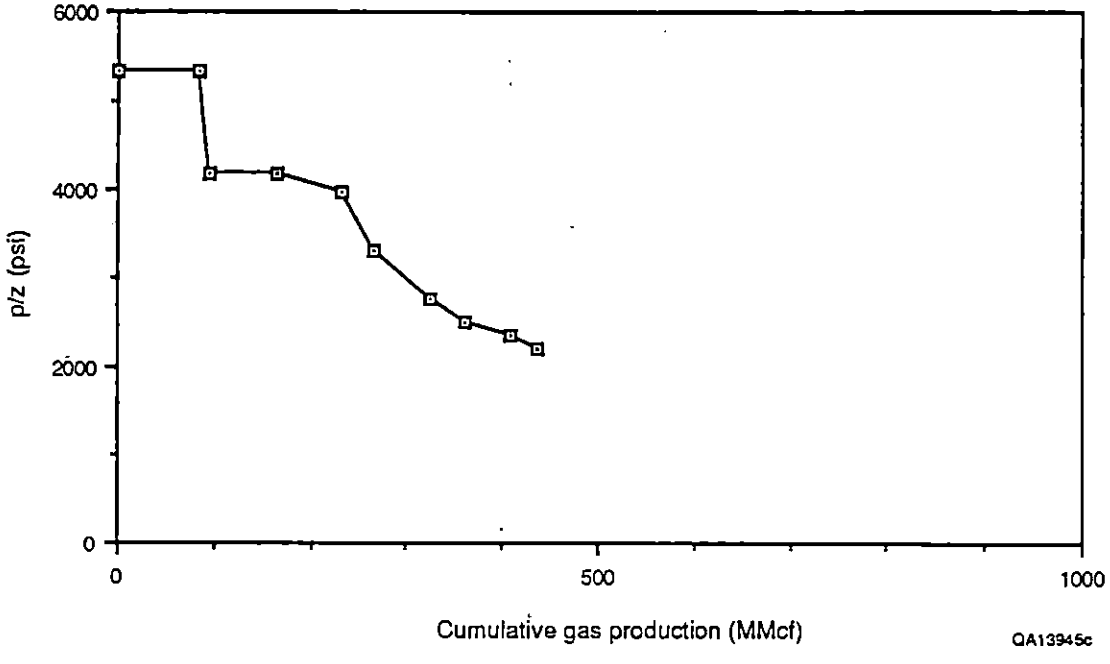

Figure A-20. Plot of p/z versus cumulative production rate for well no. 926, Cockrell No. 1 R. A. Williams.

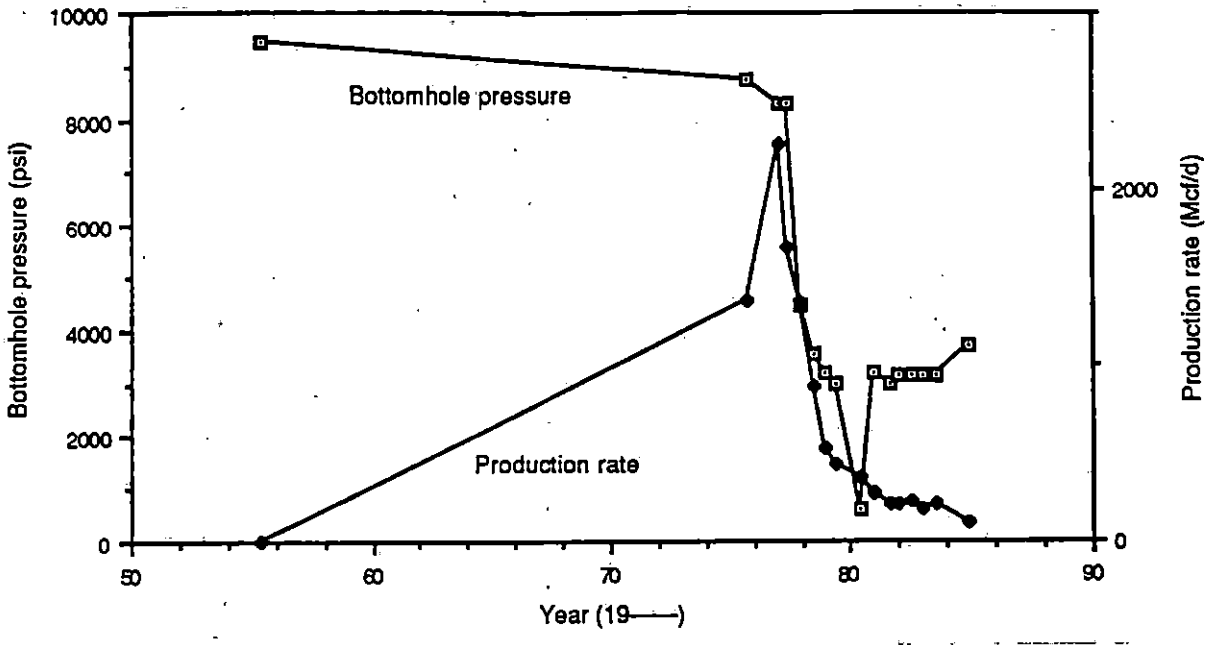

Figure A-21. Plot of bottom-hole pressure versus time for well no. 182, Superior No. 1 Cooper "B."

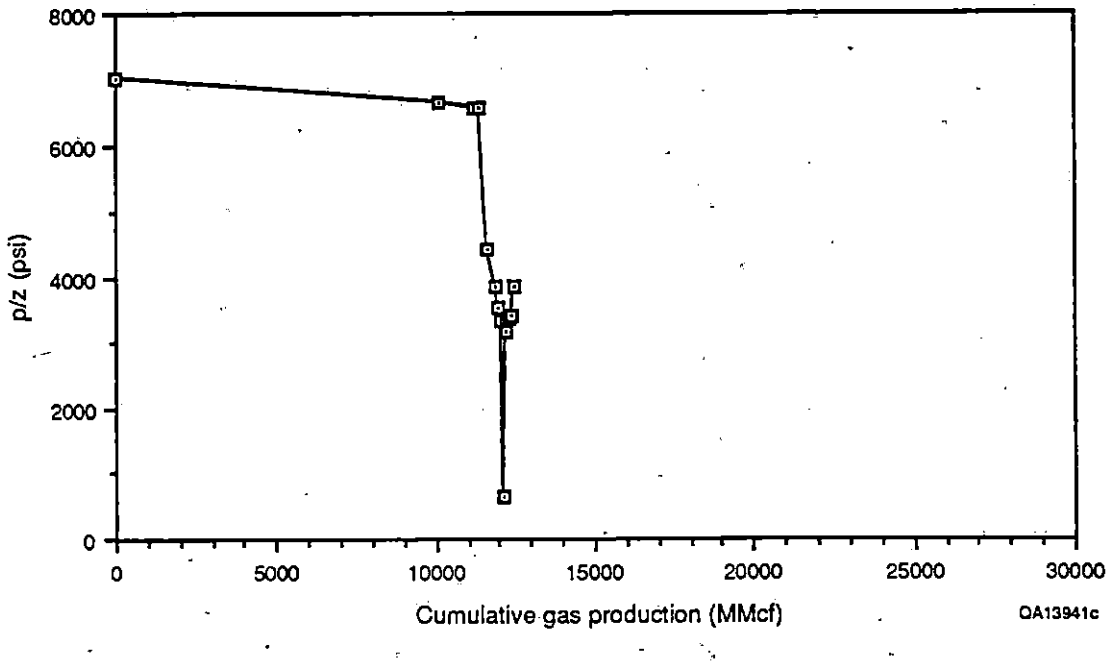

Figure A-22. Plot of p/z versus cumulative production rate for well no. 182, Superior No. 1 Cooper "B."

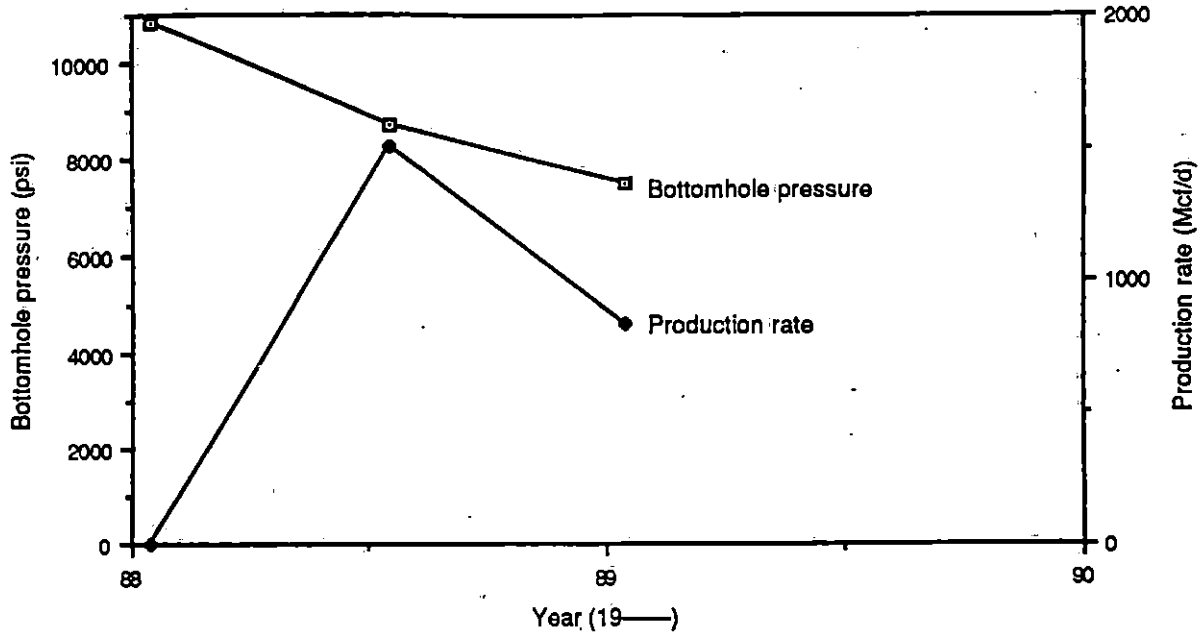

Figure A-23. Plot of bottom-hole pressure versus time for well no. 67, Phillips No. 2-A O'Daniel.

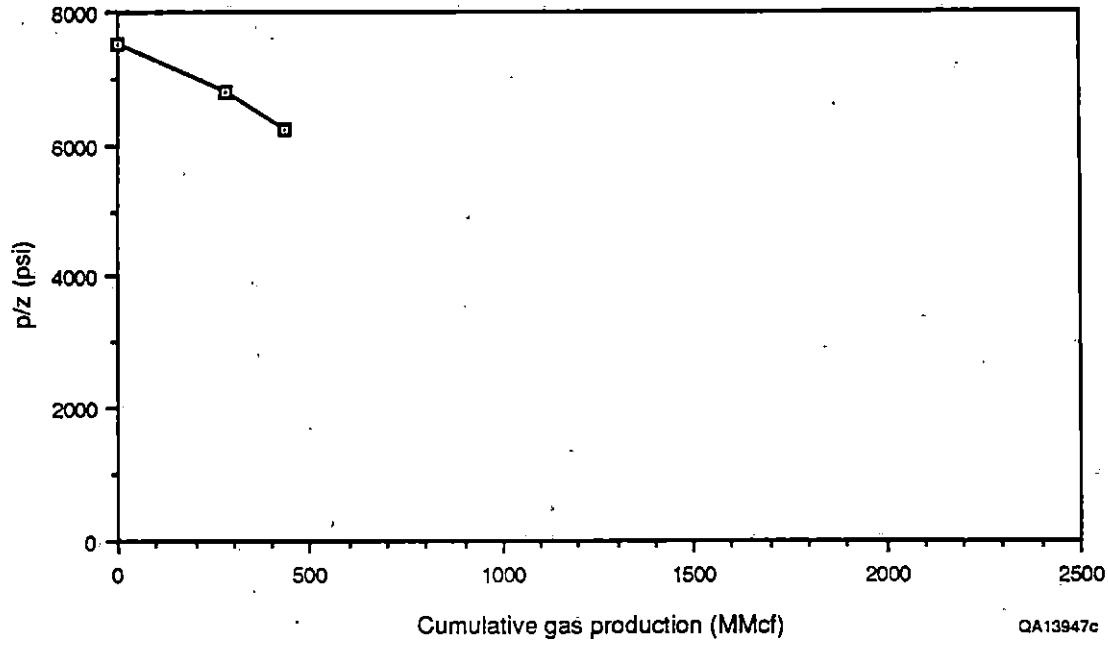

Figure A-24. Plot of p/z versus cumulative production rate for well no. 67, Phillips No. 2-A O'Daniel.

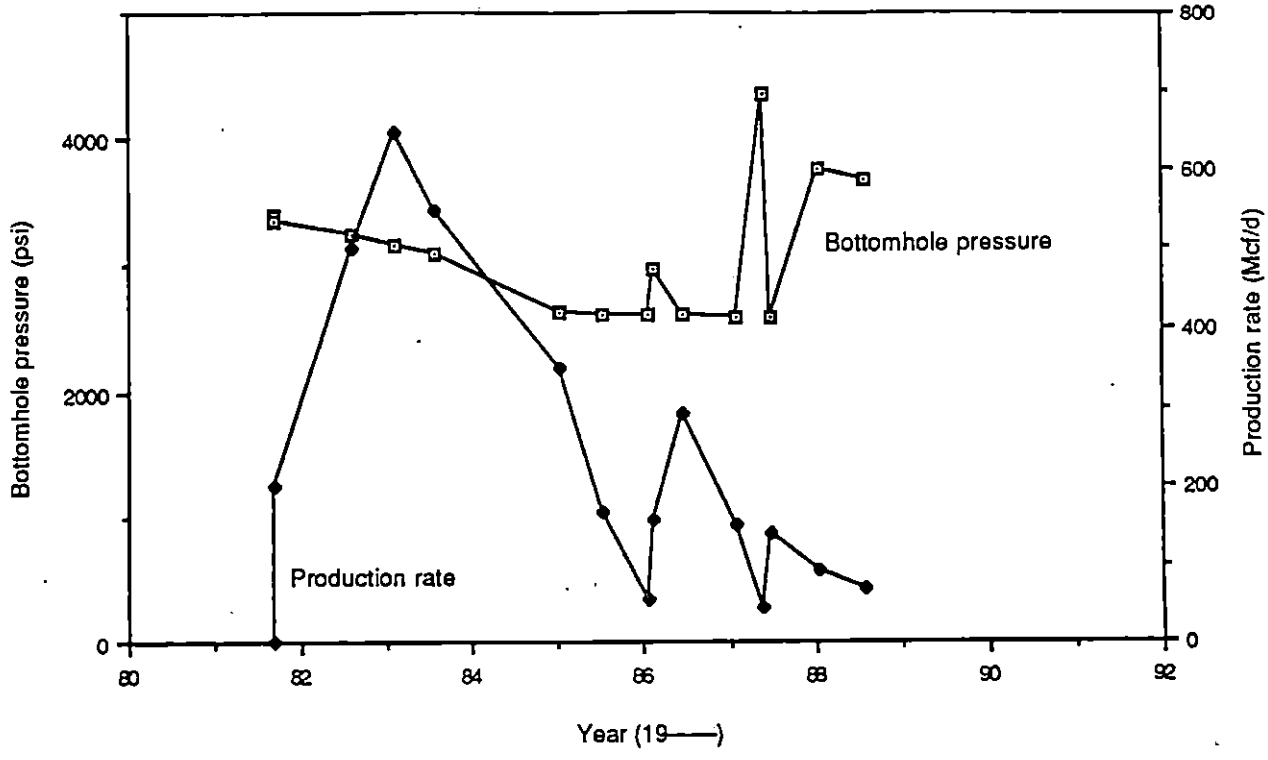

Figure A-25. Plot of bottom-hole pressure versus time for well no. 48, Phillips No. 1 Adriance.

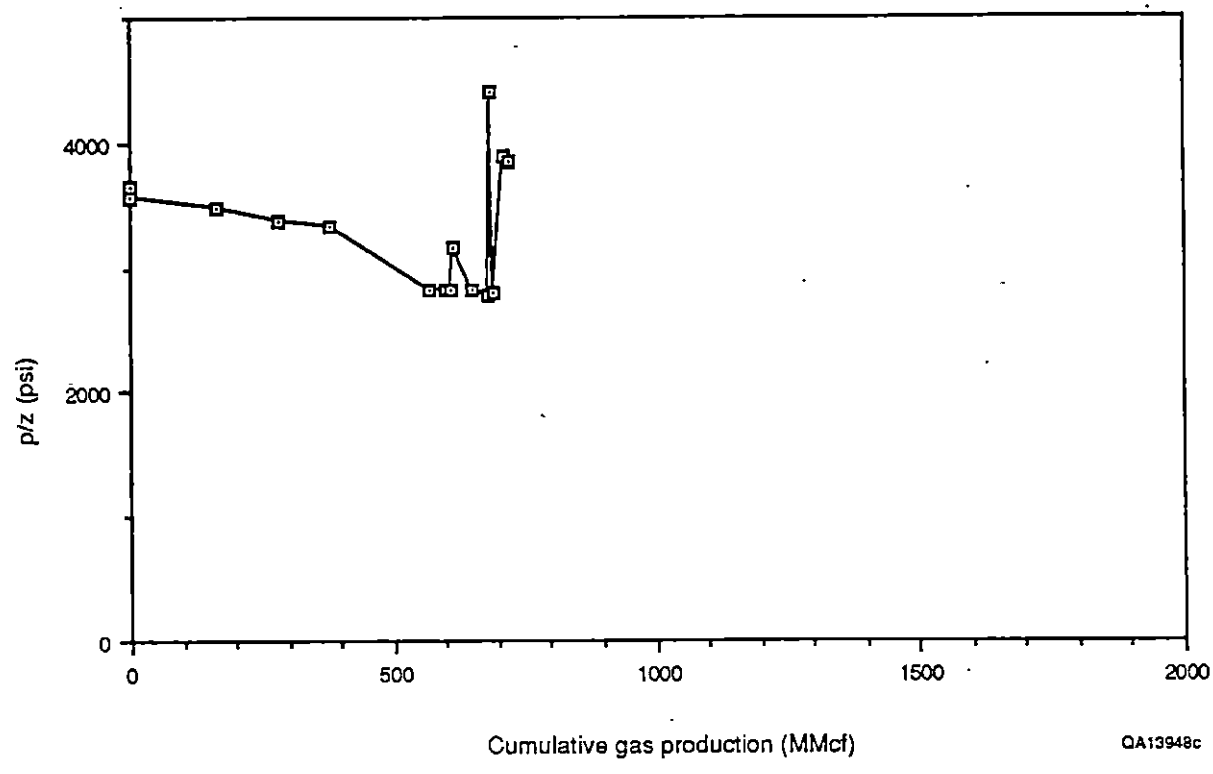

Figure A-26. Plot of p/z versus cumulative production rate for well no. 48, Phillips No. 1 Adriance.

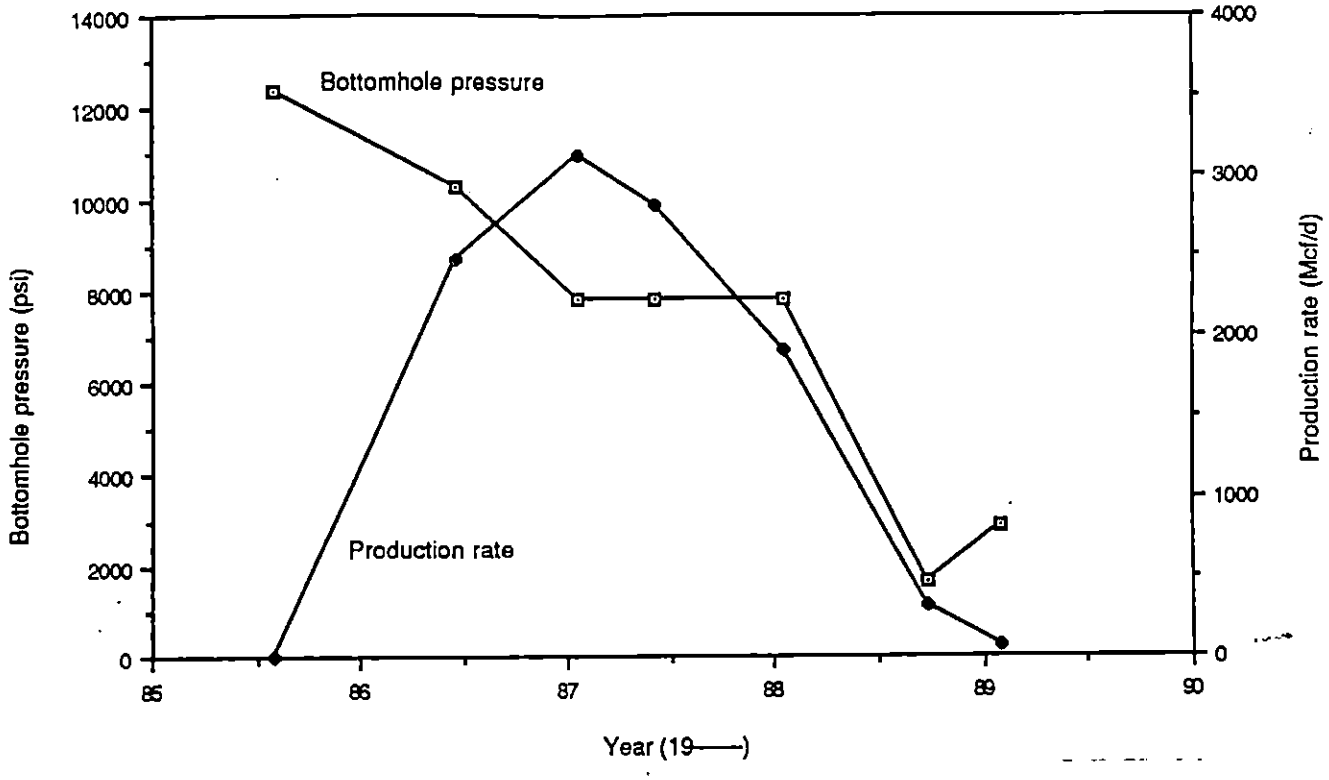

Figure A-27. Plot of bottom-hole pressure versus time for well no. 931, Denovo No. 1 U.S. National Bank of Galveston.

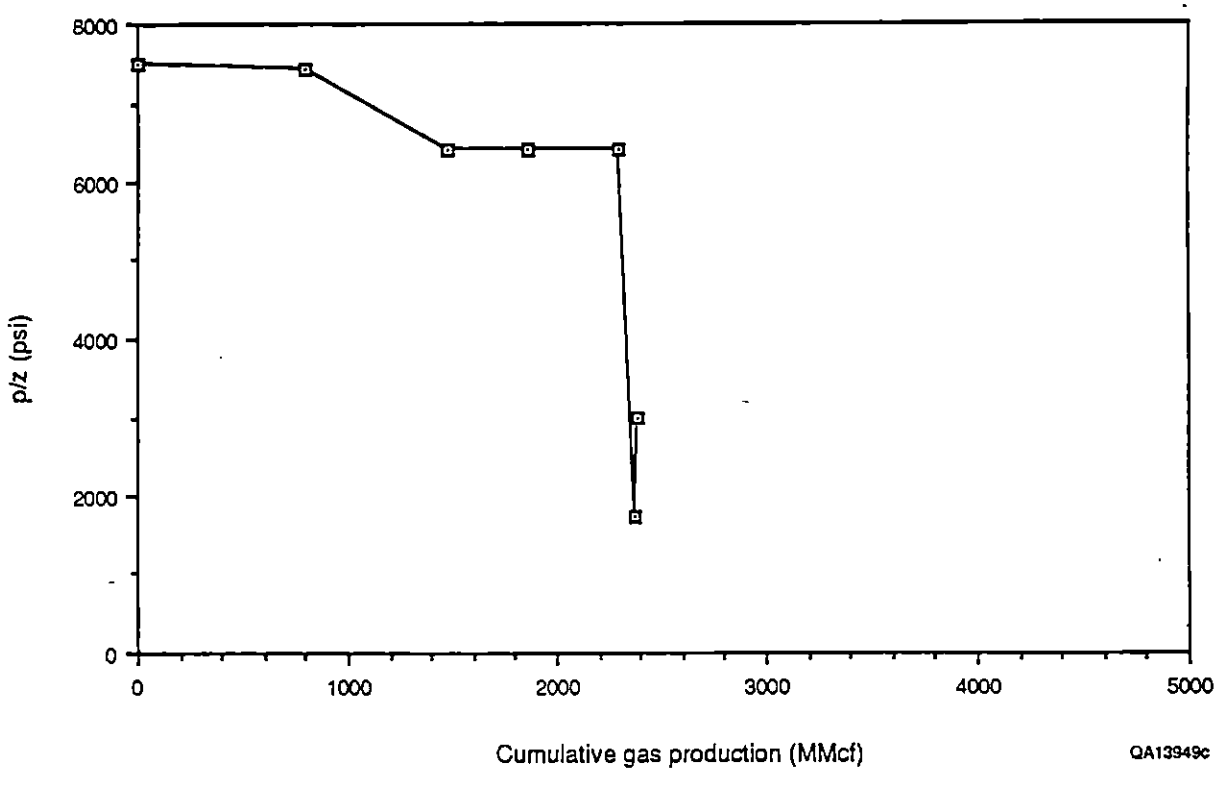

Figure A-28. Plot of p/z versus cumulative production rate for well no. 931, Denovo No. 1 U.S. National Bank of Galveston.

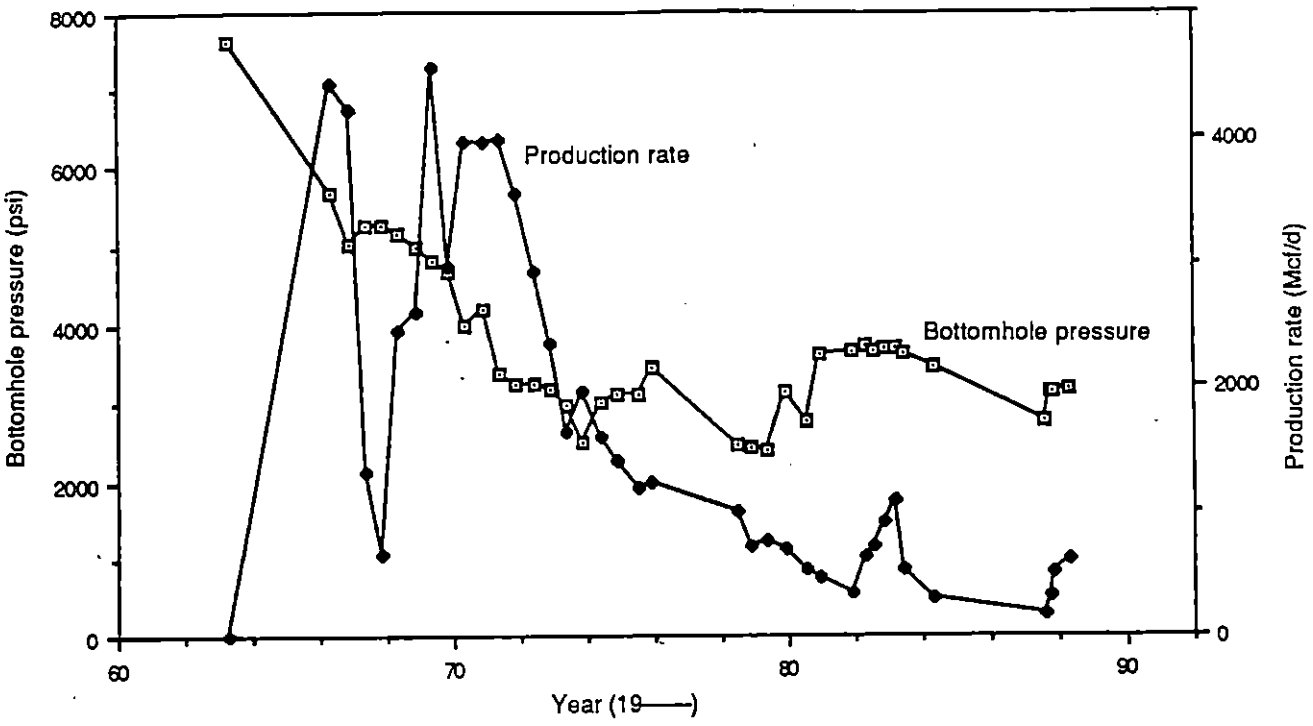

Figure A-29. Plot of bottom-hole pressure versus time for well no. 269, Superior No. 2 Lockhart Bank Unit 1.

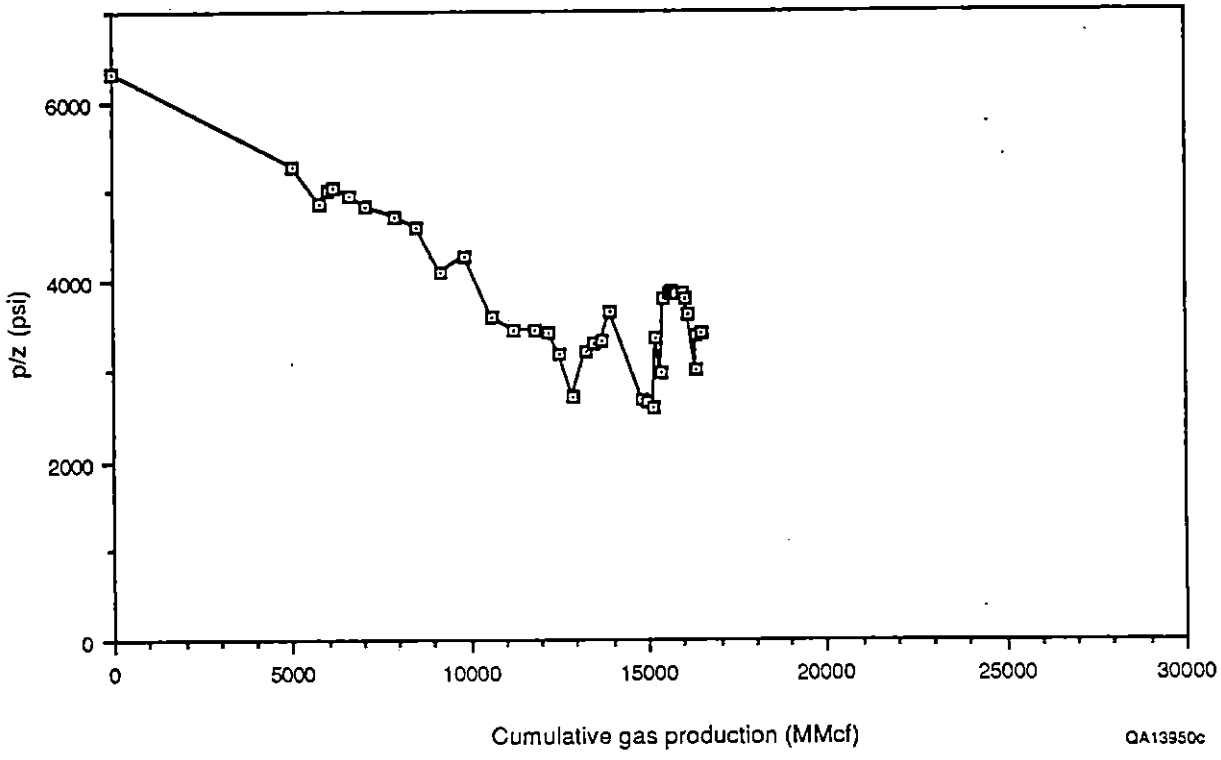

Figure A-30. Plot of p/z versus cumulative production rate for well no. 269, Superior No. 2 Lockhart Bank Unit 1.

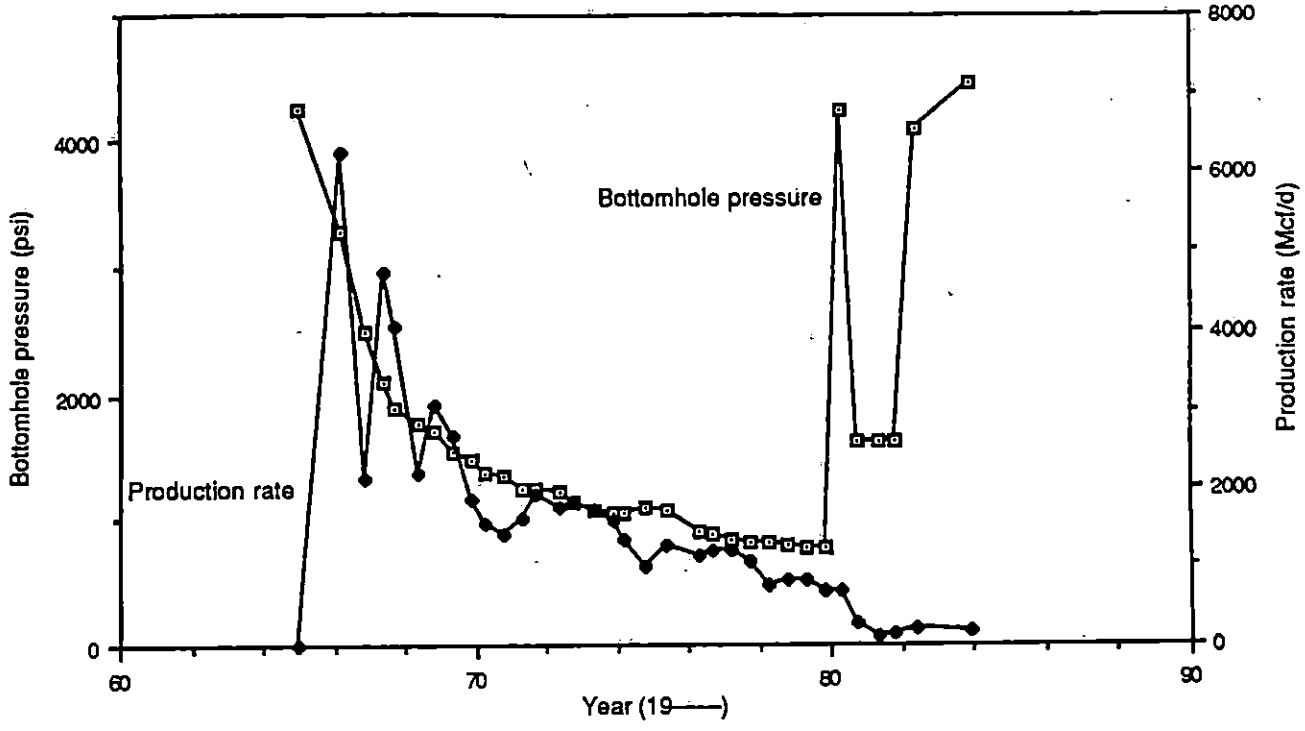

Figure A-31. Plot of bottom-hole pressure versus time for well no. 110, Phillips No. 2U Cozby.

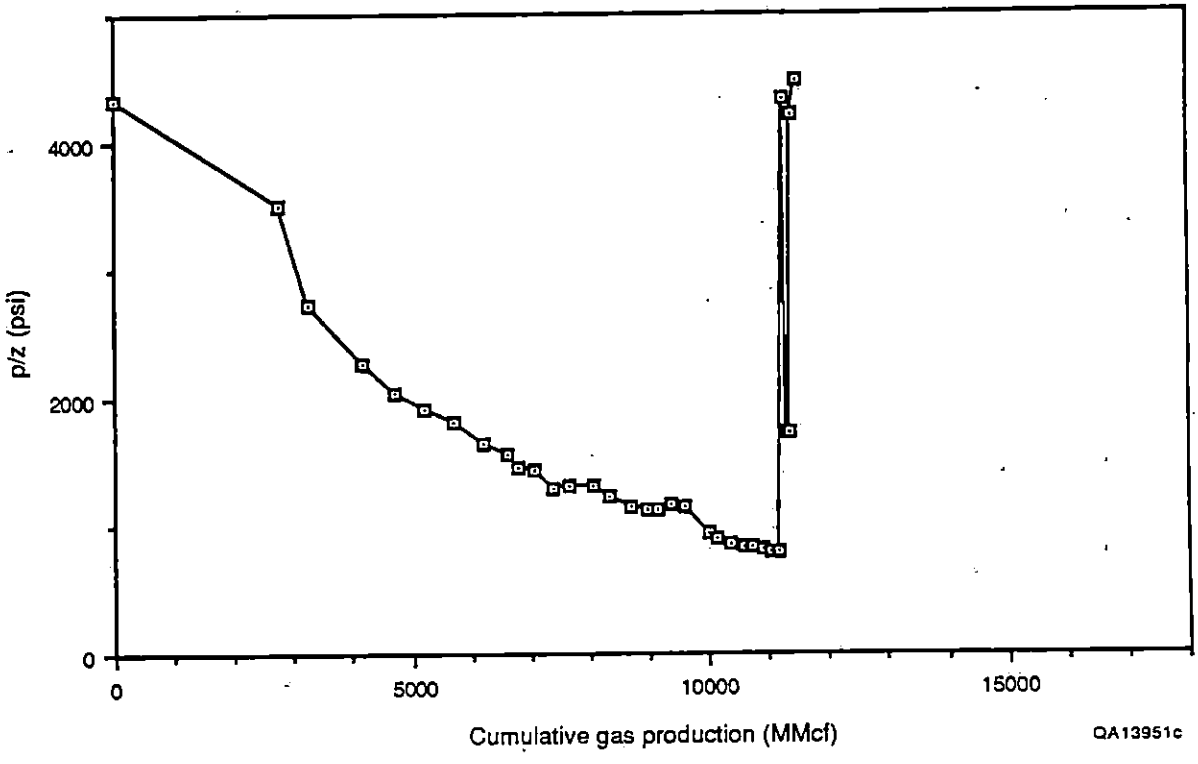

Figure A-32. Plot of p/z versus cumulative production rate for well no. 110, Phillips No. 2U Cozby.

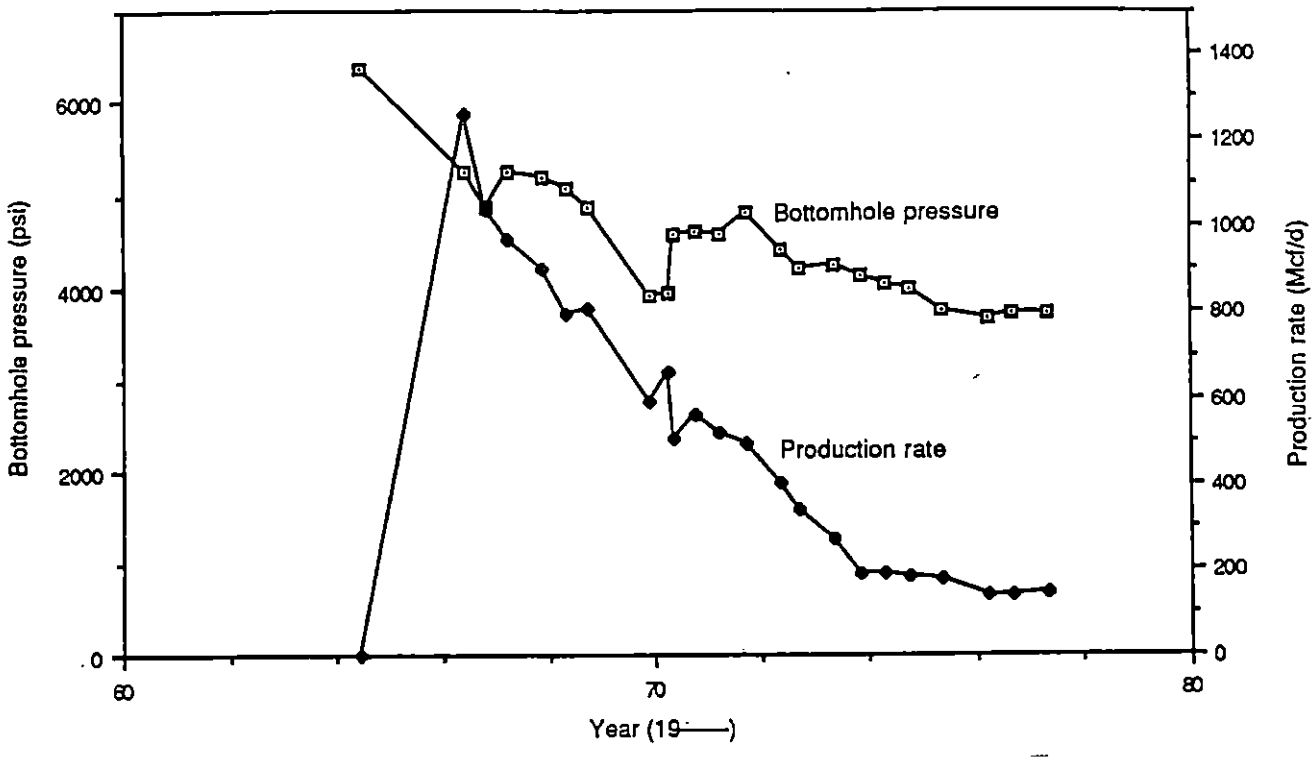

Figure A-33. Plot of bottom-hole pressure versus time for well no. 122, Phillips No. 3 Angle.

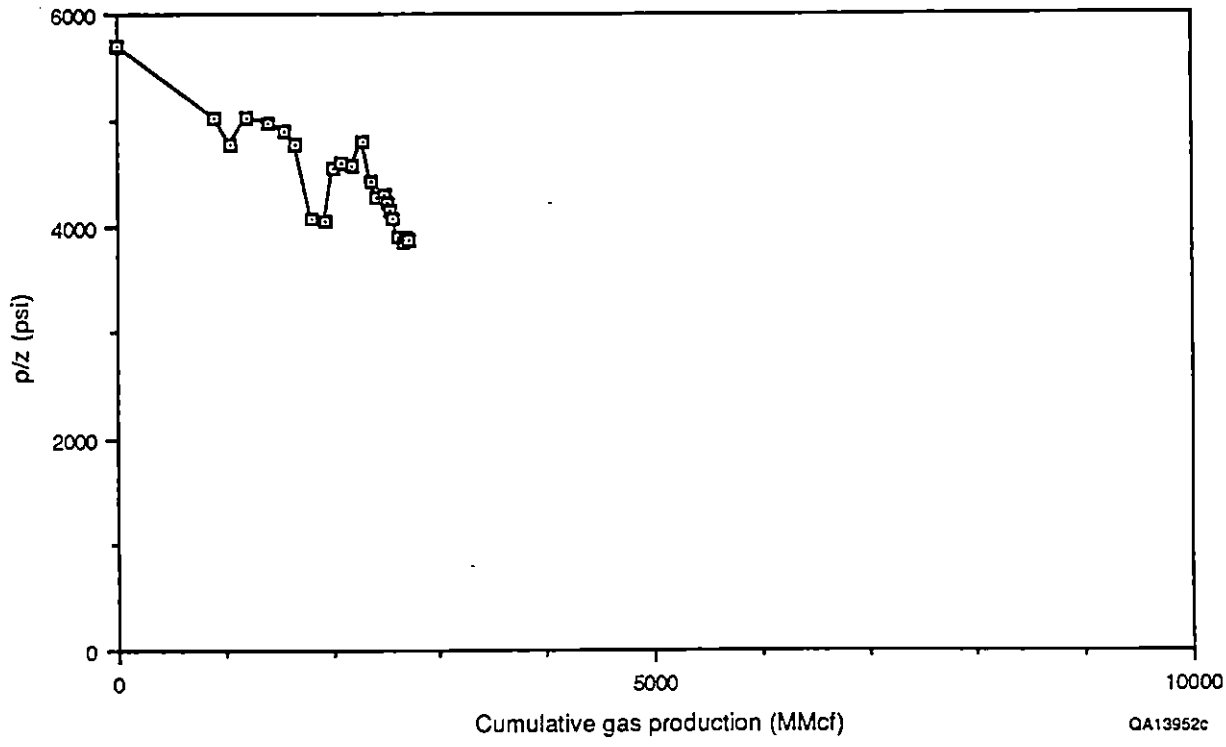

Figure A-34. Plot of p/z versus cumulative production rate for well no. 122, Phillips No. 3 Angle.

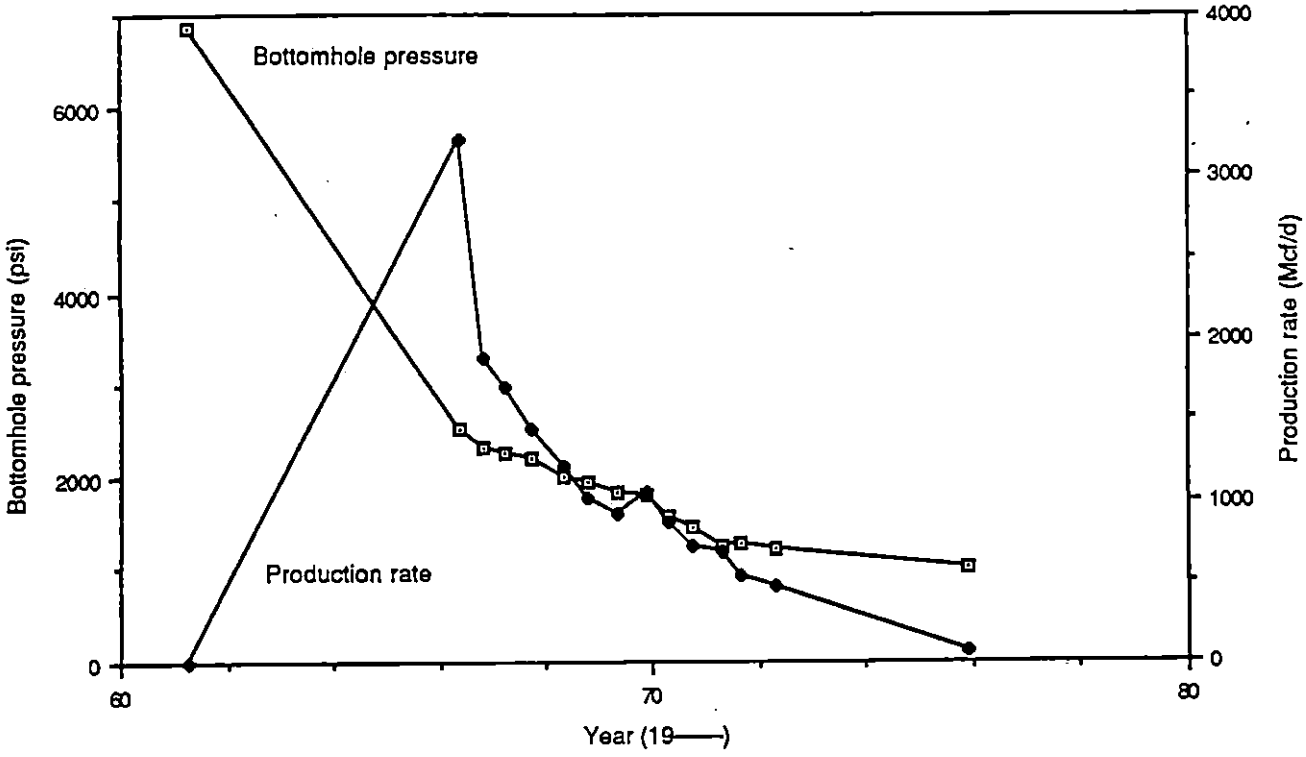

Figure A-35. Plot of bottom-hole pressure versus time for well no. 98, Phillips No. K-1 Houston Farms.

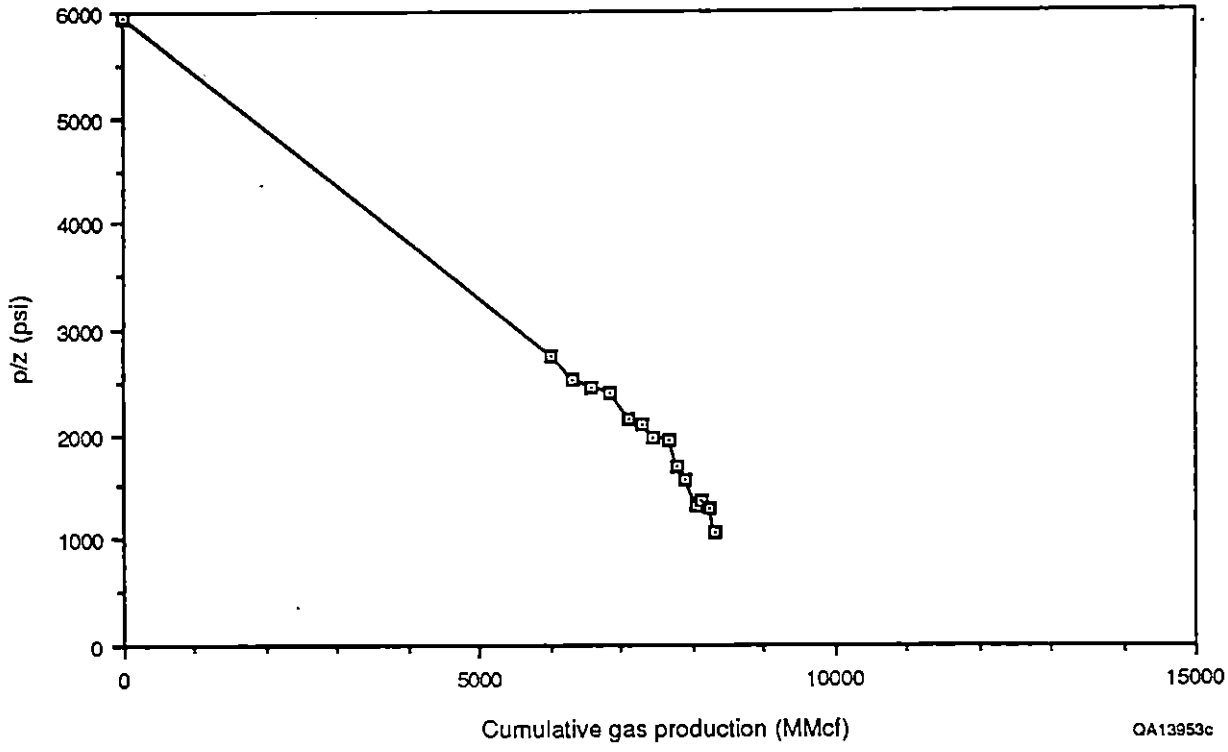

Figure A-36. Plot of p/z versus cumulative production rate for well no. 98, Phillips No. K-1 Houston Farms.

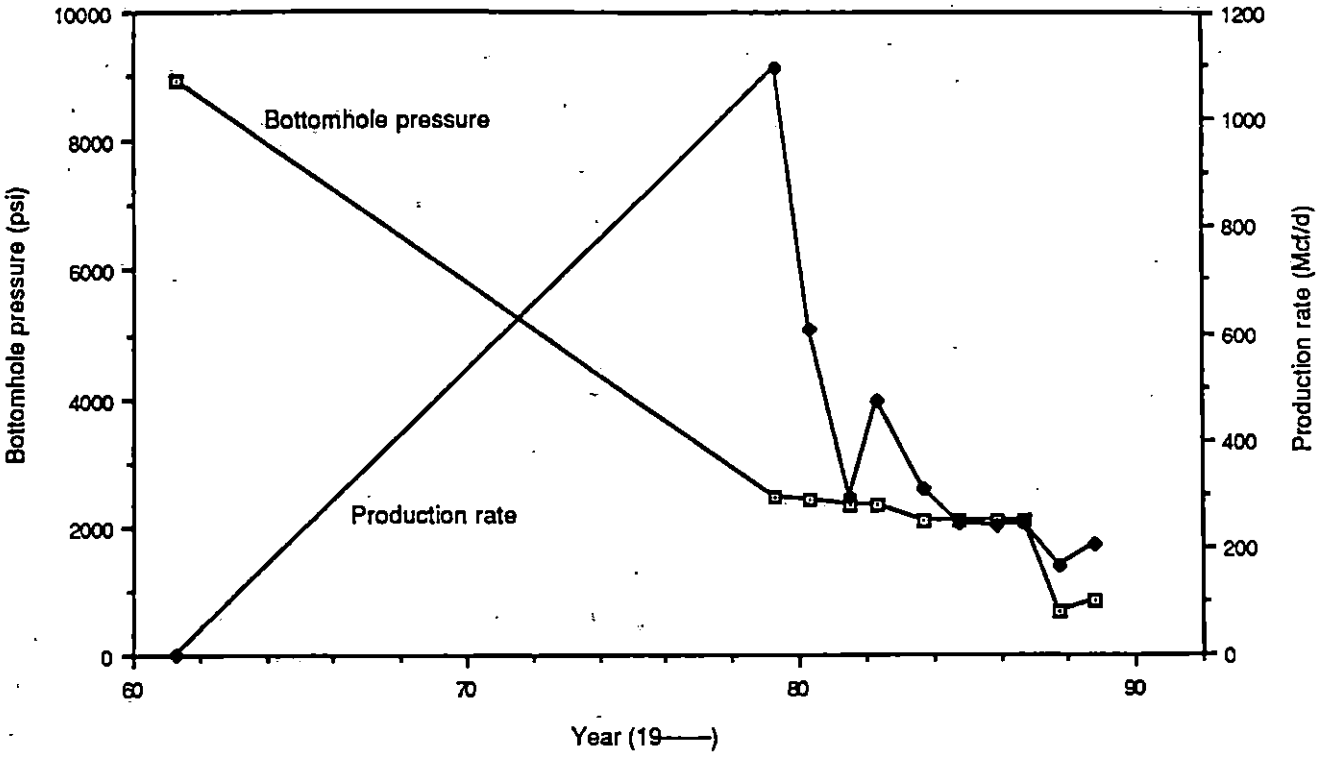

Figure A-37. Plot of bottom-hole pressure versus time for well no. 186, Phillips No. 1 Houston Farms.

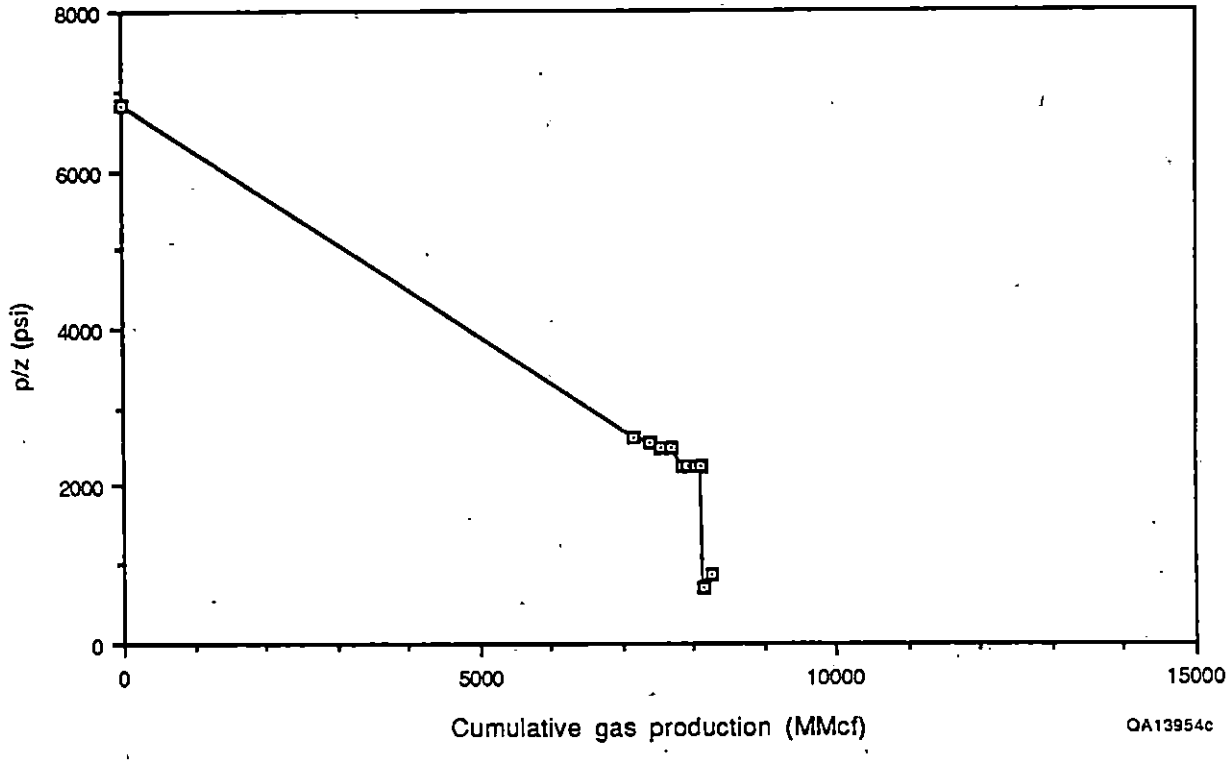

Figure A-38. Plot of p/z versus cumulative production rate for well no. 186, Phillips No. 1 Houston Farms.

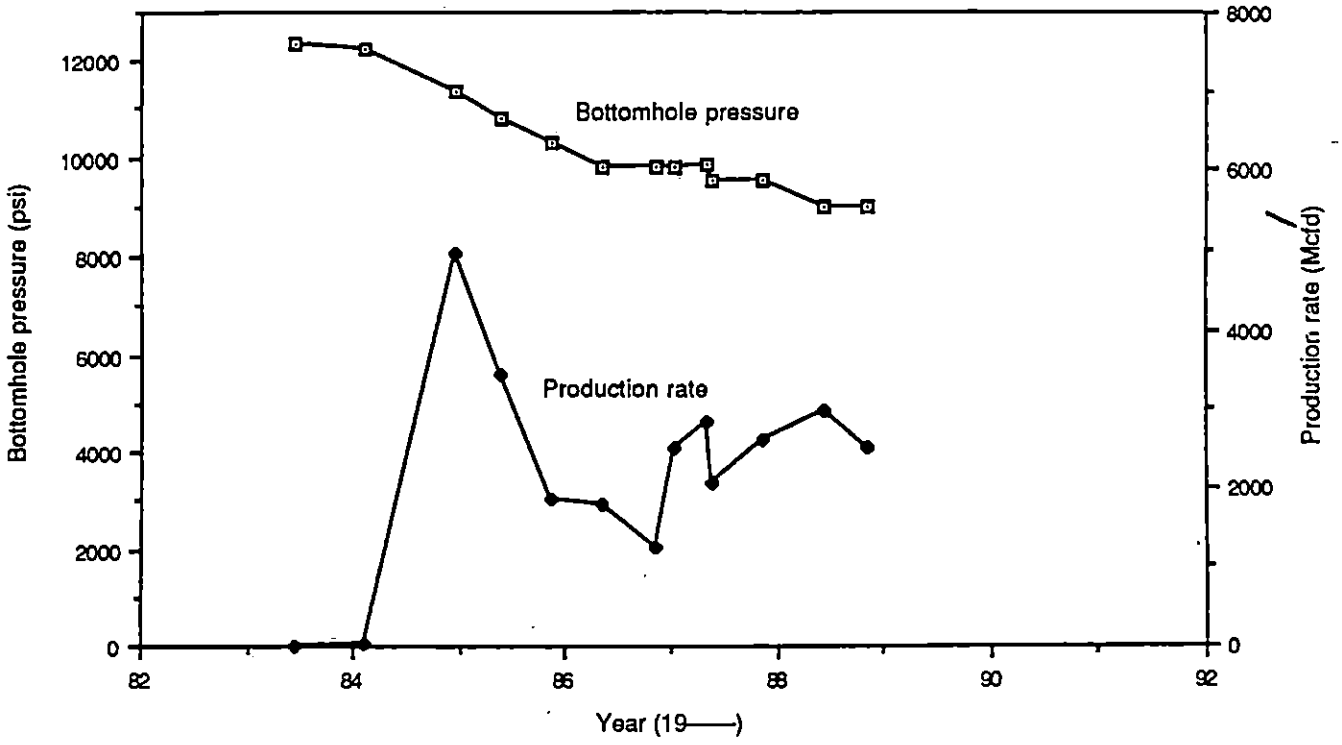

Figure A-39. Plot of bottom-hole pressure versus time for well no. 913, Rutherford No. 1-L I. P. Farms.

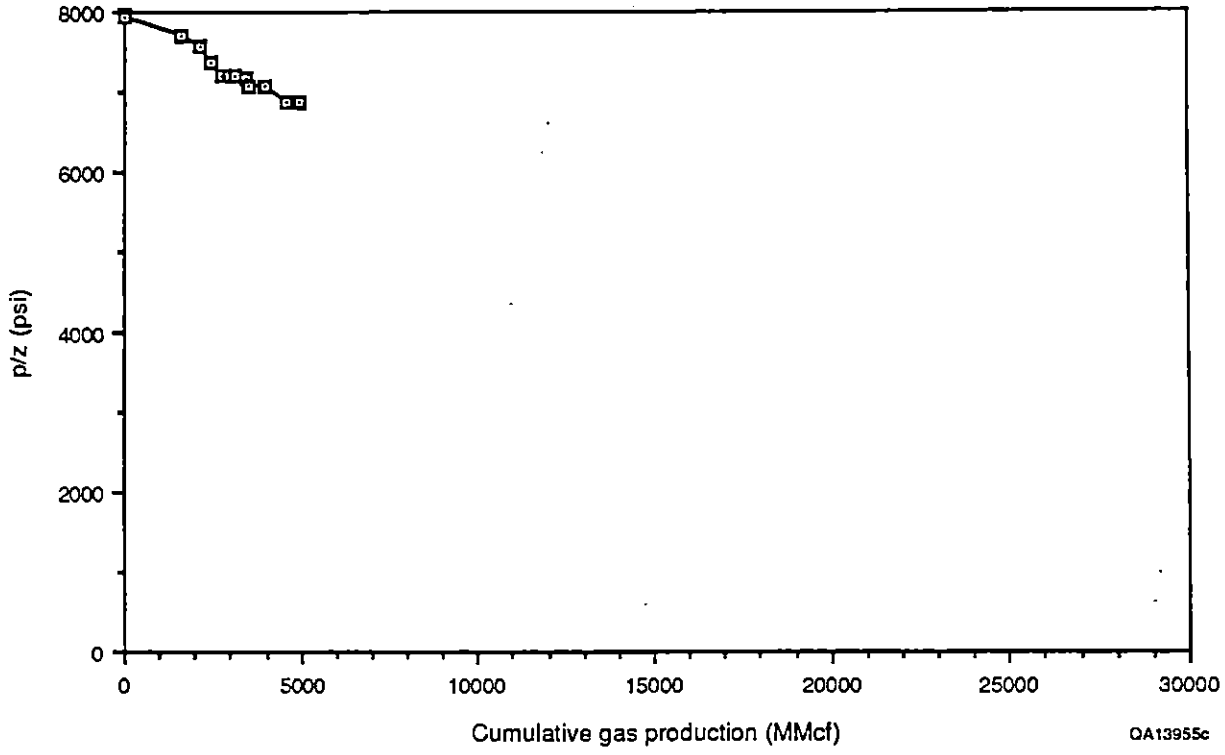

Figure A-40. Plot of p/z versus cumulative production rate for well no. 913, Rutherford No. 1-L I. P. Farms.

Table A-1. Well data base. Well numbers correspond to numbers on cross sections.

Field name	Well name	Log no.	Interval (ft)	Status	Date	BHP (psi)	Date	BHP (psi)
Chocolate Bayou,N (10400)	No. 1 Potter	18	10099-10103	P&A	11/30/73	4349		
Chocolate Bayou,N	No. 1 Robnett	29		NA				
Chocolate Bayou,N	No. 1 Herring	17		NA				
Chocolate Bayou,N (10800)	Bright Gas Unit No. 1	911	10811-10816	ACT	78/03/27	4353	88/12/30	1629
Chocolate Bayou,N(10400)	Triwallinder No. 1 T	910	10376-10380	ACT			89/01/16	2914
Chocolate Bayou,S	No. FF-1 Houston Frm.	150	15311-15276	P&A	7/12/76	12288		
Chocolate Bayou,S (Banfield)	No. FF-1 Houston Frm.	150	13890-13652	ACT	77/03/15	9504	88/11/10	5435
Chocolate Bayou,S (S)	No. EE-1 Houston Frm	153	14682-14667	P&A	4/4/64	12422		
Chocolate Bayou,S (12300 Frio)	I.P. Farms No. 2 UT Well No. 2U	903	12298-12320	ACT			88/11/12	5772
Chocolate Bayou,S (I.P.)	I.P. Farms Well No. 1L	913	14150-14194	ACT			88/11/06	8981
Chocolate Bayou,S (P Frio)	Houston Farms Dev. Co. UT 1-A Well No. 1		12162-12172	ACT	76/05/14	1587	84/04/11	1111
Chocolate Bayou,S (S)	No. JJ-1 Houston Frm.	151		P&A				
Chocolate Bayou,S (S)	Houston 'K' No. 2	96	11968-11988	P&A	4/9/58	8397		
Chocolate Bayou,S (S)	No. GG-1 Houston	156	14850-14817	S/I	5/18/65	11227		
Chocolate Bayou,S (Harris)	Houston 'CC' No. 1	149	12838-12823	ACT	63/04/17	10577	881020	3702
Chocolate Bayou,S	No. 1 Houston Frm	186		NA	7/5/60	9800		
Chocolate Bayou,S	No. LL-1 Houston Frm.	152A		NA				
Chocolate Bayou,S	No. KK-1 Houston	152	14684-14649	P&A	9/30/65	9784		
Chocolate Bayou,S	No. 1 Halls Bayou	165		NA				
Chocolate Bayou,SE (13500)	No. 1 McIlvaine Gas Unit	89	13566-13577	P&A	10/10/76	10921		
Chocolate Bayou (P Frio)	No. 1 Houston Farms Dev.	904 or 133	12509-12471	ACT	61/04/21	8926	88/10/23	843
Chocolate Bayou (P Frio)	No. 3 Houston Farms Dev.	905 or 184	12510-12518	ACT	61/04/23	8640	88/10/29	1042
Chocolate Bayou (Freeman)	Wilson R.K. GU No. 1 Well No. 1	906 or 107	10424-10442	ACT	87/11/23	372	88/07/28	262
Chocolate Bayou (11500 Wieting No. 2)	Houston -P-No. 1	136	11490-11510	REC	50/10/13	6955	—	—
Chocolate Bayou (Banfield)	Angle Well No. 3	122	10897-10916	REC	47/08/12	6255	—	—
Chocolate Bayou (Weiting Upper)	Angle Well No. 3	122	11434-11449	S/I	64/06/03	6362	77/05/02	3704
Chocolate Bayou (12000)	No. 2 Rekdhal	106A	12086-12076	REC	57/06/15	8943	—	—
Chocolate Bayou (Banfield)	Banfield N O Well No. 1	124	10972-10992	REC	45/06/05	5100	—	—
Chocolate Bayou (Banfield)	Weiting A.W. G/U O/A Well No. 12	907	10809-10864	ACT	74/08/07	1350	88/09/02	1184
Chocolate Bayou (Harris)	Weiting A.W. G/U O/A Well No. 17	908	10250-10263	ACT	80/09/26	2860	88/09/03	1400
Chocolate Bayou (Andrau)	Stafford Gas Unit Well No. 1		11250-11256	REC	59/05/05	2871	—	—
Chocolate Bayou (12800 R1A)	Houston -R-No. 1-A	146A	12846-12854	REC	52/04/28	9473	52/08/13	10165
Chocolate Bayou (Andrau)	R.W. Wilson G.U.No. 1 Well No. 6	179	12098-12120	ACT	86/02/18	10133	88/06/13	9134
Chocolate Bayou (Andrau)	Houston -M-No. 1	914	11390-11428	REC	50/02/15	4607	—	—

Table A-1. (cont.)

Field name	Well name	Log no.	Interval (ft)	Status	Date	BHP (psi)	Date	BHP (psi)
Chocolate Bayou (Frio P)	Houston -M-No. 1	914	10871-10877	ACT	88/09/18	3718	89/01/19	3739
Chocolate Bayou (Weiting Upper)	Houston -K- Well No. 1	98	11348-11371	P&A	61/04/11	6584	75/12/01	1008
Chocolate Bayou (Weiting Upper)	Wilson R.K. Gas Unit No. 1 Well No. 2	909	11280-11290	ACT	72/05/24	2321	88/09/04	889
Chocolate Bayou (Weiting Upper)	No. 1-H Houston	95		P&A				
Chocolate Bayou (Weiting Upper)	Gewill No. 1T	901	11354-11364	ACT	63/01/18	4872	88/10/20	1000
Chocolate Bayou (Weiting Upper)	Houston -G-No. 1 T	100	11279-11303	ACT	66/05/13	2163		
Chocolate Bayou (Weiting Upper)	Houston -L-No. 1	902	11450-11474	ACT	62/03/06	6724		
Chocolate Bayou (Weiting Lower)	Gewill No. 2	106	11446-11474	REC	60/09/27	6986	—	—
Chocolate Bayou (Banfield)	Cozby No. 1C	111	10760-10780	ACT	47/05/23	6324		
Chocolate Bayou (Weiting Lower)	Gardiner1 Well No. 1	147	11779-11746	S/I	64/09/09	6871	2/17/66	7594
Chocolate Bayou (Andrau S SEG)	Cozby No. 2	110	12196-12160	REC	53/11/01	9905	—	—
Chocolate Bayou (Schenck)	Cozby No. 2U	110	10905-11005	S/I	64/12/17	4245	86/12/06	4446
Chocolate Bayou (HO. FMS. VI-A-Z)	Banfield Well No. 1	915 or 257	10141-10148	P&A			85/01/05	2910
Chocolate Bayou (12000)	Cozby No. 4	912	11870-11876	ACT	86/04/16	8047	88/11/10	4616
Chocolate Bayou	Fresling No. 1	5		NA				
Chocolate Bayou	No. 3 Houston Farm	184		NA				
Chocolate Bayou	No. S-1 Houston Frm. Dev.	97	12048-12008	P&A	1/11/53	5803		
Chocolate Bayou	No. F-3 Houston Frm.	101		P&A				
Chocolate Bayou	No. 2-A Schenck	114		S/I			—	—
Chocolate Bayou	No. 1 Gunderson			NA				
Chocolate Bayou	No. T-1 Houston Frm.	92		NA				
Chocolate Bayou	No. 2 Gunderson	99		NA				
Chocolate Bayou	Houston 'W' No. 1	94		NA				
Chocolate Bayou	Cozby Well No. 5	178		NA				
Chocolate Bayou	Schenck No. 3 C	116	10793-10890	S/I	53/05/23	4639	67/03/16	1266
Chocolate Bayou	Schenck No. 3T	116	11360-11230	S/I	61/06/27	6897	87/05/21	254
Chocolate Bayou	Schenck No. 3U	116	10985-10957	S/I	68/02/05	2707	89/03/31	1102
Chocolate Bayou	No. U-1 Houston	91		NA				
Chocolate Bayou	No. 1 McIlvaine	90		NA				
Chocolate Bayou	No. Z-1 Houston Frm.	143		NA				
Chocolate Bayou	Houston Farms Dev. Co.	145		NA				
Chocolate Bayou	No. B Houston Frm.	130		NA				
Chocolate Bayou	Houston 'AA' No. 1	144		NA				
Chocolate Bayou	Houston 'Y' No. 1	142		NA				
Chocolate Bayou	No. X-1 Houston Frm.	141	12104-12064	NA	12/17/54	7056		
Chocolate Bayou	No. 2 Houston Farm Dev. Co.	140		NA				

Table A-1. (cont.)

Field name	Well name	Log no.	Interval (ft)	Status	Date	BHP (psi)	Date	BHP (psi)
Chocolate Bayou	Houston Farms Dev. Co.No. 1	177	15031-14989	NA	11/21/67	9556		
Chocolate Bayou	Archibald No. 1	199	11796-11812					
Chocolate Bayou	Andrau No. 1	193						
Chocolate Bayou	Houston Farms Dev. Co.No. 1	241						
Chocolate Bayou	No. 1 Persimmon Bayou Tract 151	139						
Chocolate Bayou	Houston Farms Dev. Co.No. 1	181						
Martin Ranch (S)	No. 5 T.Martin Fee	188	14889-14999	ACT	5/24/74	12660		
Martin Ranch	No. 3 Martin	933		NA				
Martin Ranch (Frio 14600)	Martin, T., Fee Well No. 1	929 or 261	14664-14684	S/I	73/01/10	12723	86/04/14	5286
Martin Ranch (Frio 14600)	Martin, T., Fee Well No. 4	930	13876-13880	P&A	74/02/12	12199	83/05/08	4965
Liverpool	No. 1 Callahan	198	8757-8762	P&A(O)				
Liverpool	No. 1 M.F. Baugh	197	10566-10583	NA				
Liverpool	Todd Unit No. 1		10170-10206	ACT	84/08/04	7079	89/01/17	2753
Liverpool	Hary GroupeNo. 1	239						
Liverpool	FingerNo. 1	173						
Danbury	South Texas Dev. Co. NCT-1 Well No. 1	263						
Danbury	R.W. ViemanNo. 1	174	13251-13264		11/15/63	10633		
Danbury	No. 2 S.D. Hawley	243		NA				
Danbury	No. 1 S.D. Hawley	242		NA				
Danbury	No. 1 Houston Frm.	181		NA				
Danbury	No. 1 J.M. Skrabanek	175		NA				
Danbury	No. 1 Houston Frm.	186	12154-12126	NA				
Danbury,S	M.E. Hunter No. 1	176						
Danbury,S (Anomlina 2, Frio 10)	No. 1 Vieman	244	10822-10775	S/I	5/24/65	10633		
Danbury,S (Frio 11700)	No. 2 R.W. Vieman		11320-11302	P&A	1/10/77	7769		
Danbury,SW (Frio Lower 12550)	No. 1 H.L. Peterson	246	12564-12544	ACT	77/06/04	9095	88/11/29	1972
Danbury,SW (12100-A)	No. 1 Marmion, James R.	259	12078-12120	ACT	78/10/11	7617	88/11/29	1945
Danbury,SW (12900-E)	No. 1 Renn, Phillips	260	12890-12910	ACT	12/20/78	10563	88/11/29	1838
Algoa,NW. (Frio F-46)	No. 1 William R A	926	10506-10475	ACT	6/4/83	5582	88/12/29	2029
Algoa (47)	No. 1 Cooper Williams Gas Unit	218	11535-11502	P&A	10/16/78	7956		
Algoa (45)	No. 1 Winton Gas Unit	215	11487-11439	ACT	67/10/30	7006	86/04/05	3552
Algoa (45)	Cooper 'B' Unit No. 1	182	11514-11524	P&A	55/05/16	8015	83/07/06	3150
Algoa (48)	No. 1 Cooper Unit	217	11676-11644	ACT	54/09/25	9207	2/19/79	7685
Wildcat, Algoa Area	Algoa Townsite Well No. 1	214						
Wildcat,Algoa Orchard Area	Joe Tocker O/ANo. 1	36		NA				
Algoa Orchard	Orchard Gas(Oil) Unit No. 1 O/A	39A						

Table A-1. (cont.)

Field name	Well name	Log no.	Interval (ft)	Status	Date	BHP (psi)	Date	BHP (psi)
Rattlesnake Mound,W (Schenck)	No. 1 Shell Point	185	14283-14279	ACT	74/12/15	10442	881218	1059
Rattlesnake Mound (Andrau)	No. 1 Houston Frm.			P&A				
Rattlesnake Mound	No. 1 S/L 66709		12390-12371	NA	1/5/77	9696		
Rattlesnake Mound	No. 3 Alligator Point Unit		11107-11106	NA	8/23/77	9049		
Rattlesnake Mound	No. 1 Alligator Point Unit	187	11499-11498	NA	2/6/76	9587		
Rattlesnake Mound	No. BB-1 Houston Frm.	189	11278-11250	NA	11/3/62	10000		
Hoskins Mound	No. 1 Hoskins Mound Fee			NA				
Hoskins Mound	Hoskin Mound Fee NCT-1 Well No. 1			NA				
Alta Loma (Schenck)	No. A-1 Christensen	82	12778-12743	P&A	4/12/56	8122		
Alta Loma (Weiting Lower)	No. A-2 Tacquard	66A	13014-13022	P&A	9/29/64	10755		
Alta Loma (Weiting Lower)	Evan ANo. 1	69		P&A				
Alta Loma (10200 Frio)	No. 1-1 C.S. Thompson et al	256		P&A				
Alta Loma	No. B-1 J.W. Harris	34		NA				
Alta Loma	No. 1 Crane Gas	255		NA				
Alta Loma	No. 2 C.E. Franks Gas UN.		11444-11409	NA	6/6/64	5665		
Alta Loma	No. 1 Corine Scott	212		NA				
Alta Loma	No. 1-A Tacquard et al	51	12368-12372	NA	10/13/57	9693		
Alta Loma	No. 2-A Tacquard et al		12254-12228	NA	11/1/66	3871		
Alta Loma	No. 2 SH Green et al UN.	252	11375-11354	NA	3/14/64	7693		
Alta Loma	No. B-2 Pabst	53		NA				
Alta Loma	No. 1 Hulen	84		NA				
Alta Loma	No. 1 Halls Bayou Ranch	76		NA				
Alta Loma	No. 1 Nana	87	10136-10143	NA	12/27/57	4810		
Alta Loma	No. B-13 Macomstewart			NA				
Alta Loma	No. 4 Erwin-Bishop			NA				
Alta Loma	No. 2 Camp Wallace	934	11501-11469	NA	9/6/65	6880		
Alta Loma	No. 1 A.G. Crouch et al		10829-10802	NA	5/22/63	7103		
Alta Loma	No. 2 Camp Wallace	937	11513-11494	NA	4/24/64	5941		
Alta Loma	No. 1 Hervey et al	935	12457-12427	NA	3/4/58	6340		
Alta Loma	No. 1 Beaver G.A.	211	12247-12205	NA	10/5/59	5700		
Alta Loma	No. 1 Stewart Gas Unit	210	10729-10742	NA	2/2/60	4785		
Alta Loma	No. 1 Joe Black Trustee		11202-11210	NA	6/4/80	1699		
Alta Loma	No. 1 Tibaldo Louis Unit	924	11041-11003	NA	4/24/82	4495		
Alta Loma,W (Banfield)	No. 1 Adriance	920	11165-11162	ACT	10/8/80	4022	87/01/26	2577
Alta Loma,W (Schenck)	No. 2 H. Sayko et al	50	11279-11285	P&A	11/20/64	5630		
Alta Loma,W (Schenck Upper)	No. 2 H. Sayko et al	50	11164-11214	P&A	11/20/64	3058		

Table A-1. (cont.)

Field name	Well name	Log no.	Interval (ft)	Status	Date	BHP (psi)	Date	BHP (psi)
Alta Loma,W	Pabst BNo. 3	49	11410-11373	P&A	6/8/68	7809		
Alta Loma,W (R-1 A)	No. 1 W.N. Zinn	45	12862-12839	P&A	8/2/73	9207		
Alta Loma,W (Hulen)	No. 1 T. Hulen	86	14461-14441	P&A	6/6/75	12450		
Alta Loma,W	No. 1 J.M. Harris	44	12678-12683	NA	2/5/72	10508		
Alta Loma,W (S-1)	No. 1-B Harrus, J.W. -B-	936		P&A				
Alta Loma,S (Frio 12600)	No. 1 SUN-AMOCO Feeleas	81	12547-12528	P&A	6/3/75	10214		
Alta Loma,S (Tacquard)	No. 1 Reitmeyer-Brisco	85	13036-13014	P&A	10/2/77	10405		
Alta Loma,SW (Schenck)	No. 1 A.B. Marshall	161	12808-12784	P&A	7/21/69	10505		
Alta Loma,SW(Banfield)	No. 1 A.B. Marshall	161	12590-12564	P&A	7/21/69	10397		
Alta Loma,SW (Andrau)	No. 1 Lucille Konzack	79		P&A				
Alta Loma,SW	No. 2 A.B. Marshall	77		NA				
Alta Loma,SW	No. 3 A.B. Marshall	160		NA				
Alta Loma,SW	No. 1 G Mc Ilvaine O No. 1	89 or 919	13564-13549	NA	10/10/76	10921		
Alta Loma,SW (14280)	U.S. NAT. Bank OF Galy TR.Well No. 1	931	14280-14288	ACT	8/1/85	12191	89/01/30	2849
Alta Loma,E (S Sand)	No. 1 Ben Sase	59		P&A				
Alta Loma,E	No. 1 3RD Ntl Bk Nashvll	923	11260-11255	NA	8/27/81	6825		
Alta Loma,E	Firth Unit No. 1 Well No. 1	917	11710-11680	NA	2/19/79	9290		
Alta Loma,E	No. 1 S.L. Henck	64	12834-12842	S/I	2/15/59	9256		
Alta Loma,E (Andrau Lower)	Mc VeaNo. 1	70		P&A				
Alta Loma,E (Andrau Lower)	No. 3 O'Daniel	71	14578-14540	P&A	1/26/66	11048		
Alta Loma,E (S)	O Daniel Unit No. 2 A	927	13825-13840	ACT	88/01/15	10854	89/01/16	7473
Alta Loma	No. 1 Clark B	262	13000-13030					
Alta Loma	Proctor Gas Unit No. 1	208						
Alta Loma (Lower Houston Farm)	R.B. Wilkins No. 1	54	11300-11308		3/22/59	8714		
Alta Loma	No. 3 Craig	74	9240-9250					
Wildcat,Alta Loma Area	Oldham No. 1	267						
Wildcat,Alta Loma Area	Mc Kinley No. 1	209						
Wildcat,Alta Loma Area	No. 1 L.B. Bishop Unit	216	10738-10750		2/5/59	4740		
Wildcat, Alta Loma Area	Brisco-Dycene No. 1	37						
Alta Loma,N	W.E. Eggers Gas Unit No. 1	32						
Hitchcock	Prets No. 1	180		NA				
Hitchcock	No. 1-1 Hitchcock Gas Unit	183		NA				
Alvin,S	No. 1 Concklin Oil UN.	221	11775-11717	NA	10/18/69	7525		
Alvin,S (No. 39 SEG D)	No. 3 Lockkkhart BK U	224	10950-10899	ACT(O)	10/10/76	7951		
Alvin,S	No. 1 Tiemann	219	11191-11150	NA	10/13/51	7100		
Alvin,S	No. 1 Krauss L M Gas UN		11835-11779	NA	12/11/63	7275		

Table A-1. (cont.)

Field name	Well name	Log no.	Interval (ft)	Status	Date	BHP (psi)	Date	BHP (psi)
Alvin,S (No. 46)	Lockhart Bank Unit No. 1 Well No. 2	269 or 928	10497-10525	ACT	63/04/01	7614	88/05/02	3167
Wildcat, Alvin Area	C.P. TongNo. 1	223						
Rowan,N	No. 1 E.L. Summers	229	10861-10805	NA	1/9/68	7176		
Rowan,N	No. 1 Rosa Clark et al.	230		NA	7/11/53	7515		
Rowan,N	E.W. WissnerNo. 1	236						
Rowan,N	NW. Rowan Gas Unit1 Well No. 1	237						
Rowan,S	Manual Rudy No. 1	200	10167-10179		11/1/62	4430		
Angleton,NE	Dan Moody No. 1	266	11480-11520					
Oliver	R.C. Parsley Estate No. 1	225						

SECTION II: HYDROCHEMICAL STUDIES FOR LONG-TERM-FLOW TESTING OF PLEASANT BAYOU GEOPRESSURED GEOTHERMAL WELL NO. 2

Regina M. Capuano and Mark E. Erwin

ABSTRACT

Results of chemical analyses of 18 formation-fluid samples produced during long-term-production testing of the Pleasant Bayou No. 2 geopressured geothermal well were compiled and evaluated for short-term and long-term trends, or both, during high-rate production from May 30, 1988, through April 4, 1989. Errors introduced into the data as a result of sampling procedures and analytical limitations for each element are discussed, as well as batch accuracies from a duplicate analysis of selected ions on the initial 14 brine samples. Taking these errors into consideration, measurable changes in brine chemistry of both major and minor elemental concentrations and trends in concentration changes were determined.

Overall brine salinity (TDS), as well as the concentration of many major elements, increased rapidly during the first 40 d of production and then more slowly through the remainder of production. Short-term changes in brine chemistry were also observed. Some were within the limits of analytical uncertainty, but some were not.

Possible causes of both long- and short-term changes in brine chemistry were investigated, including production-induced chemical changes, shifts in fluid source, and natural variations in the production-zone fluid chemistry. The large analytical uncertainties associated with most elements (5 to 25 percent), combined with a lack of chemical control both laterally and vertically away from the Pleasant Bayou No. 2 well, prohibit any definitive statements on the cause or causes of chemical changes in the formation fluid produced through the current production period. However, several lines of evidence suggest that natural lateral variations in the production-zone fluid composition may be responsible for the changes observed.

INTRODUCTION

The hydrochemistry of the brines produced from Pleasant Bayou No. 2 well and brines from surrounding areas was evaluated to determine if there were measurable chemical changes over time that might be indicative of changes in the source of water being produced. To do so required a three-step approach: (1) a review of sampling procedures, (2) an evaluation of hydrochemical data over the recent flow-testing program, and (3) a comparison of data from current testing to previously collected data.

REVIEW OF SAMPLING AND ANALYTICAL PROCEDURES AND SCHEDULES

Within the first task three subtasks need to be considered:

1. Interaction with the organizations and institutions that are sampling and analyzing fluids at Pleasant Bayou to ensure that the procedures currently being used are providing samples that are representative of the deep-reservoir brine.
2. In conjunction with the Institute of Gas Technology (IGT), design and implementation of an on-site chemical monitoring program that would permit sampling procedures to be modified in the event that a significant chemical change occurs.
3. Preparation of a sampling and analysis schedule that will allow timely prediction of changes in fluid composition, by estimation of the largest sampling interval and least number of different analyses on each sample to provide data needed for this prediction.

The proper collection and analysis of samples is required to permit the quantitative hydrochemical research proposed in this study. To obtain scientifically meaningful samples and analyses of geopressured geothermal reservoir fluids, sampling procedures must be used that differ from those commonly used to collect and analyze shallower water samples. Some of the concerns are that (1) analytical techniques be tailored to highly concentrated sodium-chloride

brines, (2) standardization and quality assurance be practiced, (3) gas and liquid samples be properly preserved for later analysis, (4) gas and liquid compositions be collected from the samples simultaneously whenever possible, (5) wellhead pressure and temperature be recorded when fluids are sampled, (6) sample separation pressure and temperature be recorded, (7) key analyses be done on site immediately after sample collection, and (8) the full suite of necessary analyses be completed.

Interactions with Organizations That Have Current Sampling Responsibilities

Bureau of Economic Geology (BEG) personnel conducted three site visits and had numerous phone conversations with IGT personnel to review sampling and on-site analysis procedures. IGT personnel collected brine and gas samples monthly to semimonthly under the site management of Eaton Operating Company.

Brine samples were collected using a preservation technique developed earlier in the history of the Geopressured Geothermal Program by M. Thomson at Rice University in Houston, Texas (P. L. Randolph, 1989, personal communication). The current procedure for collection of samples (see discussion below) was developed early in the program when it was only necessary to stabilize those elements in the brine samples that were needed to solve corrosion and scaling problems, such as iron and bicarbonate in the brine. Reviewing the brine sampling procedures reveals that the samples are not adequately preserved to stabilize those elements needed to characterize the reservoir fluid or to document hydrochemical changes occurring in response to long-term production. Much research has been conducted on the proper methods of collecting and preserving geothermal brine samples for hydrochemical studies (see for example, Kindle and Woodruff, 1981; Lico and others, 1982). We suggest that the brine-sampling procedure be revised to provide more useful samples. Some of the problems resulting from inadequate preservation techniques are addressed later. Suggestions for the need for greater analytic accuracies for several elements also appear later.

Design and Implementation of an On-site Chemical-Monitoring Program

This task was proposed to permit sampling procedures to be modified in the event that significant chemical changes occur. When this project was proposed, however, limited IGT and Eaton Operating Company funds for FY89 did not permit its implementation.

Preparation of a Sampling and Analysis Schedule That Will Allow Timely Prediction of Changes in Fluid Composition

More frequent sampling of a conservative element such as chloride could permit a better comparison than can be drawn from the current sampling schedule between wellhead pressure and chemical changes in the reservoir fluid. These small-scale changes, rather than those described for the long-term-production period in the next discussion may give insights into the effects of pressure reduction on the drainage of shale layers. This subject is discussed briefly in the section on hydrogeology (p. 22). In addition to chloride samples, a brine sample could also be collected and stored for later analysis if determined important. The timing between these samples should be shorter than the timing between the wellhead-pressure drop of interest.

EVALUATION OF HYDROCHEMICAL DATA FROM CURRENT TESTING SCHEDULE

A three-step program was proposed for studying the temporal changes in fluid composition during the long-term-production testing of Pleasant Bayou No. 2 well scheduled for FY89. The first two steps scheduled for completion in FY89 are (1) to evaluate whether well-bore and production-related perturbations in chemistry significantly altered formation fluid and gas composition and (2) to evaluate shifts in fluid chemistry that may result from shifts in fluid sources or hydrologic regimes. The third and final step, not scheduled for completion in FY89,

includes a quantitative characterization of the liquid and gas resources of the Pleasant Bayou reservoir and identification of recharge fluids and their sources.

Long-term Production Testing—Sample Collection

The Pleasant Bayou No. 2 well commenced long-term-production testing on May 27, 1988. Brine production initially averaged between 19,000 and 20,000 barrels/day (bpd) and currently averages around 17,000 bpd (fig. 1). Brine, gas, and condensate samples were collected for analysis by IGT representatives on a roughly semimonthly basis beginning May 30, 1988. Fluid compositions from these long-term-production samples are taken from Eaton Operating Company monthly reports prepared for the Department of Energy. Chemical analyses provided in Eaton Operating Company's monthly reports, up to and including June 1989, were considered. Analyses available after that time will be considered next year if funding permits. This study focuses on the changes in the composition of the brine samples through the period described earlier.

Production-related data, such as bottom-hole pressure and fluid temperature, were collected on a daily basis during the long-term testing and are also compiled in the Eaton Operating Company Monthly Reports to DOE. These reports are the source of production data presented later.

Brine samples were collected close to the wellhead just after the first choke. The pressure at the collection point was maintained between approximately 900 and 1,000 psi during most of production. Surface brine samples were also collected just before reinjection, but these analyses are not discussed in this report because of the additional chemical changes that could have resulted during flow to the disposal well.

Brine samples were collected using a preservation technique developed earlier in the history of the Geopressured Geothermal Program by M. Thomson at Rice University in Houston, Texas (P. L. Randolph, personal communication, 1989). Upon collection the brine ran

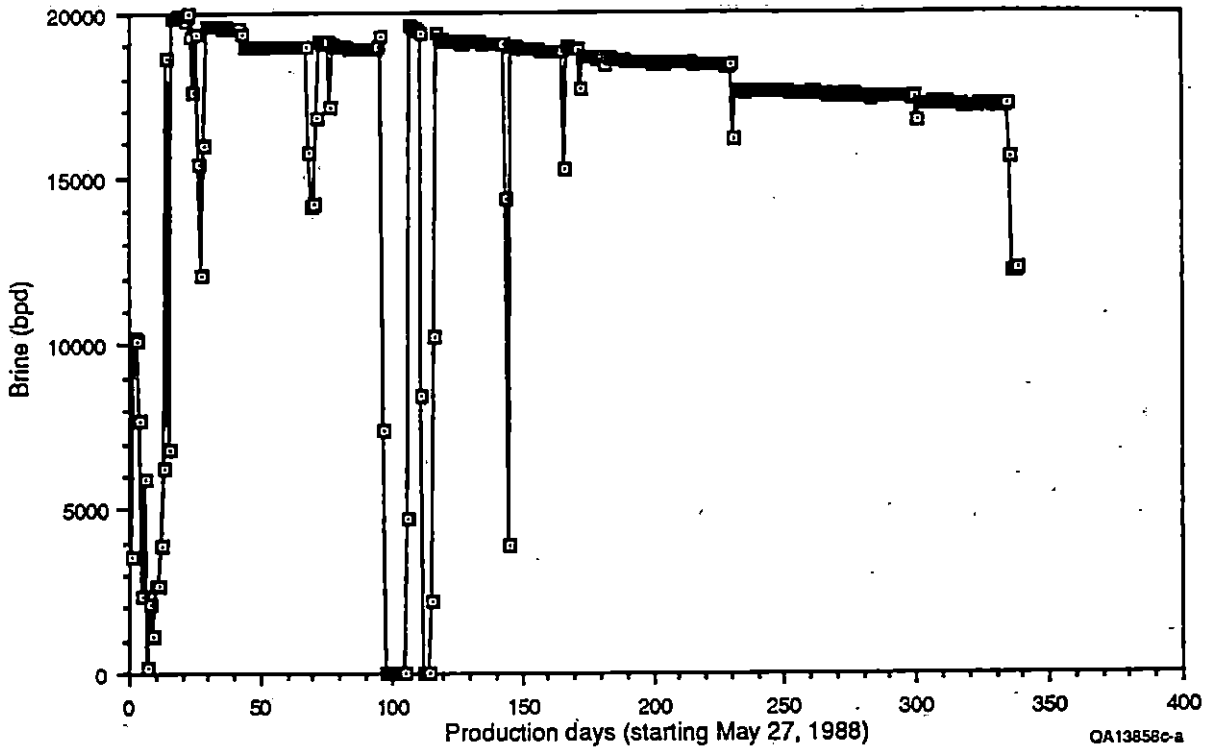

Figure 1. Daily brine production (bbl/d) of Pleasant Bayou No. 2 through the current production period (May 27, 1988, through April 30, 1989). The large drops in pressure represent well shut-ins.

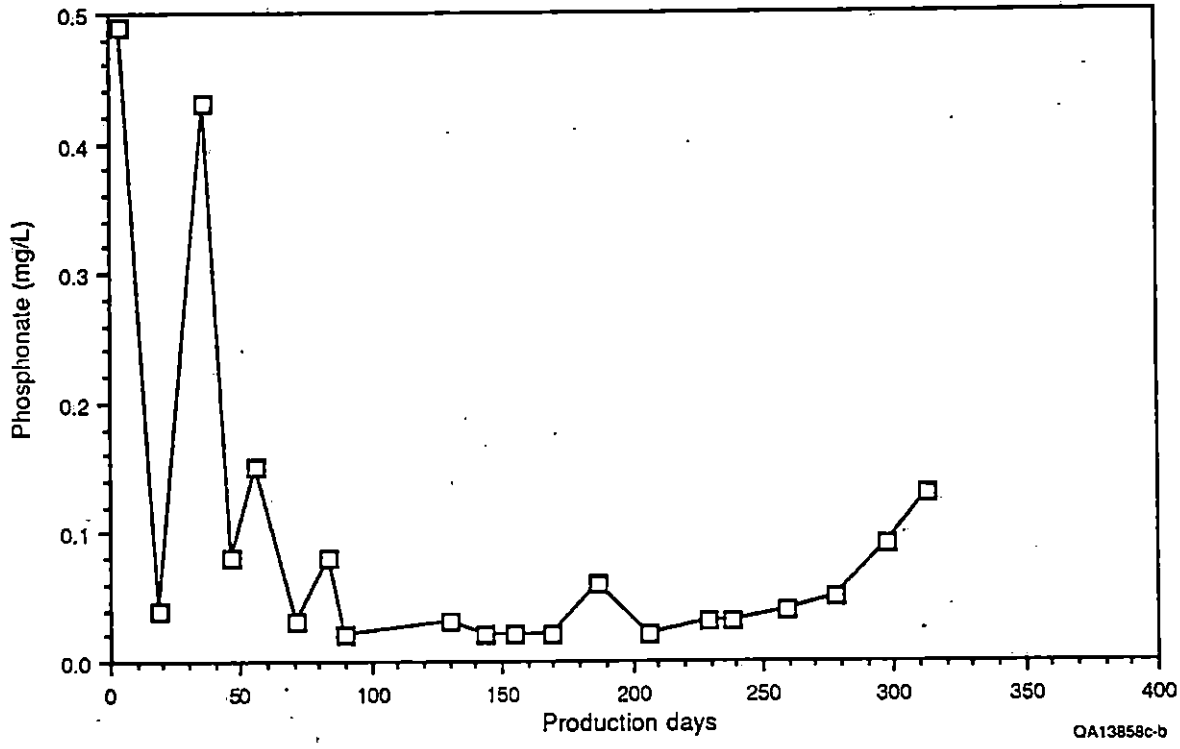

Figure 2. Phosphonate- (scale inhibitor) concentration data (mg/L) of Pleasant Bayou No. 2 through the current production period.

through a stainless steel cooling coil and flowed into a polyethylene bottle that was open to the atmosphere. As the sample flowed into the bottle, carbon dioxide was bubbled into it, and when the polyethylene sample bottle was full it was immediately capped. The corrosion inhibitors that were injected between the wellhead and the first choke were not stopped before sample collection. Within a couple of days, alkalinity was analyzed; then the samples were able to be shipped to a laboratory where the remainder of the chemical analyses were performed. The samples were not filtered and no other precautions were taken to stabilize chemicals in solution. We suspect that many of the elements in solution may have become unstable as a result of the large decrease in fluid pressure from approximately 10,000 psi and temperature from approximately 147°C to the sample collection pressure and temperature at atmospheric conditions. We suggest that the brine-sampling procedure be revised to provide more useful samples. Some of the problems resulting from inadequate preservation techniques are addressed later.

Brine Analyses

Brine samples were analyzed at the BEG Mineral Studies Laboratory for sodium (Na), magnesium (Mg), calcium (Ca), potassium (K), strontium (Sr), barium (Ba), iron (Fe), manganese (Mn), zinc (Zn), lithium (Li), silica (SiO_2), boron (B), chloride (Cl), ammonia (NH_3), bromide (Br), fluoride (F), iodide (I), sulfate (SO_4), arsenic (As), chromium (Cr), lead (Pb), nickel (Ni), cadmium (Cd), copper (Cu), mercury (Hg), and tin (Sn), as well as for alkalinity and total dissolved solids (TDS). Analytic procedures, their accuracy, and their detection limits when applicable, are listed in table 1. For some elements the relative batch accuracies are also listed. These batch accuracies are taken as the relative standard deviations for a set of analyses and are generally much lower than the analytic accuracy. Eight of these elements were not detected above the instrumental detection limits: arsenic, chromium, lead, nickel, cadmium, copper, mercury, and tin.

Table 1. Analytic procedures, accuracies, and detection limits of elements analyzed.

Element	Accuracy (relative)	Batch accuracy[a]	Detection limit[b]	Analytic procedure
	(%)	(%)		Reference
Na	5	2		Koppenaal, 1987a
Mg	5	1		Koppenaal, 1987a
Ca	5	2		Koppenaal, 1987a
K	5	4		Koppenaal, 1987a
Sr	25	4		Koppenaal, 1987a
Ba	25	2		Koppenaal, 1987a
Fe	25	7.2		Koppenaal, 1987a
Mn	25	4.4		Koppenaal, 1987a
Zn	25	21		Koppenaal, 1987a
Li	25	8		Koppenaal, 1987a
SiO_2	25	6		Koppenaal, 1987a
B	25	6		Koppenaal, 1987a
Cl	5	1		Koppenaal, 1986a, Tweedy, pers. comm.(1989)
NH^3	5			Tweedy, pers. comm.(1989)
Br	5			Koppenaal, 1986b
F	2			Koppenaal, 1987b
I	15			Koppenaal, 1986d
SO^4	5			Koppenaal, 1986c
Alkalinity	5			Koppenaal, pers.comm.(1988)
TDS[c]	2[d]			Tweedy, pers. comm.(1989)
As	BDL[e]		<0.5	Koppenaal, 1987a
Cr	BDL		<0.1	Koppenaal, 1987a
Pb	BDL		<1	Koppenaal, 1987a
Ni	BDL		<0.25	Koppenaal, 1987a
Cd	BDL		<0.1	Koppenaal, 1987a
Cu	BDL		<0.1	Koppenaal, 1987a
Hg	BDL		<0.025	ASTM, 1984, D3223-80
Sn	BDL		<0.25	Koppenaal, 1987a

[a] relative standard deviation for analyses performed in a group
[b] units in mg/L unless otherwise noted
[c] TDS = total dissolved solids
[d] represents precision, not accuracy
[e] BDL = below detection limits in all cases

Change in Brine Chemistry during Long-term Production

Eighteen analyses of brine samples collected from the Pleasant Bayou No. 2 well during long-term production were available for study as of July 24, 1989. These analyses, listed in table 2, cover a period beginning May 30, 1988—4 d after the start of production—through April 4, 1989—313 d after the start of production. In the following section, errors introduced into the data as a result of sampling and analysis are discussed for each element analyzed in the brine. Then, taking these errors into consideration, we determine whether measurable changes in the concentration of these elements occur during production and whether these changes follow a trend over time.

The inaccuracies of the majority of the chemical analyses conducted on the brine samples are generally high, 5 to 25 percent (table 1). One reason is the high concentration of the brine (>120,000 mg/L). Some of these relative errors may be reduced by adjusting the analytic procedure (S. Tweedy, personal communication, 1989); we thus recommend that the analytic procedures be reviewed in order that methods be found to improve accuracy of future sampling at this well.

Because of the possibly large inaccuracies in the data, we tried to focus on the trends revealed within the limits of the inaccuracies. After all, for some elements the potential errors were actually lower than those listed in table 1. A series of duplicate analyses conducted on the initial 14 brine samples were thus compared with the original analyses. These duplicate samples were run in a single batch, and a batch accuracy was provided with the data (table 1). In all cases except one the batch accuracies were more than 50 percent better than the analytic accuracies. The results of these duplicate analyses were compared with the initial analytic results to estimate whether the accuracy considered in this report could be taken as the lower batch accuracy or value intermediate between the batch and the relative accuracy of the

Table 2. Pleasant Bayou No. 2 flow-test brine chemistry.

Date of sample	Data source	BHP (psi)	WHP (psi)	Brine (bpd)	Gas (Mcfd)	Gas/brine (cf/b)	Brine-cum (mb)	Gas-cum (MMcf)	Brine temp. (°F)	S.G. (60F)	TDS (mg/L)	Alk. (mg $CaCO_3$/L)	NH_3 (mg/L)
05/30/88	1		4037	7699	186.4	24.21	65.93	1.555	240	1.085	127000	309	
05/30/88	2												
06/14/88	1	10092	3061	19895	481.2	24.19	203.17	4.82	288	1.082	124000	310	83
06/14/88	2												
07/01/88	1	10138	3123	19531	462.7	23.69	519.31	12.26	290	1.08	132900	211	83
07/01/88	2												
07/21/88	1	10091	3120	18940	444.8	23.48	902.22	21.32	290	1.08	132900	291	85
07/21/88	2												
08/05/88	1	10330	3507	14132	332.9	23.56	1173.45	27.68	288	1.07	132600	295	86
08/05/88	2												
08/24/88	1	10038	3048	18854	447.3	23.72	1529.32	36.05	291	1.08	133900	301	86
08/24/88	2												
10/03/88	1	10007	2997	19075	458.8	24.05	2021.82	47.81	291	1.085	133000	286	87
10/03/88	2												
10/17/88	1		3226	14303	342.9	23.97	2283.74	54.11	261	1.087	134100	283	88
10/17/88	2												
28/17/88	1	9949	2970	18858	451.3	23.93	2476.6	58.73	291	1.084	133400	292	86
28/17/88	2												
11/11/88	1	9920	2936	18903	454.3	24.03	2736.3	64.96	291	1.085	134300	299	89
11/29/88	1	9908	2935	18535	447.3	24.13	3070.72	73.02	291	1.082	134200	311	89
11/29/88	2												
12/19/88	1	9884	2910	18446	445.4	24.15	3440	81.95	291	1.08	133800	315	89
12/19/88	2												
01/10/89	1	9822	2889	18325	439.3	23.97	3845.01	91.71	291	1.079	132800	305	88
01/10/89	2												
01/20/89	1	9889	2957	17566	423.3	24.1	4019.92	95.92	289	1.081	133900	272	88
01/20/89	2												
02/09/89	1	9865	2939	17515	423.6	24.18	4370.68	104.34	290	1.088	133100	208	88
02/28/89	1	9846	2926	17407	421.1	24.19	4702.61	112.29	290	1.091	134900	226	88
03/20/89	1	9836	2915	17414	418.8	24.05	5050.9	120.68	290	1.086	135100	227	88
04/04/89	1	9841	2929	17206	412.2	23.96	5308.7	126.87	290	1.085	133700	245	90

Data source: 1= BEG original analyses, Eaton Operating Co., Inc., monthly report, May 1989; 2= BEG duplicate analyses (Steve Tweedy, personal communication, 1989). **BHP** = bottom-hole pressure. **WHP** = wellhead pressure. **Brine-cum** = cumulative brine production. **Gas-cum** = cumulative gas production. **S.G.** = specific gravity (at 60° Fahrenheit). **TDS** = total dissolved solids. **Alk** = alkalinity. Blanks in the data set represent undetermined values.

Table 2. (cont.)

Date of sample	Data source	As (mg/L)	Ba (mg/L)	B (mg/L)	Br (mg/L)	Cd (mg/L)	Ca (mg/L)	Cl (mg/L)	Cr (mg/L)	Cu (mg/L)	F (mg/L)	I (mg/L)	Fe (mg/L)	Pb (mg/L)	Li (mg/L)	Mn (mg/L)
05/30/88	1	< 0.5	803	23		< 0.1	7620	70200	< 0.1	< 0.1			44	<1	30	14
05/30/88	2		741	25.9			7380	70310					47.1	<1	29.6	15.9
06/14/88	1	< 0.5	805	23	74	< 0.1	7700	70400	< 0.1	< 0.1	1.5	23	42	<1	30	14
06/14/88	2		757	32.1			7520	69590					47.2	<1	29.4	16.3
07/01/88	1	< 0.5	757	24	80	< 0.1	7760	72200	< 0.1	< 0.1	1.6	21	45	<1	31	15
07/01/88	2		742	29.6			7570	71590					59.7	<1	28.6	16.6
07/21/88	1	< 0.5	765	25	73	< 0.1	7940	71200	< 0.1	< 0.1	1.5	22	45	<1	31	16
07/21/88	2		752	27.1			7710	72340					49.5	<1	25.3	17.3
08/05/88	1	< 0.5	769	25	78	< 0.1	7890	72400	< 0.1	< 0.1	1.7	22	47	<1	32	16
08/05/88	2		751	27.2			7810	71660					47.7	<1	24.4	17.6
08/24/88	1	< 0.5	767	25	75	< 0.1	7960	72000	< 0.1	< 0.1	1.6	23	45	<1	32	16
08/24/88	2		743	26.4			7690	72230					46.9	<1	24.9	17.2
10/03/88	1	< 0.5	770	20	73	< 0.1	8010	71700	< 0.1	< 0.1	1.5	20	55	<1	30	19.2
10/03/88	2		746	26.6			7760	71700					46.7	<1	25.8	17.5
10/17/88	1	< 0.5	760	19	77	< 0.1	7970	72000	< 0.1	< 0.1	1.4	21	58	<1	29	19.3
10/17/88	2		747	26.6			7720	72030					50.7	<1	26.3	17.6
28/17/88	1	< 0.5	750	19	75	< 0.1	7890	71600	< 0.1	< 0.1	1.5	21	56	<1	29	19.2
28/17/88	2		749	27			7740	71560					49.9	<1	26.1	17.8
11/11/88	1	< 0.5	770	20	75	< 0.1	7860	72700	< 0.1	< 0.1	1.4	21	52	<1	32	19.1
11/29/88	1	< 0.5	770	20	75	< 0.1	7900	72900	< 0.1	< 0.1	1.4	21	54	<1	31	19.2
11/29/88	2		782	27.4			8010	72640					18.4	<1	26.1	18.4
12/19/88	1	< 0.5	780	27	78	< 0.1	7940	71600	< 0.1	< 0.1	1.4	21	54	<1	27	18.3
12/19/88	2		778	26.8			7940	71590					54	<1	23.9	18.3
01/10/89	1	< 0.5	760	27	76	< 0.1	7860	71700	< 0.1	< 0.1	1.4	21	49	<1	27	18.1
01/10/89	2		761	26.7			7860	71650					49.1	<1	24	18.1
01/20/89	1	< 0.5	770	29	75	< 0.1	7890	72300	< 0.1	< 0.1	1.5	21	53	<1	27	17.9
01/20/89	2		768	27.1			7890	72270					51.4	<1	23.3	17.9
02/09/89	1	< 0.5	790	31	75	< 0.1	7920	71900	< 0.1	< 0.1	1.7	75	49	<1	29	17
02/28/89	1	< 0.5	790	31	77	< 0.1	7990	72900	< 0.1	< 0.1	1.8	20	49	<1	29	17
03/20/89	1	< 0.5	790	31	77	< 0.1	7940	72800	< 0.1	< 0.1	1.9	21	49	<1	29	17
04/04/89	1	< 0.5	790	31	70	< 0.1	7970	72900	< 0.1	< 0.1	1.7	19	49	<1	29	17

Table 2. (cont.)

Date of sample	Data source	Mg (mg/L)	Hg (mg/L)	Ni (mg/L)	K (mg/L)	SiO_2 (mg/L)	Na (mg/L)	Sr (mg/L)	SO_4 (mg/L)	Sn (mg/L)	Zn (mg/L)
05/30/88	1	553		< 0.25	522	103	35000	838			0.60
05/30/88	2	560			531	87.9	36400	895			0.41
06/14/88	1	564	< 0.005	< 0.25	530	100	35300	855	13		0.70
06/14/88	2	577			557	92.3	37500	955			0.43
07/01/88	1	593	< 0.005	< 0.25	542	106	35900	864	1	< 0.25	0.50
07/01/88	2	571			544	94.6	36200	911			0.40
07/21/88	1	603	< 0.005	< 0.25	554	106	36400	866	4	< 0.25	0.40
07/21/88	2	578			535	82.3	36900	903			0.35
08/05/88	1	604	< 0.005	< 0.25	565	108	36900	827	2	< 0.25	0.60
08/05/88	2	579			581	81.7	36900	985			0.43
08/24/88	1	604	< 0.005	< 0.25	561	108	36700	850	6	< 0.25	0.50
08/24/88	2	572			555	81.2	36700	921			0.39
10/03/88	1	612	< 0.025	< 0.25	570	94	37400	930	1	< 0.25	0.40
10/03/88	2	582			563	80.9	36000	877			0.40
10/17/88	1	609	< 0.025	< 0.25	580	88	36800	930	1	< 0.25	0.30
10/17/88	2	584			578	80.9	37400	933			0.39
28/17/88	1	603	< 0.025	< 0.25	570	92	36500	900	1	< 0.25	0.40
28/17/88	2	580			582	81.4	37600	955			0.43
11/11/88	1	574	< 0.025	< 0.25	540	90	35800	892	1	< 0.25	0.30
11/29/88	1	577	< 0.025	< 0.25	550	90	35700	870	4	< 0.25	0.30
11/29/88	2	589			588	82.6	38700	959			0.33
12/19/88	1	590	< 0.025	< 0.25	600	88	37000	950	1	< 0.25	0.20
12/19/88	2	590			601	79.7	38100	952			0.21
01/10/89	1	590		< 0.25	580	89	36700	880	1	< 0.25	0.30
01/10/89	2	588			580	80.6	37700	882			0.25
01/20/89	1	590		< 0.25	580	85	36500	910	1	< 0.25	0.20
01/20/89	2	587			584	78	37600	915			0.25
02/09/89	1	584		< 0.25	600	91	35900	930	4	< 0.25	0.40
02/28/89	1	588		< 0.25	600	89	36700	930	4	< 0.25	0.40
03/20/89	1	585		< 0.25	610	90	36100	900	4	< 0.25	0.40
04/04/89	1	588		< 0.25	610	90	35900	900	3	< 0.25	0.40

procedure. On the basis of these comparisons, a probable analytic error was estimated as a value between the batch and analytical accuracies.

Scale-inhibitor-pill Injection

On April 20, 1988, a scale-inhibitor pill containing 514 kg of aminotrimethylenephosphonic acid (ATMP) was injected into the reservoir. During clean-up flow, 220 kg of ATMP was recovered from the reservoir, leaving 294 kg. An additional 38 kg of ATMP was produced between the clean-up flow and July 21, 1988 (56 d of flow), leaving about 256 kg of ATMP in the reservoir (Eaton Operating Co., Inc., 1988a).

Brine samples produced from the well were periodically analyzed for phosphonate. The results of these analyses are shown in figure 2 (data from Eaton Operating Co., Inc., 1989a and 1989b). Phosphonate levels fell off quickly between the time of injection (0.5 mg/L) and August 1988 (0.03 mg/L) and remained at levels of around 0.03 mg/L until February 1989 when phosphonate levels inexplicably began to increase. They stabilized at about 0.13 mg/L in April 1989. The effects of injection of the scale inhibitor on brine chemistry is not fully understood, although at current low concentrations in the brine, it probably does not contribute significantly to major element concentrations.

Chloride, TDS

Chloride was analyzed by titration with silver nitrate according to BEG Specific Work Instruction 1.1 (D. W. Koppenaal, 1987a). Although a potential analytical error of ±1 percent is reported as typical for analyses of solutions containing a high chloride concentration, such as the Pleasant Bayou brines, the chief chemist responsible for the analyses suggested a potential error of ±5 percent be used for the Pleasant Bayou brine analyses (S. W. Tweedy, personal communication, 1989). Figures 3, 4, and 5 show the data for chloride concentration with no

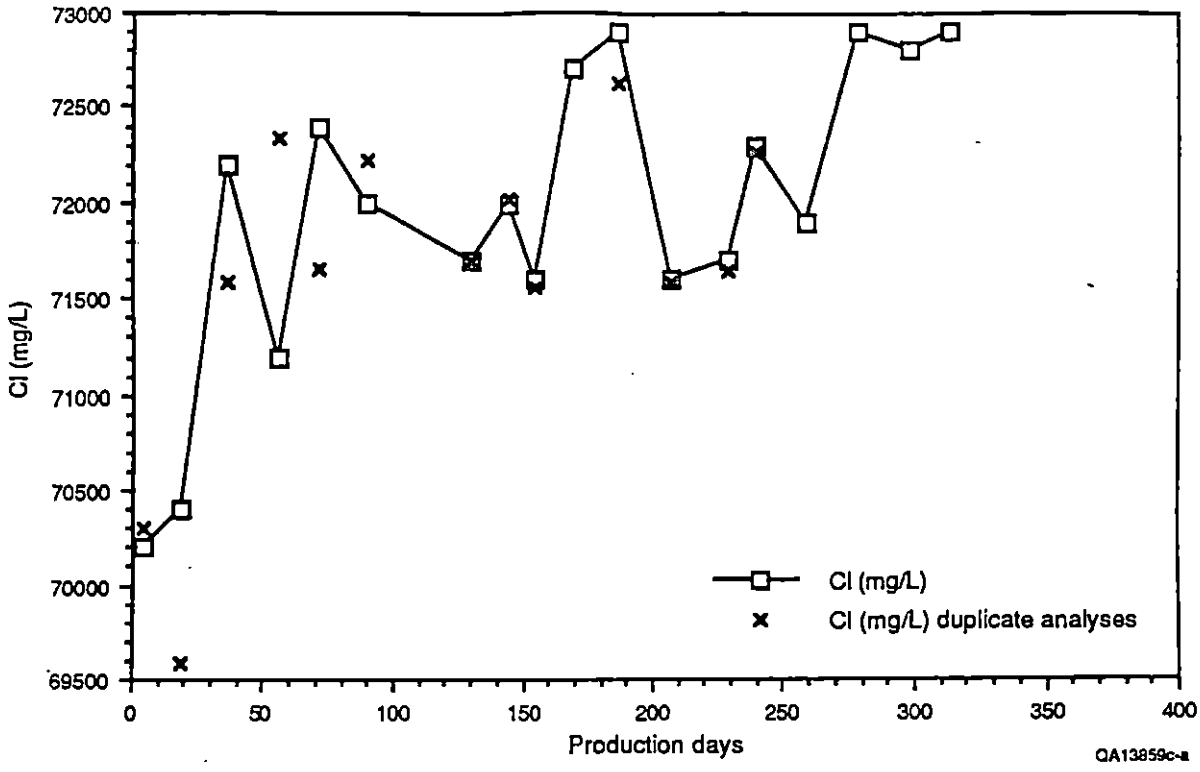

Figure 3. Chloride-concentration data (mg/L) of Pleasant Bayou No. 2 through the current production period with values of duplicate analyses.

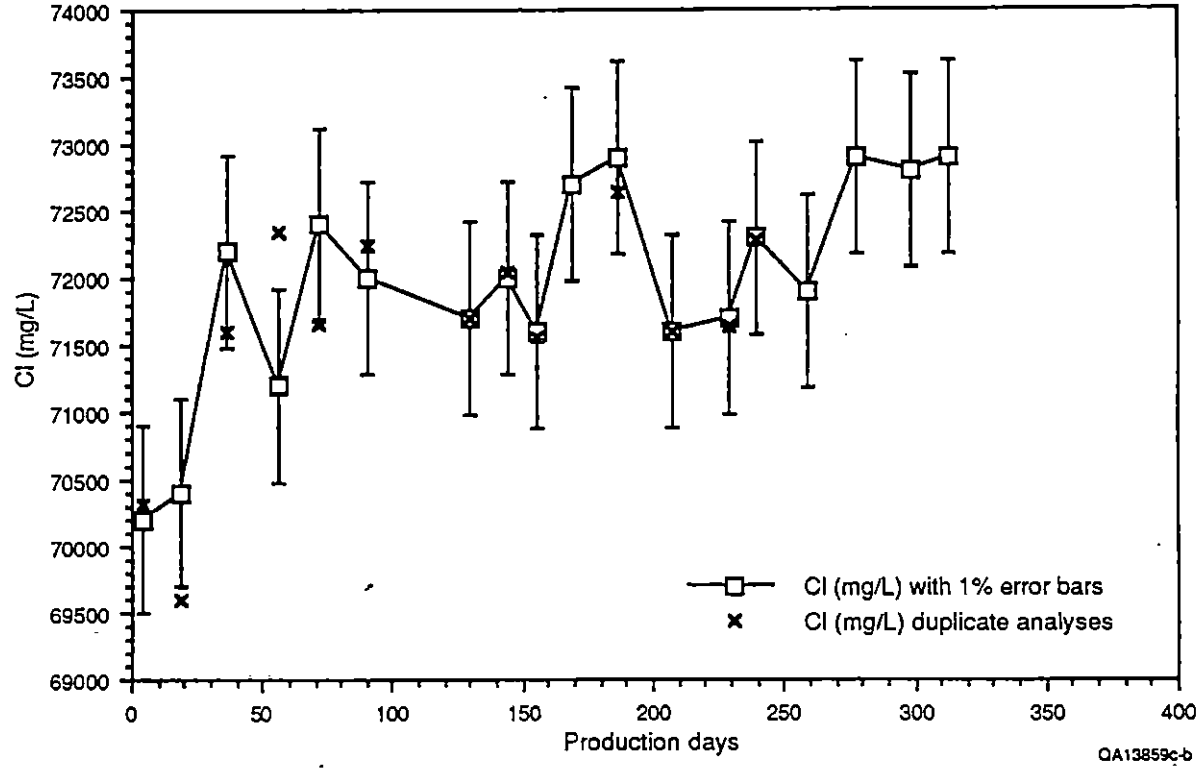

Figure 4. Chloride-concentration data (mg/L) of Pleasant Bayou No. 2 through the current production period with ±1 percent relative error bars and values of duplicate analyses.

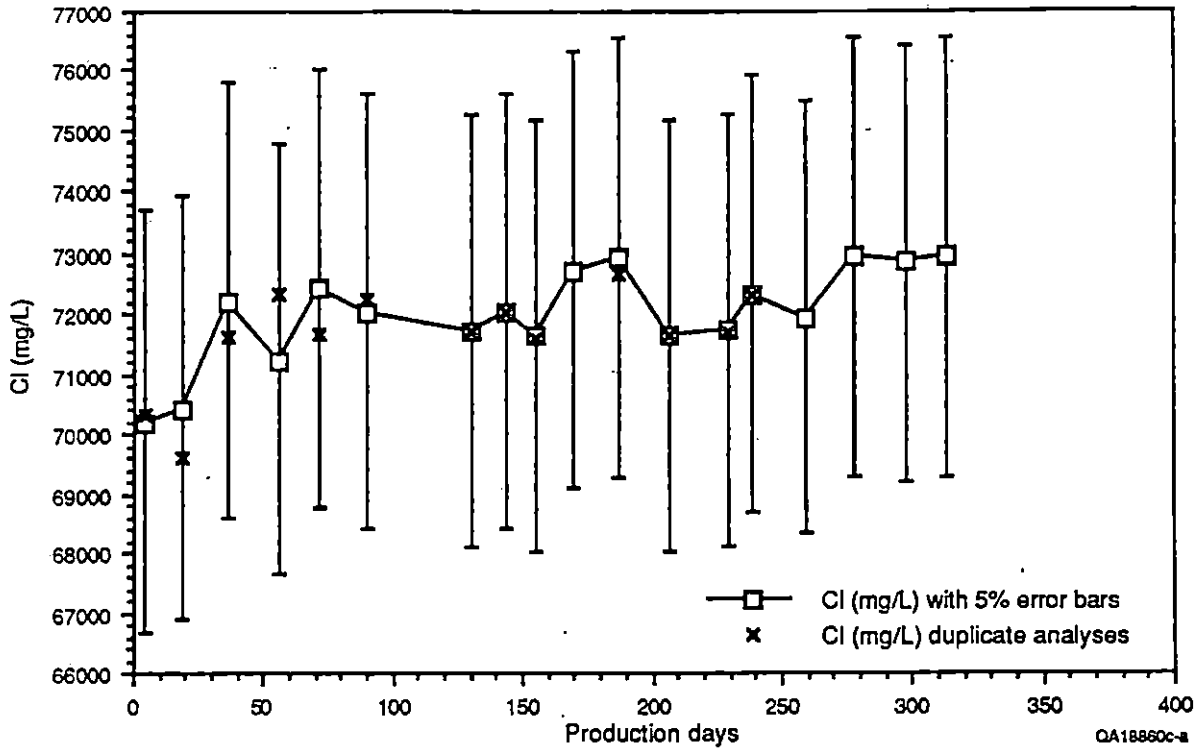

Figure 5. Chloride-concentration data (mg/L) of Pleasant Bayou No. 2 through the current production period with ±5 percent relative error bars and values of duplicate analyses.

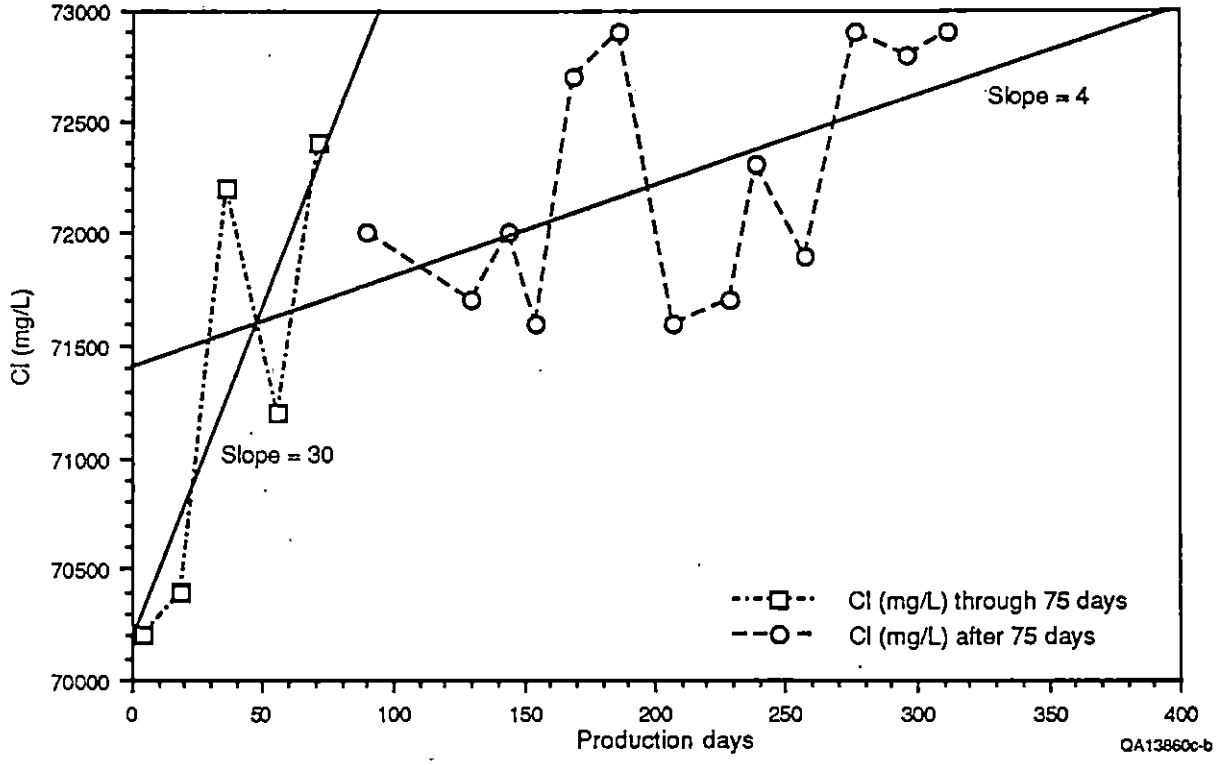

Figure 6. Chloride-concentration data (mg/L) of Pleasant Bayou No. 2 divided into samples collected within the first 75 d of production and samples collected after the first 75 d of production. A straight line is fit to each of the data sets to graphically depict the change in concentration trends.

error bars, error bars of ±1 percent, and ±5 percent, respectively, as well as the values for duplicate analyses run to investigate possible batch effects during analysis. Batch accuracy, the relative standard deviation for analyses performed in a group, is reported as 1 percent for chloride. With two exceptions, all duplicate runs are within 1 percent of the original analyses, suggesting that 1 percent is a reasonable value to use for potential error.

Whether 1 or 5 percent is used for the potential relative error, chloride concentrations appear to rise more quickly during initial and early production (less than 75 d after production began) than production after approximately 75 d. Chloride concentrations start at 70,200 mg/L and rise to 72,400 mg/L within 75 d, an apparent increase of more than 2,000 mg/L.

Subsequent production ranged from 71,600 mg/L to 72,900 mg/L in the last sample (April 4, 1989). Figure 6 graphically shows the change in chloride-concentration trends. The data set was divided into samples collected during the first 75 d of production, and samples collected after the first 75 d of production, and a straight line was fit to each of the data sets. The slope of the line for the earlier production was approximately 30, whereas the slope of the line through the latter data set is closer to 4, indicating an initial rise in chloride concentration of more than seven times that of chloride-concentration increases in later production. This pattern is closely mimicked by TDS, which initially rises rapidly and then levels off significantly (fig. 7). The overall slope of the chloride-concentration trend is close to 5.5, thus clearly suggesting an overall increase in chloride concentration with time (fig. 8).

In addition to its overall increase as production continues, chloride shows smaller scale variations monthly and bimonthly that may be related to short-term changes in production. These smaller scale changes are probably real because they are greater than the uncertainties in the analyses.

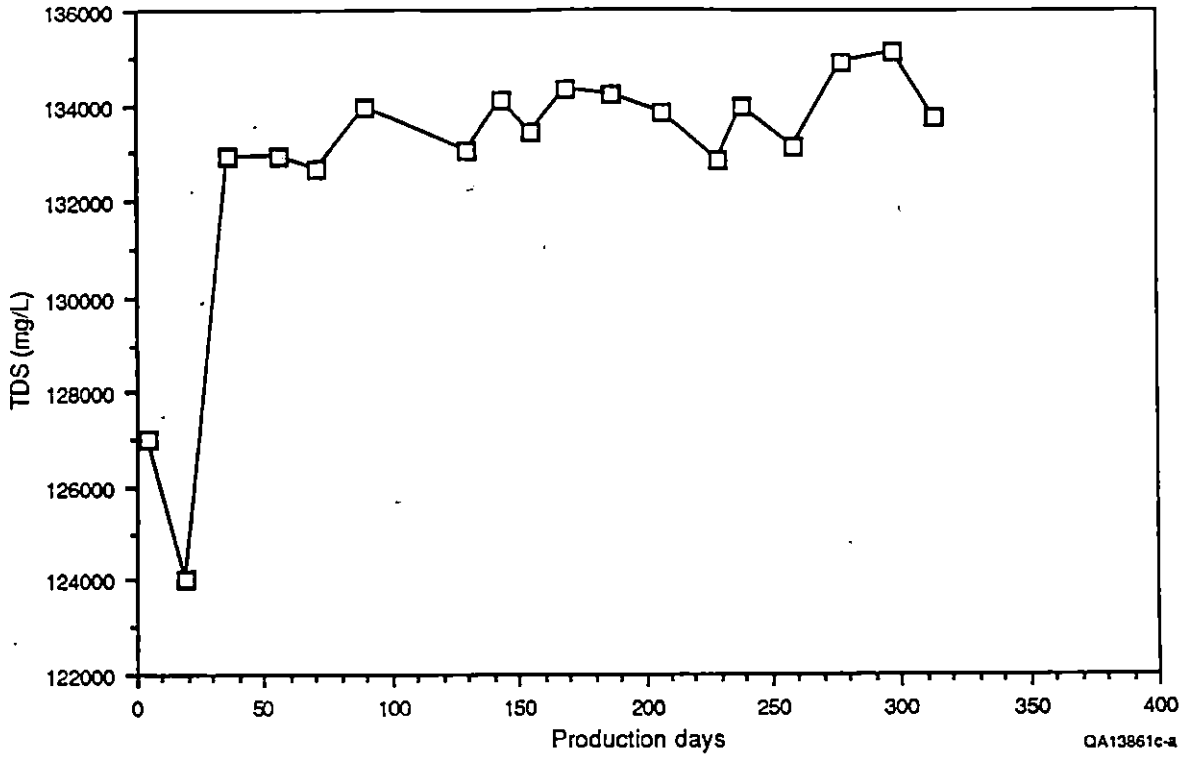

Figure 7. Total-dissolved-solids- (TDS) concentration data (mg/L) of Pleasant Bayou No. 2 through the current production period.

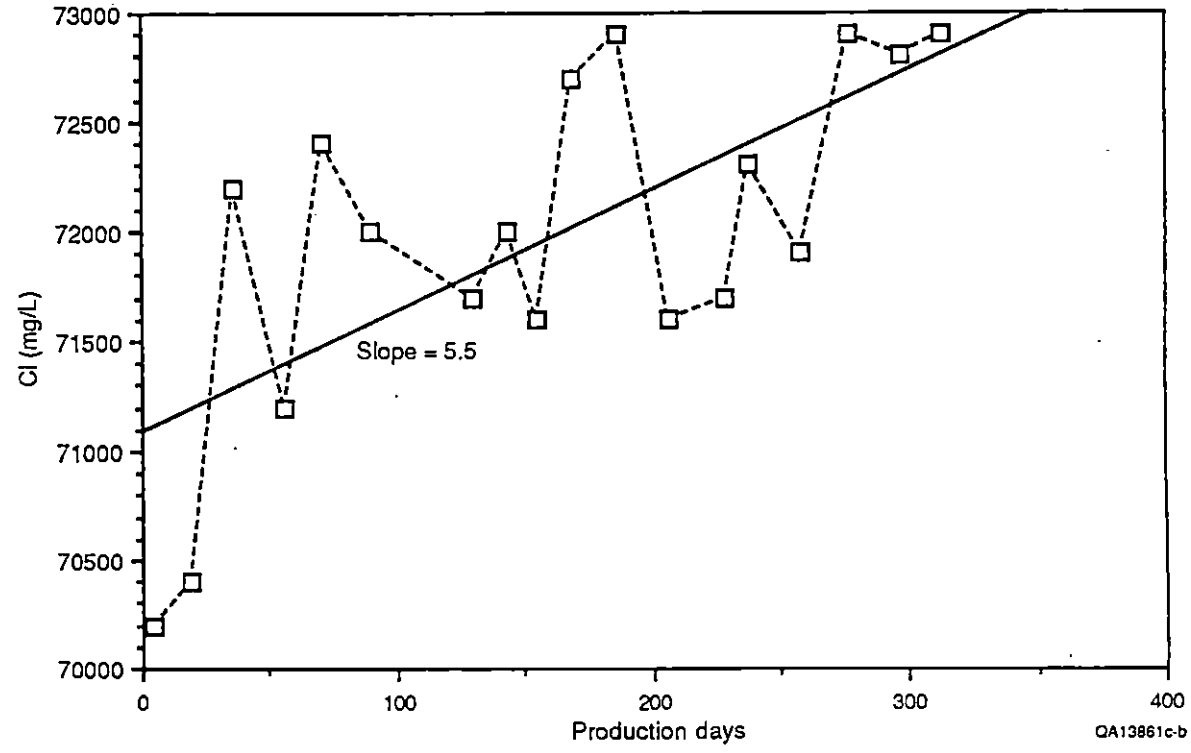

Figure 8. The complete chloride-concentration data (mg/L) of Pleasant Bayou No. 2 set with a straight line fit to graphically depict the overall concentration trend since the beginning of current production.

Sodium

Sodium was analyzed by a direct-reading inductively coupled plasma-optical emission spectrometer (ICP-OES)(Koppenaal, 1987a). The reported maximum potential error for Na is ±5 percent relative. Figure 9 shows sodium-concentration data with 5 percent relative error bars. The data shown are both the initial analyses and the duplicate analyses, which were run to investigate possible batch effects. The duplicate analyses were run to compare relative concentrations of various elements through the sampling period, with little attention paid to absolute accuracy. Therefore, duplicate analyses should not be used in place of the original data (S. W. Tweedy, personal communication, 1989). Batch accuracy for sodium is reported as 2 percent.

Assuming a potential relative error of ±5 percent, whether any long-term trends in sodium concentration can be detected is questionable. It is possible that any trends observed can be accounted for by batch effects or other sources of analytical error. However, acknowledging these limitations, we divided sodium-concentration data into two data sets (fig. 10) to compare it with observed chloride-concentration trends (fig. 6). Interestingly, both Na and Cl concentrations appear to increase steadily through the first 75 d of production. After approximately 75 d, chloride concentrations generally appear to increase, though at a much slower rate, while sodium concentrations appear to level off or decrease slightly. Whether these trends are a coincidental analytical effect or a consequence of real trends in sodium and chloride concentrations is difficult to determine with the high analytical error for sodium.

Calcium

Calcium was analyzed using ICP-OES with a maximum potential error reported as ±5 percent (Koppenaal, 1987a) and a batch accuracy of ±2 percent. Calcium values obtained

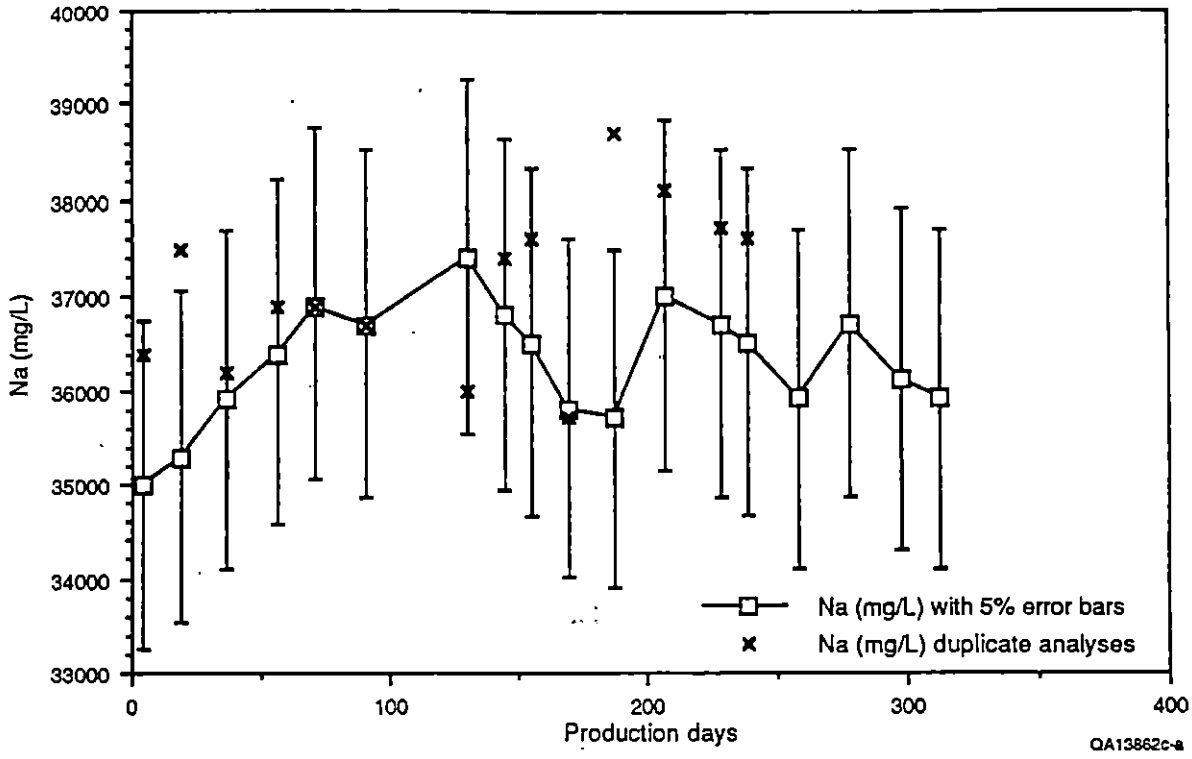

Figure 9. Sodium-concentration data (mg/L) of Pleasant Bayou No. 2 through the current production period with ±5 percent relative error bars and values of duplicate analyses.

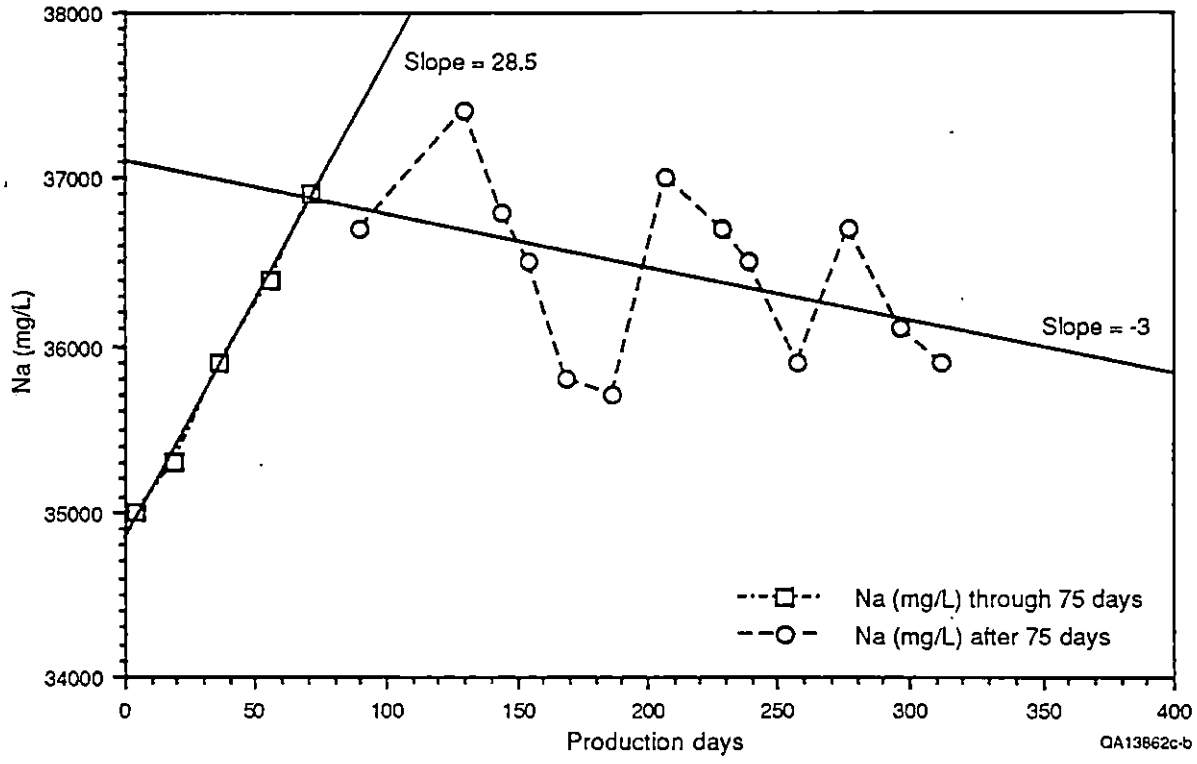

Figure 10. Sodium-concentration data (mg/L) of Pleasant Bayou No. 2 divided into samples collected within the first 75 d of production and samples collected after the first 75 d of production. A straight line is fit to each of the data sets to graphically depict the change in concentration trends.

from the original analyses range from 7,620 mg/L to 8,010 mg/L, all duplicate analyses (run to investigate possible batch effects) falling within ±5 percent of the original data (fig. 11) and most falling within ±3 percent (fig. 12). Duplicate analyses were run with little attention to absolute accuracy, so they should not be used in place of the original data (S. W. Tweedy, personal communication, 1989). Also shown in figure 12 are calcium concentration data reported by IGT on samples analyzed by atomic absorption/atomic emission spectroscopy. These values also fall within ±3 percent of the original BEG analyses and further indicate that a probable error of ±3 percent is a reasonable value to use.

Figure 13 shows the calcium-concentration data divided into two data sets: those samples obtained during the first 75 d of production and samples obtained after the first 75 d of production. A simple first-order polynomial was fit to each of the data sets to compare calcium-concentration-data trends to possible trends observed in sodium- and chloride-concentration data (figs. 6 and 10). The same general pattern seems to exist in concentration trends of all three of these elements—a rapid increase during the first 75 d followed by a leveling off of the rate of increase or even a slight subsequent decrease. Calcium concentrations rise from 7,620 mg/L to around 7,900 mg/L within the first 75 d of production, an apparent increase of 4 percent, compared with an apparent increase of 5 percent in sodium and an apparent increase of 3 percent in chloride through the same time period. After about 75 d of production, calcium concentrations appear to level off. Duplicate analyses seem to support the reality of these observed trends for calcium and chloride, whereas duplicate analyses bring into question the reality of the Na trends.

Potassium

Potassium was analyzed by ICP-OES with a maximum potential error reported as ±5 percent (Koppenaal, 1987a). Potassium values range from 522 mg/L to 610 mg/L over the

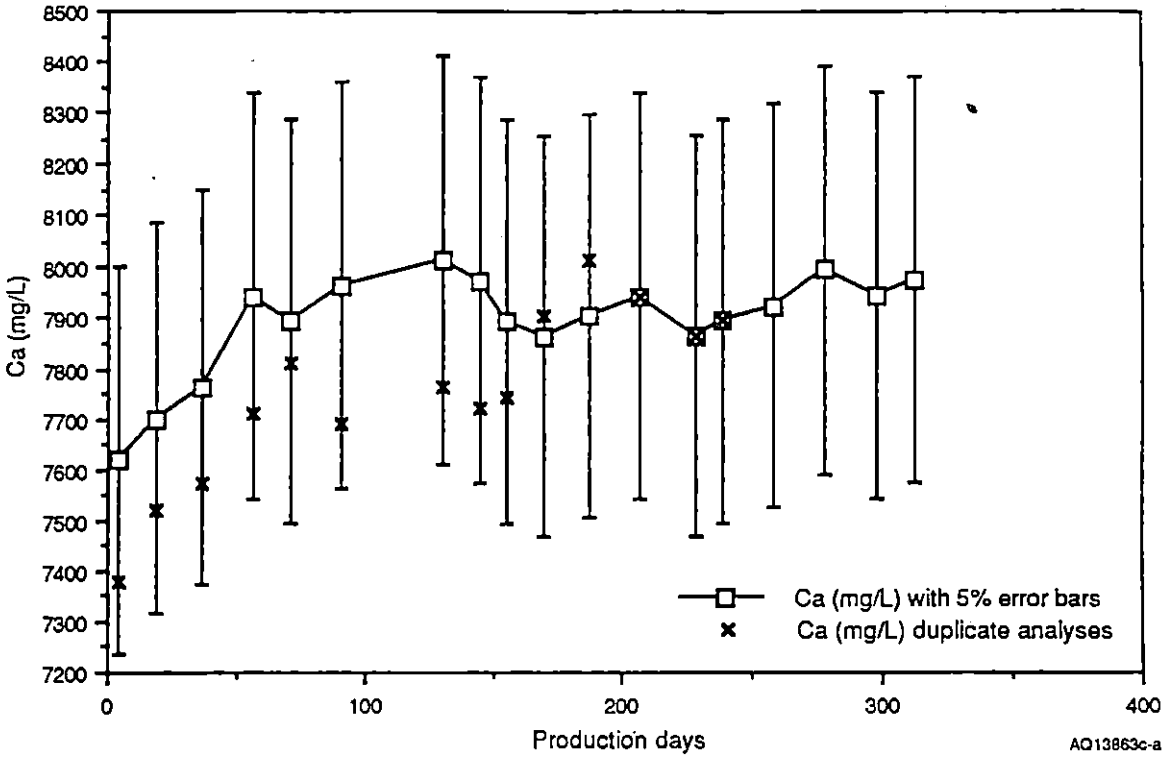

Figure 11. Calcium-concentration data (mg/L) of Pleasant Bayou No. 2 through the current production period with ±5 percent relative error bars and values of duplicate analyses.

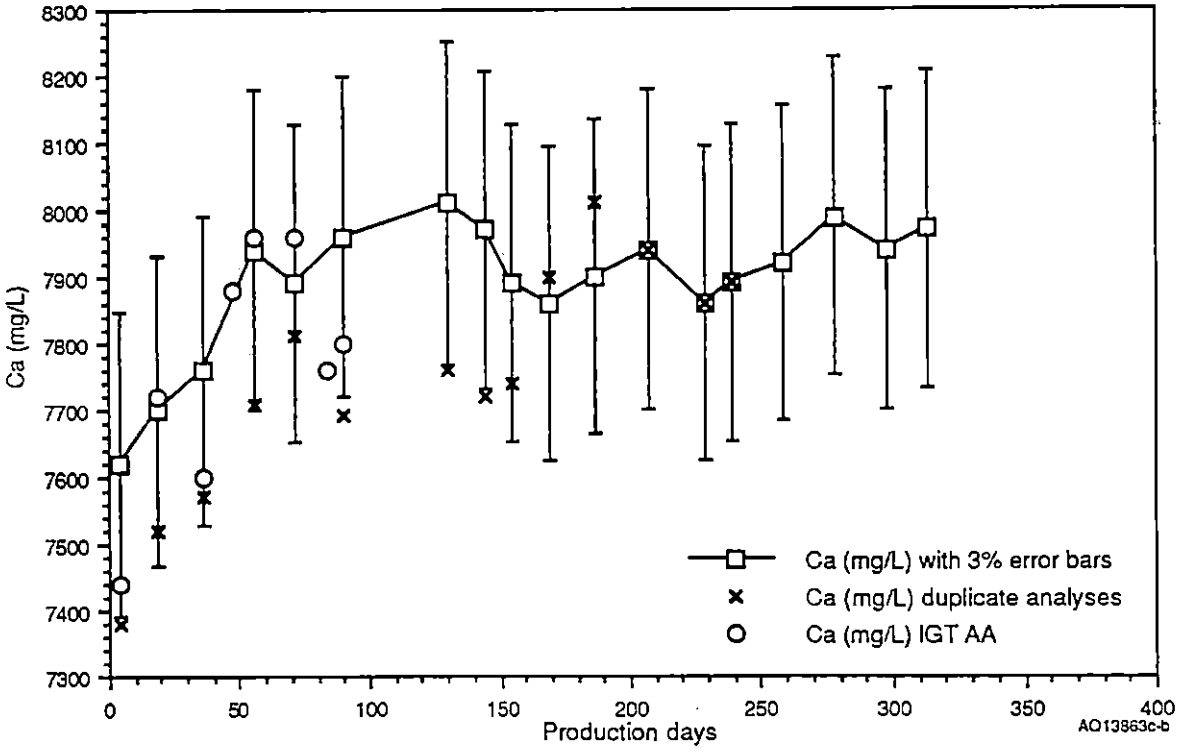

Figure 12. Calcium-concentration data (mg/L) of Pleasant Bayou No. 2 through the current production period with ±3 percent relative error bars and values of duplicate analyses. Also shown are calcium concentration values reported by IGT obtained by atomic absorption analyses (Eaton Operating Co., Inc., 1988a).

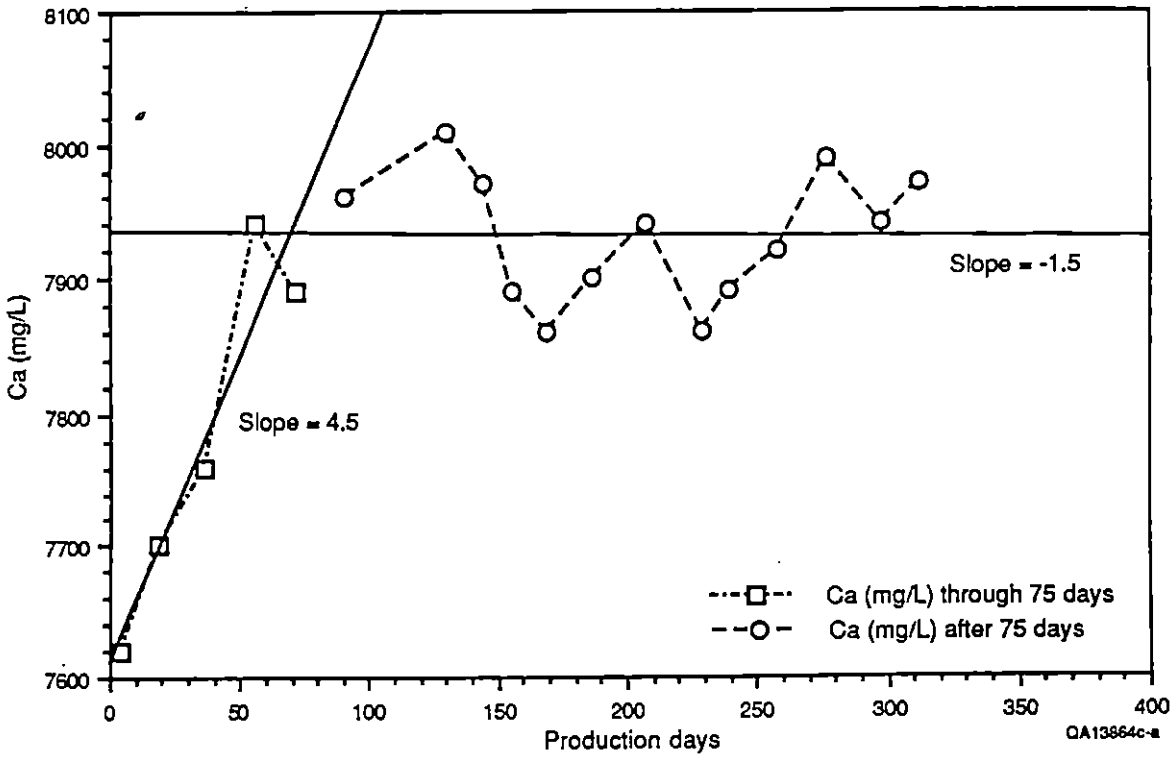

Figure 13. Calcium-concentration data (mg/L) of Pleasant Bayou No. 2 divided into samples collected within the first 75 d of production and samples collected after the first 75 d of production. A straight line is fit to each of the data sets to graphically depict the change in concentration trends.

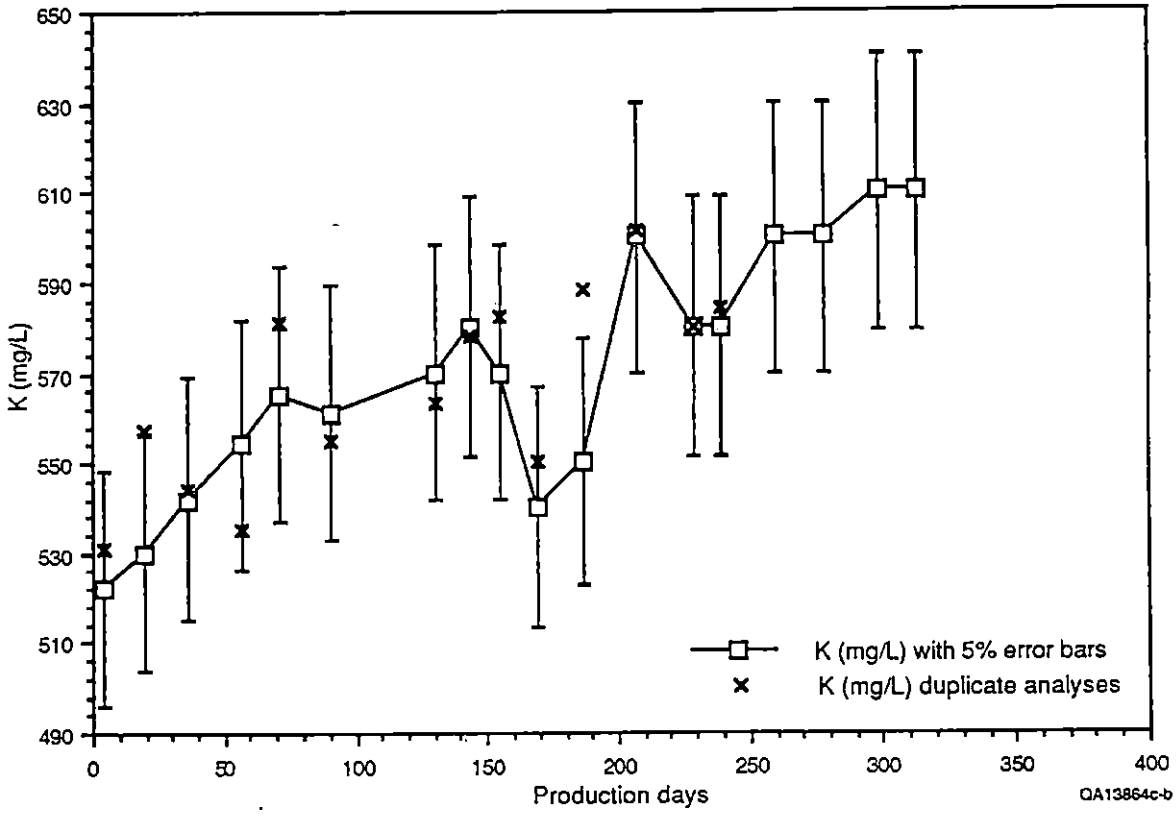

Figure 14. Potassium-concentration data (mg/L) of Pleasant Bayou No. 2 through the current production period with ±5 percent relative error bars and values of duplicate analyses.

span of currently sampled production (May 27, 1989, through April 30, 1989), all but one duplicate analysis falling within ±5 percent of the original data (fig. 14).

Figure 14 reveals that potassium concentrations have risen more or less steadily since production began. In order to compare potassium concentration trends with trends of other major elements, a straight line was fit through potassium data from the first 75 d of production, and through the potassium data from samples obtained after the first 75 d of production (fig. 15). Potassium increased steadily from 522 mg/L to 565 mg/L (8 percent) within the first 75 d. Subsequently, potassium increased more erratically by another 8 percent through the remainder of production. These trends are similar to chloride- and calcium-concentration trends. Duplicate analyses are more scattered but seem to indicate that an apparent overall increase of potassium concentrations through time is not a product of batch effects.

Silica

We worried that silica-concentration data for the Pleasant Bayou No. 2 well brine samples may be unreliable because of a lack of preservation of dissolved silica and the large analytical uncertainty of analyses. Because calculation of equilibrium between aqueous silica and quartz is a useful tool for confirming subsurface temperatures, detecting mixing trends, and delineating source areas of geothermal fluids that have temperatures greater than about 100°C, added precaution may be necessary to preserve dissolved silica in the Pleasant Bayou geothermal waters. A standard procedure for preserving silica is to collect a sample and immediately dilute it 50 percent or more to ensure that the brine remains undersaturated with respect to amorphous silica and possibly chalcedony and cristobalite at surface temperatures. If samples are not diluted, silica may polymerize and begin to form a siliceous precipitate, resulting in silica analyses that are substantially lower than actual silica concentrations in the subsurface samples.

Silica concentrations in fluid samples collected from the Pleasant Bayou site by Kharaka and others (1980), who used the preservation method of on-site dilution, indicate that silica is

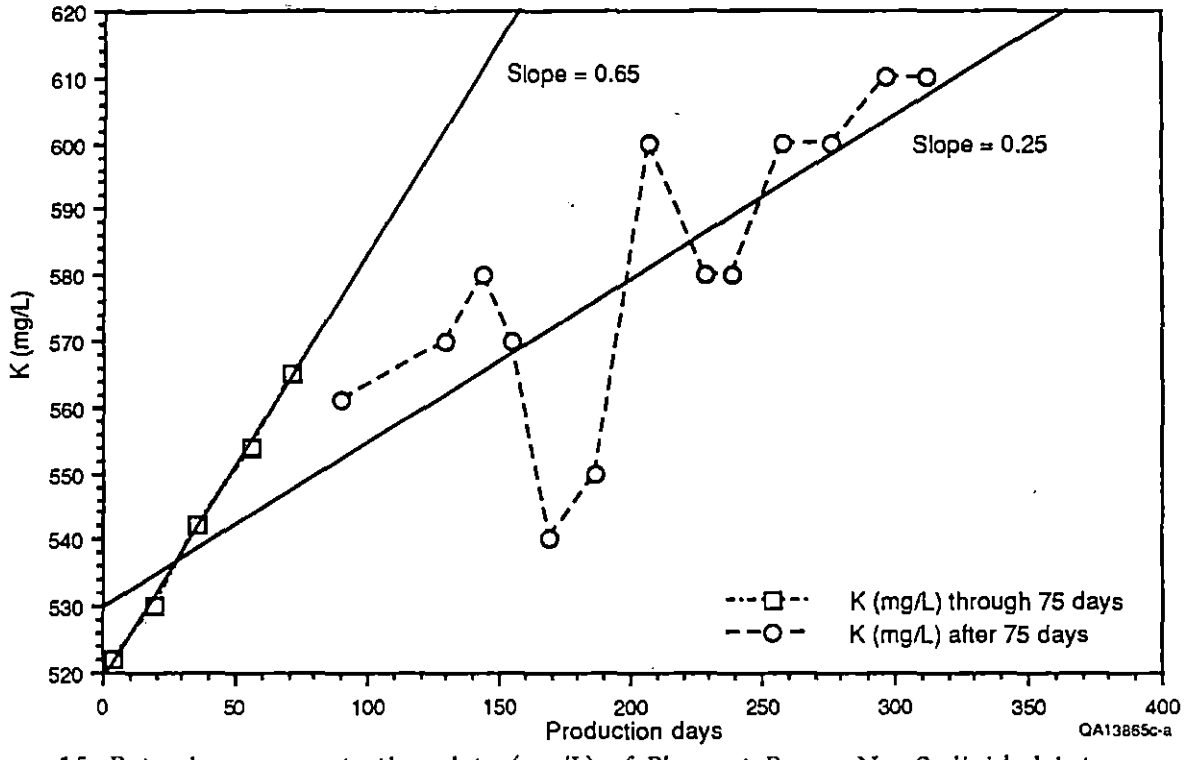

Figure 15. Potassium-concentration data (mg/L) of Pleasant Bayou No. 2 divided into samples collected within the first 75 d of production and samples collected after the first 75 d of production. A straight line is fit to each of the data sets to graphically depict the change in concentration trends.

at or near equilibrium with quartz at the temperatures and pressures of the Pleasant Bayou reservoir (Capuano, 1988)(fig. 16). Figure 16 shows silica concentration versus temperature for the Pleasant Bayou samples reported by Kharaka and others (1980). Superimposed are calculated equilibrium-saturation curves for quartz and amorphous silica. Apparently, upon cooling to surface temperatures (25°C), brine samples from the Pleasant Bayou reservoir may become supersaturated with respect to amorphous silica, and silica may begin to precipitate out, thus invalidating subsequent analysis. Diluted samples collected by Kharaka and others (1980), at depths of 14,682 ft and 15,589 ft and bottom-hole temperatures of 138 and 150°C, respectively, have silica concentrations of 120 and 200 mg/L, respectively (fig. 17). Undiluted, and therefore unpreserved samples, obtained during long-term testing yield silica concentrations ranging from 78 to 108 mg/L, compared with a value of 118 mg/L for a recently collected sample diluted upon collection (fig. 17). The three samples collected with silica preserved by dilution have higher reported silica concentrations than any sample collected without dilution. Therefore, to obtain a brine sample that more accurately reflects subsurface silica concentrations, future workers should include a separate filtered and diluted sample for silica analysis to prevent extensive silica polymerization.

A second significant problem with reported silica concentrations in Pleasant Bayou brine samples is the large analytical uncertainty associated with the ICP-OES method of analysis. Reliability for silica-concentration analyses, as well as several other minor and trace elements, is ±25 percent, virtually obscuring any definitive trends for these elements (fig. 18). Because minor- and trace-element trends are important in delineating changes in brine sources, more accurate analytical methods for determining concentrations of these elements are recommended. Unless significant improvement is made in the areas of silica preservation and reduced analytical uncertainty, changes in silica concentrations are unlikely to prove useful in predicting or documenting changes in reservoir brine source areas.

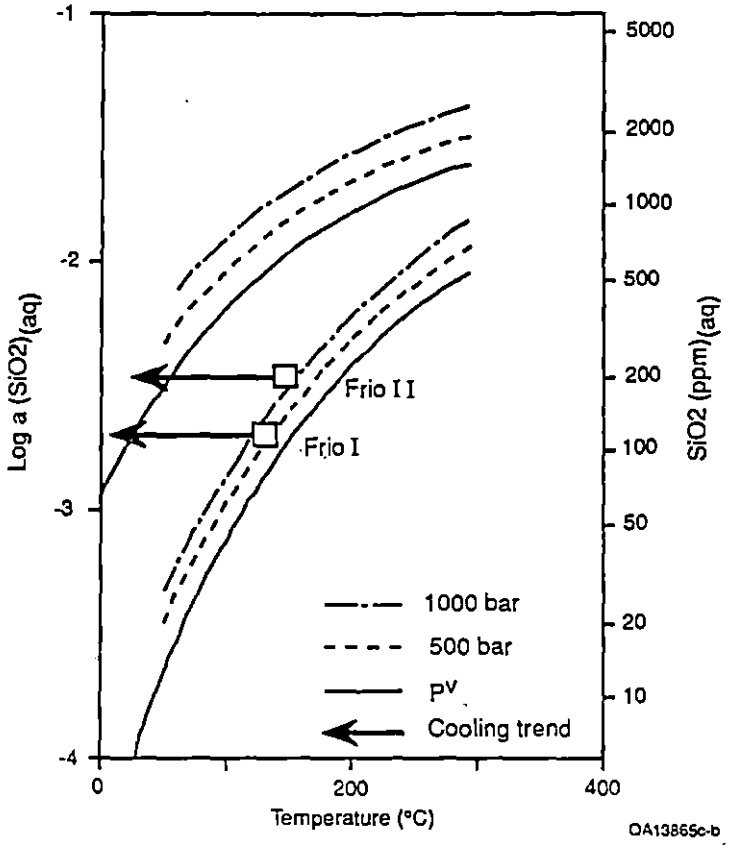

Figure 16. Quartz and amorphous silica solubility as a function of temperature at pressures of the vapor pressure of water (P^V)(solid line), 500 bars (dashed line), and 1,000 bars (dot-dashed line)(Capuano, 1988). Pleasant Bayou No. 2 brine samples reported by Kharaka and others (1980) (Frio I [C-zone] and Frio II [F-zone]) are shown to be at or near equilibrium with respect to quartz at reservoir temperatures and pressures, but upon cooling to surface temperatures may become oversaturated with respect to quartz and amorphous silica.

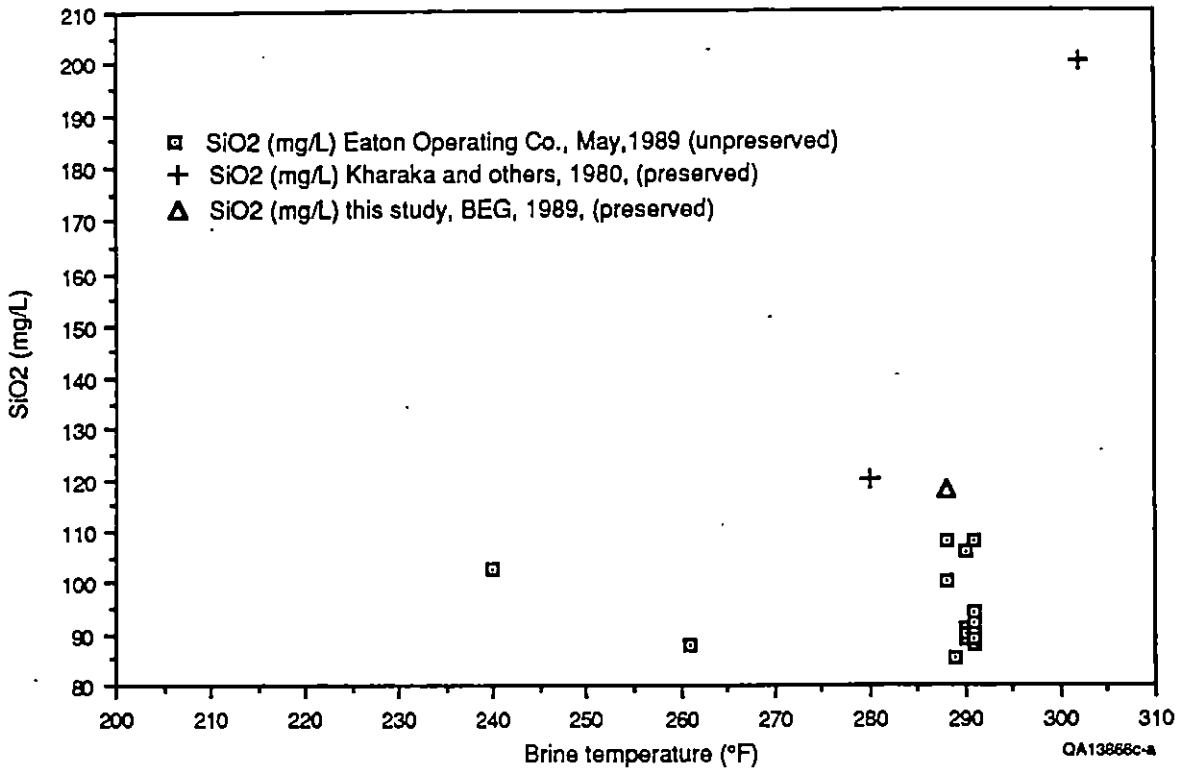

Figure 17. Brine-sample silica concentrations (mg/L) of Pleasant Bayou No. 2 as a function of temperature. Note that diluted, and therefore preserved, samples have higher reported silica concentrations than all samples not diluted upon collection (data from tables 2 and 3).

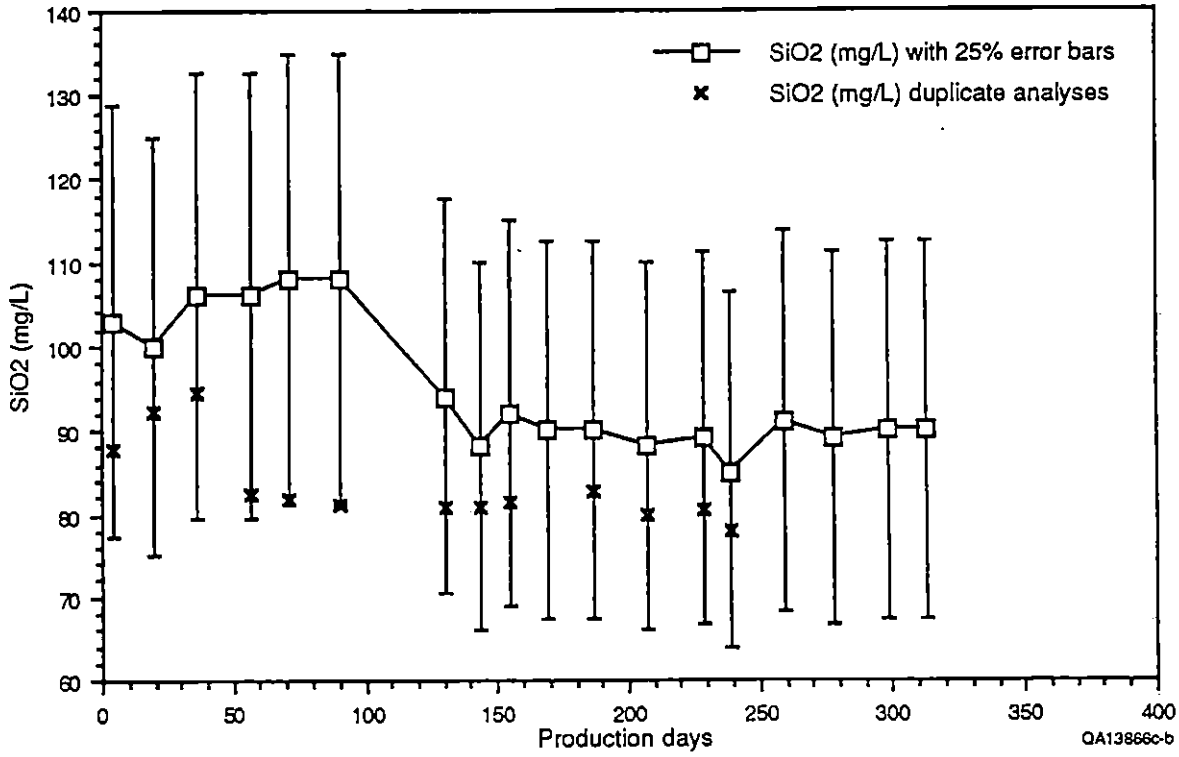

Figure 18. Silica-concentration data (mg/L) of Pleasant Bayou No. 2 through the current production period with ±25 percent relative error bars and values of duplicate analyses.

Ammonia

Ammonia is measured as ammonium by steam distillation and spectrophotometry (S. W. Tweedy, personal communication, 1989) and converted to ammonia for reporting. Maximum potential error is reported as ±5 percent (fig. 19). A fairly steady concentration increase through time is observed, even though the error is not negligible. Ammonia increases from 83 mg/L during early production to 90 mg/L during later production, an increase of 8 percent.

A good correlation exists between ammonia- (shown as ammonium) concentration trends and potassium-concentration trends, particularly during the first 40 d of production (fig. 20, shown in meq/L). A plot of molar ratios (fig. 21) shows potassium is roughly three times as abundant as ammonium and the ratio appears to be increasing fairly consistently, with the exception of two data points at about 170 and 190 d of production.

Alkalinity

Alkalinity concentrations of the brine samples were measured both on site and at the BEG laboratory. The brine samples were cooled, collected under a blanket of carbon dioxide, and kept cool until analyses were under way. This was done to prevent precipitation of calcium carbonate, which would lower alkalinity concentrations (Eaton Operating Co., Inc., 1988b). BEG brine samples were analyzed by titration using standardized hydrochloric acid to a pH end point of 8.3, 4.5, or 2.5, depending on sample and suspected acid neutralizing constituents (D. W. Koppenaal, personal communication, 1988). Apparently the steps taken to prevent calcium carbonate precipitation were not sufficient over extended periods of time. The on-site analyses were usually performed within a day or two of sample collection, whereas the BEG analyses were run in batches, sometimes requiring lengthy storage of samples (3 to 10 wk). This lengthy sample storage at the BEG has resulted in excessively low values reported for alkalinity, as

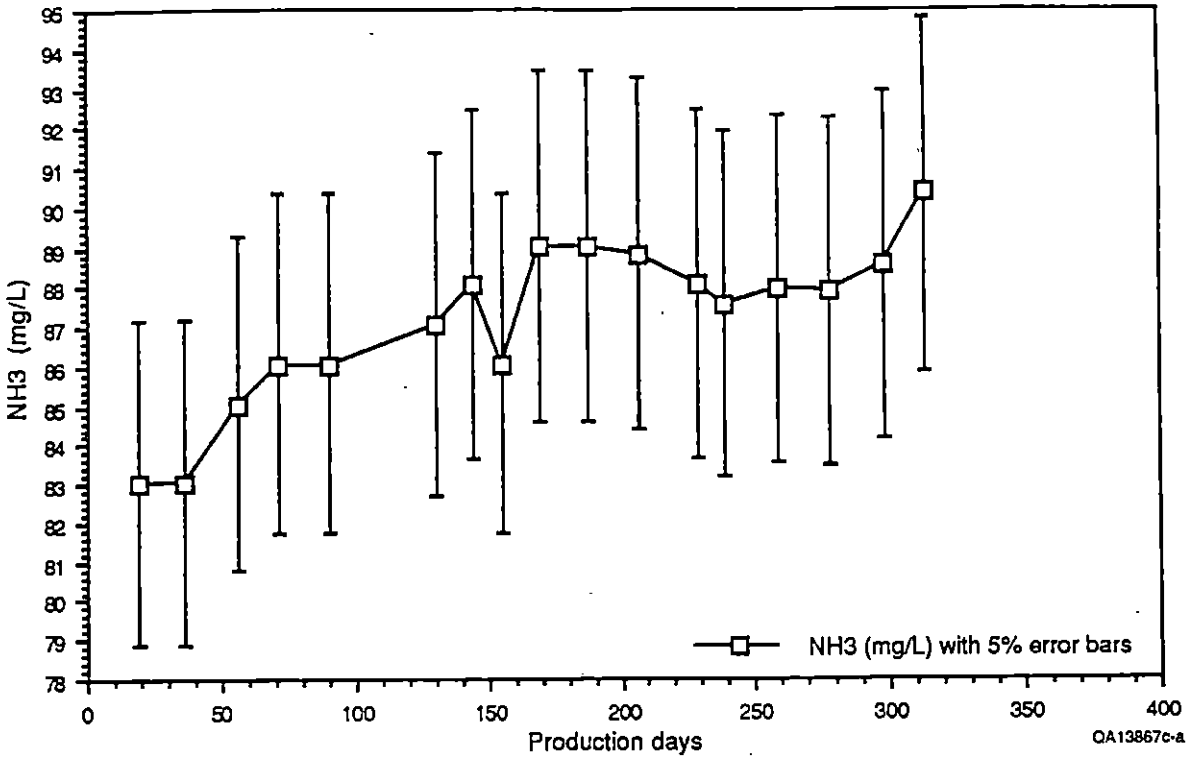

Figure 19. Ammonia-concentration data (mg/L) of Pleasant Bayou No. 2 through the current production period with ±5 percent relative error bars.

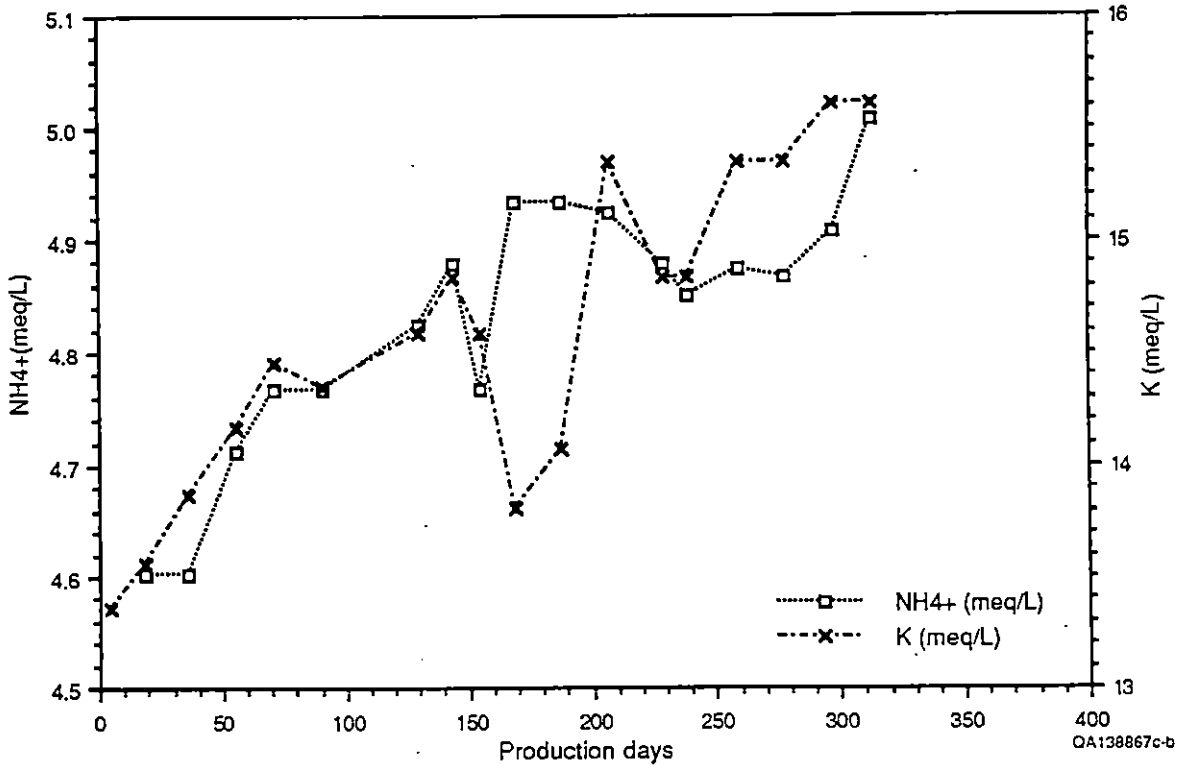

Figure 20. Ammonium- and potassium-concentration data (meq/L) of Pleasant Bayou No. 2 through the current production period, showing very good correlation, particularly during early production.

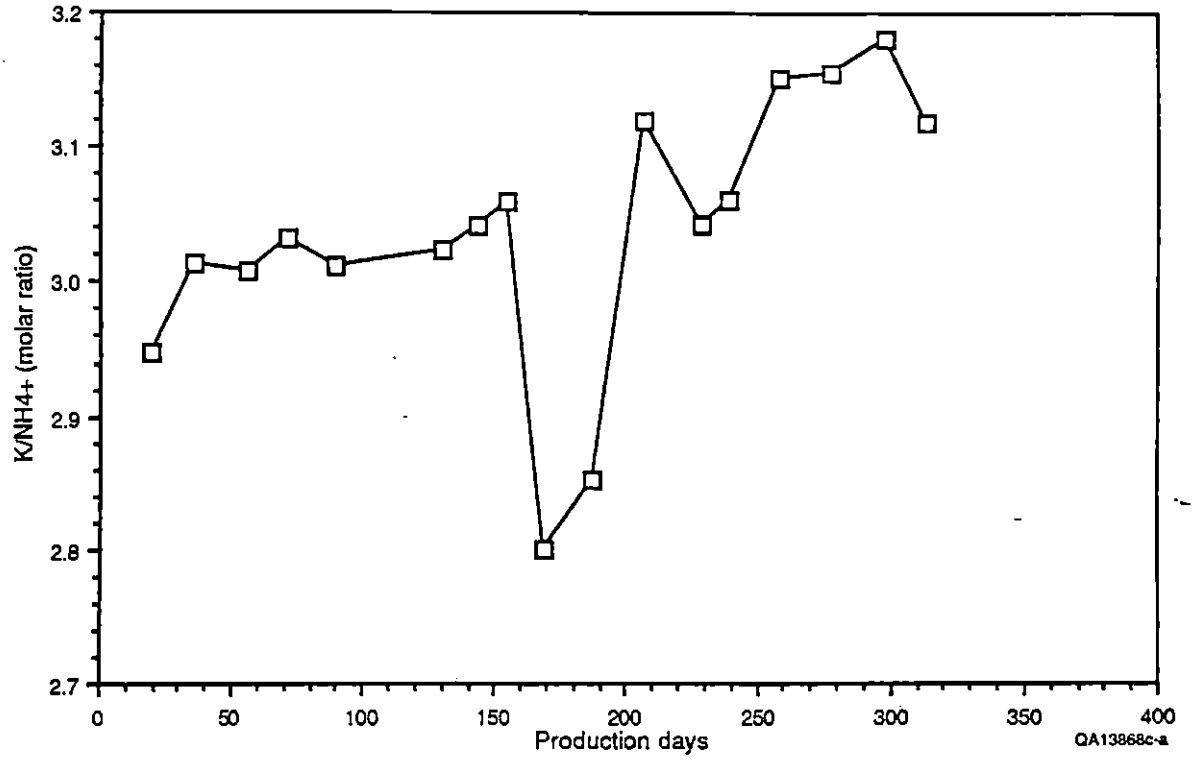

Figure 21. Potassium/ammonium molar ratio (meq/L) of Pleasant Bayou No. 2 through the current production period.

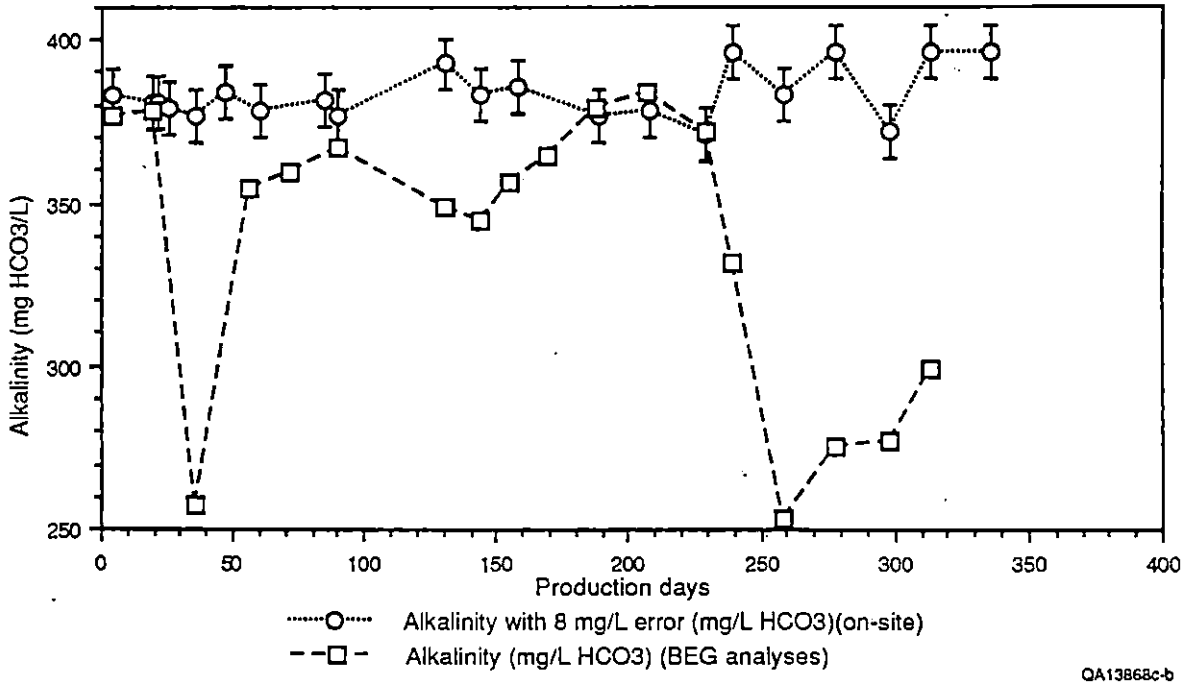

Figure 22. Alkalinity-concentration data (in mg HCO_3/L) of Pleasant Bayou No. 2 through the current production period.

compared with those during the on-site analyses (fig. 22). In general, the longer the sample-storage time, the lower the reported alkalinity concentrations. Therefore, the BEG alkalinity data will not be used. Although the on-site analyses have higher alkalinities than do the BEG analyses, problems in preserving alkalinity in solution and possible interferences with carbonate equilibria by the bubbling of carbon dioxide into the solution during collection and by the injecting of corrosion and scale inhibitors into the flow before collection have led to the decision not to use alkalinity data in the investigation to determine current and future source areas of brine production in the Pleasant Bayou reservoir.

Others

Iron, magnesium, and manganese appear to show a trend toward increasing concentration through current production (figs. 23, 24, and 25). Iron concentrations, although apparently increasing, are suspect because IGT gas analyses have shown iron corrosion losses of about 21 lb/d (46 kg/d) from production tubing (Eaton Operating Co., Inc., 1988a), possibly contaminating brine samples with iron. Observed batch effects and a large analytical uncertainty (±25 percent) also negate the further use of iron in this investigation. Magnesium and manganese also show possible trends toward increased concentrations, but having the pronounced batch effects for both elements and a ±25-percent relative error for manganese analyses, these trends are not definitive.

Lithium, iodide, and zinc may be showing trends toward decreasing concentrations. However, the trends for lithium (fig. 26) and iodide (fig. 27) are within the large analytical error (±25 percent and ±15 percent, respectively). The perceived trend in the original zinc-concentration data is not seen in the duplicate, single-batch run (fig. 28), indicating that the observed trend may be a result of batch effects. No duplicate analyses were run for iodide, thereby prohibiting comparison in order to determine the existence of batch effects for iodide.

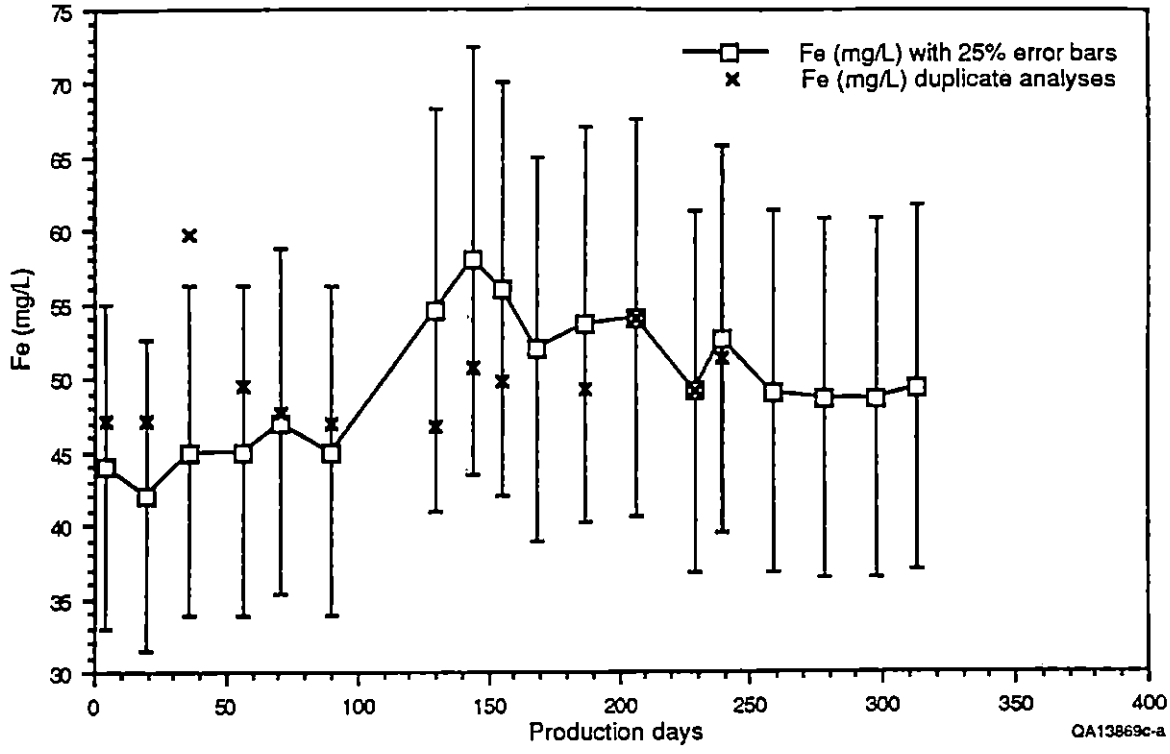

Figure 23. Iron-concentration data (mg/L) of Pleasant Bayou No. 2 through the current production period with ±25 percent relative error bars and values of duplicate analyses.

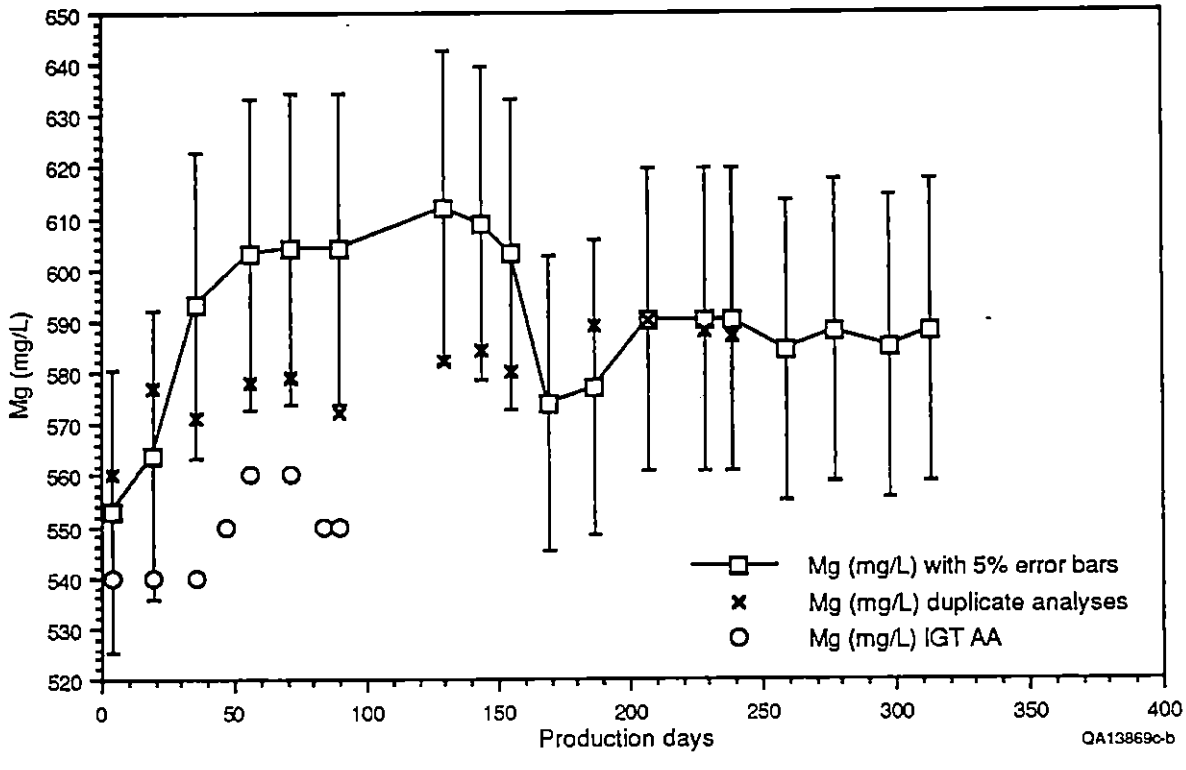

Figure 24. Magnesium-concentration data (mg/L) of Pleasant Bayou No. 2 through the current production period with ±5 percent relative error bars and values of duplicate analyses; and magnesium-concentration values reported by IGT obtained by atomic absorption analyses (Eaton Operating Co., Inc., 1988a).

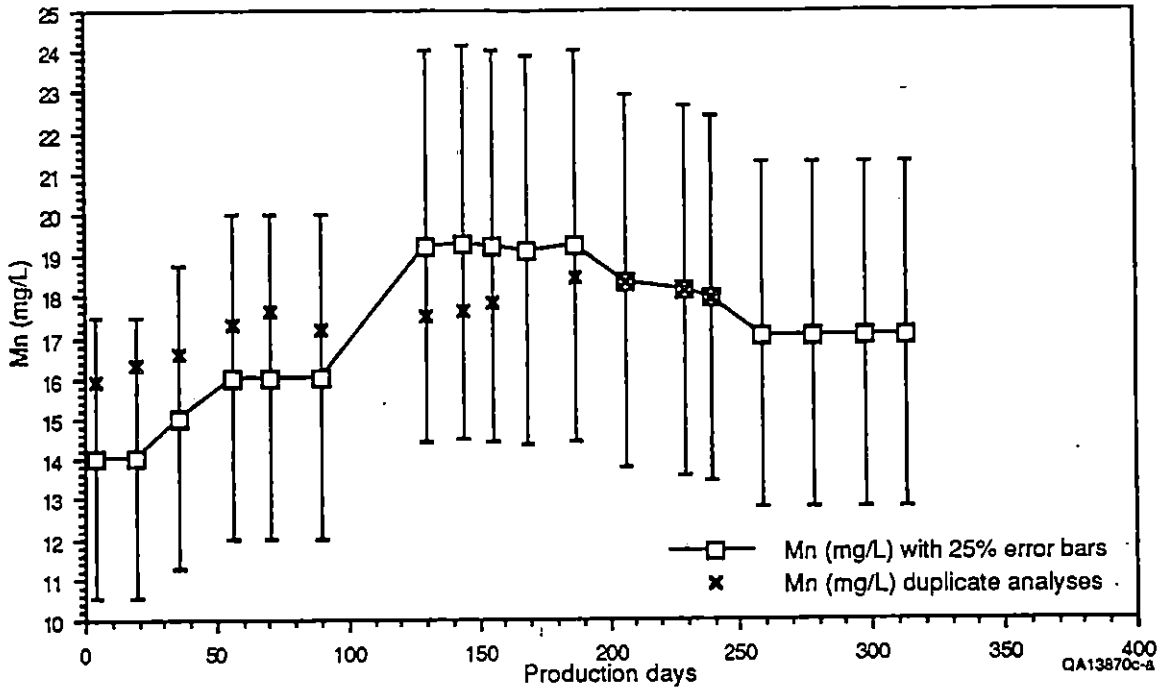

Figure 25. Manganese-concentration data (mg/L) of Pleasant Bayou No. 2 through the current production period with ±25 percent relative error bars and values of duplicate analyses.

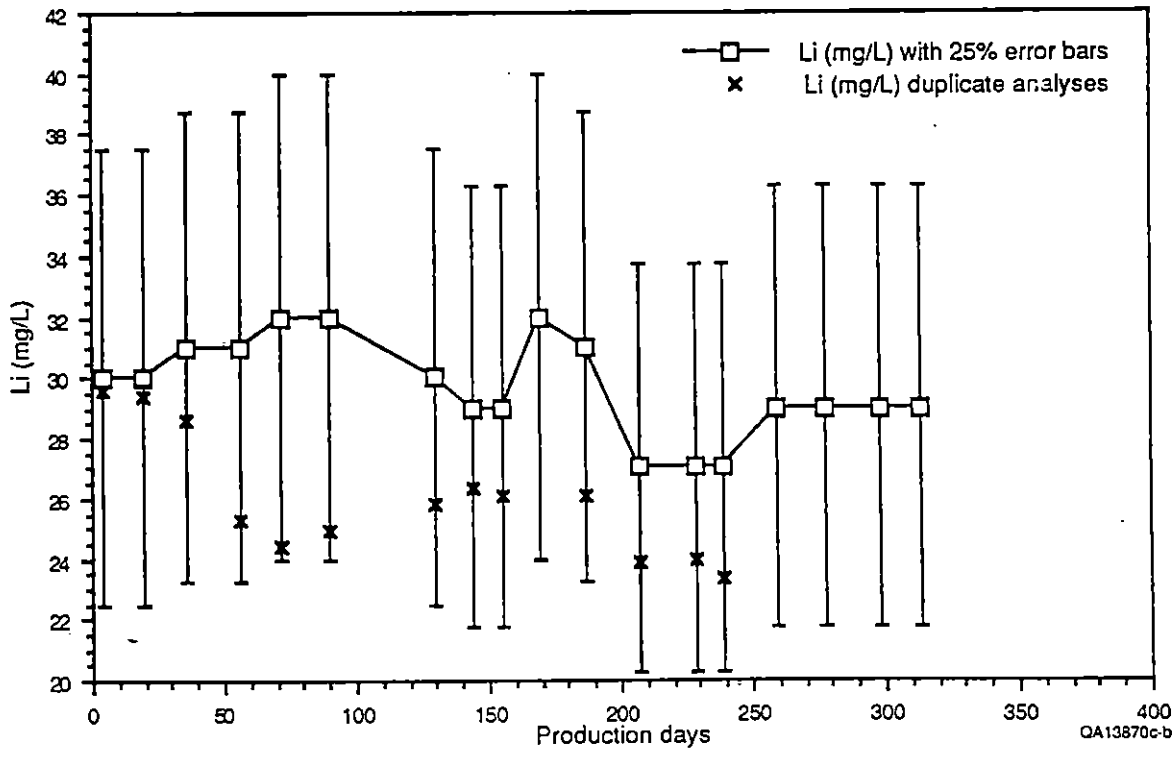

Figure 26. Lithium-concentration data (mg/L) of Pleasant Bayou No. 2 through the current production period with ±25 percent relative error bars and values of duplicate analyses.

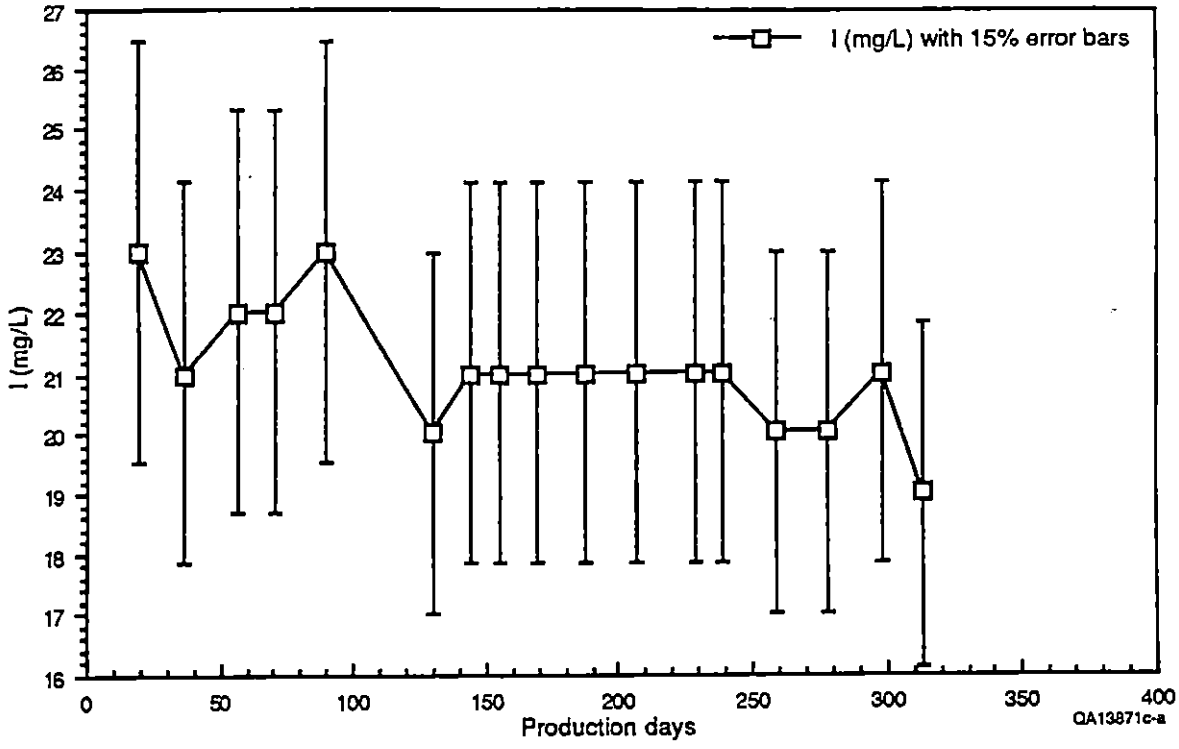

Figure 27. Iodide-concentration data (mg/L) of Pleasant Bayou No. 2 through the current production period with ±15 percent relative error bars.

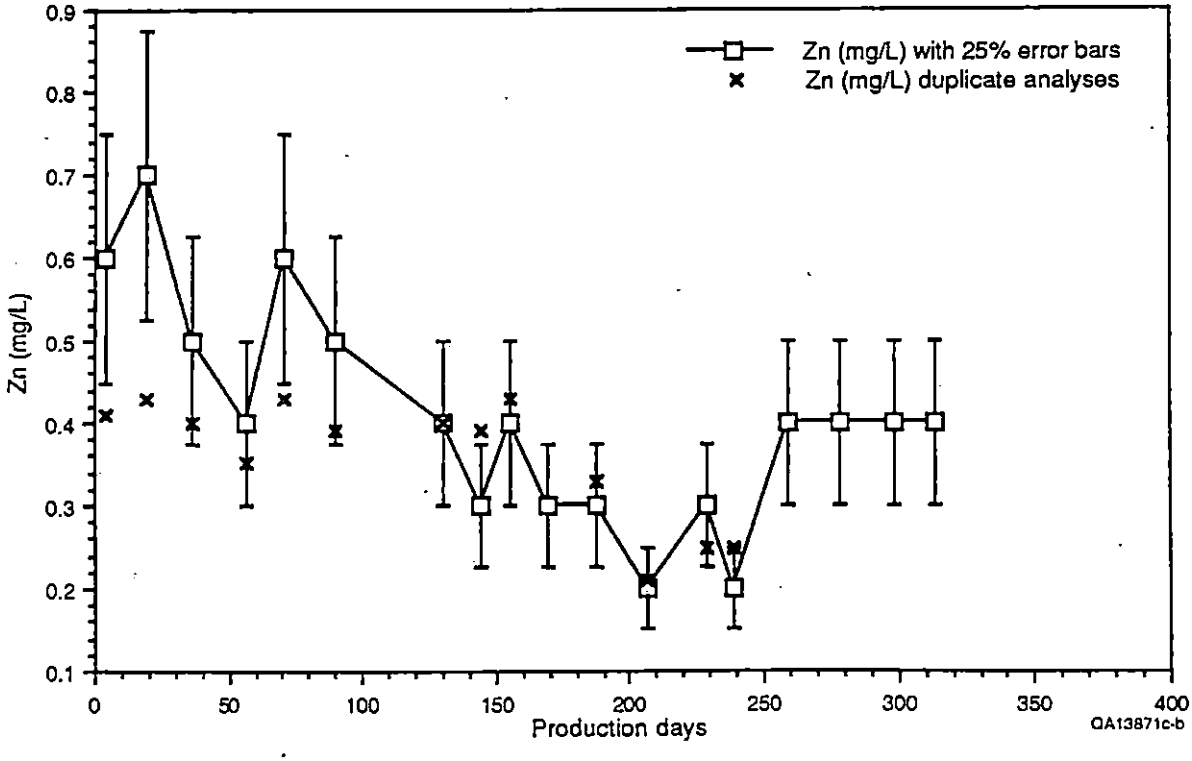

Figure 28. Zinc-concentration data (mg/L) of Pleasant Bayou No. 2 through the current production period with ±25 percent relative error bars and values of duplicate analyses.

Barium-, boron-, bromide-, fluoride-, strontium-, and sulfate-concentration data show no definitive long-term trends. Barium concentrations range from 740 to 780 mg/L with no trends apparent, particularly when viewed in terms of the ±25-percent potential analytical error (fig. 29). Original boron-concentration data are shown to be strongly influenced by batch effects through duplicate analyses (fig. 30). Boron shows no perceivable trends, most values falling between 26 and 27 mg/L. Bromide-concentration values range from 72 to 80 mg/L (fig. 31), with no trends apparent. Fluoride values (fig. 32) range from 1.5 to 1.9 mg/L, and although an increase occurs between 230 and 310 production days, no other element corroborates this trend and it cannot be considered definitive. All strontium-concentration data, both original BEG data and duplicate BEG data, and IGT atomic absorption analyses show considerable scatter. All three sets of data fall within ±25 percent relative uncertainty of the original BEG data (fig. 33). No long-term trends are apparent in the strontium-concentration data, although the high strontium concentrations (approximately 900 mg/L) are worth noting. Sulfate initially decreased from 13 mg/L to around 1 mg/L, but subsequently has varied between 1 and 4 mg/L (fig. 34). No distinct trend can be seen, especially if the anomalously high first data point is excluded. Although bromide, fluoride, and sulfate lack a consistent long-term trend, they do show small-scale monthly or semimonthly concentration changes that are greater than analytic uncertainty.

Elements below Detection Limits

Several elements analyzed were never found to be above the detection limits of the methods of analysis used. These elements are arsenic, cadmium, chromium, copper, lead, mercury, nickel, and tin. The analyses may not, however, reflect the true upper limit on the concentration of these elements because all these elements may have been unstable in the samples as they were collected. Samples are generally acidified to prevent all these elements from forming precipitates or from bonding with the polyethylene sample bottle. In the case of

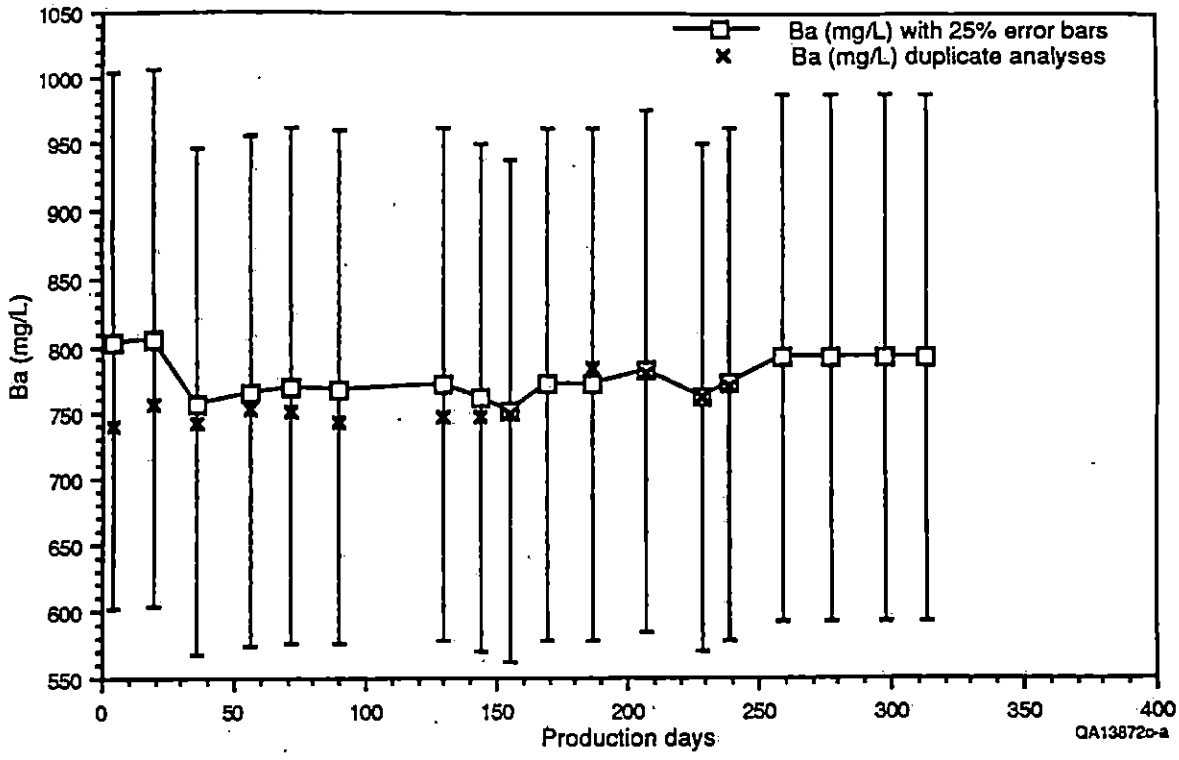

Figure 29. Barium-concentration data (mg/L) of Pleasant Bayou No. 2 through the current production period with ±25 percent relative error bars and values of duplicate analyses.

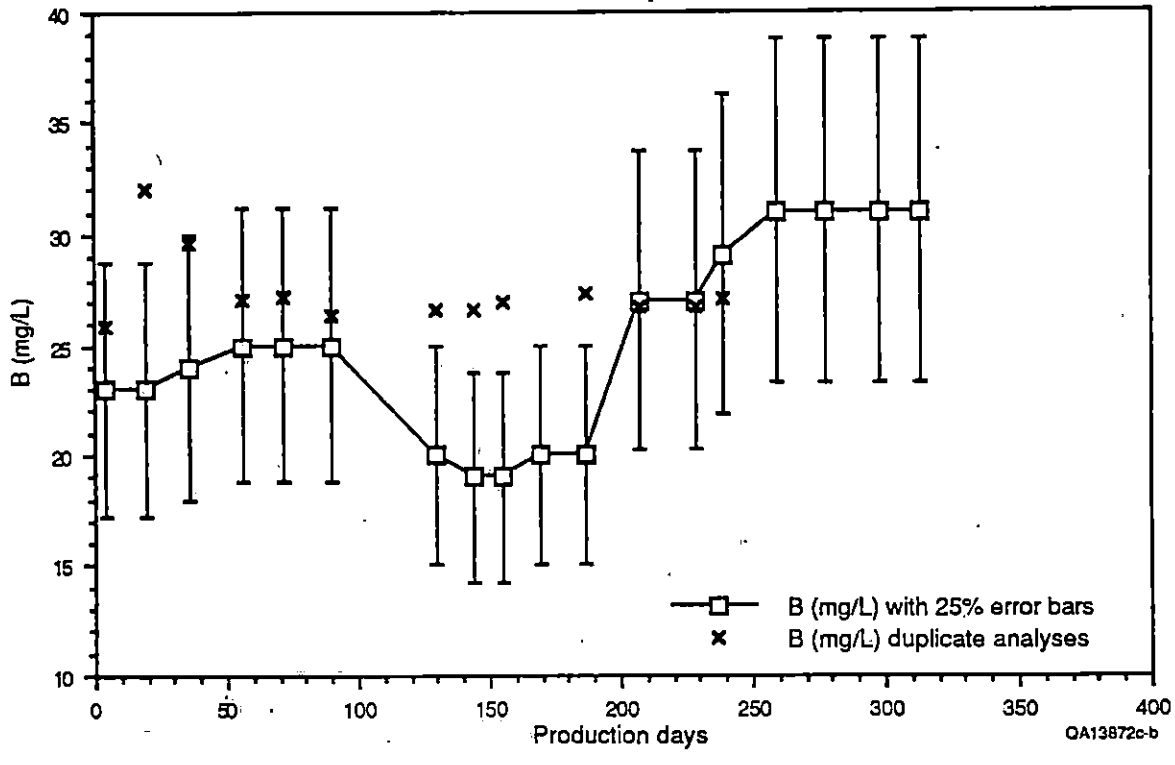

Figure 30. Boron-concentration data (mg/L) of Pleasant Bayou No. 2 through the current production period with ±25 percent relative error bars and values of duplicate analyses.

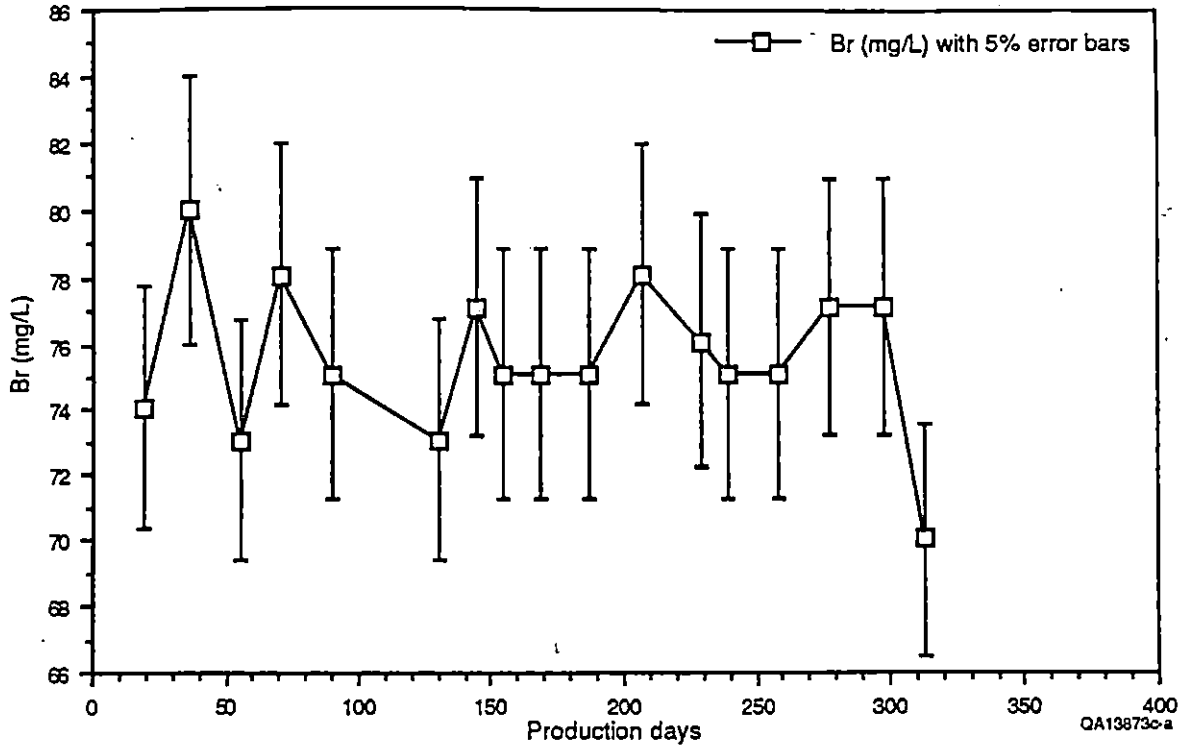

Figure 31. Bromide-concentration data (mg/L) of Pleasant Bayou No. 2 through the current production period with ±5 percent relative error bars.

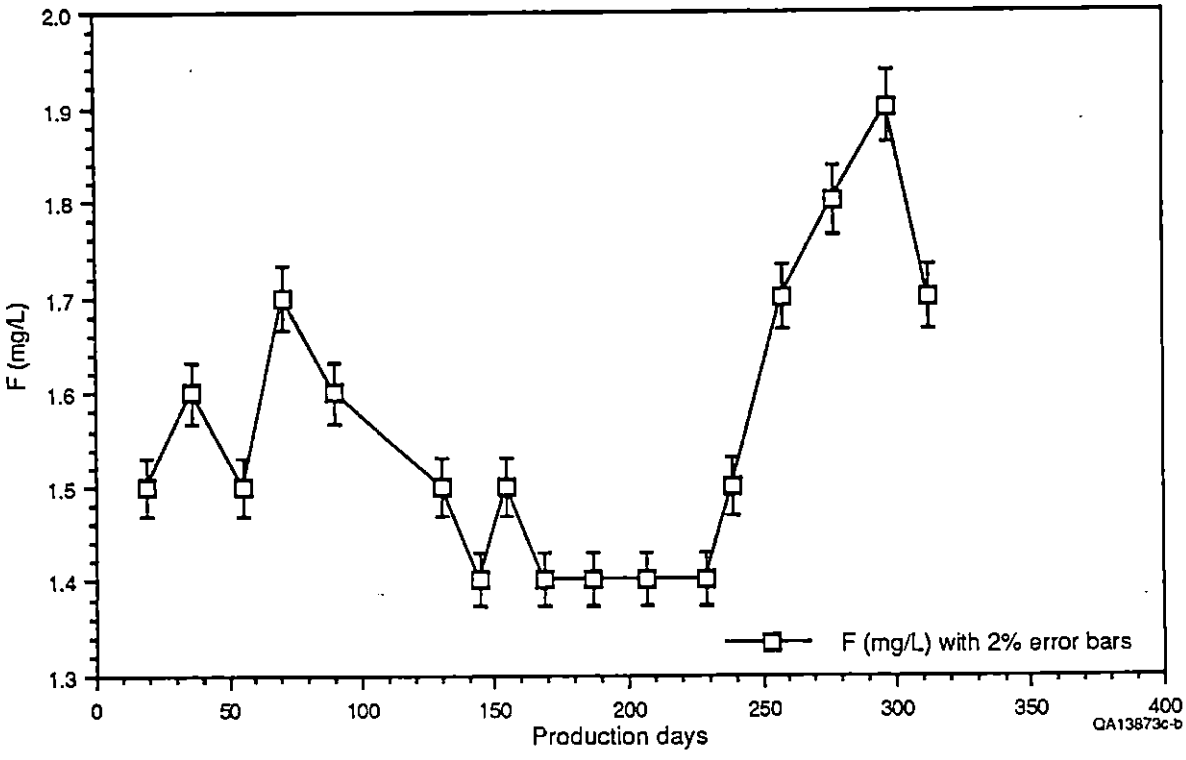

Figure 32. Fluoride-concentration data (mg/L) of Pleasant Bayou No. 2 through the current production period with ±2 percent relative error bars.

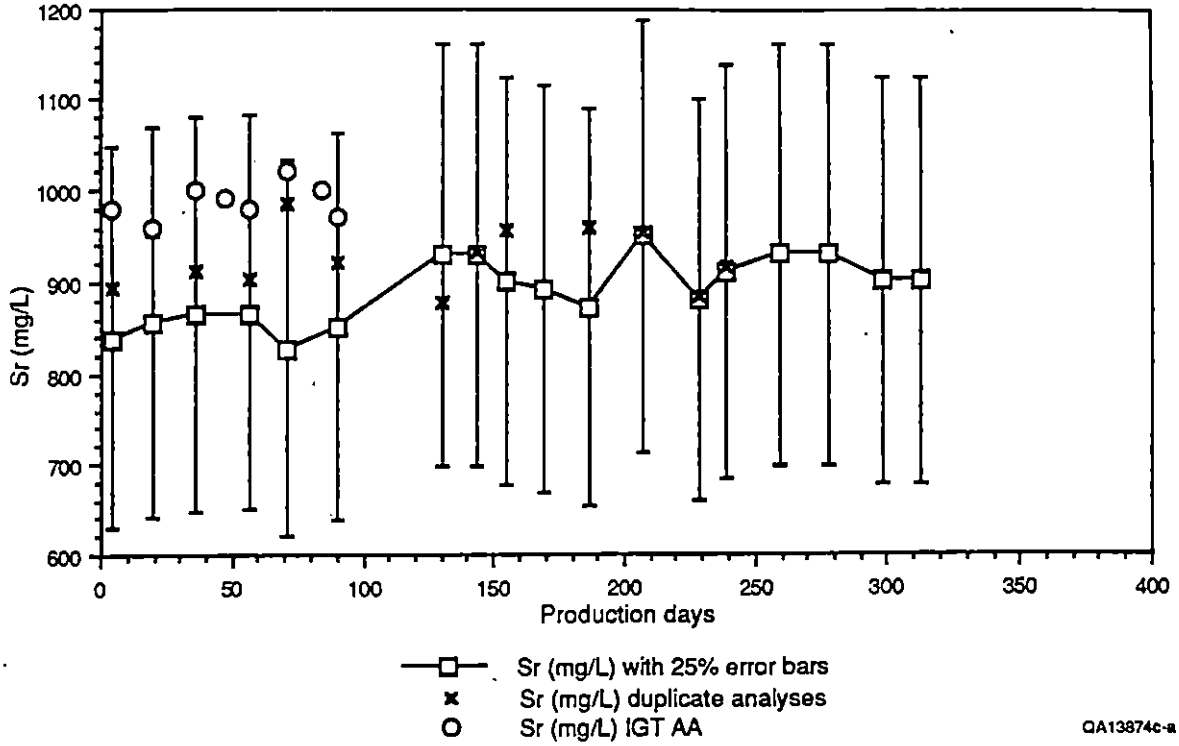

Figure 33. Strontium-concentration data (mg/L) of Pleasant Bayou No. 2 through the current production period with ±25 percent relative error bars and values of duplicate analyses. Also shown are strontium-concentration values reported by IGT obtained by atomic absorption analyses (Eaton Operating Co., Inc., 1988a).

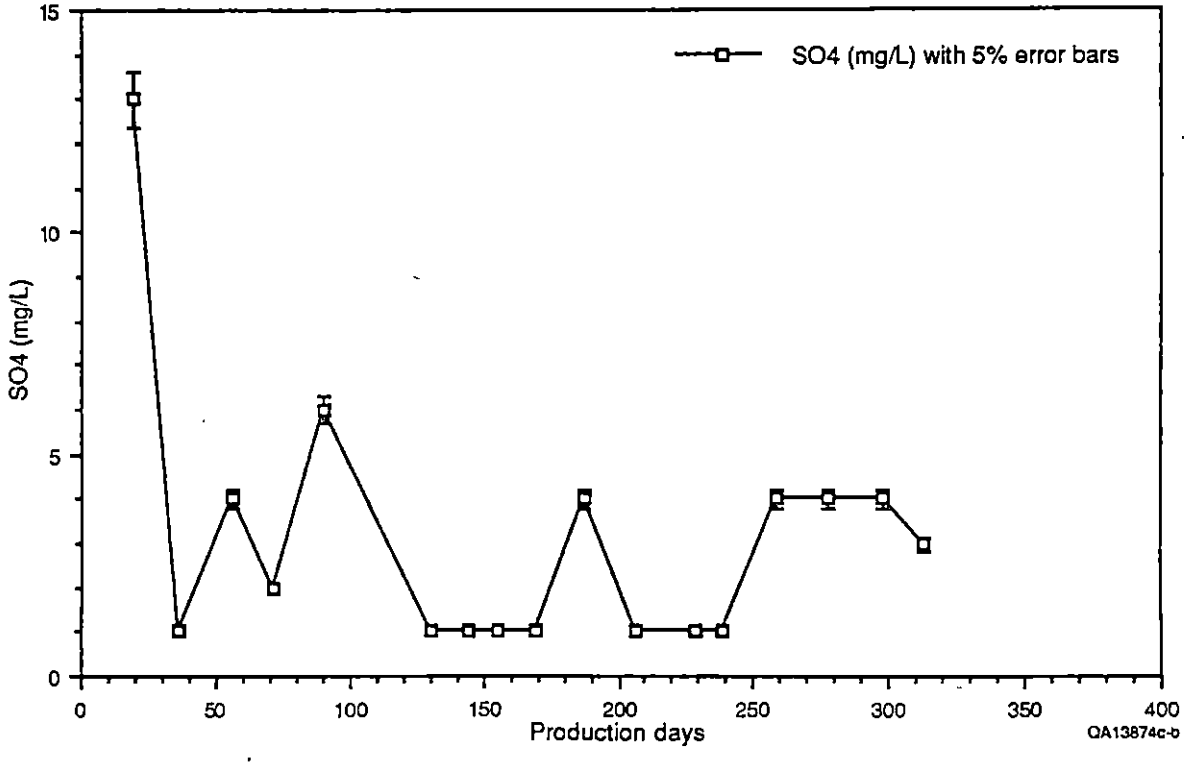

Figure 34. Sulfate-concentration data (mg/L) of Pleasant Bayou No. 2 through the current production period with ±5 percent relative error bars.

mercury, samples should be collected in a glass container because mercury can escape through polyethylene as a vapor. Generally mercury analyses on brines need to be done immediately. These elements will not be discussed further.

Summary of Compositional Changes

The overall salinity of the brine produced increased dramatically during the first 40 d of production, as evidenced by both TDS and chloride-concentration data. A possible initial decrease in salinity (first 20 d) may or may not be real because it is within the limits of uncertainty. TDS increased from 127,000 to 133,000 mg/L within the first 40 d, an increase of 4.6 percent, whereas chloride increased from 70,310 to 72,240 mg/L, an increase of 2.7 percent. After approximately 40 d, the salinity of the brine increased more gradually as evidenced by concentration increases of 1 percent for TDS and 0.1 percent for chloride throughout the remainder of brine production sampled. Sodium-concentration data may have initially increased and then slightly decreased or leveled off, but large errors and inconsistent duplicate analyses obscure any trends. The problems with sodium-concentration data make calculation of the solution's charge balance difficult.

Certain cations appeared to show an overall increase in concentration with or without sharp changes in the rate of increase. Calcium-concentration data increased rapidly at first and then increased more gradually or leveled off, suggestive of chloride and TDS. Overall, Calcium concentrations increased from 7,620 to 7970 mg/L, an increase of 4.5 percent. Potassium and ammonia both increased through current production, with good correlation of concentration trends. Manganese concentrations also appeared to be increasing, both in original and duplicate analyses. Duplicate analyses showed an increase from 16 to 18 mg/L, an increase of more than 11 percent.

Zinc and iodide both showed a trend toward decreasing concentrations. Zinc declined from around 0.6 mg/L to around 0.3 or 0.4 mg/L, a sharp decrease of at least 40 percent. Iodide

also decreased from 23 to 19 mg/L (19 percent), but a large relative error (±15 percent) precludes definitive observations. Bromide and lithium also appeared to be decreasing, but within analytical uncertainty.

The overall change in brine composition is thus marked by a general increase in brine concentration, with corresponding increases in chloride, calcium, potassium, ammonium, and manganese, and overall decreases in zinc and iodide, and perhaps sulfate, bromide, and lithium.

Short-term Compositional Changes

In the preceding discussion, long-term concentration changes and overall trends through the current production period were described. Short-term changes and trends were not discussed, and most elements that were described as having no trends may indeed exhibit short-term, small-scale changes. Some of these short-term changes are within the analytical uncertainty (for example, sodium and calcium, figs. 9 and 11), whereas some are definitely beyond the analytical uncertainty (for example, fluoride and sulfate, figs. 32 and 34).

An attempt was made to correlate the timing of small-scale changes among various elements. A possible short-term event may be observed between 150 and 200 production days, as reflected by an increase in phosphonate, chloride, and perhaps lithium, and a decrease in potassium and possibly sodium, but no consistent trends were observed. Given the current sampling interval and large relative uncertainties, short-term compositional changes were difficult to detect and document, but apparently short-term concentration changes did take place. These short-term changes might be correlated with interruptions in well production. In general, it appears that small-scale changes in choride (and thus TDS) occur at roughly the same frequency as well shut-ins (fig. 35).

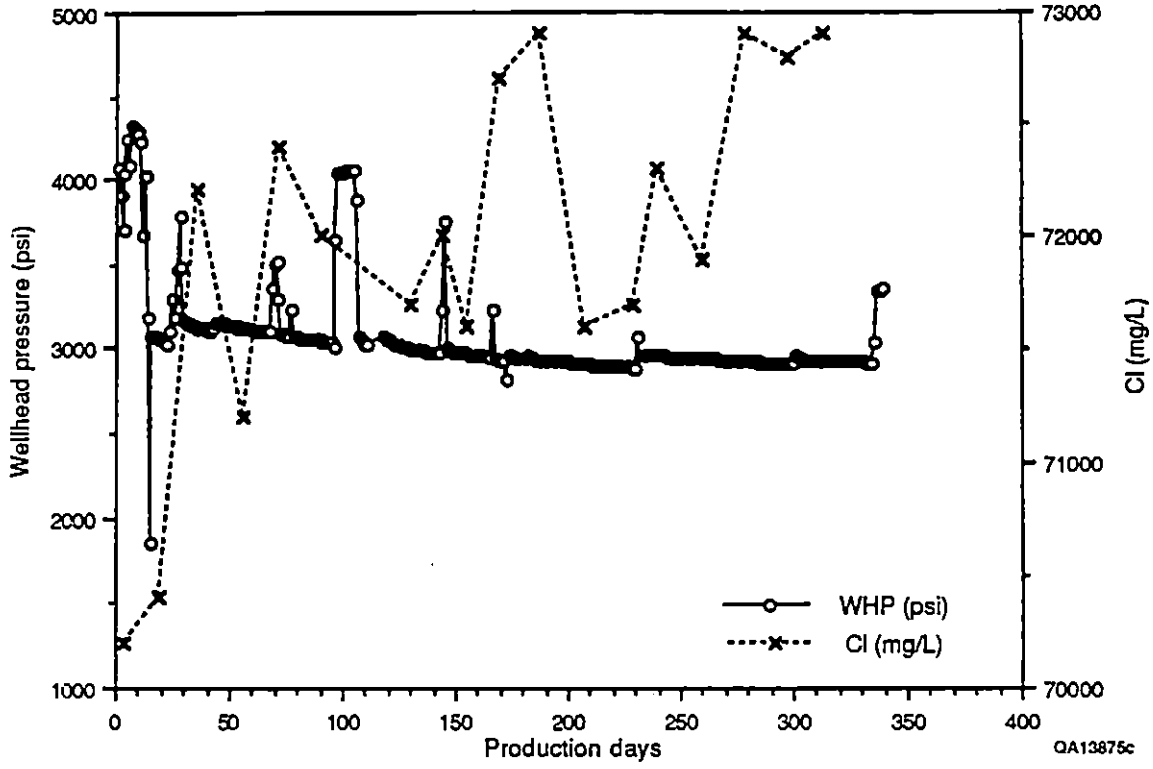

Figure 35. Wellhead pressure (psi) and chloride concentration (mg/L) of Pleasant Bayou No. 2 through the current production period (sharp increases in wellhead pressure correspond to well shut-ins).

COMPARISON OF CURRENT PLEASANT BAYOU NO. 2 SAMPLES WITH PREVIOUSLY COLLECTED SAMPLES

During the 10 yr since the Pleasant Bayou No. 2 well was drilled, numerous production and sampling programs have been conducted. Three samples collected from the well, two immediately after it was drilled (Kharaka and others, 1980) and one approximately 1 yr later (Morton and others, 1981), provided information adequate enough to be compared with that of the samples collected during current long-term production. One of these three earlier samples is particularly instructive in that it was collected from a depth in the well greater than the current production depth.

Drilling of the Pleasant Bayou No. 2 well was completed to a total depth of 5,029 m (16,500 ft) on May 28, 1979. Packers were set and the well was perforated and tested at increasingly shallower depths throughout June and July 1979. During that time two fluid samples were collected by Kharaka and others (1980), the first from 4,749 m (15,589 ft) in the Frio T5 unit F zone and the second from 4,474 m (14,682 ft) in the Frio T5 unit C zone, the current production zone. That the fluid sampled was not contaminated with drilling fluid had to be ensured because these samples were collected during the production test immediately after completion of the well. To do this, we collected the samples only after the conductivity of the production fluid showed no variation for approximately 1.5 h, suggesting that the fluid no longer contained a significant fraction of drilling fluid (Kharaka and others, 1980).

In early 1981, another sample was collected by the operator and analyzed at the BEG Mineral Studies Laboratory (Morton and others, 1981). The procedure for collection of this sample is uncertain. The Pleasant Bayou No. 2 well was produced numerous times between collection of this 1981 sample and that of Kharaka and others (1980). Determining the production history from the field reports available was impossible.

The compositions of these earlier samples are compared with those from the current long-term-production testing in figure 36a through r. Several elements follow a similar pattern between 1979 and 1989. This pattern is typified best by chloride and calcium (fig. 36c and d) and is marked by a decrease in brine concentration (as reflected in chloride concentrations) of about 3 percent between 1979 and 1981, a further decrease of about 11 percent between 1981 and 1988, followed by a trend toward increasing concentration through the current high-rate production (an increase of about 4 percent). This trend is observed in TDS, chloride, calcium, potassium, magnesium, manganese, and possibly strontium and boron, although large errors obscure details of these last two. The pattern is offset somewhat in trends of current TDS values, which may be anomalously high. Reported TDS values are approximately 10,000 mg/L higher than the corresponding summation of elements for that analysis.

Lithium, zinc, and iodide represent another pattern observed (fig. 36m through o). These three elements appear to have sharply decreased in concentration from 1979 to 1988 (about 23 percent, 18 percent, and 53 percent, respectively) (no 1981 data available) and then continued to decrease (18 percent, 16 percent, and 71 percent, respectively) during current high-rate-production testing. Ammonia, bromide, sodium, and sulfate increase from 1979 to 1981, decrease from 1981 to 1988, and increase or show no trend through current production. Other elements show no discernible trend or do not fit any observed pattern.

Noting these three separate patterns, the dominant long-term trend of overall brine salinity, typified by calcium and chloride, appears to be (1) a small to moderate decrease (3 percent in chloride) between 1979 and 1981, (2) another larger decrease from 1981 to 1988 (11 percent in chloride), followed by (3) a turnaround toward increased brine salinity during current long-term, high-rate production testing (4-percent increase in chloride).

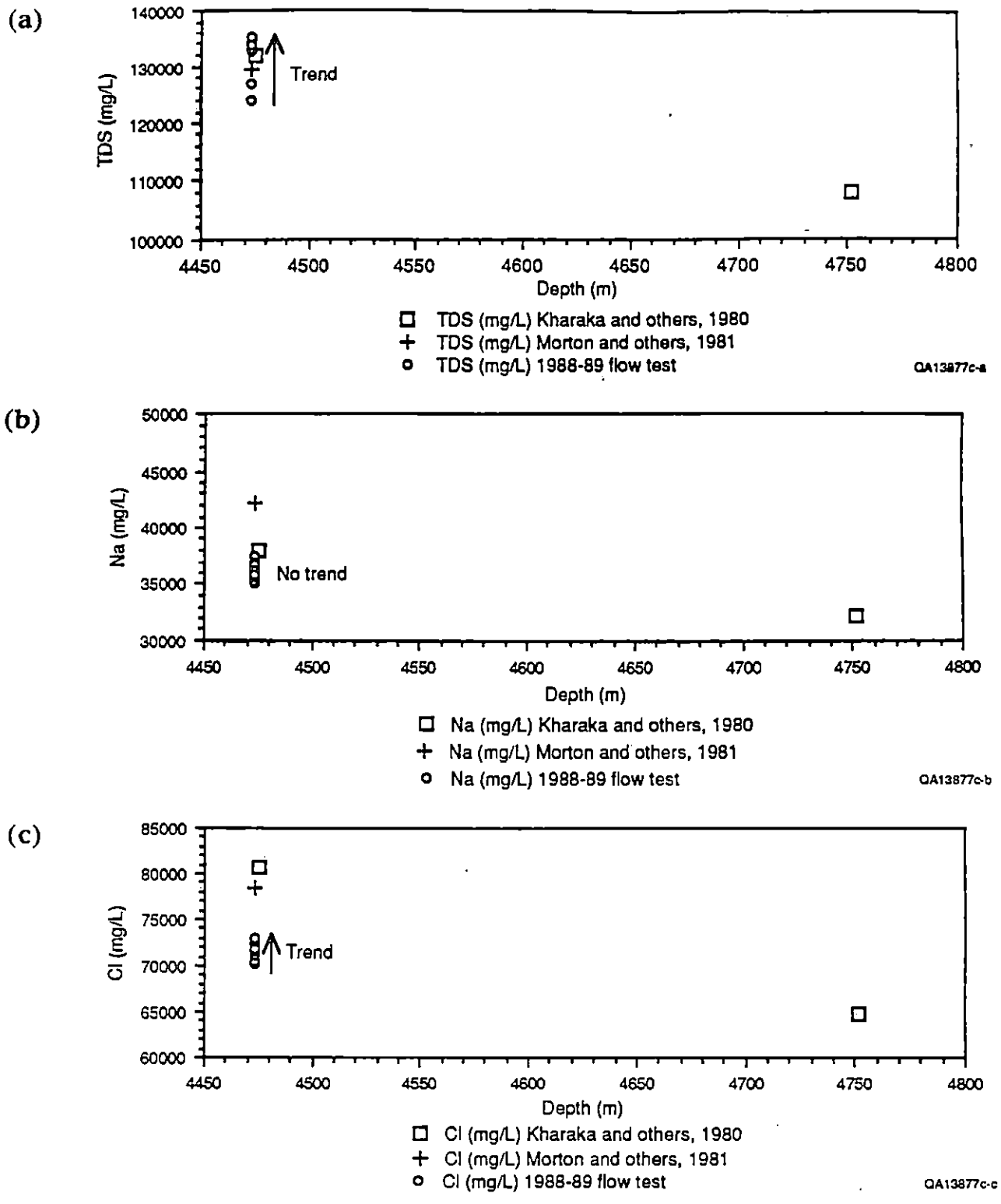

Figure 36. Concentration (mg/L) versus depth plots comparing current Pleasant Bayou No. 2 C-zone brine concentrations (1988–1989 flow test [data in table 2]) with previous C-zone brine analyses (Kharaka and others, 1980; Morton and others, 1981) and a previous F-zone brine analysis (Kharaka and others, 1980)(data in table 3). Also shown is the 1988–1989 flow-test trend (arrow) toward increasing or decreasing concentration with continued production. (a) TDS. (b) Sodium. (c) Chloride. (d) Calcium. (e) Ammonia. (f) Potassium. (g) Magnesium. (h) Manganese. (i) Strontium. (j) Bromide. (k) Sulfate. (l) Fluoride. (m) Lithium. (n) Zinc. (o) Iodide. (p) Iron. (q) Barium. (r) Boron.

(d)

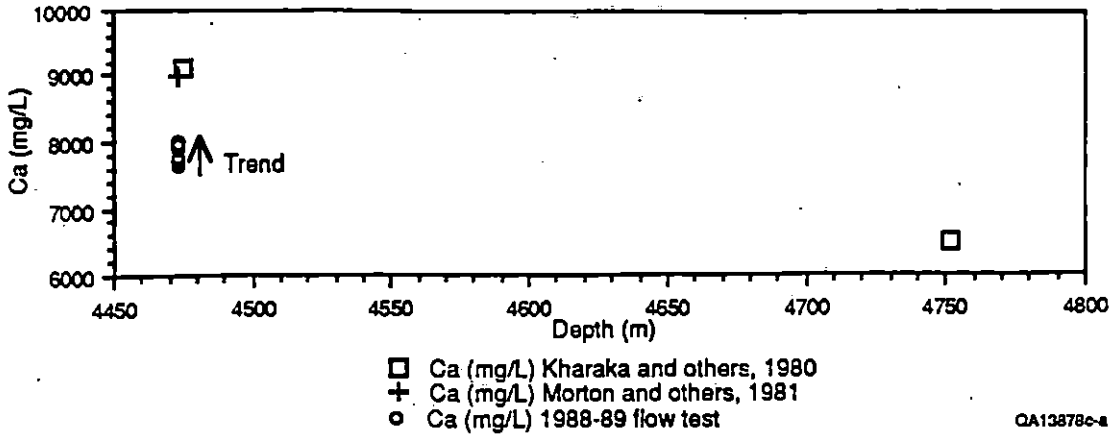

(e)

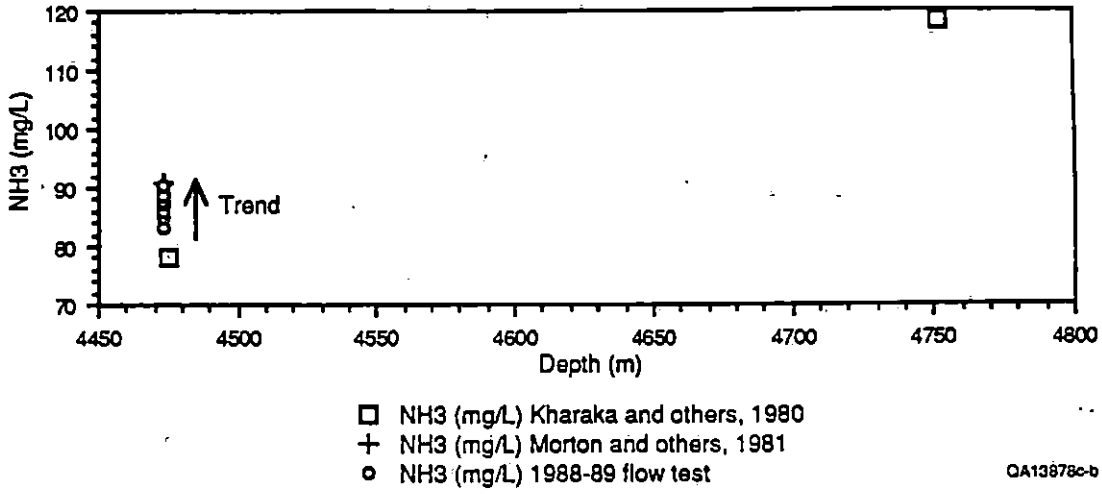

(f)

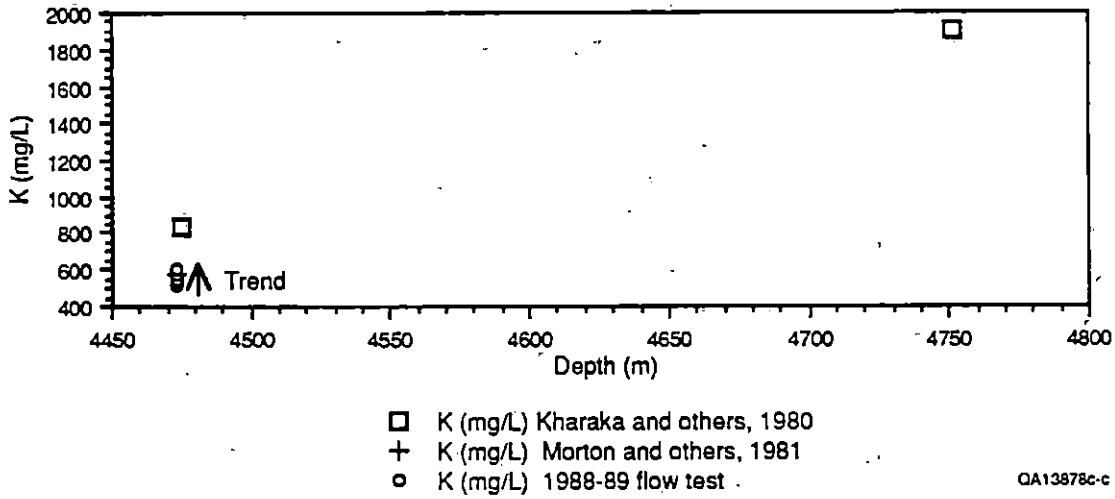

Figure 36. (cont.)

(g)

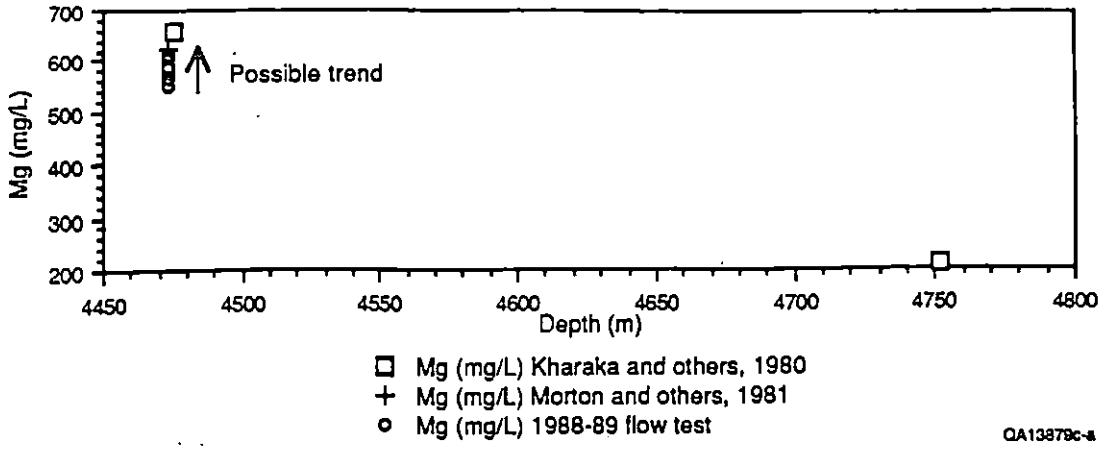

(h)

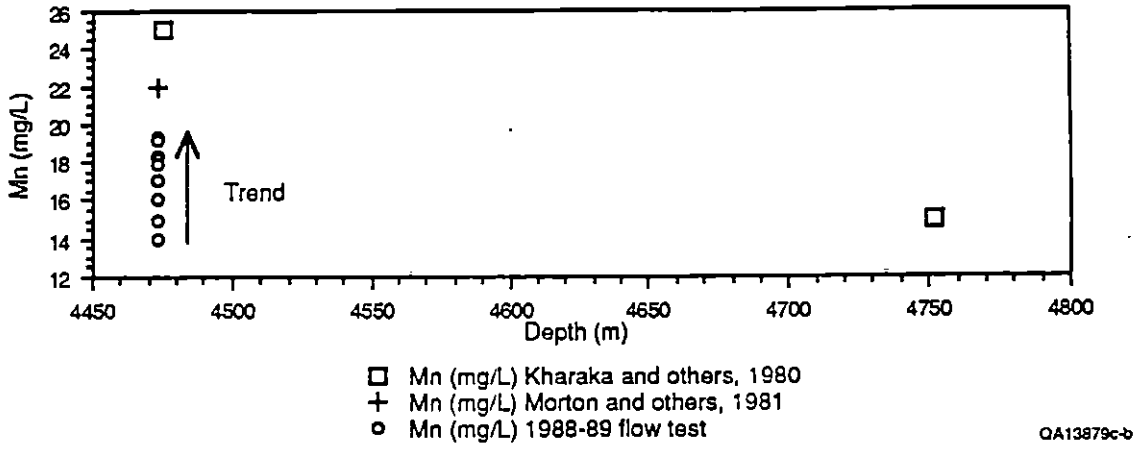

(i)

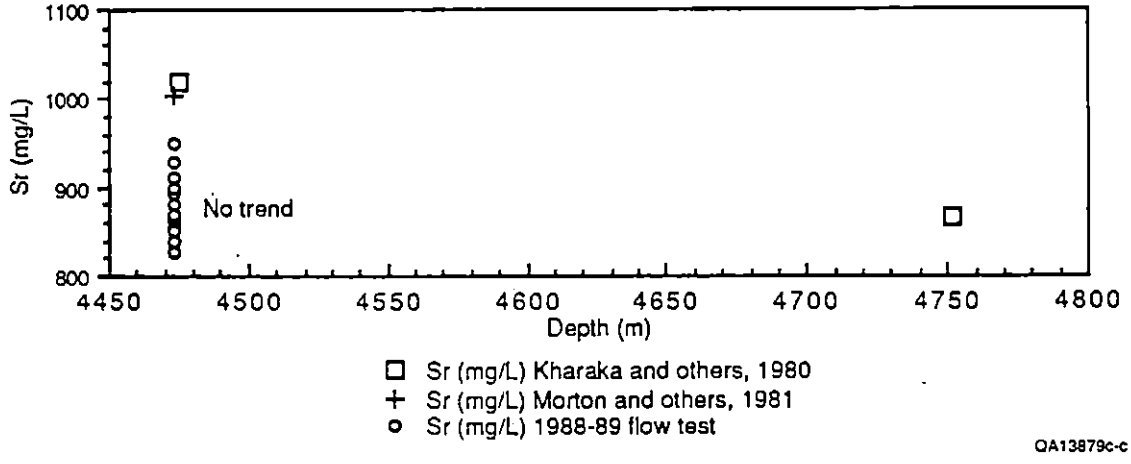

Figure 36. (cont.)

(j)

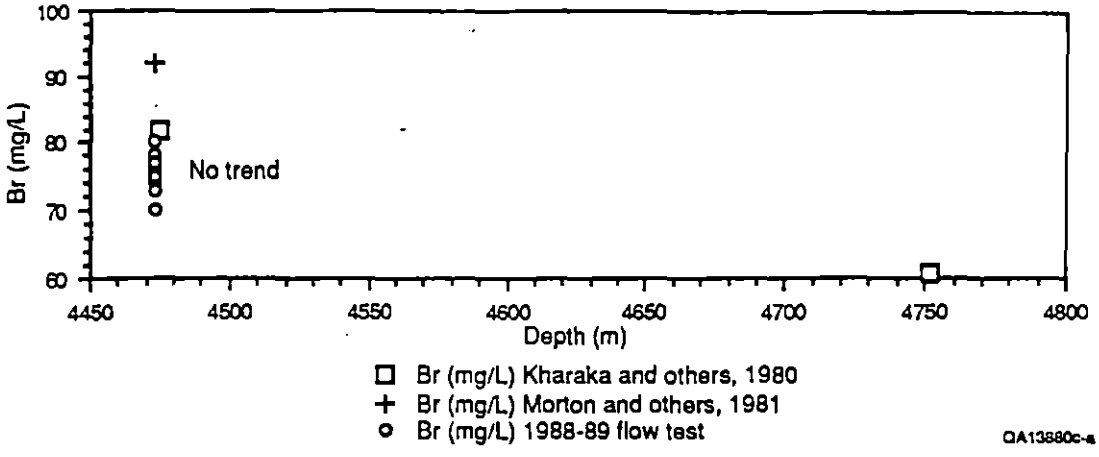

(k)

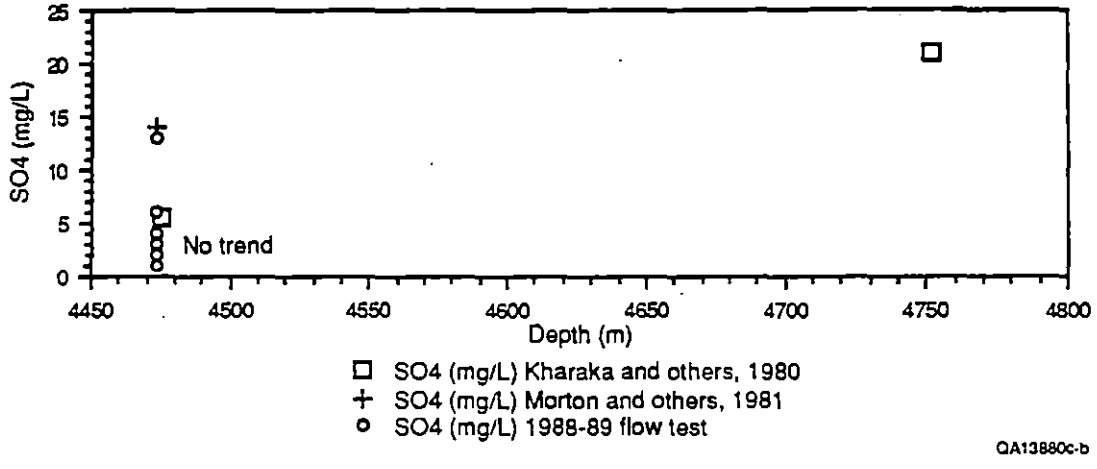

(l)

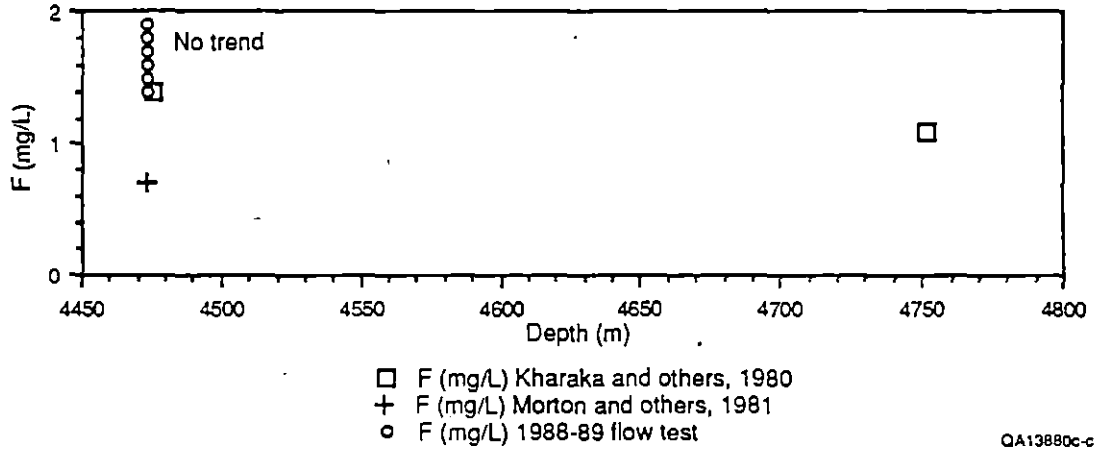

Figure 36. (cont.)

(m)

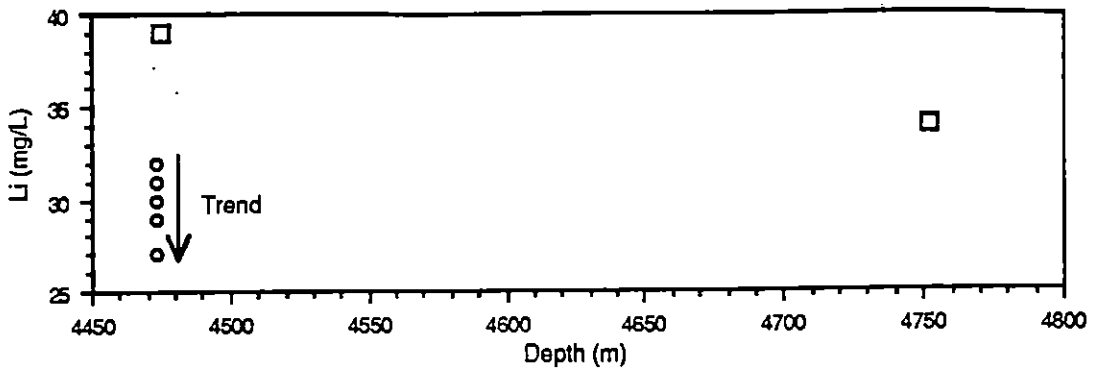

Li (mg/L) Kharaka and others, 1980
Li (mg/L) 1988-89 flow test

QA13881c-a

(n)

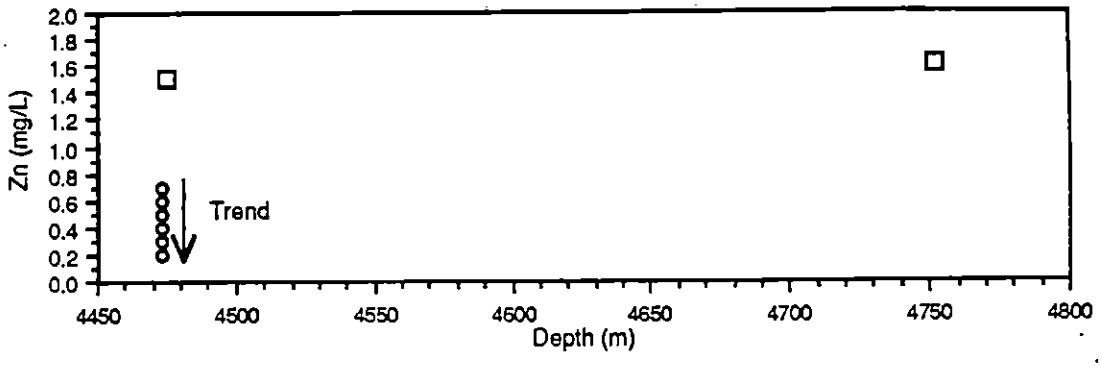

Zn (mg/L) Kharaka and others, 1980
Zn (mg/L) 1988-89 flow test

QA13881c-b

(o)

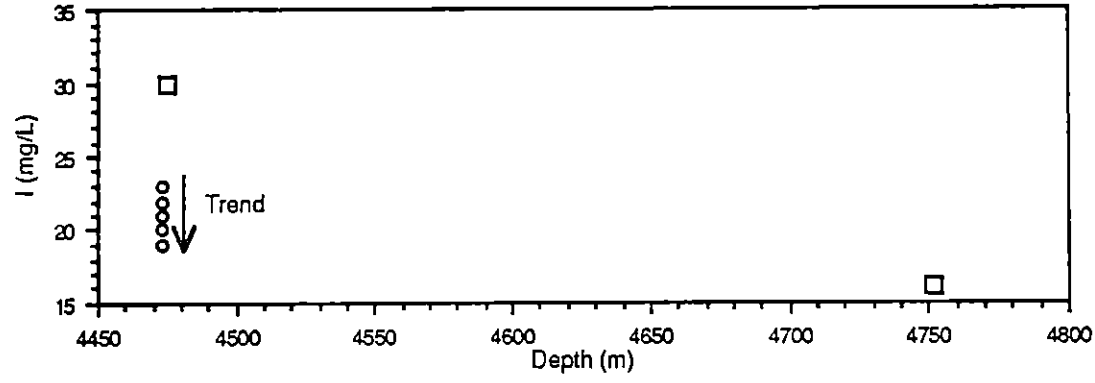

I (mg/L) Kharaka and others, 1980
I (mg/L) 1988-89 flow test

QA13881c-c

Figure 36. (cont.)

(p)

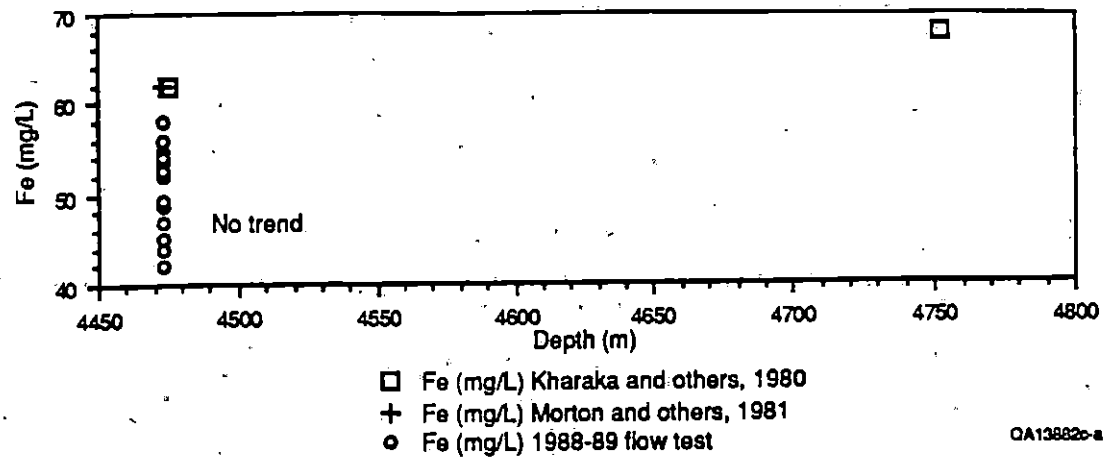

(q)

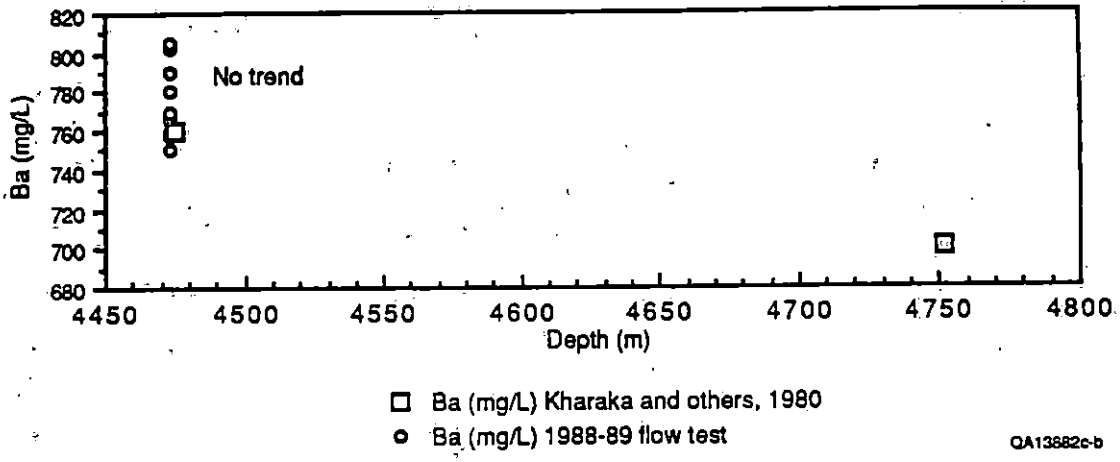

(r)

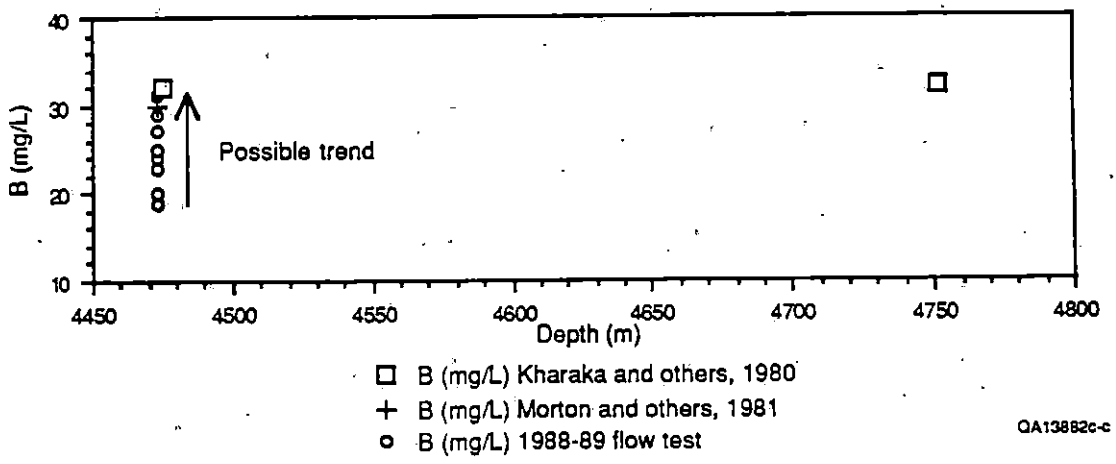

Figure 36. (cont.)

POSSIBLE CAUSES OF CHEMICAL CHANGES DURING LONG-TERM PRODUCTION

Chemical changes in the Pleasant Bayou No. 2 fluid during long-term production may be caused by production changes, natural chemical variations in pore fluids present in the C-zone sandstone, or a shift in the source of the produced fluid. These possibilities are reviewed below.

Production-induced Chemical Changes

Chemical variations during long-term production could be induced by operators, by their changing the separation pressure, injecting a scale or corrosion inhibitor, or changing sampling method or location. Reviewing these possibilities, the shifts in fluid chemistry were probably not the result of production changes—the location and methodology for collection of the brine and gas samples have not changed during the year of sample collection. The separator pressures and production pressures have also remained nearly constant, except for periodic shut-downs of the well.

A phosphonate-scale inhibitor, ATMP, was injected into the C-zone before long-term production began. Recovery concentrations of phosphonate show levels ranging from an initial high of 0.5 mg/L to a low of 0.03 mg/L (fig. 2), suggesting that elements in the phosphonate did not contaminate the samples sufficiently to be of concern. Other possible effects of the scale inhibitor, such as causing the dissolution of formation minerals, were not considered because of data insufficient to calculate aqueous equilibria in the reservoir.

If, however, compositional changes were induced by the scale inhibitor, they would probably follow a pattern comparable to the one created by changes in phosphonate concentration in the fluid. The only correlation that might be made is the initial drop in ATMP during the first 50 d of production with the initial increase in chloride, sodium, calcium, and potassium. The scale inhibitor, however, would probably not affect the chloride content of the

reservoir fluid as a result of mineral reactions. Mineral dissolution due to the injection of scale inhibitor would not be expected to result in an increase in chloride because chloride is a rare component of C-zone minerals around the Pleasant Bayou well. The correlation between chloride, sodium, calcium, potassium, and phosphonate probably reflects changes in the fluid source or natural variations in the reservoir fluid composition.

Champion's Corton RN-97, a corrosion inhibitor, has been injected into the surface brine flow between the wellhead and the brine-sampling location since August 5, 1988. The corrosion inhibitor is present in the brine samples in concentrations of less than 10 mg/L (except between August 5 and September 10, 1988, when the corrosion inhibitor was present in concentrations of between 10 and 20 mg/L)(fig. 37). Therefore, the corrosion inhibitor probably does not affect inorganic elemental concentrations. One exception is iron, which would likely be a product of corrosion. Iron analyses, however, do not correlate with corrosion-inhibitor injection (compare figs. 23 and 37). This is not considered a problem because variations in iron analyses are not accurate enough for use because of the large analytic errors.

We therefore conclude that the variations in concentration of most of the elements analyzed in the brine are the result of natural variations or changes in fluid source area, rather than of artificial inducement during field operations.

Natural Variations in the Composition of C-Zone Reservoir Fluid

Most changes in concentration of the major elements recorded during long-term production are small changes, on the order of 10 percent or less (except potassium). These relatively small compositional changes could be the result of natural variations in the fluid composition within the C-zone reservoir. Unfortunately, chemical analyses of C-zone brine collected from other wells in or around the Pleasant Bayou fault block were not available. Without data for the C-zone from other wells within the 1-mi^2 area influenced by production,

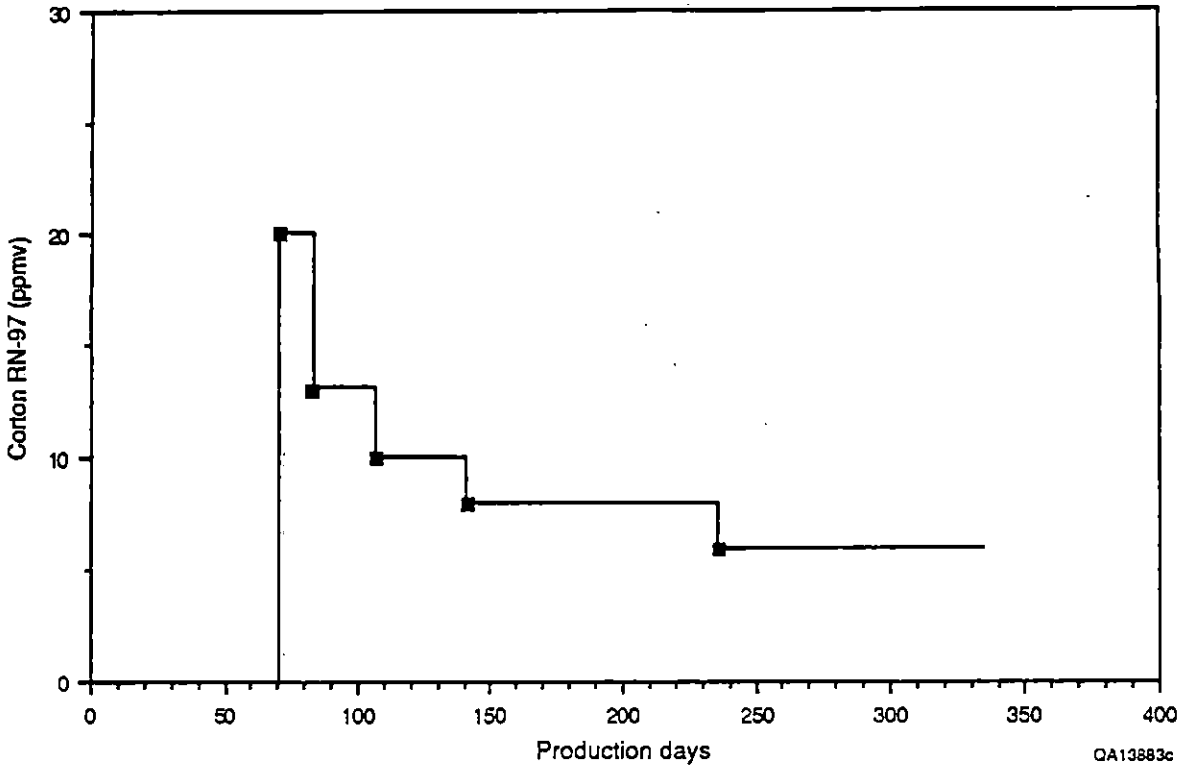

Figure 37. Average concentration (ppm volumetric) of the injected corrosion inhibitor (Corton RN-97) in the brine of Pleasant Bayou No. 2 through the current production period.

predicting the influence of natural variations in C-zone fluids on chemical changes in the brine during current production is difficult.

The uniformity or lack thereof in the composition and depositional history of the C-zone sandstone within the Pleasant Bayou fault block could provide information on possible variations in fluid composition within the reservoir. Any predictions would be based on an assumption that the composition of the C-zone reservoir fluid is governed by both the composition of the reservoir sandstone and the fluid trapped during geopressuring.

The C-zone sandstone is the product of deltaic-distributary-channel and channel-mouth-bar deposition (Tyler and Han, 1982; Hamlin and Tyler, 1988). All lower Frio sediments in the Pleasant Bayou area have a common source area (Loucks and others, 1980, 1981). Thus, detrital mineralogy should be fairly uniform. Some compositional variations in the C-zone sand may result from lateral changes in the amount of intergranular clay matrix and interbedded shale that are commonly observed in a heterogeneous deltaic environment. A wide variation in the composition of the pore fluids in C-zone sandstones within the Pleasant Bayou block would therefore be unexpected on the basis of mineralogical and host-rock compositional changes.

An exception to this assumption of a uniform mineralogical composition within the C-zone is the possible presence of salt deposits, such as those found at Danbury Dome and Hoskin's Mound just to the northwest and south, respectively, of the Pleasant Bayou fault block (fig. 38). Both of these salt domes penetrate the C-zone more than 5 mi from the Pleasant Bayou No. 2 well. An increase in the sodium and chloride content of the C-zone aquifer fluid would be expected as it neared these salt domes. The Anschultz H. L. Peterson No. 1 well, located in Danbury Dome field outside the Pleasant Bayou fault block at a depth of 12,536 ft, produces from the T5 unit C-zone (T. G. Walter, personal communication, 1989). The produced fluid has a chloride concentration of 152,000 mg/L, more than twice that of the Pleasant Bayou No. 2 brine (approximately 72,000 mg/L)(data from table 3), representative of the highly concentrated brine expected to be found in the proximity of salt domes. Therefore, it cannot be ruled out that the increased chloride concentration with increased production may result

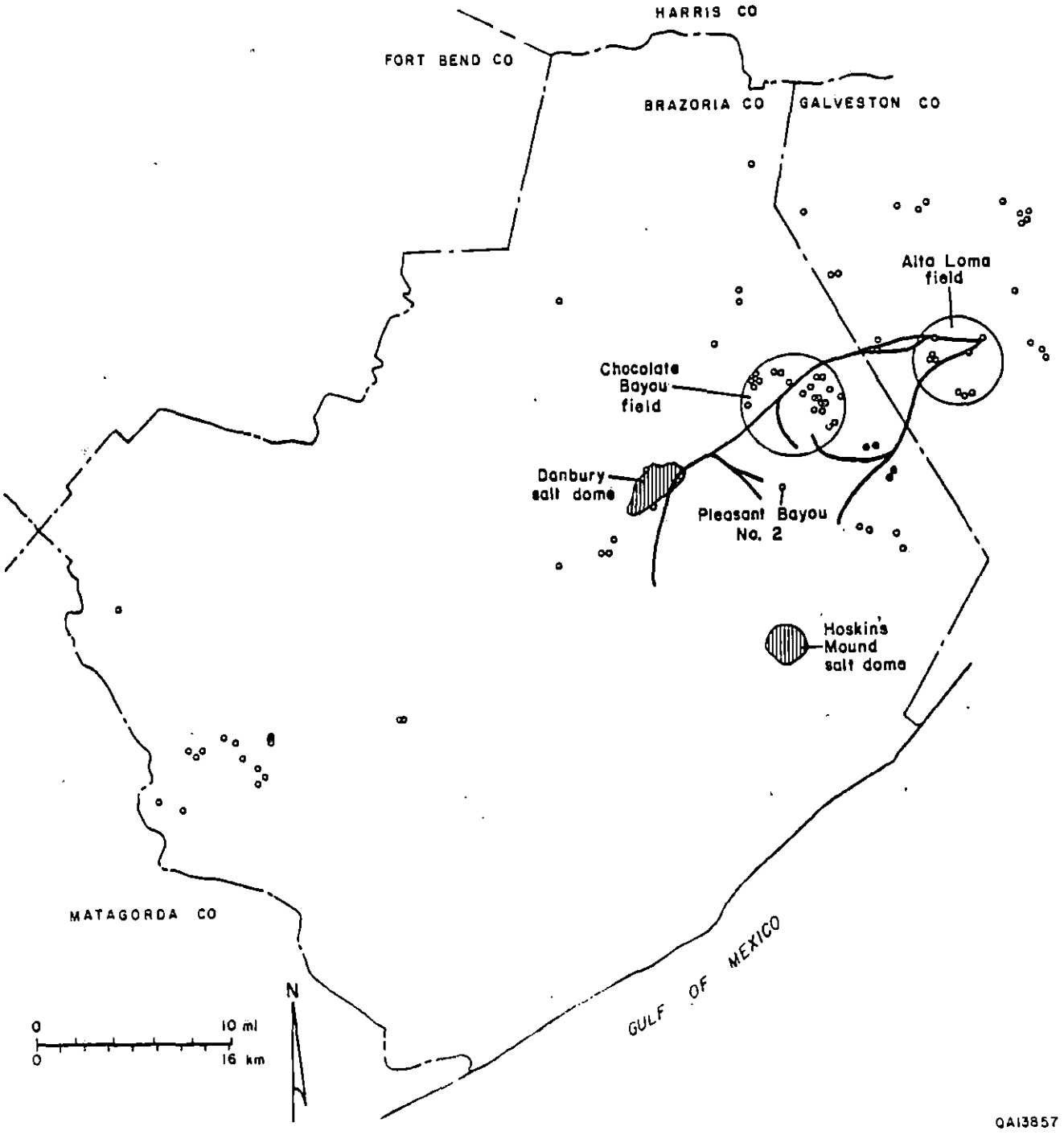

Figure 38. Location map (Universal Transverse Mercator coordinates) of Brazoria County showing the Pleasant Bayou fault block, the Pleasant Bayou No. 2 well, and wells for which water analyses were available. Also shown are Chocolate Bayou and Alta Loma fields and Danbury Dome and Hoskin's Mound salt domes. (Dome locations from Seni and others, 1984.)

Table 3. Brine-chemistry data base for Galveston and Brazoria Counties.

Index no.	Well name	Field	Data source	County	Production zone	Latitude	Longitude	Lat (UTM)	Long (UTM)
1	Mobil T. Martin Fee #4	T. Martin Ranch	1	Brazoria		29.2270	95.1625	581396.7	3233249.3
2	Mobil T. Martin Fee #1	T. Martin Ranch	1	Brazoria		29.2226	95.1537	582255.5	3232767.9
3	Mobil State Use 66709 #1	T. Martin Ranch	1	Brazoria		29.2200	95.1300	584561.3	3232496.7
4	Mobil Houston Farms #1	Houston Farms	1	Brazoria		29.2100	95.1250	585055.5	3231392.3
5	Superior Lockhart Bank unit1 #2	S Alvin	2	Brazoria		29.4057	95.2625	571552.6	3252983.5
6	Superior Lockhart Bank unit1 #3	S Alvin	2	Brazoria		29.3980	95.2625	571558.0	3252130.4
7	Anschutz, H.L. Peterson #1	SW Danbury	2; 3	Brazoria		29.2188	95.3725	560991.1	3232213.4
8	Union Texas, E.L. Summers #1	N Rowan	2	Brazoria		29.3662	95.2844	569454.6	3248593.8
9	Superior Cooper unitB #1	Algoa	2	Galveston		29.4156	95.1825	579306.8	3254132.2
10	Superior Winton unit1	Algoa	2	Galveston		29.4167	95.1769	579849.2	3254257.9
11	Hunt Oil F. Ghinaudo #1	Alta Loma	2	Galveston		29.3679	95.0537	591845.3	3248941.4
12	Hunt Oil Green #2	Alta Loma	2	Galveston		29.3575	95.0663	590631.5	3247779.2
13	Hunt Oil Sayko #2	Alta Loma	2	Galveston	T4 unit	29.3553	95.0969	587663.0	3247512.1
14	Hunt Oil Tacquard #1	Alta Loma W	2; 4	Galveston	T5 unit 'D' zone	29.3673	95.0948	587856.6	3248843.3
15	Superior Eastham Jocku Sonn unit1	Hastings SE	2	Galveston		29.4638	95.2050	577087.6	3259457.7
19	Shell No.1, J.O. Evans	Old Ocean	5	Brazoria		29.0701	95.7011	529093.8	3215612.8
20	Shell No.1, McKinney	Old Ocean	5	Brazoria		29.0731	95.7101	528217.0	3215943.0
21	Shell No.1, J.W. Reynolds	Old Ocean	5	Brazoria		29.0751	95.6701	532109.7	3216174.8
23	Shell, Stanolind-From Heating Treater	Old Ocean	5	Brazoria		29.0721	95.6721	531916.0	3215841.9
24	Shell, Stanolind-From Heating Treater	Old Ocean	5	Brazoria		29.0715	95.6715	531974.6	3215775.5
25	Phillips No.1, Andrau	Chocolate Bayou	5	Brazoria	Andrau ?	29.3374	95.2203	575697.5	3245442.6
26	Humble No.C-1, Blakeley	Danbury	5	Brazoria		29.2719	95.3438	563747.8	3238111.8
27	Humble No.B-1, Moller	Danbury	5	Brazoria		29.2423	95.3375	564378.4	3234835.7
28	Humble No.1, Mettler	Angleton	5	Brazoria		29.2000	95.4200	556384.5	3230106.7
29	Humble No.16, C. Brown	Hastings	5	Brazoria		29.5000	95.2500	572698.1	3263439.7
30	Humble No.1, M. McFarland	Pledger	5	Brazoria		29.1700	95.8000	519448.4	3226660.3
31	Stanolind, Separator Sample	Sandy Point	5	Brazoria		29.4000	95.4170	556565.8	3252267.2
33	Phillips No.3, Lobit	League City	5	Galveston		29.4700	95.1000	587264.0	3260218.7
34	Phillips No.4, Lobit	League City	5	Galveston		29.4649	95.1063	586657.5	3259648.9
35	Humble No.1, Bayou Development Co.	Dickinson	5	Galveston		29.4550	95.0150	595520.1	3258623.4
36	Humble No.2, E.C. Wilson	Dickinson	5	Galveston		29.4600	95.0200	595030.6	3259173.3
37	Humble No.A-19, A. Stewart	Dickinson	5	Galveston		29.4024	95.0250	594599.1	3252787.0

Data source: 1 = Lundergard, 1985; 2 = Morton and others, 1981; 3 = Morton unpublished data, 1981; 4 = Morton and Land, 1987; 5 = Jessen and Rolshausen, 1944; 6 = Taylor, 1975; 7 = Kharaka and others, 1977; 8 = Carothers and Kharaka, 1978, 1980; 9 = Eaton Operating Company, Inc., 1988a and b.

Table 3. (cont.)

Index no.	Well name	Field	Data source	County	Production zone	Latitude	Longitude	Lat (UTM)	Long (UTM)
38	Humble No.B-1, San Leon Co.	Dickinson	5	Galveston		29.4520	95.0180	595232.0	3258288.5
39	Humble No.1, R.B. Peters	Dickinson	5	Galveston		29.4700	95.0350	593566.8	3260269.2
40	Humble No.1, Fream	Dickinson	5	Galveston		29.4620	95.0125	595756.0	3259401.1
43			6	Brazoria	Clay	29.0400	95.6800	531156.7	3212283.4
44			6	Brazoria	Clay	29.0500	95.6800	531153.7	3213391.3
45			3	Brazoria		29.0200	95.7460	524735.3	3210052.0
46			3	Brazoria		29.0250	95.7670	522689.2	3210601.7
48			3	Brazoria		29.0580	95.6940	529788.4	3214274.0
49			3	Brazoria		29.0600	95.7340	525894.0	3214486.1
50			3	Brazoria		29.0640	95.7290	526379.7	3214930.4
51			3	Brazoria		29.0640	95.7400	525308.9	3214928.0
53			3	Brazoria		29.0860	95.5580	543016.2	3217418.1
54	Phillips Houston Fms "A" #2	Chocolate Bayou	3	Brazoria	"A" sand	29.2862	95.1550	582078.4	3239813.8
55	Phillips Kriesling #1	Chocolate Bayou	3	Brazoria	"B" sand	29.3432	95.2488	572926.4	3246067.1
56	Phillips Barsodi #1	Chocolate Bayou	3	Brazoria	9100' sand	29.3356	95.2500	572815.3	3245224.3
57	Phillips Smiley-Benson #1	Chocolate Bayou	3	Brazoria	L. Weiting	29.3454	95.2331	574449.0	3246320.8
58	Phillips Plummer #1	Chocolate Bayou	3	Brazoria	Andrau	29.3388	95.2475	573055.7	3245580.4
59	Phillips Angle #1	Chocolate Bayou	3	Brazoria	"A" sand	29.3399	95.1963	578025.7	3245735.4
60	Phillips Diecken #1	Chocolate Bayou	3	Brazoria	Alibel	29.3251	95.1763	579979.0	3244109.1
61	Phillips Kempner #1	Chocolate Bayou	3	Brazoria	Banfield	29.3399	95.1938	578268.5	3245737.1
62	Phillips Gunderson #2	Chocolate Bayou	3	Brazoria	Andrau	29.3037	95.1825	579393.6	3241733.8
64	Phillips Thompson Trustee #1	Hitchcock	3	Galveston	9100' sand	29.3635	95.0125	595848.4	3248487.0
65	Phillips League City	League City	3	Galveston	8700' sand	29.4670	95.1250	584842.4	3259867.8
66	Phillips Tacquard #2	Alta Loma	3	Galveston	L. Weiting	29.3264	95.0638	590901.8	3244335.3
67	Phillips Adriance #1UT	Alta Loma	3	Galveston	Upper Schenck	29.3525	95.1000	587364.5	3247199.6
68	Phillips Bernand #6	Chocolate Bayou	7; 8	Brazoria	"A" sand	29.3434	95.2275	574994.1	3246102.8
55	Phillips Kresling #1	Chocolate Bayou	7; 8	Brazoria	"B" sand	29.3432	95.2488	572926.4	3246067.1
56	Phillips Barsodi #1	Chocolate Bayou	7; 8	Brazoria	Upper Grubbs	29.3356	95.2500	572815.3	3245224.3
71	Phillips Kitchen #1	Chocolate Bayou	7; 8	Brazoria	"B" sand	29.3383	95.2525	572570.6	3245521.9
72	Phillips Banfield #1	Chocolate Bayou	7; 8	Brazoria	Upper Houston Farms	29.3279	95.2071	576986.2	3244398.6
73	Phillips Houston "M" #1	Chocolate Bayou	7; 8	Brazoria	"P" Sand	29.3200	95.2550	572340.8	3243492.8
74	Phillips Angle #3	Chocolate Bayou	7; 8	Brazoria	Upper Weiting	29.3329	95.2016	577516.5	3244956.3
75	Phillips Cozby #1-shallow	Chocolate Bayou	7; 8	Brazoria	Banfield	29.3220	95.1938	578282.1	3243753.8
75	Phillips Cozby #1-deep	Chocolate Bayou	7; 8	Brazoria	Upper Weiting	29.3220	95.1938	578282.1	3243753.8

Table 3. (cont.)

Index no.	Well name	Field	Data source	County	Production zone	Latitude	Longitude	Lat (UTM)	Long (UTM)
77	Phillips Schenck #3	Chocolate Bayou	7; 8	Brazoria	Upper Weiting	29.3240	95.1975	577921.3	3243972.9
78	Phillips Alibel #1	Chocolate Bayou	7; 8	Brazoria	Alibel	29.3202	95.1931	578351.5	3243554.8
79	Phillips Old #2	Chocolate Bayou	7; 8	Brazoria	Alibel	29.3152	95.1988	577801.8	3242997.0
80	Phillips Houston "K" #1	Chocolate Bayou	7; 8	Brazoria	Upper Weiting	29.3015	95.1860	579055.3	3241487.6
81	Phillips Cozby #2	Chocolate Bayou	7; 8	Brazoria	Schenck T4 unit	29.3208	95.1923	578428.7	3243621.8
82	Phillips Gardiner #1	Chocolate Bayou	7; 8	Brazoria	Lower Weiting	29.2880	95.1488	582679.2	3240017.6
83	Texaco Weiting #5	Chocolate Bayou	7; 8	Brazoria	Alibel	29.3300	95.1853	579101.3	3244645.9
84	Texaco Wilson "A" #2	Chocolate Bayou	7; 8	Brazoria	Alibel	29.3150	95.1934	578326.3	3242978.4
87	Phillips Houston "FF" #1	Halls Bayou	7; 8	Brazoria	Schenck T4 unit	29.2626	95.1363	583914.1	3237212.2
88	Phillips Houston "CC" #1	Halls Bayou	7; 8	Brazoria	Harris T4 unit	29.2683	95.1330	584230.1	3237846.1
89	Phillips Huff "A" #1	Hitchcock	7; 8	Galveston	9100' sand	29.3525	95.0000	597072.1	3247278.5
90	Phillips Prets #1	Hitchcock	7; 8	Galveston	9100' sand	29.3586	95.0031	596765.4	3247951.8
91	Phillips Pabst "B" #3	Alta Loma S	7; 8	Galveston	Upper Schenck	29.3531	95.0963	587723.2	3247268.8
92	Phillips Evans "A" #1	Alta Loma E	7; 8	Galveston	T5 unit 'B' zone	29.3240	95.0700	590301.9	3244064.6
92	Phillips Evans "A" #1	Alta Loma E	3	Galveston	T5 unit 'G' zone	29.3240	95.0700	590301.9	3244064.6
93	Pleasant Bayou #2 1980a	Pleasant Bayou	7	Brazoria	T5 unit 'F' zone	29.2557	95.2280	575009.6	3236385.5
93	Pleasant Bayou #2 1980b	Pleasant Bayou	7	Brazoria	T5 unit 'C' zone	29.2557	95.2280	575009.6	3236385.5
93	Pleasant Bayou #2 (Day #15, 1988-89)	Pleasant Bayou	9	Brazoria	T5 unit 'C' zone	29.2557	95.2280	575009.6	3236385.5
93	Pleasant Bayou #2 1981-272	Pleasant Bayou	2	Brazoria	T5 unit 'C' zone	29.2557	95.2280	575009.6	3236385.5
96	Anschutz Phillips Renn #1	NW Danbury	3	Brazoria		29.2105	95.3773	560529.5	3231291.3
97	Anschutz J.R. Marmion #1	NW Danbury	3	Brazoria		29.2102	95.3815	560121.4	3231255.9
102	Phillips McVea #1	Alta Loma E	3	Galveston	T5 unit 'G' zone	29.3265	95.0740	589911.3	3244338.5

Table 3. (cont.)

Index no.	Date of analysis	Gas/water (volume)	Well type	Depth (m)	Temp (°C)	Press (MPa)	S.G.	pH	Na (mg/L)	K (mg/L)	Ca (mg/L)	Mg (mg/L)	Sr (mg/L)	SiO_2 (mg/L)	Cl (mg/L)	Total alk (mg/L)
1	1985			4540.9	157				36700	434	15912	1000	947	83	90800	180
2	1985			4457.7	157				40500	490	19176	1137	993	71	103500	216
3	1985			3768.9	133				5200	58	61	9	7	129	7000	1227
4	1985			3816.1	128											
5	1981	2.85		3211.4	103			7.8	37900	292	1010	180	157	60	59500	
6	1981		oil	2961.7	98			7.8	30600	216	903	196	154	56	49100	
7	1981	6.77		3821	126			5.2	69700	1218	22600	1535	1080	60	152000	
8	1981	0.18		3310.4	119				22700	171	330	59.7	49.7	95.2	34000	
9		0.53		3475.6	109			6.1	44000	624	8350	710	350	25	83600	
10		4.28		3500.6	128			5.9	42400	643	8580	670	380	22	80900	
11			oil	3291.8	103			8	24900	180	606	88.4	116	102	36700	
12			oil	3438.1	108			8	20900	185	1190	153	143	44.5	33100	
13			oil	3429.6	116			8.1	22700	192	783	95.1	145	114	35200	
14			oil	3741.4	129		1.016	7.4	29800	230	1490	151	272	83.5	46300	536
15		11.76		2979.4	101			7.4	49300	371	4260	660	381	8.5	83600	
19	1944			3082.4											14600	
20	1944			3087.6											18100	
21	1944			3082.4					10750		333	21			16450	
23	1944			3089.8					14155		137	64			21276	
24	1944			3078.5					7180		24	17			9928	
25	1944			3476.9					29170		2244	360			49951	
26	1944			2016.9					16625		638	112			26500	
27	1944			1728.2					27400		1104	29			43800	
28	1944			3225.1					17581		1688	68			29800	
29	1944			1864.8					38852		1804	322			64000	
30	1944			2072.6					6890		253	72			10900	
31	1944			1980.3					36262		1808	338			59927	
33	1944			2821.5					39996		2374	486			67012	
34	1944			2778.9					37432		1886	400			61921	
35	1944			2766.7					20435		512	235			32750	
36	1944			2447.5					27106		2852	496			48100	
37	1944			2612.1					16542		746	68			26700	

Table 3. (cont.

Index no.	Date of analysis	Gas/water (volume)	Well type	Depth (m)	Temp (°C)	Press (MPa)	S.G.	pH	Na (mg/L)	K (mg/L)	Ca (mg/L)	Mg (mg/L)	Sr (mg/L)	SiO_2 (mg/L)	Cl (mg/L)	Total alk (mg/L)
38	1944			2453					34170		2910	380			58750	
39	1944			2467.4					23783		2288	265			41000	
40	1944			2579.8					19056		1880	41			32300	
43	1941			3087.9			1.024	7.9	12370		184	31			18450	
44	1941			3082.4			1.018	8	9145		90	18			13000	
45	1967			3284.5				6.8	15467		384	78			24300	
46	1967			3180				7	17520		344	64			27300	
48	1967			3084.3				7.4	14258		144	39			21600	
49	1967			3131.8				7.1	9361		120	44			13400	
50	1967			3155.3				7.4	14480		160	49			22000	
51	1967			3099.2				7.3	13152		96	39			19700	
53	1959			3651.8				6.1	24388		1547	206			40100	
54	1946			2645.1	99				15165		425	98			24181	
55	1953			2671	98				15124		302	81			23151	
56	1963			2792.3					16467		292	72			25234	
57	1945			3322.3					18043		827	138			29289	
58	1961			3487.5	120				20400		1600	185			34625	
59	1946			2690.5	100				13843		441	101			21459	
60	1956			2859	107				18306		582	101			28934	
61	1952			3371.7	120				23994		1104	168			39102	
62	1948			3731.7	132				27820		4319	595			52600	
64	1968			2773.7				7.6	15680		480	98			24650	
65	1968			2642.3				7.1	41030		4320	708			72700	
66	1967	27.3		3967.9				6.9	15200		880	183			25180	
67	1967	40.3		3407.7				6.2	18170		660	134			29260	
68		34.7		2624	94	28.1		7	16250	140	380	70	25	68	24000	1610
55		131		2625.9	94	28.1		7.1	15250	120	280	60	22	75	22500	1620
56		223.3		2696	98	26.7		7	15750	110	180	40	19	74	22400	1240
71		357.7		2625.9	96	28.1		7	16500	130	290	60	22	70	23200	1660
72		654.6		2980.9	103	31.7		6.9	16500	120	130	30	22	84	23800	1270
73		62333.3	gas	3326.9	110	50.8		5.1	2.2	0.1	1.3	0.1	0.14	1.5	3	
74		761.2		3462.8	118	52.4		5.9	26500	400	2000	220	365	87	42700	455
75		623.7		3258.9	117	46.3		7	25000	280	710	90	130	81	36300	818
75		66000	gas	3393.6	124	52.4		5.2	600	7.5	23	2.5	5.1	3	900	

Table 3. (cont.)

Index no.	Date of analysis	Gas/water (volume)	Well type	Depth (m)	Temp (°C)	Press (MPa)	S.G.	pH	Na (mg/L)	K (mg/L)	Ca (mg/L)	Mg (mg/L)	Sr (mg/L)	SiO_2 (mg/L)	Cl (mg/L)	Total alk (mg/L)
77		12666.7		3402.8	123	52.4		5.9	22000	270	1700	200	360	63	37500	409
78		67.5		2820.9	105	31.4		7	13000	90	130	25	12	84	18100	1909
79		620.7		2830.1	102	31.4		6.7	14000	90	160	35	13	95	19600	1520
80		766.2		3440	122	52.4		6.3	23250	220	610	95	150	87	35200	818
81		47750	gas	3908.8	111	46.7		5.2	1075	8.5	100	3	5.8	2	1740	
82		56.5		3573.8	127	52.3		6.3	24000	300	2000	235	380	87	40500	530
83		834.3		2827.9	103	31.5		7.4	14000	100	140	30	14	78	20400	1730
84		1067.2		2828.8	106	31.5		7.2	12500	100	170	30	13	79	19600	1540
87		1222.8		4160.8	150	80		6.8	20500	180	1800	170	170	110	34500	409
88		6857.1		3892	138	73.7		6.7	17750	240	1600	185	170	95	29300	395
89		755.1		2722.8	100	39.7		7.1	19000	180	550	95	45	66	26400	1060
90		86.7		2722.8	100	39.7		6.9	17000	160	470	85	35	65	25200	1120
91		182.3		3376.9	118	46.2		6.4	19500	190	700	90	130	80	31000	788
92		5875	gas	3960	154	71.2		5.9	18250	190	1230	170	150	99	29300	561
92	1968			4400.4			1.024	7.8	12190		616	59			19510	
93		4.8		4739.6	150	84.3		6.2	32100	1900	6500	210	867	200	64700	
93		3.7		4461.7	138	78.7		6.5	38000	840	9100	660	1020	120	80600	
93	Jun-88	5.8		4500.1	144		1.082		35300	530	7700	564	855	100	70400	376
93	1981			4465.3				7.4	42100	570	8980	625	1005	131	78500	
96	1981	70.9	gas	4105.7				5	184		14.9	1.2	1.6	0.8	320	
97	1981	106	gas	3687.8				4.5	116		12.9	0.6	0.83	0.4	150	
102	1969	1.6		4434.9			1.015	6.8	7954		316	39			12700	

Table 3. (cont.)

Index no.	HCO_3 (mg/L)	Org alk (mg/L)	TDS (mg/L)	Fe (mg/L)	Al (mg/L)	Mn (mg/L)	Ti (mg/L)	B (mg/L)	P (mg/L)	NH_3 (mg/L)	SO_4 (mg/L)	F (mg/L)	Br (mg/L)	CO_2 (mg/L)	H_2S (mg/L)	Rb (mg/L)
1	88	92	146000													
2	113	103	166000													
3	744	484	13300													
4																
5	600		98500	0	0.5	0.5	0.13	65.4	1.3	66.4	12.4	1	94			
6	340		81726	0	0.5	0.3	0.13	45.5	1.3	35.8	11.4	2.8	63			
7	30		235000	0.1	0.5	0.3	0.13	96.5	1.3	15.6	15.6	0.5	342			
8	1280		58888	8	0.5	0.5	0.13	56	1.3	21	21	1.4	80.5			
9	88		139000	0.1	<1.0	4	<.25	67.7	<2.5	120	2	0.5	81.3			
10	94.3		133000	<0.05	<1.0	6.5	<0.25	64.5	<2.5	125	2.9	1.7	80			
11	848		63665	0.1	<.5	0.7	<.13	43.7	<1.3	23.3	6.2	0.8	48			
12	547		55800	4.5	<.05	1.5	<.13	38.4	<1.3	24	1	0.6	43.7			
13	628		59969	0.1	<.5	1	<.13	39.2	<1.3	1708	7.5	0.8	43.3			
14	536		79900	3.9	<.5	1.4	<.13	53.6	<1.3	27	18.3	0.9	57.4			
15	219		136000	0.1	<.5	4.5	<.13	62.1	<1.3	76.5	51	0.7	95.4			
19																
20																
21	1348										tr.					
23	1507										151					
24	1808		19213								256					
25	580		82342								37					
26	976		44926								75					
27	921															
28	854		49991													
29	183		105161													
30	665															
31	244										69					
33	453		110361								40					
34	450										25					
35	616		54548													
36	488		79042													
37	561		44617													

Table 3. (cont.)

Index no.	HCO_3 (mg/L)	Org alk (mg/L)	TDS (mg/L)	Fe (mg/L)	Al (mg/L)	Mn (mg/L)	Tl (mg/L)	B (mg/L)	P (mg/L)	NH_3 (mg/L)	SO_4 (mg/L)	F (mg/L)	Br (mg/L)	CO_2 (mg/L)	H_2S (mg/L)	Rb (mg/L)
38	458		96668													
39	561		67897													
40	885		54187								25					
43	1720		32849								69			36		
44	2180		24512								68			35		
45	781		41026								16					
46	878		46120								14					
48	1270		37343								32					
49	2310		25285								50					
50	1270		37991								32					
51	1440		34473								46					
53	468		67389								730					
54	1596		41405								58					
55	1635		40339								46					
56	1437		43580								78					
57	655		48991								39					
58	394		57322								38					
59	1630		37498								24					
60	1093		49091								24					
61	649		65147								34					
62	369		86685								1					
64	1122		42085	17												
65	793		119339	13							1					
66	673		42223								13					
67	630		49034	89							7					
68	361	1300	42800	1.4		0.5		45		10.5	43	1	59		BDL	0.3
55	427	1290	40200	0.1		0.4		44		12	43		59		BDL	0.25
56	525	735	40000	0.2		0.2		45		10	42		50		1.5	0.2
71	397	1290	42100	0.1		0.5		42		9.8	39	1.05	60		1.64	0.35
72	582	640	42000	0.5		0.2		40		8.5	25		38		1.94	0.35
73	7		156	8.6				1.4		23	0.1	<0.1	<1		5.94	<0.2
74	334	285	73300	10.2		2.2		35		28.5	2.7	0.83	52		1.21	0.4
75	269	550	63700	0.1		0.6		35		18.5	11	1	59		3.25	0.4
75	50		1570	17		0.6		1.5		9	<0.1	<0.1	<1		2.22	0.2

Table 3. (cont.)

Index no.	HCO_3 (mg/L)	Org alk (mg/L)	TDS (mg/L)	Fe (mg/L)	Al (mg/L)	Mn (mg/L)	Ti (mg/L)	B (mg/L)	P (mg/L)	NH_3 (mg/L)	SO_4 (mg/L)	F (mg/L)	Br (mg/L)	CO_2 (mg/L)	H_2S (mg/L)	Rb (mg/L)
77	269	270	63000	15		2.1		27		22	5.4		43		0.17	0.6
78	562	1200	33400	0.2		0.2		48		6.9	57		46		1.76	0.2
79	632	970	35800	7.8		0.5		47		10.5	59	3.3	37		1.76	0.2
80	302	610	60700	7.7		1.2		33		19.5	11		49		0.79	0.3
81	90		3140	11				1.8		8.8	12	0.05	1		0.85	<0.2
82	317	285	68600	8.1		2.8		30		26	0.6	0.87	45		0.32	0.4
83	596	1110	36600	1		0.3		48		7.4	17		33		2.49	0.25
84	484	1170	34300	2.4		0.4		50		8.7	59		32		2.62	0.2
87	356	53	58100	22		1.7		91		13	16		32		1.41	0.9
88	400	150	50200	17.2		1.6		46		15	6.2	1	31		3.55	0.85
89	334	760	47600	0.5		0.4		44		18.5	31	1.3	26		0.9	0.4
90	643	750	44600	0.1		0.4		41		17	34		25		0.62	0.4
91	787	470	53100	6.8		0.9		30		17.5	11		32		0.58	0.4
92	506	195	50400	41		1		59		19.5	7.7	2.4	49		0.98	0.75
92	964		33398	5.4							17					
93	498		108000	68		15		32		118	21	1.1	61		2	8.4
93	365		132000	62		25		32		78	5.4	1.4	82		0.5	6.3
93	376		124000	42		14		23		83	13	1.5	74			
93			129600	62				30			14		92			
96	54		550	58	<.25	0.7	<.06	4.2	<1.0	18.7	14	0.4	0.8			
97	<1.0		250	2.1	<.25	0.09	<.06	1.8	<.6	13.7	69	0.4	0.4			
102	403		21448	8.1							18					

Table 3. (cont.)

Index no.	Ba (mg/L)	I (mg/L)	Li (mg/L)	δO^{18} per mil,aq	δD per mil,aq	δC^{13} per mil CO_2,aq	Oil/condensate (m^3/day)	Water (m^3/day)	Gas (1000m^3/day)	oil (m^3)/ brine (m^3)	CH^3COO (mg/L)
1				8.5		−9.2					
2				8.5		−4.8					
3				7.3		−3.1					
4											
5											
6											
7											
8											
9											
10											
11											
12											
13											
14				4.3							
15											
19											
20											
21											
23											
24											
25											
26											
27											
28											
29											
30											
31											
33											
34											
35											
36											
37											

Table 3. (cont.)

Index no.	Ba (mg/L)	I (mg/L)	Li (mg/L)	δO^{18} per mil,aq	δD per mil,aq	δC^{13} per mil CO_2,aq	Oil/condensate (m^3/day)	Water (m^3/day)	Gas (1000m^3/day)	oil (m^3)/ brine (m^3)	CH^3COO (mg/L)
38											
39											
40											
43											
44											
45											
46											
48											
49											
50											
51											
53											
54											
55											
56											
57											
58											
59											
60											
61											
62											
64	5										
65	323										
66	94										
67	84										
68	11	26	3.8			−3.7	9.9	325.9	11.3	0.03	1186
55	8.5	25	3.3			−8.9	7.2	112.2	14.7	0.06	1180
56	11	19	3.5	4.91	−9.5	−1.4	0	31.8	7.1	0	679
71	9	27	3.4	4.65	−8.1	−2	3.8	26	9.3	0.15	1280
72	12	14	3.7		−13	−7	0.6	19.4	12.7	0.03	578
73	1.6	1	<0.01				1.4	0.3	18.7	4.67	100
74	290	16	9.9	5.7	−17	−2.2	0.5	6.7	5.1	0.07	271
75	61	19	6.7	4.93	−18.8	−4.3	1	95.4	59.5	0.01	513
75	2.2	<1.0	0.15				1.4	0.6	39.6	2.33	50

Table 3. (cont.)

Index no.	Ba (mg/L)	I (mg/L)	Li (mg/L)	δO^{18} per mil,aq	δD per mil,aq	δC^{13} per mil CO_2,aq	Oil/condensate (m^3/day)	Water (m^3/day)	Gas (1000m^3/day)	oil (m^3)/ brine (m^3)	CH^3COO (mg/L)
77	240	16	7.4			−5.3	1.6	2.4	30.4	0.67	254
78	7.1	20	3.2			−1.5	4.1	41.5	2.8	0.1	1103
79	6.8	20	3.2			−1.1	0.3	8.7	5.4	0.03	920
80	6.6	20	6		−18.4	−1.8	0.2	23.1	17.7	0.01	566
81	0.4	<1	0.16				1.9	0.8	38.2	2.38	40
82	370	18	11	5.64	−18	−4.1	2.1	47.8	2.7	0.04	277
83	8.2	19	3.7			1.1	7.9	17.5	14.6	0.45	1027
84	7.3	22	3.2			0.7	8.9	13.4	14.3	0.66	1097
87	59	11	15		−24.6	−2.3	3.8	57.9	70.8	0.07	53
88	110	15	13		−21.6	−7	0.6	1.4	9.6	0.43	153
89	16	16	4			0.1	13.7	88.2	66.6	0.16	708
90	16	15	4		−14.5	−0.9	2.1	83	7.2	0.03	702
91	64	12	6		−18.7	−3.2	6.5	77.9	14.2	0.08	472
92	110	15	10		−21.3	−4.5	1.3	0.8	4.7	1.63	195
92	37										
93	700	16	34	4.9	−25.8			384			
93	760	30	39	5.4	−20.8			230			
93	805	23	30								
93											
96											
97											
102	10										

Table 3. (cont.)

Index no.	Propionate (mg/L)	Butyrate (mg/L)	Sr_{87}/Sr_{86}	CO_2 in gas (mole%)	CH_4 in gas (mole%)	Ethane in gas (mole%)	Propane in gas (mole%)	N_2 in gas (mole%)	δC^{13} per mil CH_4 in gas	δC^{13} per mil CO_2 in gas
1				4.4	89.8	3.2			-39.2	-5.4
2				4.2	90.5	3.7			-40.3	-4.8
3				1.4	81.4	7.4			-44.3	
4				1.5	89	6.2				
5										
6										
7										
8										
9										
10										
11										
12										
13										
14			0.7099							
15										
19										
20										
21										
23										
24										
25										
26										
27										
28										
29										
30										
31										
33										
34										
35										
36										
37										

Table 3. (cont.)

Index no.	Propionate (mg/L)	Butyrate (mg/L)	Sr_{87}/Sr_{86}	CO_2 in gas (mole%)	CH_4 in gas (mole%)	Ethane in gas (mole%)	Propane in gas (mole%)	N_2 in gas (mole%)	δC^{13} per mil CH_4 in gas	δC^{13} per mil CO_2 in gas
38										
39										
40										
43										
44										
45										
46										
48										
49										
50										
51										
53										
54										
55										
56										
57										
58										
59										
60										
61										
62										
64										
65										
66										
67										
68	88	26			91	5	1.2			
55	80	26			93.6	3.6	1.3			
56	37	18			92.9	3.8	1.9			
71	95	18			91.8	4.1	1.3			
72	44	9			93.3	5.7	1			
73										
74	15	Tr			89.4	5.3	2.9			
75	37	BDL								
75										

Table 3. (cont.)

Index no.	Propionate (mg/L)	Butyrate (mg/L)	Sr_{87}/Sr_{86}	CO_2 in gas (mole%)	CH_4 in gas (mole%)	Ethane in gas (mole%)	Propane in gas (mole%)	N_2 in gas (mole%)	δC^{13} per mil CH_4 in gas	δC^{13} per mil CO_2 in gas
77	15	BDL			89.1	5.3	2.2			
78	66	26			96	2.8	0.4			
79	37	13			96.3	3.1	0.6			
80	37	9			88.1	5.5	2.4			
81										
82	7	BDL			89	6	2.1			
83	66	18								
84	73	BDL								
87	BDL	BDL			90.6	4.7	1.5			
88	BDL	BDL			90.2	4.9	1.5			
89	44	9			89.4	5.2	2.7			
90	37	9			89.9	5.3	2.8			
91	Tr	Tr			90.9	4.7	2			
92	Tr	Tr								
92										
93				5.24	88.93	4.65		0.67		
93				10.54	84.51	2.97		0.57		
93				11.63	83.75	2.83	0.89	0.49		
93										
96										
97										
102										

from a salinity gradient produced by nearby salt deposits. And as is shown below, chloride/bromide ratios suggest that the source of chloride in these waters is the dissolution of evaporites. The fact that this well is outside the Pleasant Bayou block and the lack of chemical control between the salt deposits and the Pleasant Bayou No. 2 test well prohibit any definitive statements about the range and magnitude of a lateral salinity gradient around these domes or their effect on the salinity of the produced Pleasant Bayou brines.

In contrast, fluid samples from Alta Loma field (approximately 8 mi [13 km] to the northeast of the Pleasant Bayou No. 2 well), located mostly within the Pleasant Bayou fault block (fig. 38), indicate that the maximum TDS concentrations in fluids from above and below the C-zone are less than or equal to 80,000 mg/L (fig. 39a)(data from table 3). The maximum TDS value (80,000 mg/L) was obtained from the Hunt Oil Tacquard No. 1 well, producing from within the Pleasant Bayou fault block in the Frio T5 unit D-zone, the zone directly below the Pleasant Bayou No. 2 production zone (C-zone). Assuming that the composition of the D-zone in the Pleasant Bayou No. 2 well is somewhere between that of the overlying C-zone and the underlying F-zone, a Pleasant Bayou No. 2 D-zone TDS concentration between 108,000 and 132,000 mg/L would be expected. This suggests that relatively large lateral variations in salinity, on the order of 25 percent or more, may exist within laterally continuous units in the Pleasant Bayou fault block. The 10-percent change in TDS concentrations through current production can therefore probably be accounted for by natural variations within the C-zone reservoir.

Shift in Fluid Source

Long-term production of a well or short-term-production changes, such as increased flow or pressure reduction during initial production after well shut-in, may cause the fluid source, and thereby the composition, to change. Shales and sandstones in close proximity may contain fluids of different compositions just as may sandstones and shales occuring at different depths. Thus, a shift in the source of the production fluid may result in a shift in the fluid composition.

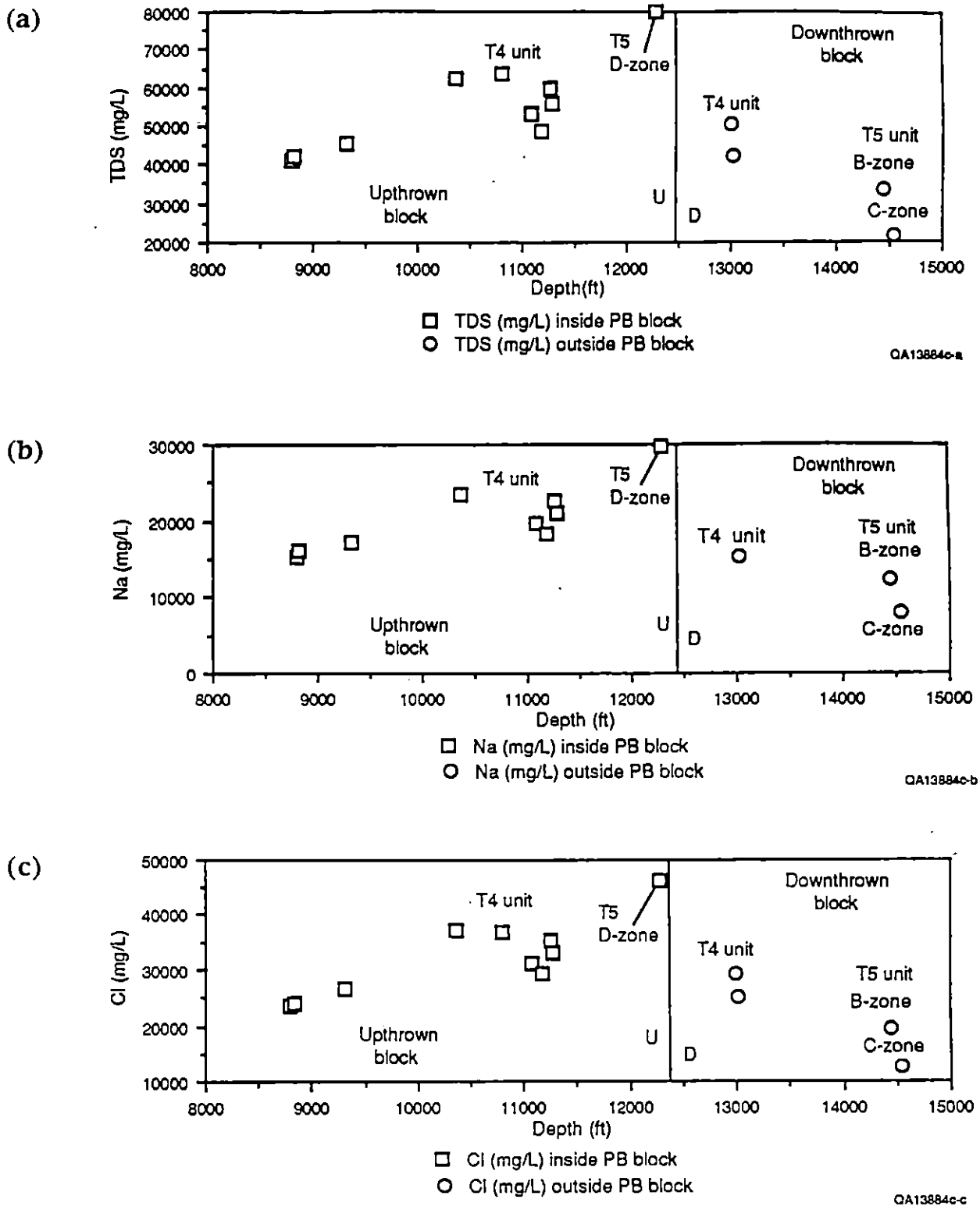

Figure 39. Depth variations of selected components for Frio Formation waters in Alta Loma field. The solid line represents the growth fault that acts as the southeastern boundary of the Pleasant Bayou fault block. Samples on the upthrown side of the fault (U) are from wells located within the fault block, whereas samples on the downthrown side of the fault (D) are from wells outside the fault block. Also shown schematically is the location of the Frio T4-T5 boundary (dashed lines) both inside and outside the fault block. (Data from table 3.) (a) TDS. (b) Chloride. (c) Sodium. (d) Calcium. (e) Potassium. (f) Ammonia. (g) Magnesium. (h) Manganese. (i) Strontium. (j) Temperature. (k) Chloride/bromide ratios. (l) Chloride/sodium ratios.

(d)

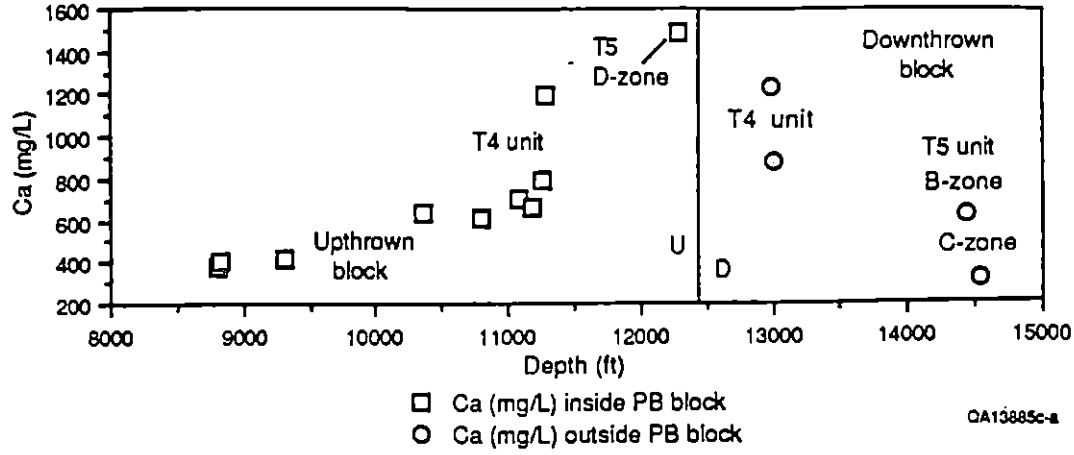

(e)

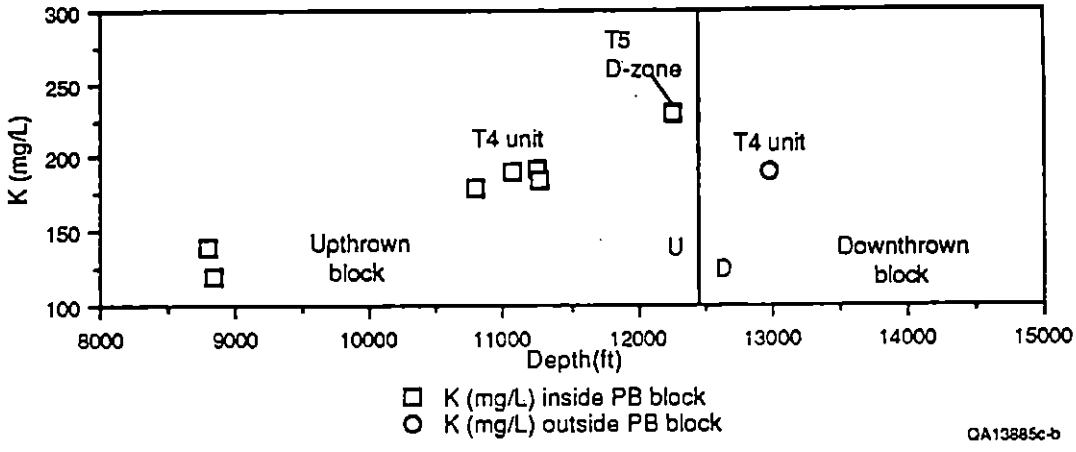

(f)

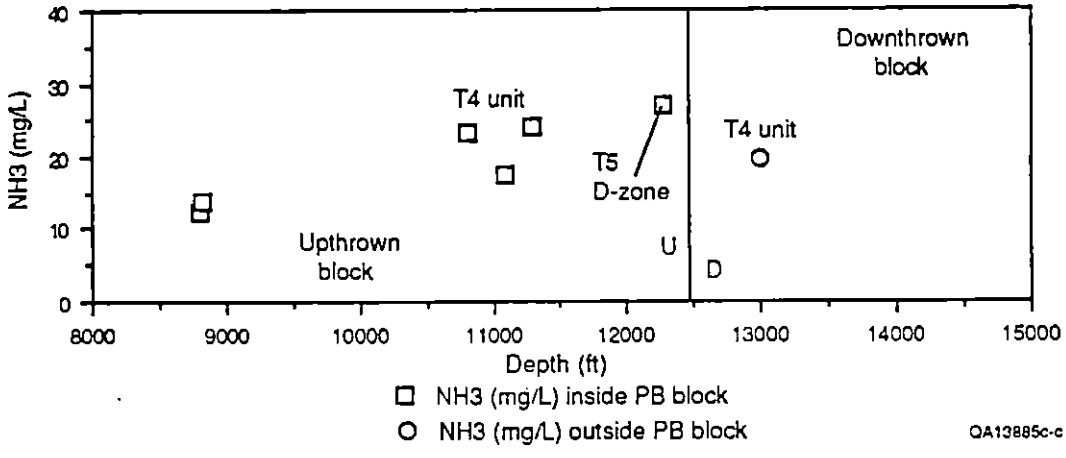

Figure 39. (cont.)

(g)

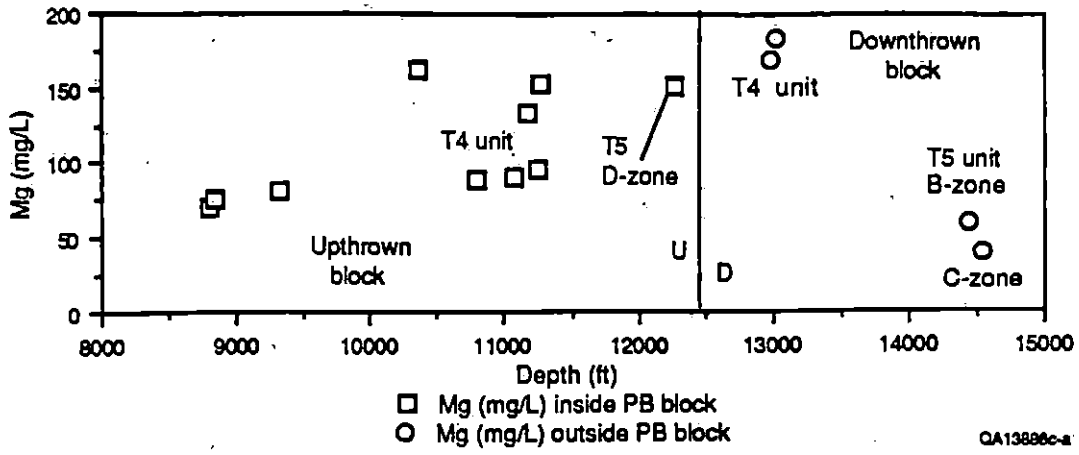

(h)

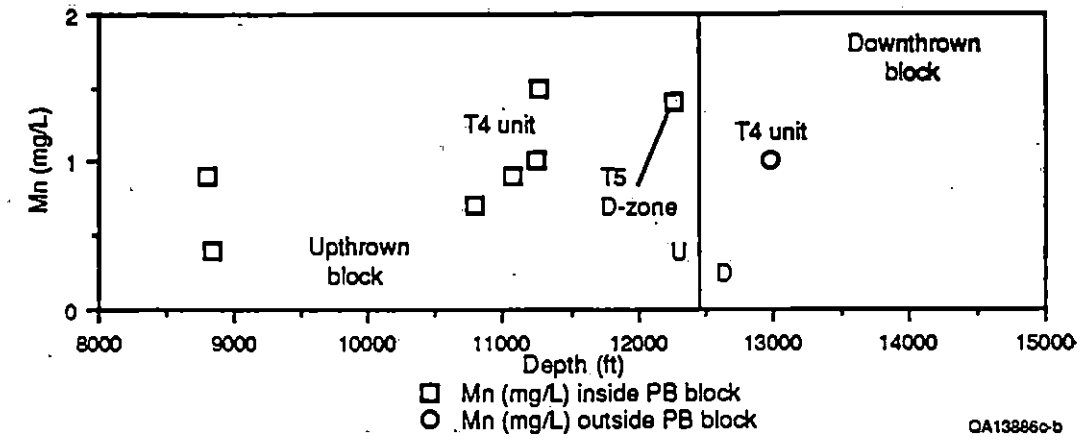

(i)

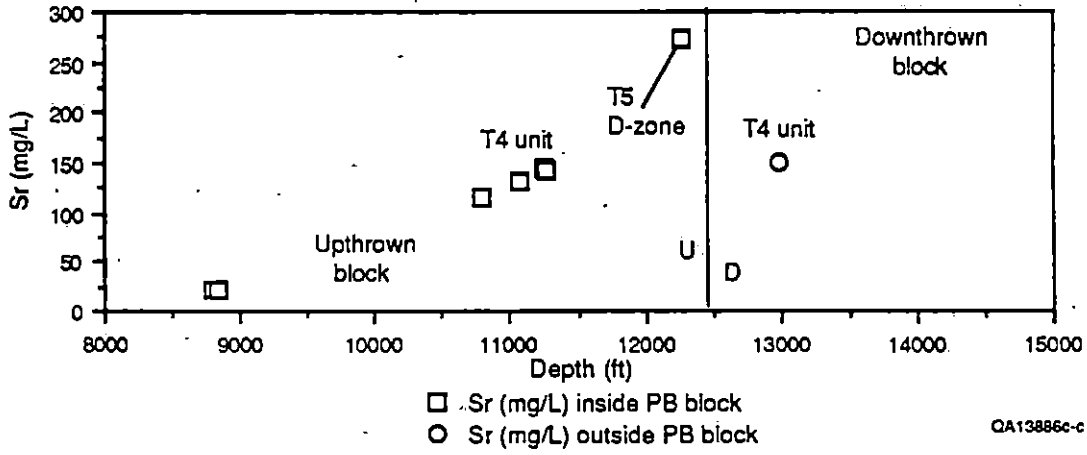

Figure 39. (cont.)

(j)

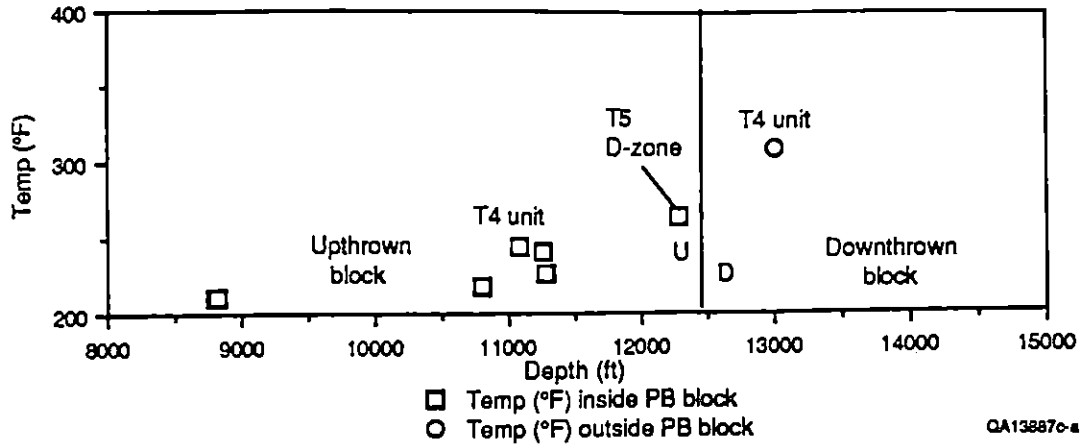

(k)

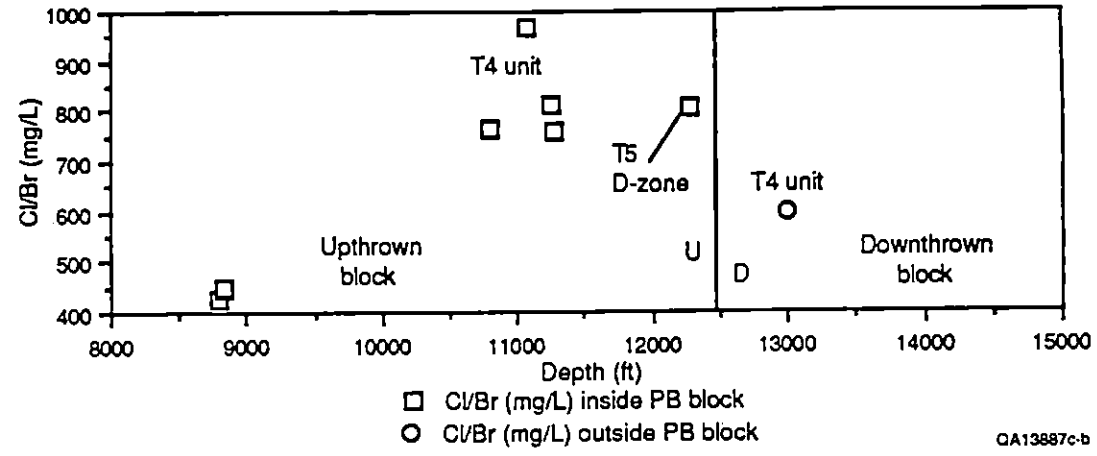

(l)

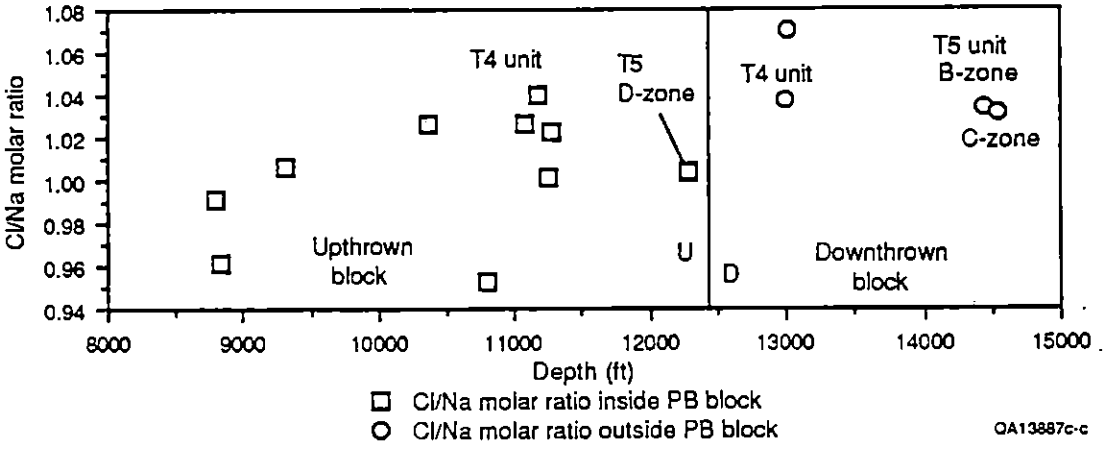

Figure 39. (cont.)

The predominant source of fluid is probably from the C-zone sandstone, and production-related changes in the source area may result in an increased component of fluid from another source. The 10 percent or less shift in concentration of most major ions suggests that if fluid from a different source is mixing with the production fluid, it is a small component or of similar composition and temperature. More important, the amount of fluid produced from the reservoir during the year of production (5,737,650 bbl) is relatively small compared to the predicted size of the C-zone reservoir (6.2 to 6.6 Bbbl effective pore volume [Hamlin and Tyler, 1988]). The area of influence, if all production is derived from the C-zone, is estimated as less than 1 mi^2.

Information on the changes in the fluid-source area as a result of long-term production is important because an increase in production of fluids derived from outside of the C-zone may significantly affect the long-term production and usage of fluids from Pleasant Bayou No. 2 well. If fluids are derived from other units, then the reservoir size would be larger than estimated when considering only C-zone production. Production of fluids from sedimentary units above or below the C-zone could result in changes in the temperature, pressure, and gas content of the reservoir, which could have significant effects on fluid usage, particularly since the gas is being used for energy production at the Pleasant Bayou site.

Similarity of Pleasant Bayou No. 2 Fluids to Frio Formation Waters

The Pleasant Bayou No. 2 well is located in the salt-dome province of the Houston Embayment. Fluids produced from the Pleasant Bayou No. 2 well are similar in composition to the sodium-chloride-dominated waters described as present in the Frio Formation within this salt-dome province (Morton and Land, 1987) and are probably similar in origin as well. This region contains highly concentrated saline formation waters (generally more than 105,000 ppm at depth)(Morton and Land, 1987). Previous work suggests that the high TDS (greater than 105,000 mg/L) and chloride/bromide weight ratios (generally greater than 200) indicate that

Frio water from the Houston Embayment is significantly influenced by evaporite dissolution (Kharaka and others, 1980; Morton and others, 1983). Morton and others (1983) postulated that the brines may have originated deeper in the basin and migrated vertically along faults and laterally through the more permeable sandstones. Chloride/bromide weight ratios of Pleasant Bayou No. 2 waters during current production range from around 900 to almost 1,050 (fig. 40). These high values are commonly accepted as a sign that the Pleasant Bayou No. 2 waters have received a significant portion of their dissolved constituents as a result of dissolution of evaporitic assemblages, particularly halite (Kharaka and others, 1978), and that these fluids have a source similar to that of other deep fluids in the Houston Embayment.

Chloride/sodium ratios are another indirect measure of the influence of evaporite dissolution on formation-water chemistry. Waters strongly influenced by halite dissolution should have chloride/sodium molar ratios near 1.0. Most deep formation waters in the Houston Embayment have chloride/sodium ratios of less than 1.3, except where calcium concentrations are greater than about 5,000 mg/L (Morton and Land, 1987). Chloride/sodium molar ratios during current production range from 1.243 to 1.324, calcium concentrations nearing 8,000 mg/L, indicating possible control by halite dissolution, modified by another process (perhaps albitization [Milliken and others, 1981]) or upward vertical migration of Mesozoic calcium-rich brines (Morton and Land, 1987). This is further supported by sodium/calcium ratios, which are generally between 10 and 100 in this area. Pleasant Bayou brines have sodium/calcium ratios near 8, which are more common in areas enriched in calcium. Chloride/bromide, chloride/sodium, and sodium/calcium ratios during long-term production do not suggest significant shifts in fluid origin from that common for fluids in the Houston Embayment. Thus, the small shift in fluid composition during long-term production probably does not mark a departure from production of fluids typical of the Houston Embayment.

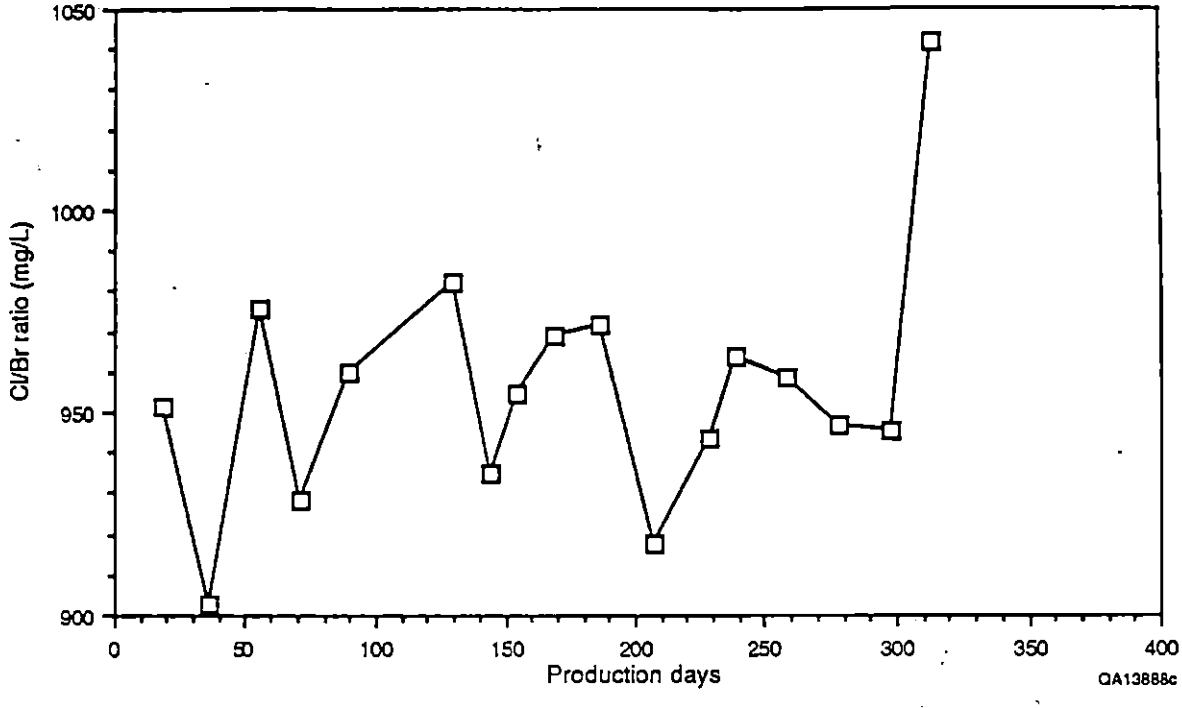

Figure 40. Chloride/bromide weight ratios of Pleasant Bayou No. 2 through the current production period.

Depth-related Compositional Changes in the Pleasant Bayou Fault Block

Depth-related changes in formation-water chemistry in the area surrounding the Pleasant Bayou No. 2 well were investigated in order to assess the possibility of shifts in fluid source to shallower or deeper reservoirs. TDS and chloride concentrations in Frio Formation waters within Brazoria and Galveston Counties appear to be largely independent of depth (fig. 41a and b)(data from table 3), as are fluid salinities in the Houston Embayment in general (Morton and Land, 1987). On a local scale, however, within individual oil fields, elemental concentrations exhibit trends consistent with depth (Morton and Land, 1987). The depth-related concentration trends were plotted for Chocolate Bayou field (fig. 42, a through o) and Alta Loma field (fig. 39a through l [data from table 3]; both fields are mostly within the Pleasant Bayou fault block, but some wells are not). The Pleasant Bayou No. 2 well is located on the extreme southeastern edge of Chocolate Bayou field (fig. 38), 4 to 5 mi from most of the wells in the field.

The plots of TDS and major elemental concentrations versus depth in Chocolate Bayou field (fig. 42a through o) show a consistent increase in concentration between 10,000 and 15,000 ft. Whereas lack of adequate brine chemistry data below 15,000 ft prohibits any definitive statement about deep concentration changes, the Pleasant Bayou No. 2 T5 unit F-zone data (Kharaka and others, 1980) suggest that brine salinity may reach a local maximum at a depth of around 15,000 ft and then decrease as depth increases through the F-zone. This suggests that the T5 unit C-zone may be at or near a localized zone of maximum salinity, and that salinity may decrease both above and below the C-zone in the Pleasant Bayou No. 2 well. Three wells in the Chocolate Bayou area have anomalously low concentrations of dissolved solids. These three wells are gas wells, as is shown in the plot of gas/water ratios (fig. 42o). Therefore, the low TDS values are probably the result of dilution by gas condensate.

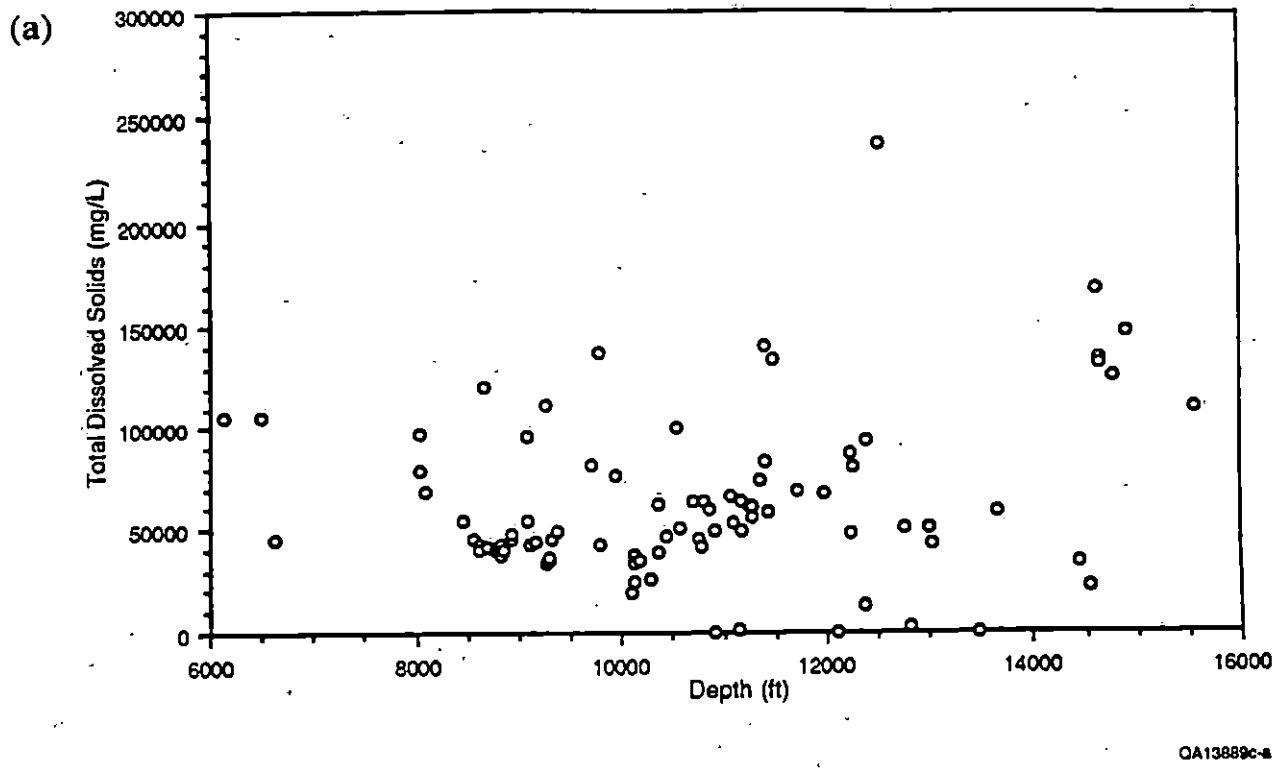

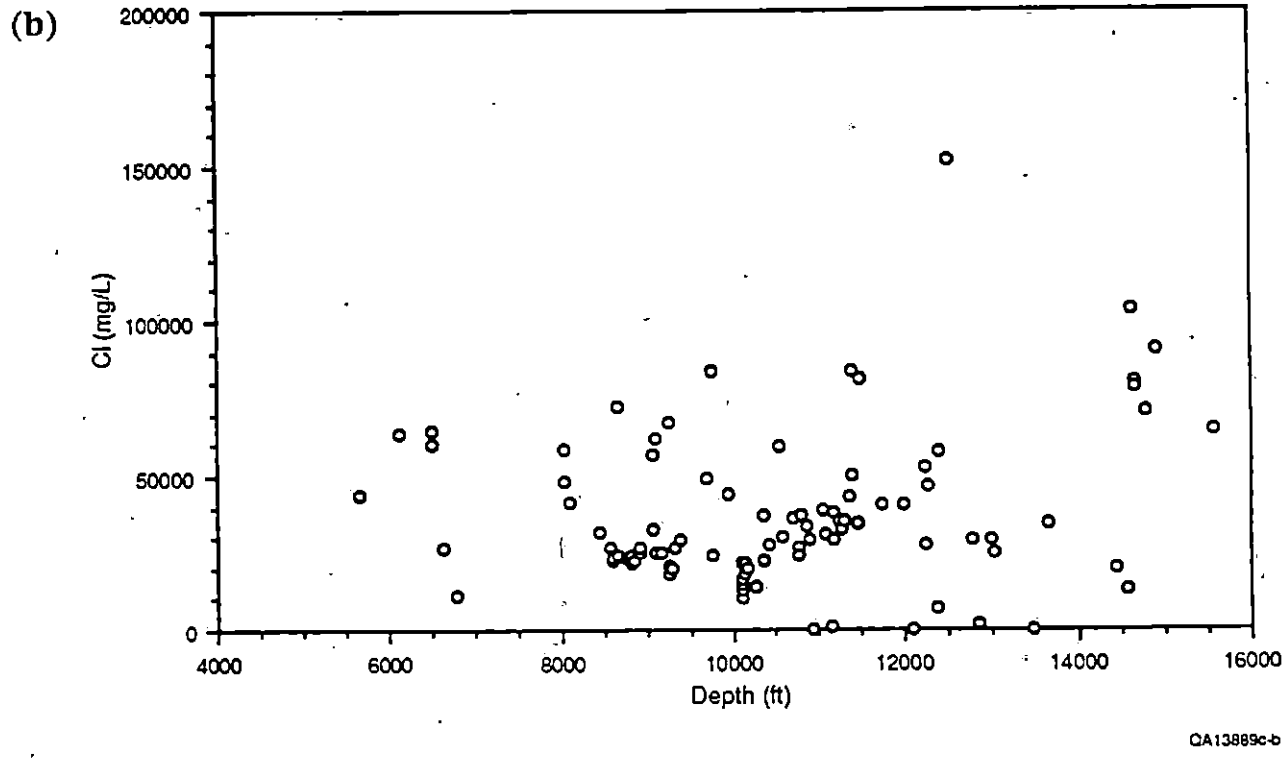

Figure 41. Concentration versus depth plot for (a) TDS and (b) chloride in Frio Formation waters within the study area (Brazoria and western Galveston Counties).

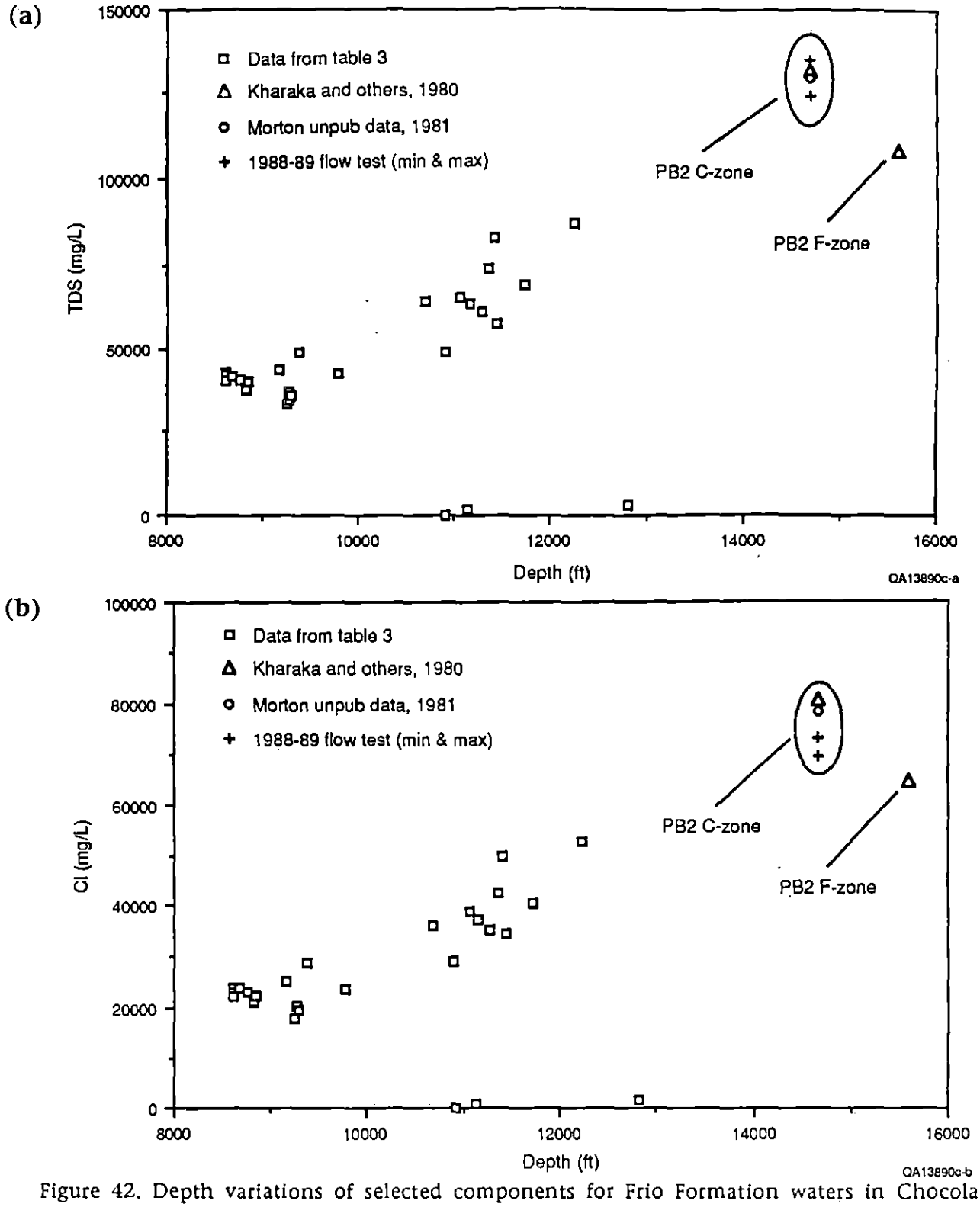

Figure 42. Depth variations of selected components for Frio Formation waters in Chocolate Bayou field. Data in these plots include Chocolate Bayou wells in table 3 (squares), Kharaka and others' (1980) analyses of Pleasant Bayou No. 2 C-zone and F-zone brines (triangles), Morton and others' (1981) analysis of a Pleasant Bayou No. 2 C-zone brine (circle), and the 1988–1989 flow-test data minimum and maximum values (crosses) (table 2) recorded for each component. (a) TDS. (b) Chloride. (c) Sodium. (d) Calcium. (e) Ammonia. (f) Potassium. (g) Manganese. (h) Magnesium. (i) Iodide. (j) Bromide. (k) Chloride/bromide ratios. (l) Strontium. (m) Pressure (psi). (n) Temperature (°F) (1988–1989 minimum temperature not reliable because of possible borehole effects). (o) Gas/water ratios.

(c)

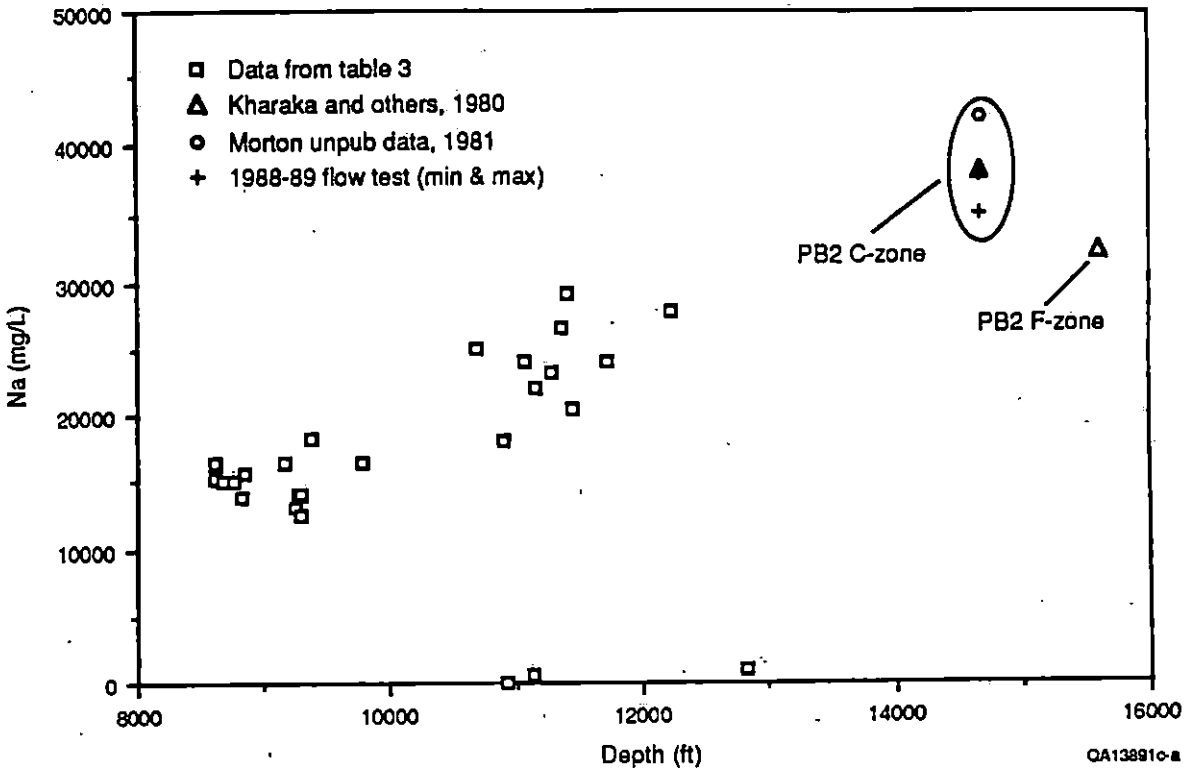

(d)

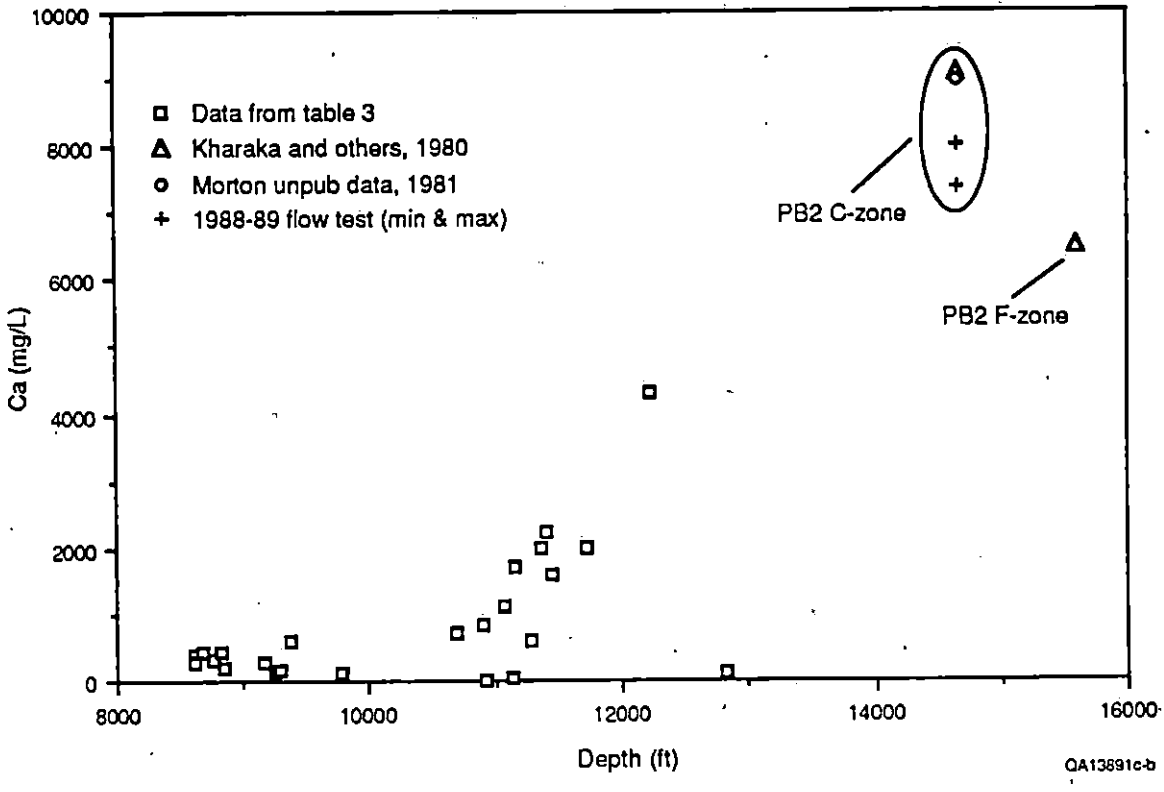

Figure 42. (cont.)

(e)

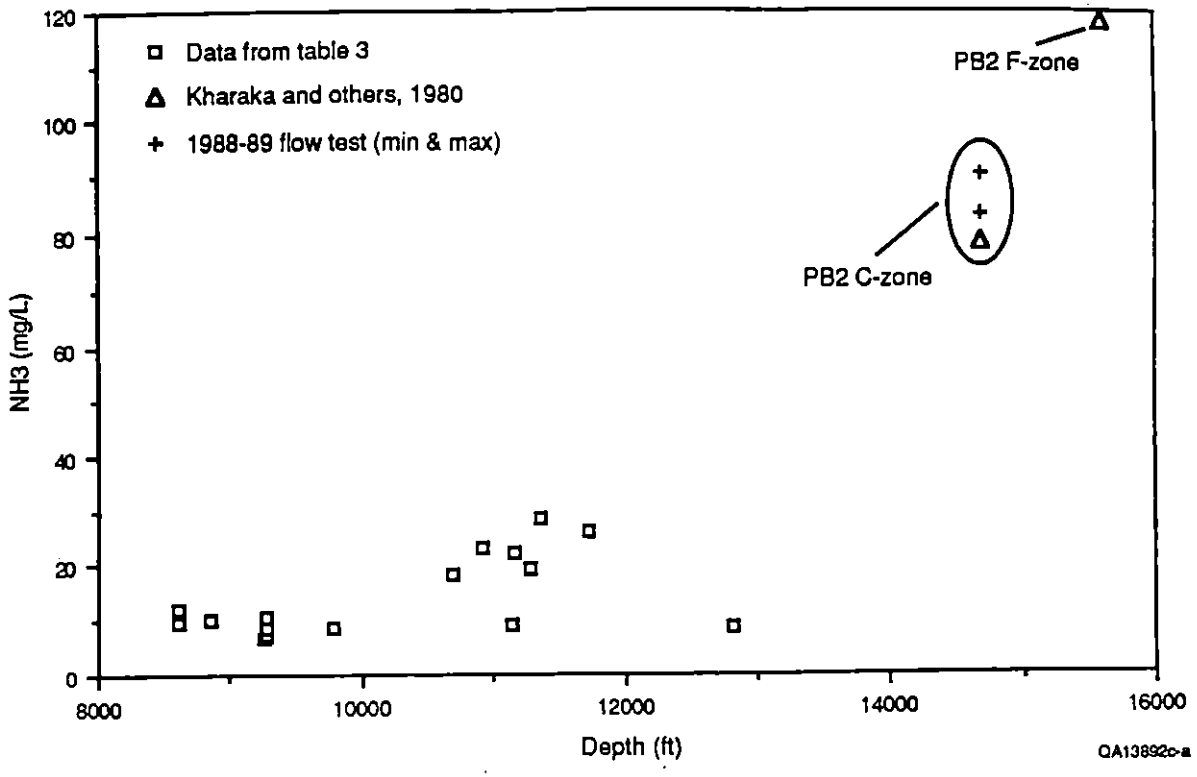

(f)

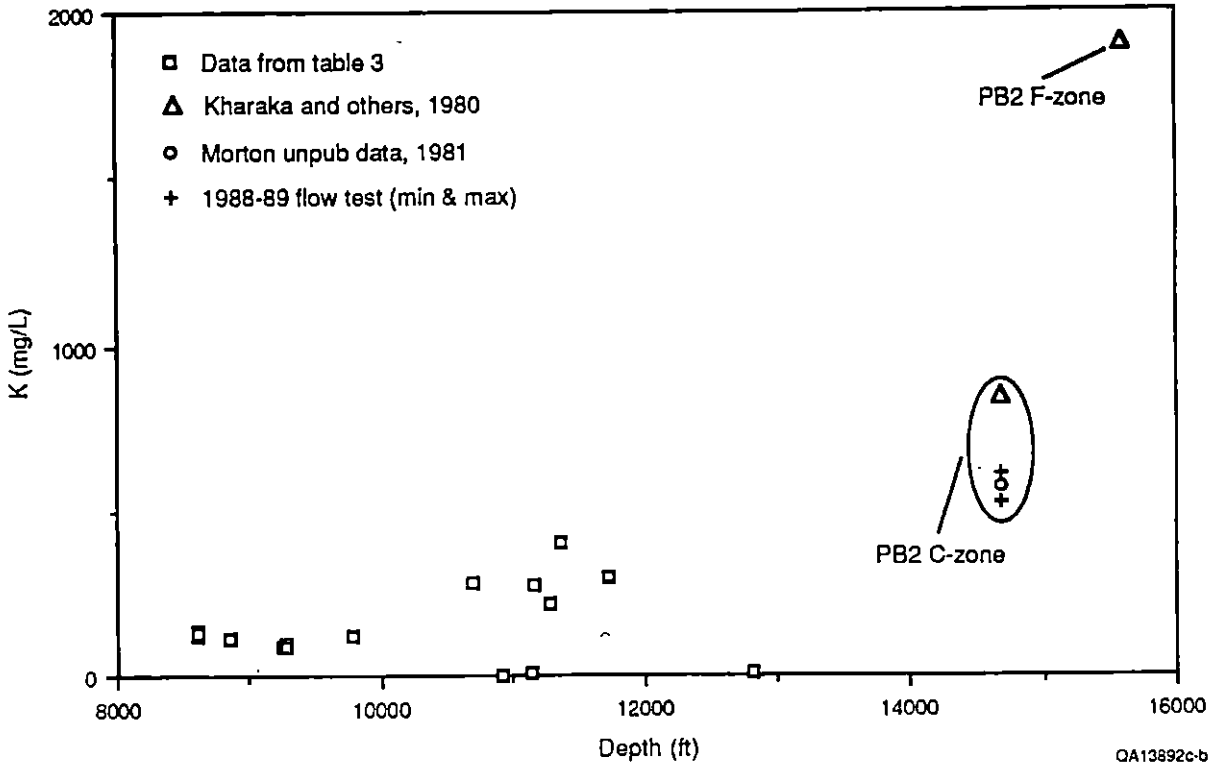

Figure 42. (cont.)

(g)

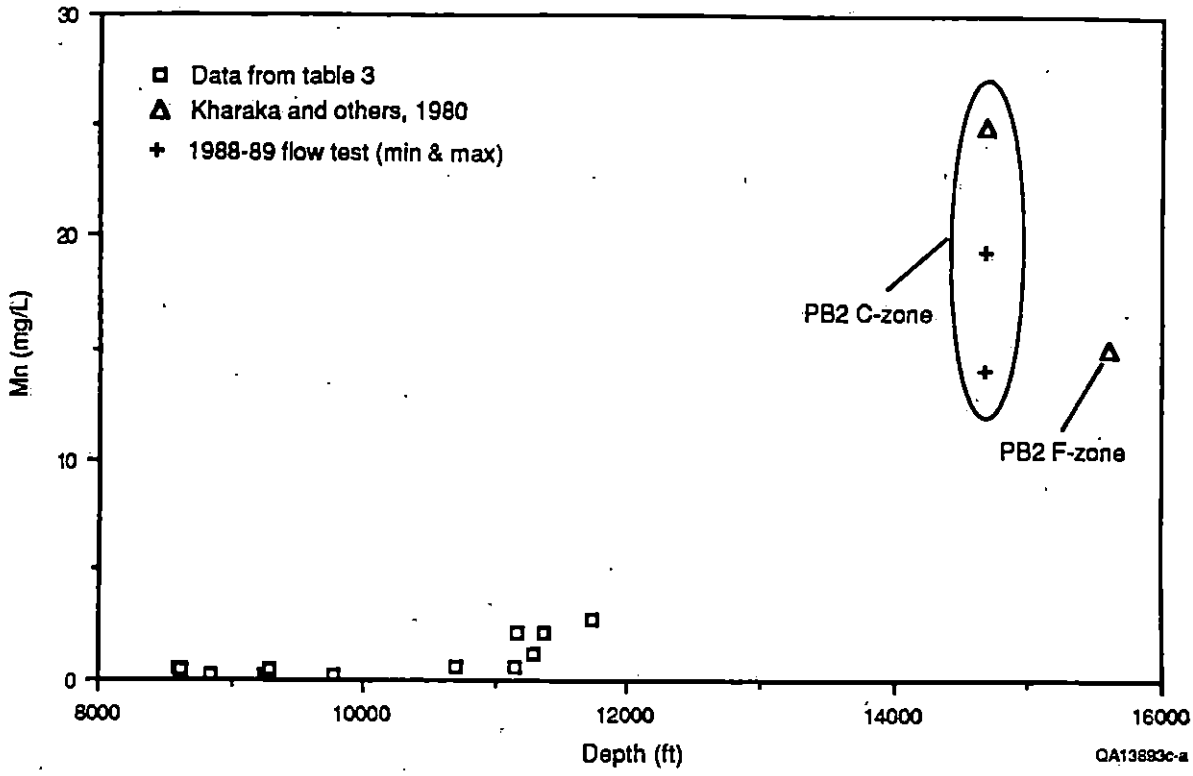

(h)

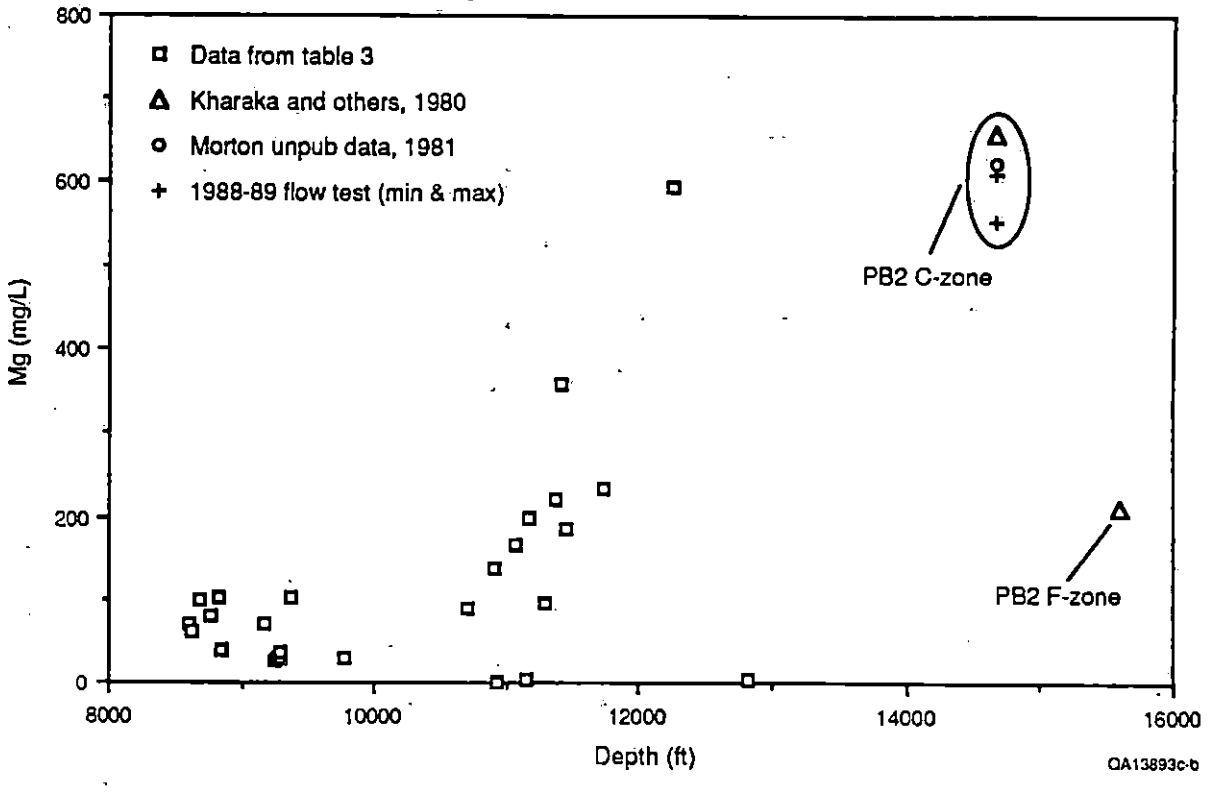

Figure 42. (cont.)

(i)

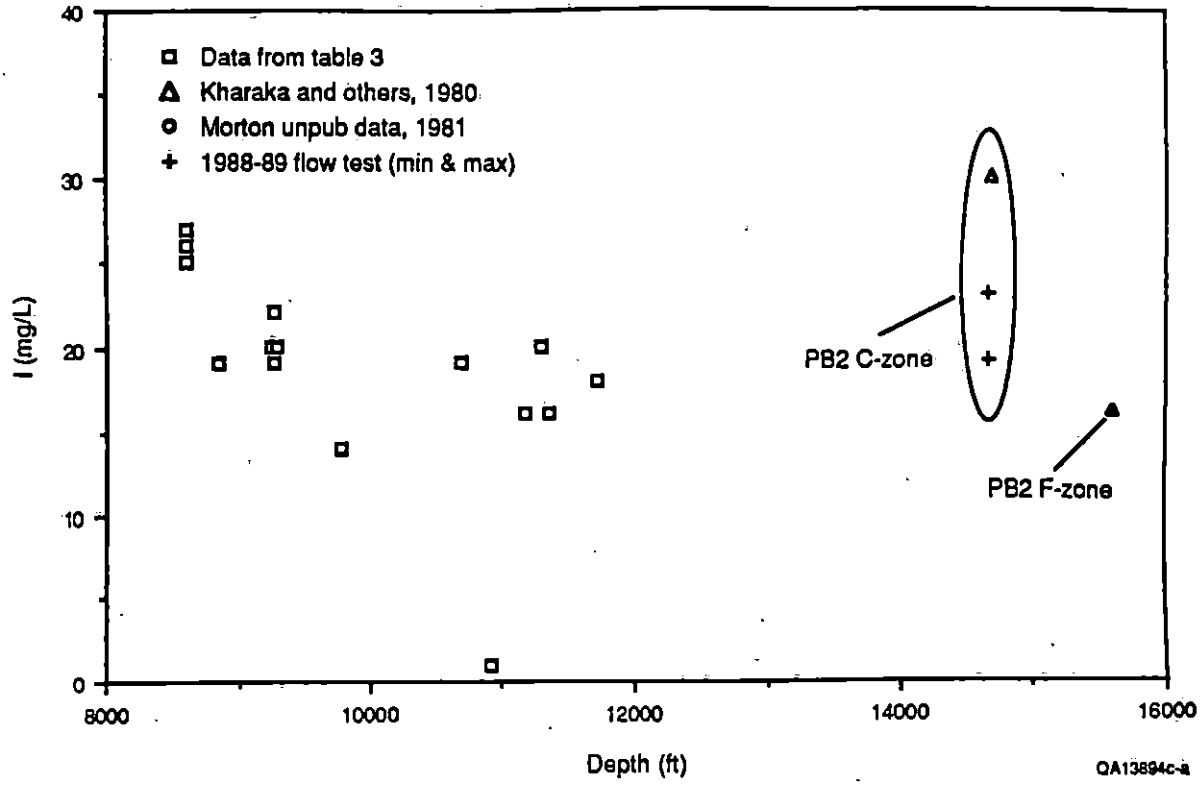

(j)

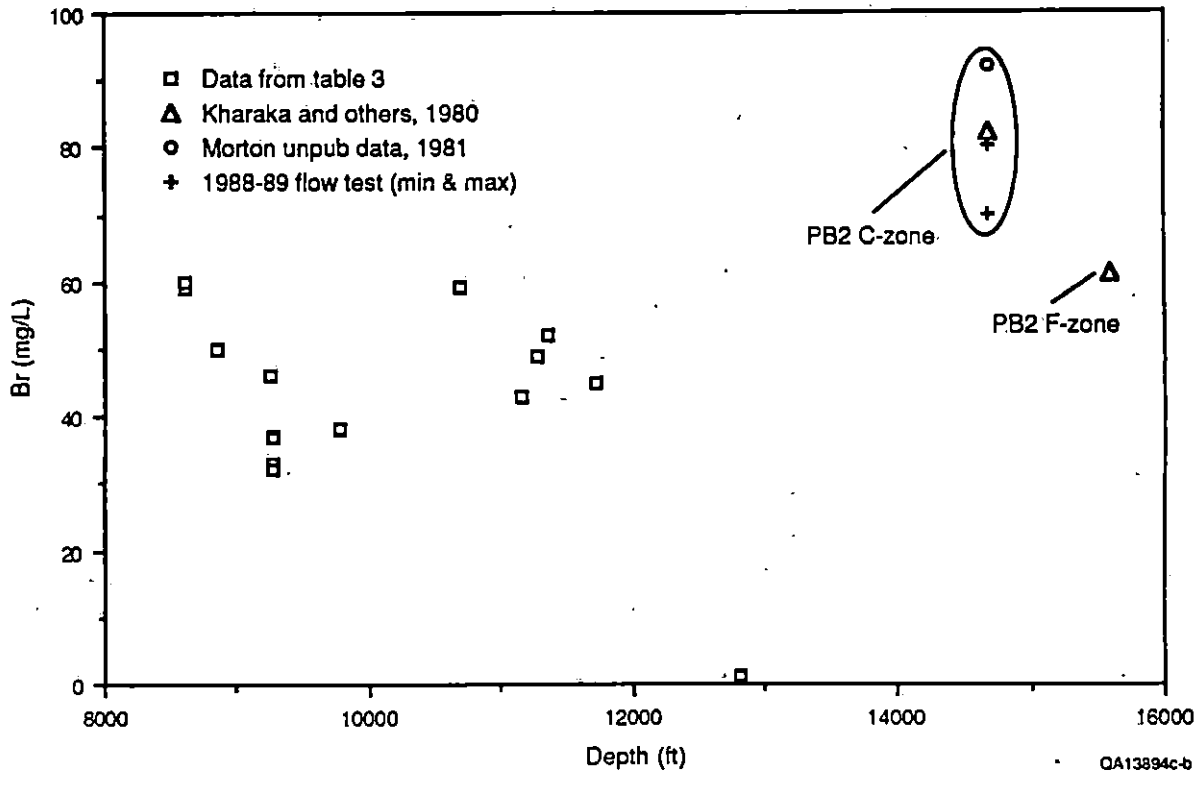

Figure 42. (cont.)

(k)

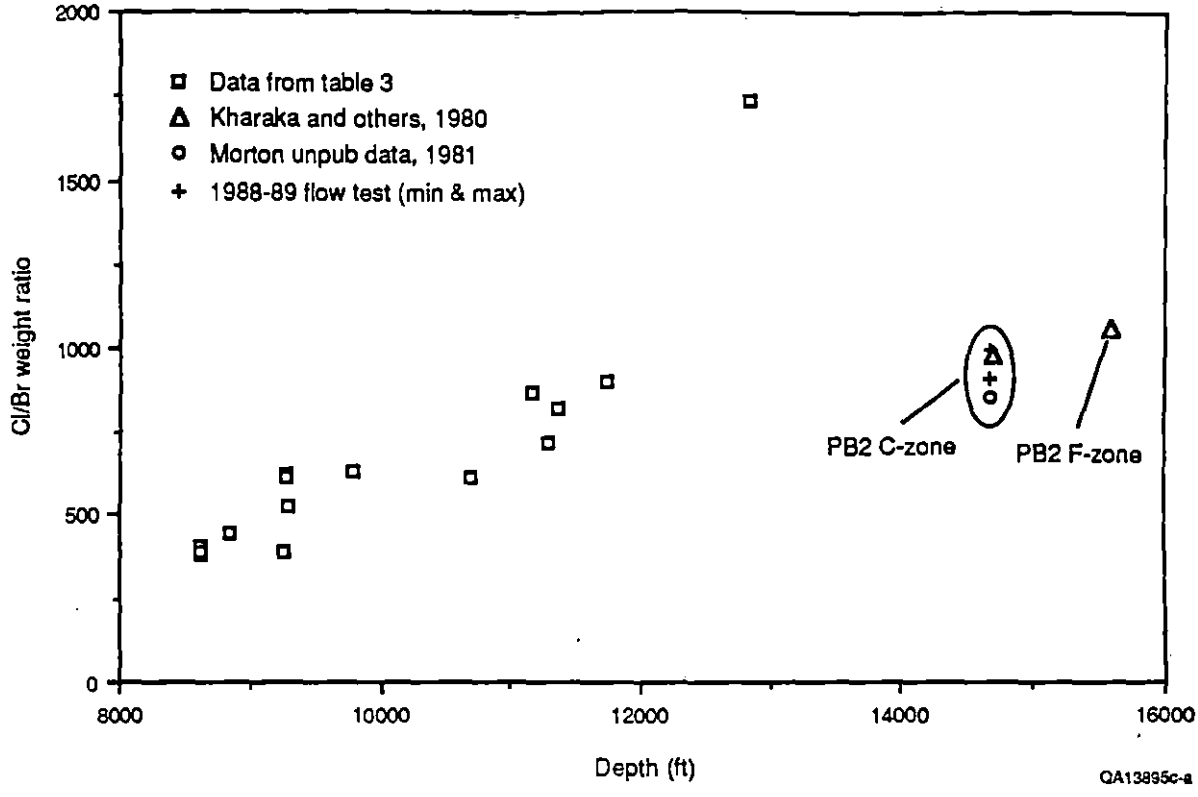

(l)

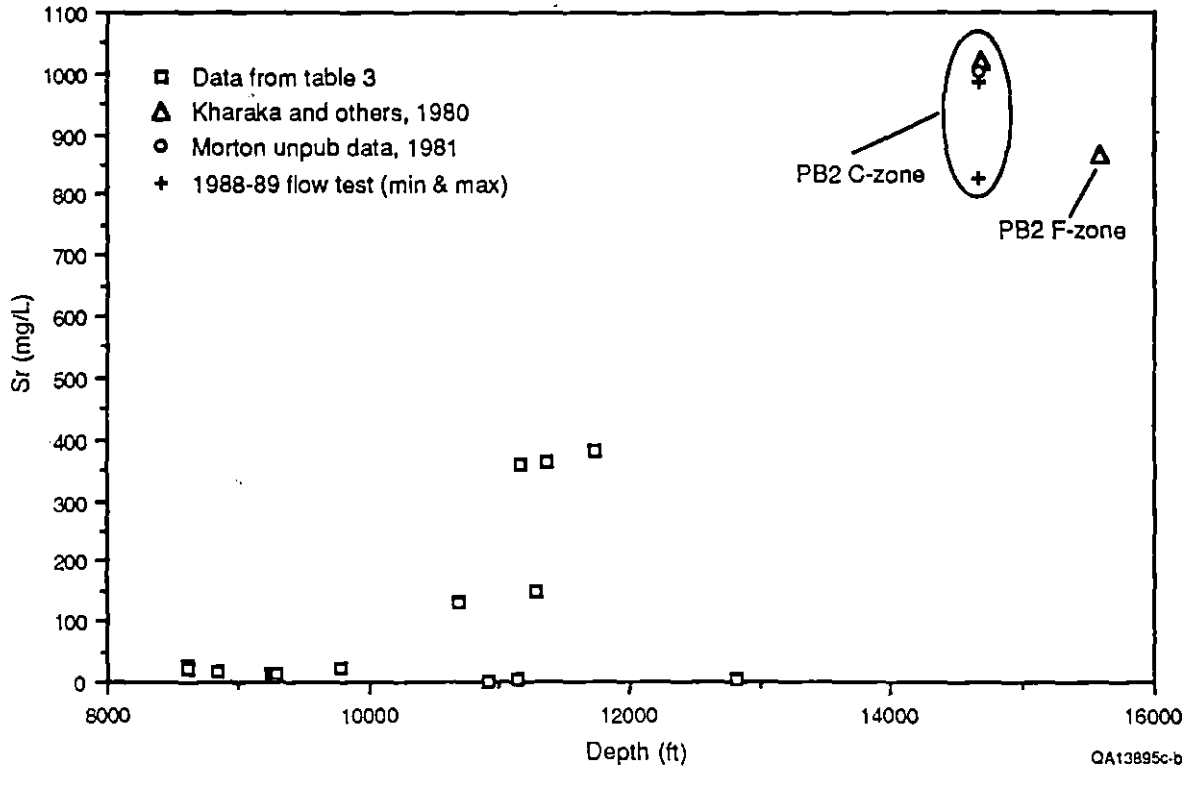

Figure 42. (cont.)

(m)

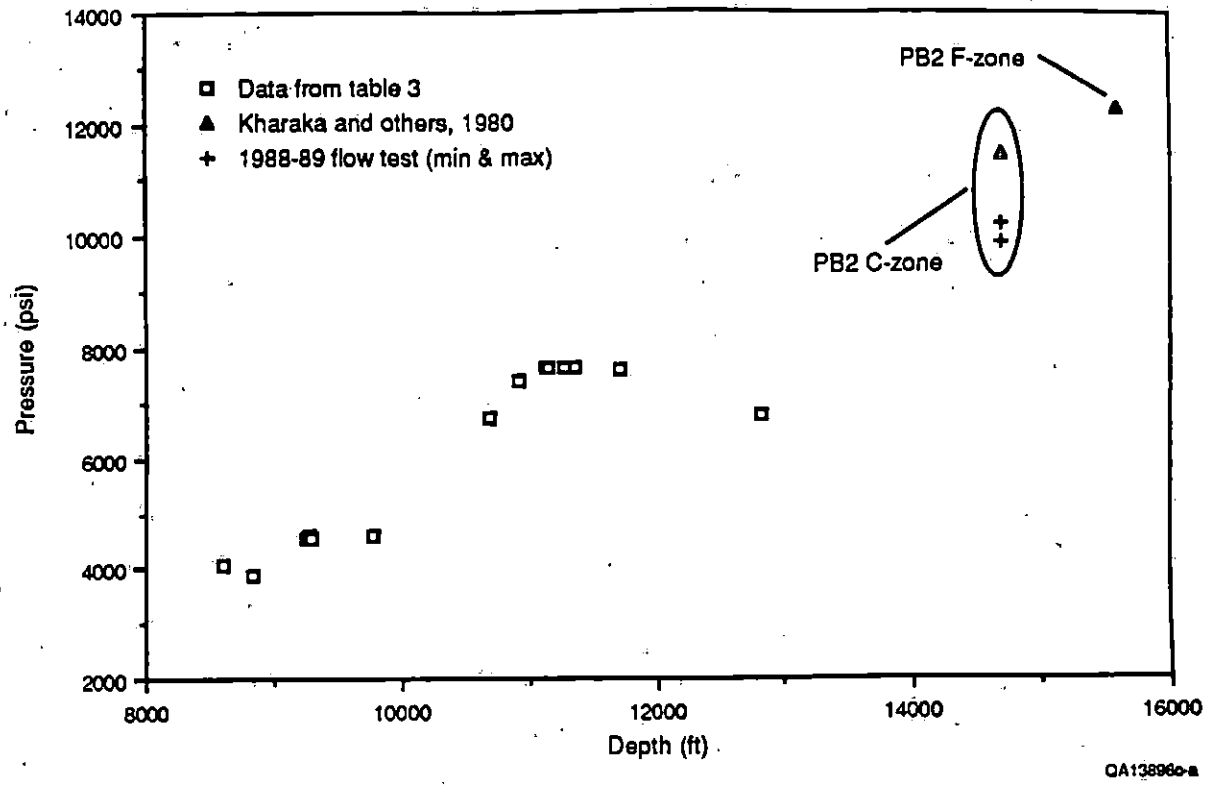

(n)

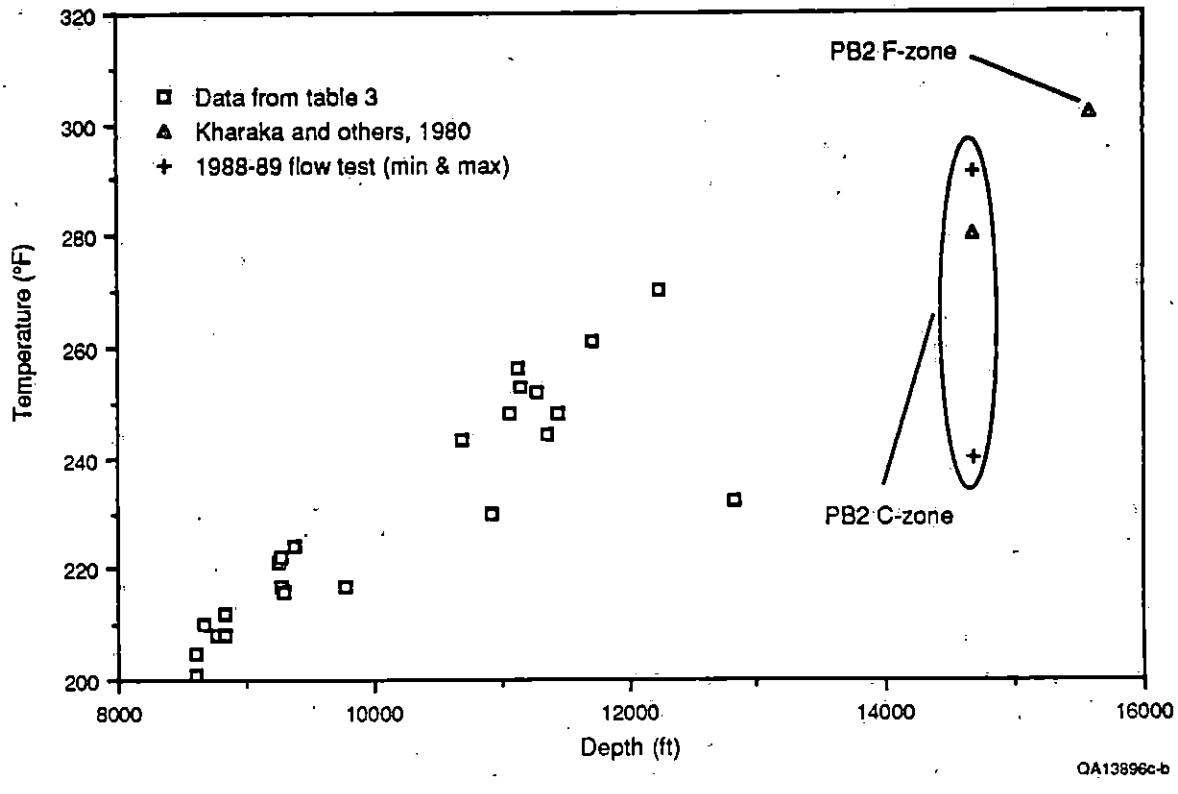

Figure 42. (cont.)

(o)

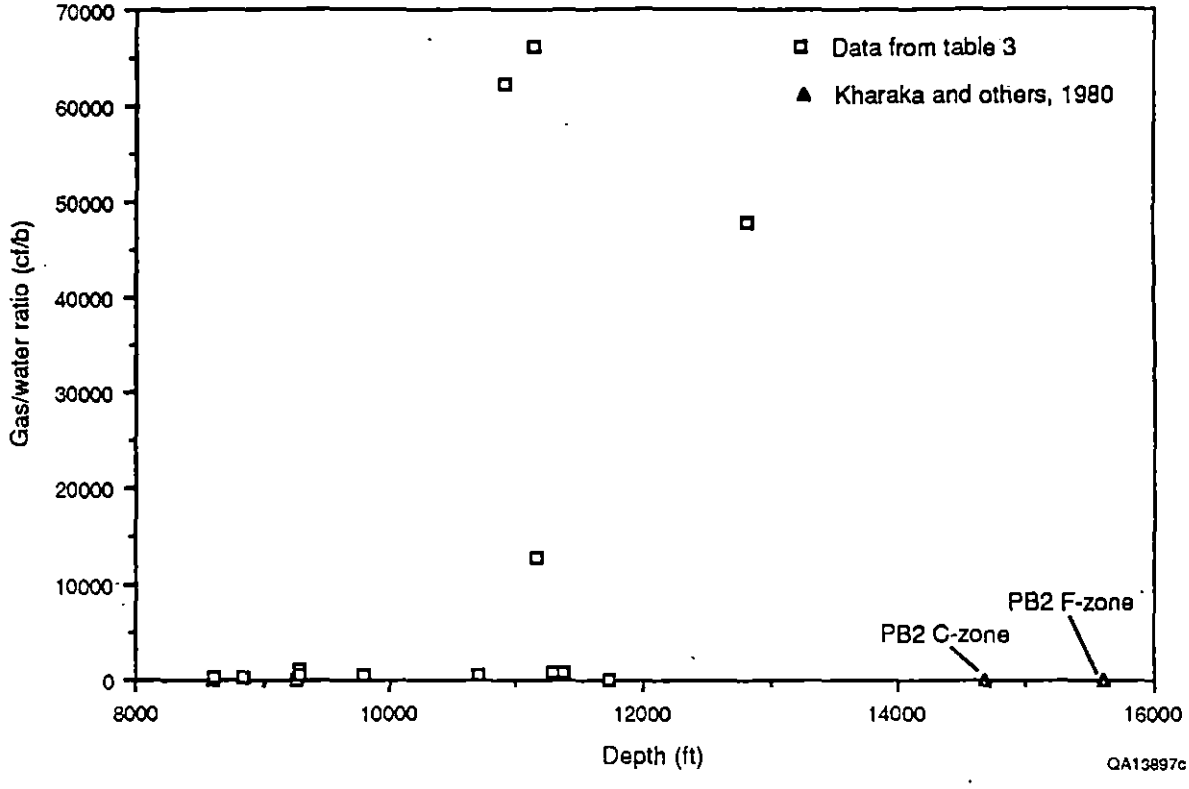

Figure 42. (cont.)

Concentration versus depth data were then plotted for TDS and major elements in Alta Loma wells (fig. 39a through l). Although it appears that concentration increases with depth to a maximum value near 12,300 ft and then decreases through 14,500 ft, the reality of this trend is obscured because samples from above and below 12,500 ft are separated by a large growth fault that marks the eastern boundary of the Pleasant Bayou fault block. The samples from depths shallower than 12,500 ft are all located inside the Pleasant Bayou fault block and show increasing concentration with depth through the deepest sample, which produces from the T5 unit D-zone (T. G. Walter, personal communication, 1989). The samples from deeper than 12,500 ft are all from wells outside the fault block and show salinities decreasing through the T5 unit B-zone and C-zone. The salinity reversal is thus neither depth dependent nor does it correspond to a particular hydrostratigraphic unit. Therefore, whereas the concentration-versus-depth trend described for Chocolate Bayou field may indeed exist in Alta Loma field, the fact that our data include samples from different, possibly hydrologically unconnected reservoirs, prohibits corroboration of the trend in Chocolate Bayou field.

The salinity maximum in the C-zone at Pleasant Bayou suggests that cross-formational flow might result in a decrease in brine salinity, but because no data are available for sand units immediately above or below the C-zone (B-zone and D-zone, respectively), and because of the likelihood of large lateral variations in brine salinity within a single zone, we cannot rule out contribution from cross-formational flow to current brine production. We can conclude, however, that fracture flow across large vertical distances (on the order of 1,000 ft) did not significantly contribute to current brine production because these fluids would likely be significantly different in composition and temperature. For example, the fluids produced from the Pleasant Bayou No. 2 F-zone (15,589 ft) have a TDS of 108,000 mg/L, whereas the overlying C-zone (14,674 ft) has a TDS of 132,000 mg/L, a difference of 24,000 mg/L. No evidence of water of this lower salinity exists in currently produced brines.

The consistency of brine temperatures and gas/brine ratios reported through the current production period also suggests that production may be confined to fluids from the C-zone

reservoir. Figure 43 shows that Pleasant Bayou No. 2 brine temperatures have remained constant near 290°F since production began (except when drilling activities have affected brine temperatures). If cross-formational flow were an important process, it might influence brine temperatures.

The consistent gas/brine ratio values (fig. 44) also suggest that production has been restricted to within or near the C-zone reservoir. Fluids from much greater or shallower depths would likely be at higher or lower pressures and temperatures, respectively. Because fluid pressure and temperature have a strong control on gas solubility, fluids from much greater or shallower depths would likely have a different gas/brine ratio. As shown in Chocolate Bayou field, gas/brine ratios can range from 10 or less to 6,000 or more (fig. 42o).

These data show the complexity in the fluid compositions vertically within an individual field. These data do not permit a determination as to whether the changes in the composition of the Pleasant Bayou fluid during long-term production are the result of cross-formation flow. The changes in composition of the Pleasant Bayou fluid during long-term production are, however, apparently smaller than the compositional changes that could be expected if the fracture flow permitted the fluid source to be shifted to much deeper or shallower samples, on the order of 1,000 ft.

Shale Dewatering

Whereas large-scale shifts in fluid source are not evidenced by current data, shale dewatering may be influencing short-term small-scale fluid compositional changes. Although causes and mechanisms of shale dewatering are not well understood, short-term pressure changes caused by shut-ins and resumptions of pumping may result in varying contributions of shale water to production. The current sampling frequency hinders attempts at correlation of pressure changes with small-scale salinity variations. However, with the long-term trend toward

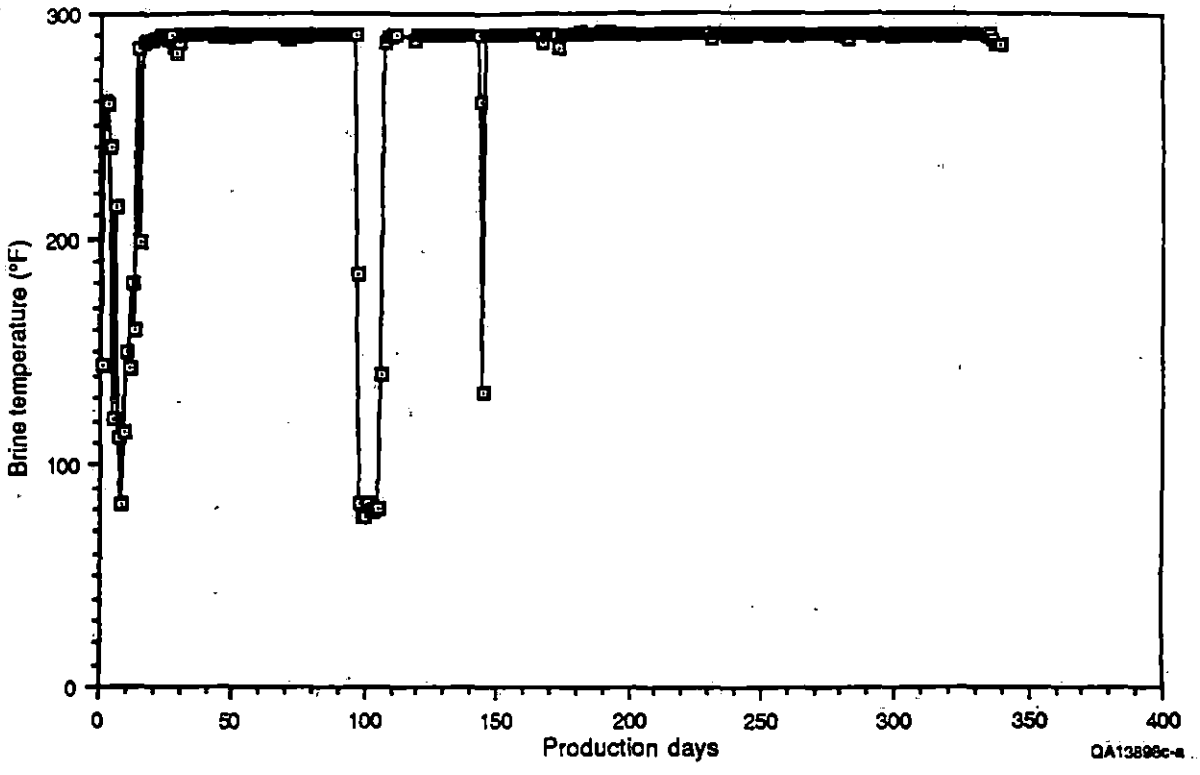

Figure 43. Brine temperatures (°F) of Pleasant Bayou No. 2 through the current production period. Large drops in temperature correspond to periods of well shut-ins.

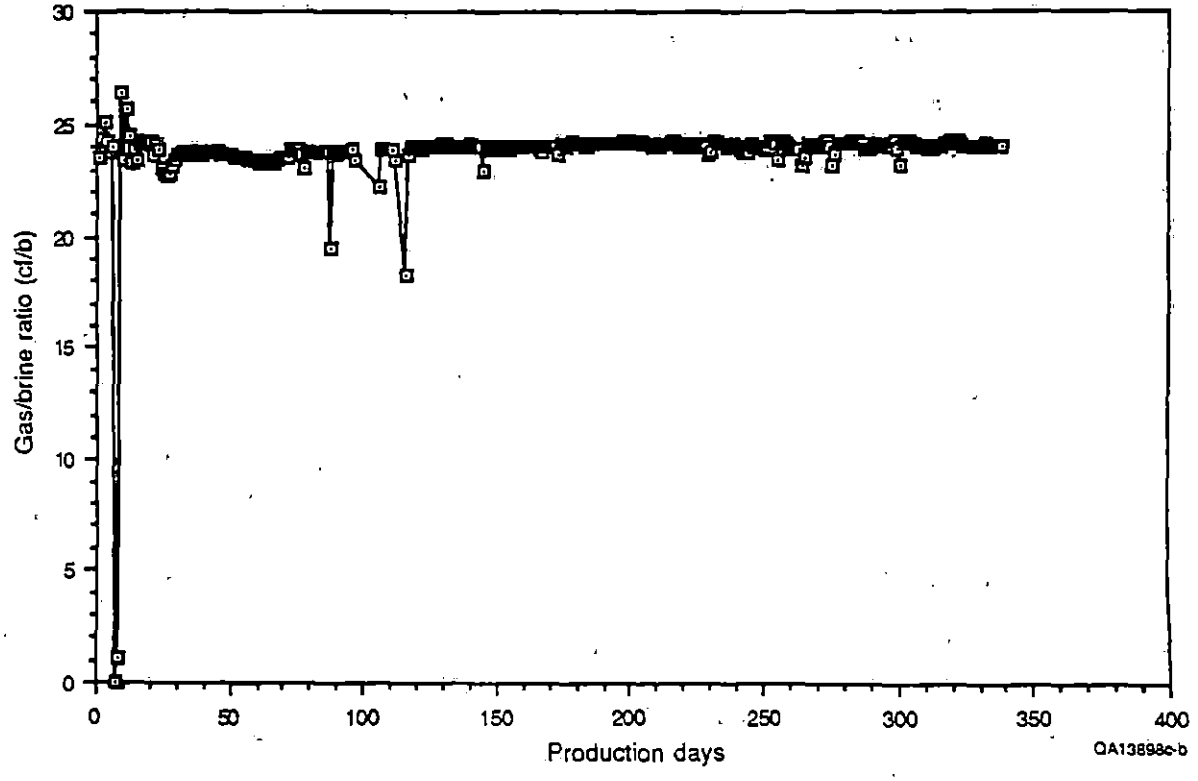

Figure 44. Gas/brine ratios (ft^3/bbl) of Pleasant Bayou No. 2 through the current production period.

increasing salinity, shale dewatering, which is expected to provide lower TDS water, does not seem to be an increasingly important process through current production.

CONCLUSIONS

The 1988–1989 flow test of the Pleasant Bayou No. 2 well was sampled periodically for chemical analyses. TDS of the brine increased through the current production period (May 27, 1988, through April 4, 1989), rapidly through the first 40 d and more slowly through the remainder of the period. Overall, TDS increased about 6 percent through the current sampling period, and most major elements followed a trend of concentration increasing through time. In addition to the long-term trend toward increased salinity, several smaller, short-term changes in brine composition were observed. Some of these were within analytic uncertainty, some were not. Their cause is unknown, but may be related to production changes.

Comparison of current Pleasant Bayou brine samples with samples obtained in 1979 and 1981 showed that several major elements (chloride, calcium, potassium, and magnesium) and the overall salinity (TDS) exhibit similar patterns: a small decrease in concentration from 1979 to 1981, a larger decrease between 1981 and 1988, and then a trend toward increasing concentration through current high-rate production. The relationship between these concentration changes and production history is uncertain.

The brines produced during current testing at the Pleasant Bayou No. 2 well are similar to those of other deep formation waters previously described in the salt-dome province of the Houston Embayment, and probably have a similar origin. Overall salinities (TDS), chloride, sodium, calcium, and other major elemental concentrations are not markedly different from typical deep formation waters from the upper Texas Gulf Coast (TDS greater than 105,000 mg/L). Chloride/bromide, chloride/sodium, and sodium/calcium ratios from Pleasant Bayou No. 2 also resemble many sodium-chloride-dominated deep formation waters from the area, particularly those that are enriched in calcium.

No correlation between production-related changes (that is, wellhead and bottom-hole pressures) and long-term concentration changes were found. The variations in brine chemistry through current production are not very large (generally 10 percent or less), rendering production of brines moving large vertical distances from above or below unlikely because concentrations vary rapidly with depth in Chocolate Bayou field. Any fluid contribution from zones other than the intended production zone would likely be limited cross-formational or small-scale fault-controlled flow. Scarcity of brine chemistry data within the Pleasant Bayou block C-zone hinders estimation of natural variations in C-zone fluids, but estimated variations of intrablock D-zone fluids and variations between C-zone fluids in and out of the fault block suggest that the variations in brine chemistry through current production can probably be accounted for by natural variations in the C-zone fluid composition. Constancy of brine temperatures and gas/brine ratios also suggests current production is largely restricted to a single reservoir.

ACKNOWLEDGMENTS

We would like to thank the following scientists at the Bureau of Economic Geology for their assistance: Scott Hamlin for information on reservoir geology, Tim Walter for correlation of well logs and information on location and production zones of the wells, Jim Tubbs for assisting in the compilation of the data base, Robert Morton for providing unpublished fluid analyses, and Steve Tweedy and Dave Koppenaal (currently with Pacific Northwest Laboratories) for information on the Pleasant Bayou No. 2 brine analyses.

We would also like to thank Phil Randolph and Chris Hayden from the Institute of Gas Technology, who were of great assistance in providing information on sampling and analytic procedure and well-production data.

Our appreciation is also extended to Lana Dieterich, who edited this manuscript, to Melissa Snell, who performed the word processing tasks, and to Patrice Porter and Tari Weaver, who prepared the illustrations under the direction of Richard L. Dillon.

REFERENCES

ASTM, 1984, Annual book of ASTM standards, Water I: Philadelphia, sec. 11, v. 11.01, 750 p.

Capuano, R. M., 1988, Chemical equilibria and fluid flow during compaction diagenesis of organic-rich geopressured sediments: Tucson, Arizona, University of Arizona, Ph.D. dissertation, 134 p.

Carothers, W. W., and Kharaka, Y. K., 1978, Aliphatic acid anions in oil-field waters—implications for origin of natural gas: American Association of Petroleum Geologists Bulletin, v. 62, no. 12, p. 2444–2445.

———— 1980, Stable carbon isotopes of HCO_3^- in oil-field waters—implications for the origin of CO_2: Geochimica et Cosmochimica Acta, v. 44, p. 326–327.

Eaton Operating Co., Inc., 1988a, Contract performance report, June 1988: technical progress report, DOE 530 Series Reports, Program Financial Summary: Houston, Texas, report prepared for the U.S. Department of Energy under contract no. DE-AC07-85ID12578, 47 p.

———— 1988b, Contract performance report, September 1988: technical progress report, DOE 530 Series Reports, Program Financial Summary: Houston, Texas, report prepared for the U.S. Department of Energy under contract no. DE-AC07-85ID12578, 43 p.

———— 1989a, Contract performance report, February 1989: technical progress report, DOE 530 Series Reports, Program Financial Summary: Houston, Texas, report prepared for the U.S. Department of Energy under contract no. DE-AC07-85ID12578, 60 p.

———— 1989b, Contract performance report, May 1989: technical progress report, DOE 530 Series Reports, Program Financial Summary: Houston, Texas, report prepared for the U.S. Department of Energy under contract no. DE-AC07-85ID12578, 45 p.

Hamlin, H. S., and Tyler, Noel, 1988, Consolidation of geologic studies of geopressured-geothermal resources in Texas: The University of Texas at Austin, Bureau of Economic Geology annual report prepared for the U.S. Department of Energy Advanced Technologies Division, under contract no. DE-FC07-85NV10412, 45 p.

Jessen, F. W., and Rolshausen, F. W., 1944, Waters from the Frio Formation, Texas Gulf Coast: Transactions of the American Institute of Mining and Metallurgical Engineers, v. 155, p. 23–38.

Kharaka, Y. K., Callender, Edward, and Carothers, W. W., 1977, Geochemistry of geopressured geothermal waters from the Texas Gulf Coast: Lafayette, Louisiana, University of Southwest Louisiana Center for Energy Studies, Proceedings, Third Geopressured Geothermal Energy Conference, v. 1, p. 138–141.

Kharaka, Y. K., Carothers, W. W., and Brown, P. M., 1978, Origin of water and solutes in the geopressured zones of the northern Gulf of Mexico basin: Proceedings, Society of Petroleum Engineers of the American Institute of Mining, Metallurgical and Petroleum Engineers, 53rd Annual Conference, SPE 7505, 8 p.

Kharaka, Y. K., Lico, M. S., Wright, V. A., and Carothers, W. W., 1980, Geochemistry of formation waters from Pleasant Bayou No. 2 well and adjacent areas in coastal Texas: Proceedings, Fourth Geopressured-Geothermal Energy Conference, v. 1, p. 168–193.

Kindle, C. H., and Woodruff, E. M., 1981, Techniques for geothermal liquid sampling and analysis: Richland, Washington, Pacific Northwest Laboratory, report prepared for the U.S. Department of Energy under contract no. DE-ACO6-76RLO 1830, 56 p.

Koppenaal, D. W., 1986a, Mineral Studies Laboratory analytical procedure; chloride by titration (Mohr method): The University of Texas at Austin, Bureau of Economic Geology Specific Work Instruction 1.1, 5 p.

———— 1986b, Mineral Studies Laboratory analytical procedure; bromide by spectrophotometry: The University of Texas at Austin, Bureau of Economic Geology Specific Work Instruction 1.2, 5 p.

———— 1986c, Mineral Studies Laboratory analytical procedure; sulfate by turbidimetry: The University of Texas at Austin, Bureau of Economic Geology Specific Work Instruction 1.3, 5 p.

———— 1986d, Mineral Studies Laboratory analytical procedure; iodide by spectrophotometry: The University of Texas at Austin, Bureau of Economic Geology Specific Work Instruction 1.4, 5 p.

———— 1987a, Mineral Studies Laboratory analytical procedure; determination of major, minor, and trace elements by ICP-OES: brine waters: The University of Texas at Austin, Bureau of Economic Geology Specific Work Instruction 1.6, 9 p.

———— 1987b, Mineral Studies Laboratory analytical procedure; determination of fluoride by ion selective electrode potentiometry: The University of Texas at Austin, Bureau of Economic Geology Specific Work Instruction 1.11, 5 p.

Lico, M. S., Kharaka, Y. K., Carothers, W. W., and Wright, V. A., 1982, Methods for collection and analysis of geopressured geothermal and oil field waters: U.S. Geological Survey Water-Supply Paper 2194, 21 p.

Loucks, R. G., Richmann, D. L., and Milliken, K. L., 1980, Factors controlling porosity and permeability in geopressured Frio sandstone reservoirs, General Crude Oil/Department of Energy Pleasant Bayou test wells, Brazoria County, Texas, *in* Dorfman, M. H., and Fisher, W. L., eds., Proceedings, Fourth Geopressured Geothermal Energy Conference: The University of Texas at Austin, Center for Energy Studies, p. 46–84.

———— 1981, Factors controlling reservoir quality in Tertiary sandstones and their significance to geopressured geothermal production: The University of Texas at Austin, Bureau of Economic Geology Report of Investigations No. 111, 41 p.

Lundegard, P. D., 1985, Carbon dioxide and organic acids: origin and role in burial diagenesis (Texas Gulf Coast Tertiary): The University of Texas at Austin, Ph.D. dissertation, 145 p.

Milliken K. L., Land, L. S., and Loucks, R. G., 1981, History of burial diagenesis determined from isotopic geochemistry, Frio Formation, Brazoria County, Texas: American Association of Petroleum Geologists Bulletin, v. 65, p. 1397–1413.

Morton, R. A., Garrett, C. M., Jr., Posey, J. S., Han, J. H., and Jirik, L. A., 1981 [1982], Salinity variations and chemical compositions of waters in the Frio Formation, Texas Gulf Coast:

The University of Texas at Austin, Bureau of Economic Geology, 1981 annual report prepared for The U.S. Department of Energy, Division of Geothermal Energy, under contract no. DE-AC08-79ET27111, 96 p.

Morton, R. A., Han, J. H., and Posey, J. S., 1983, Variations in chemical compositions of Tertiary formation waters, Texas Gulf Coast, *in* Morton, R. A., Ewing, T. E., Kaiser, W. R., and Finley, R. J., Consolidation of geologic studies of geopressured geothermal resources in Texas: The University of Texas at Austin, Bureau of Economic Geology, 1982 annual report prepared for the U.S. Department of Energy, Division of Geothermal Energy, under contract no. DE-AC08-79ET27111, p. 63–134.

Morton, R. A., and Land, L. S., 1987, Regional variations in formation water chemistry, Frio Formation (Oligocene), Texas Gulf Coast: American Association of Petroleum Geologists Bulletin, v. 71, no. 2, p. 191–206.

Seni, S. J., Mullican, W. F., III, and Hamlin, H. S., 1984, Texas salt domes: natural resources, storage caverns, and extraction technology: The University of Texas at Austin, Bureau of Economic Geology, report prepared for Texas Department of Water Resources, under interagency contract no. IAC(84-85)-1019, p. 97, 115.

Seni, S. J., Mullican, W. F., III, and Ozment, R. W., 1984, Computerized inventory of data on Texas salt domes: The University of Texas at Austin, Bureau of Economic Geology, report prepared for Texas Department of Water Resources under contract no. IAC(84-85)-1019, 34 p.

Taylor, R. E., 1975, Chemical analyses of ground water for saline-water resources studies in Texas Coastal Plain stored in National Water Data Storage and Retrieval System: Bay St. Louis, Mississippi, U.S. Geological Survey Open-File Report no. 75-79, v. 1, p. 118–123.

Tyler, Noel, and Han, J. H., 1982, Elements of high constructive deltaic sedimentation, lower Frio Formation, Brazoria County, Texas: Gulf Coast Association of Geological Societies Transactions, v. 32, p. 527–540.

SECTION III: CO-LOCATION OF HEAVY OIL AND GEOPRESSURED GEOTHERMAL BRINE RESOURCES, EXAMPLES FROM SOUTH TEXAS AND SOUTHERN CALIFORNIA

H. Scott Hamlin, Timothy G. Walter, and Charles W. Kreitler

ABSTRACT

In the San Joaquin Basin of California and the Rio Grande Embayment of South Texas, deep geopressured geothermal zones are a potential source of hot water for thermally enhanced recovery of heavy oil in shallow reservoirs. In this report we review the relevant literature and characterize geopressured geothermal zones and heavy-oil fields that are geographically co-located. The San Joaquin Basin contains billions of barrels of heavy-oil reserves, but geopressured geothermal resources there have not been adequately delineated. The regional structural setting and isolated deep-well data, however, indicate that high fluid pressures and temperatures commonly occur below 9,000 ft in the San Joaquin Basin. The geopressured geothermal potential of the Wilcox Group in South Texas is well established; upper Wilcox sandstones at depths below 8,000 ft generally have fluid temperatures and pressure gradients that exceed 250°F and 0.7 psi/ft, respectively. Yegua and Jackson heavy-oil reservoirs in the Mirando Trend overlie deep Wilcox geopressured sandstones.

INTRODUCTION

During 1989, we conducted an overview of the geologic parameters involved in thermally enhanced heavy-oil recovery using geopressured geothermal waters from underlying sandstone reservoirs in southern California and South Texas. In both regions there is widespread co-location of shallow heavy-oil reservoirs and deep geopressured geothermal zones.

The south part of the San Joaquin Basin in Kern County, California, contains about 18 billion barrels (Bbbl) of heavy oil (gravity <20° API) in 59 large reservoirs. Although most of these reservoirs are undergoing thermally enhanced oil recovery (primarily steam injection), they are currently only about 22 percent depleted. The west part of the basin contains a thick sedimentary section at depth under considerable tectonic compression, which has generated high fluid pressures and temperatures (Berry, 1973). Heavy-oil reservoirs occur in sandstones from a few hundred to several thousand feet deep. Prospective geopressured geothermal sandstones occur as shallow as 4,000 ft but are most common below about 9,000 ft. At these depths fluid-pressure gradients commonly exceed hydrostatic, salinities average about 20,000 ppm, and temperatures are probably at least 250°F.

The Los Angeles Basin in Los Angeles and Orange Counties, California, contains nearly 14 Bbbl of heavy oil in 63 reservoirs. Most reservoirs are undergoing steam injection or waterflooding and are about 19 percent depleted. The basin is dissected by northwest-southeast trending strike-slip faults, which control the distribution of the oil fields. Well data indicate that geopressured geothermal conditions are present at depth along these faults.

In South Texas deeply buried Wilcox geopressured geothermal reservoirs underlie the heavy-oil fields of the Mirando Trend. Heavy-oil reservoirs occur mainly in the Jackson and Yegua Formations at depths ranging from 100 to 5,000 ft. Original heavy oil in place (OHOIP) in the Mirando Trend is about 200 million barrels (MMbbl), of which about 30 per cent has already been produced. Geopressured upper Wilcox sandstones lie at depths ranging from 8,000 ft down to deepest well control. Temperatures in these sandstones exceed 250°F, pressure gradients are generally greater than 0.7 psi/ft, sandstone porosities range from 9 to 17 percent, and pore-fluid salinities range from 70,000 to less than 20,000 ppm NaCl.

SAN JOAQUIN BASIN

The available literature was reviewed to determine potential co-location of heavy-oil reservoirs and underlying geopressured geothermal reservoirs in the San Joaquin Basin of California. Unfortunately, actual temperature and pressure data are rarely cited; only isolated references to "overpressure" and "high temperature" are made. Most of the major heavy-oil fields (25 MMbbl or more of OHOIP) are located around the margins of the south part of the basin in Kern County (fig. 1). The west part of the basin is geologically most favorable for the occurrence of overpressured sandstone reservoirs at depth. Typical heavy-oil fields from this area—Coalinga field in Fresno County and Lost Hills, Cymric, McKittrick, and Midway-Sunset fields in Kern County—are described in this report.

Geology

The San Joaquin Basin is bounded to the east by the Sierra Nevada batholith and to the west by the San Andreas fault (fig. 1). The Temblor Range parallels the fault, composing the west edge of the south part of the basin, and is an area of uplift characterized by folds and faults in the basinal sediments (fig. 2). Structural deformation of sediments began in the middle Miocene and reached greatest intensity in the Pliocene and Pleistocene (Berry, 1973). Structural traps associated with Temblor deformation contain major heavy-oil fields.

Temblor Range deformation probably caused substantial overpressuring. On the basis of drill-stem-pressure measurements and regional structure, Berry (1973) reasoned that tectonic compaction was responsible for near-lithostatic pressures in Cretaceous sediments in the Sacramento Basin and the north and central parts of the San Joaquin Basin. The present distribution of high fluid pressures in the San Joaquin Basin appears to be related more to structural deformation than to sedimentation rates and patterns, the highest pressures

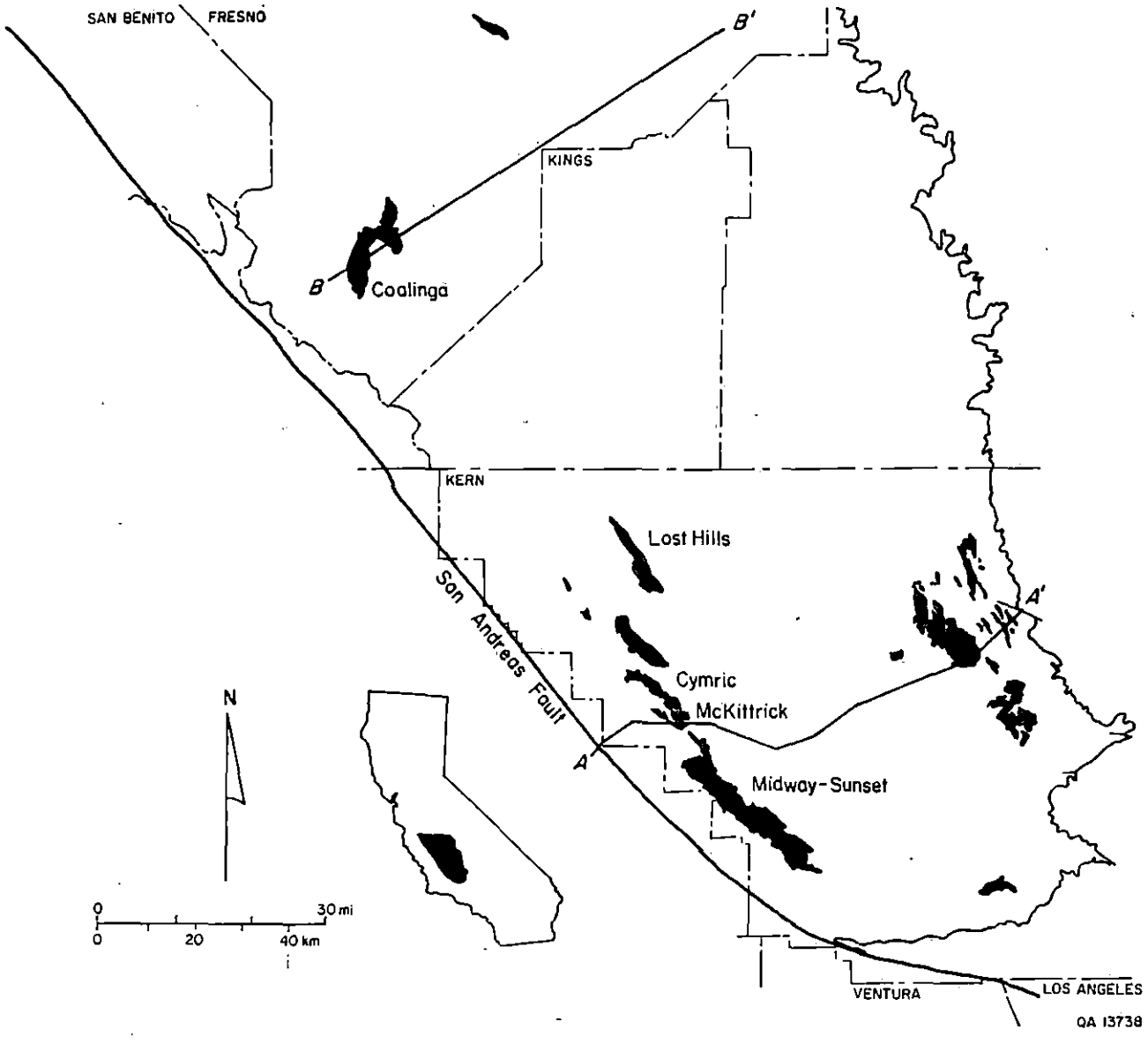

Figure 1. Location map of heavy-oil fields in San Joaquin Basin, California, containing reserves greater than 25 MMbbl of original heavy oil in place (Nehring and others, 1983). Cross section A–A′ shown in figure 2; cross section B–B′ shown in figure 3.

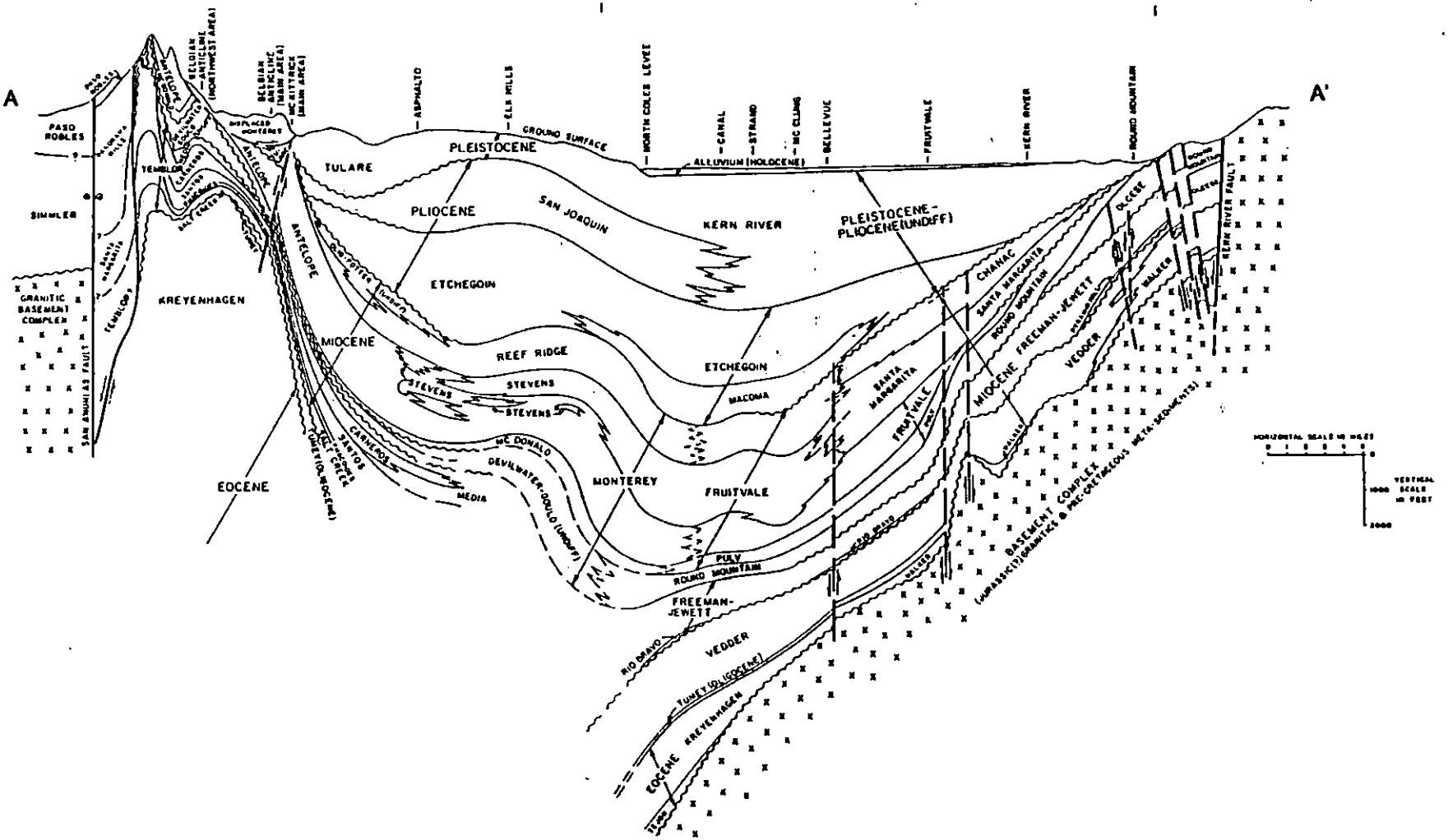

Figure 2. Generalized west-east cross section A–A' in southern San Joaquin Basin. From California Division of Oil And Gas (1973). Line of section shown in figure 1.

occurring, at depth, along the crests of folds (often coincident with overlying oil traps) and diminishing away from these structures (Berry, 1973). The San Andreas Fault to the west and a fault at depth bounding the western edge of the Sierra Nevada batholith on the east side of the basin have caught the Cretaceous Great Valley clastic sequence in a viselike grip, compressing the sediments and increasing formation pressures (Berry, 1973). The Temblor mountain-building episode was one consequence of this process.

Stratigraphic relationships in the San Joaquin Basin are generally complex. Mesozoic sediments and metasediments are typically deeply buried beneath Cenozoic (Paleocene-to-Pleistocene) sandstones, siltstones, and shales (fig. 3). Erosional unconformities, which are especially abundant adjacent to the basin margins, provide the principal basis by which the stratigraphic sequence is divided. These unconformities have provided numerous traps both in angular contacts of the beds below the unconformity, and in pinchouts of strata above unconformities (Foss and Blaisdell, 1968). Although structure plays the major role in oil accumulation (Callaway, 1968), many heavy-oil reservoirs occur in stratigraphic traps.

Heavy-oil reservoirs in the San Joaquin Basin generally occur in the shallowest horizons. The lower Pliocene Etchegoin Formation and younger Tulare Formation (figs. 2 and 3) are the dominant producing zones in the west half of the basin. However, several large heavy-oil reservoirs also occur in deeper formations, notably the Carneros Sand of the lower Miocene Temblor Formation and the Oceanic Sand of the Oligocene Tumey Formation (figs. 2 and 3). Some of the smaller fields, such as Antelope Hills and North Antelope Hills (fig. 1), produce heavy oils from the coarse sands of the lower Santos member of the Temblor Formation or from the Point-of-Rocks Sandstone of the Eocene Kreyenhagen Formation (figs. 2 and 3).

Pressure

Geopressured sandstones are more likely to occur in the west part of the basin for two reasons. First, crystalline basement is shallow and overlying sediments are thin in the east half

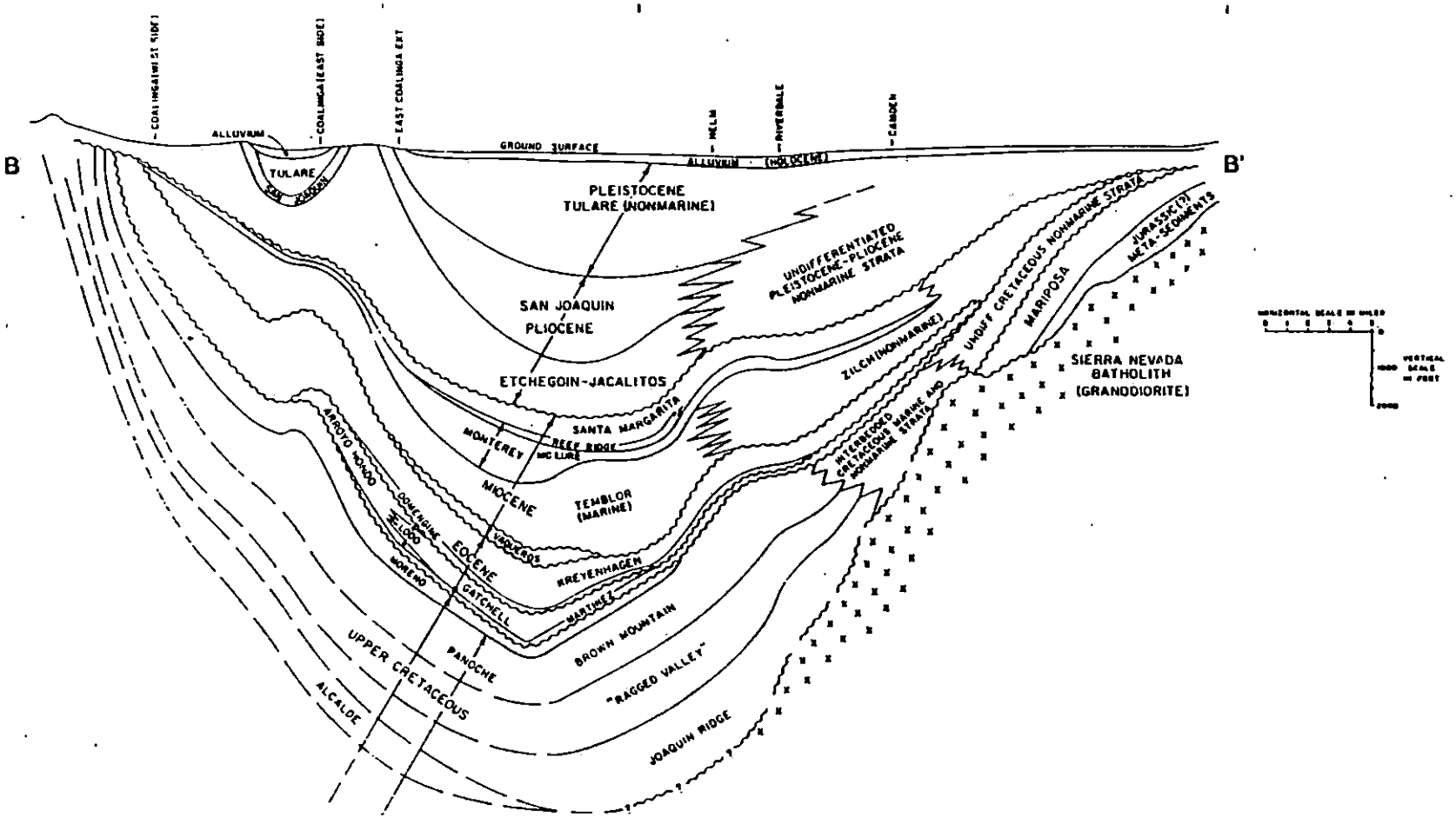

Figure 3. Generalized west-east cross section B–B′ in central San Joaquin Basin. From California Division of Oil And Gas (1973). Line of section shown in figure 1.

of the basin (figs. 2 and 3), whereas the Tertiary sedimentary package has a thickness that exceeds 15,000 ft in the west half (fig. 2). Secondly, Cretaceous strata are present only in the west half of the basin, and Cretaceous sandstones and shales have undergone the greatest tectonic compression and contain the highest fluid pressures (Berry, 1973).

Tertiary strata in the San Joaquin Basin also contain sandstones that have abnormal pressures. Wallace and others (1979) and Strongin (1981) indicated that significant overpressured zones have been found in numerous fields within the basin. Overpressured zones may be present locally at depths as shallow as 400 ft (Wallace and others, 1979). Data from Berry (1973) indicate that pressure gradients at Lost Hills field (fig. 1) are above hydrostatic within the Pliocene Etchegoin Formation at a depth of about 1,000 ft (fig. 4).

Temperature and Salinity

Few published data are available on temperatures and water chemistry for either the heavy-oil reservoirs or the potential geopressured geothermal zones. General temperature gradients for basins in California, as given by Strongin (1981), range from 2.0°F to 3.5°F per 100 ft of depth. Wallace and others (1979), however, indicated a statewide average gradient of 1.8°F per 100 ft. Van Orstrand (1934) determined gradients for several California oil fields using well data, and a basinwide average calculated from his data is approximately 1.67°F per 100 ft. Using this gradient, which is probably a conservative estimate for fields on the west side of the basin, a formation temperature would be 300°F at a depth of about 13,800 ft. Using low and high gradients from the above workers, we calculated temperature ranges for zones in several heavy-oil fields in the San Joaquin Basin (table 1).

Water salinity shows little correlation with depth or formation in the San Joaquin Basin, ranging from about 30,000 to 10,000 ppm TDS in various Tertiary zones between 500 and 10,000 ft deep (table 1). Data for geopressured horizons below 10,000 ft are not reported in

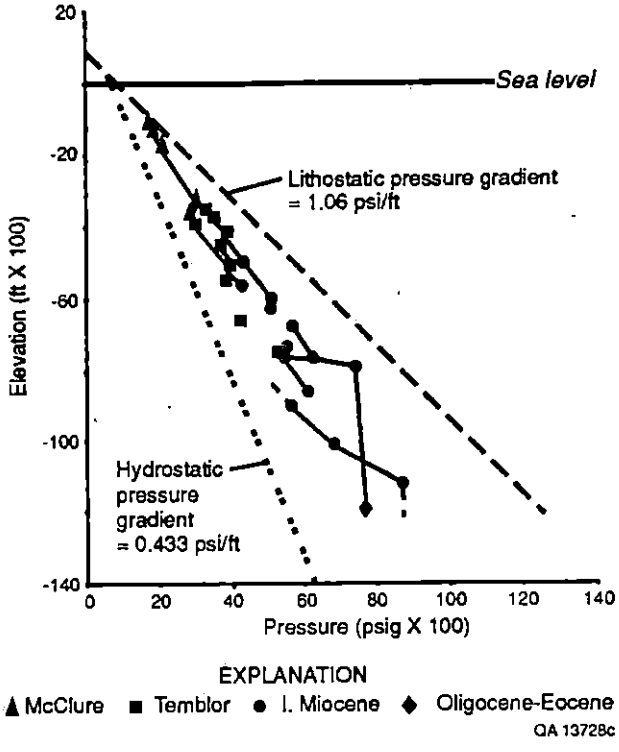

Figure 4. Plot showing pore-fluid pressure versus depth for 13 wells in Lost Hills oil field (fig. 1). From Berry (1973).

Table 1. Salinity and calculated temperature ranges for selected heavy-oil fields in San Joaquin Basin, California. Temperatures calculated using gradients of 1.67°F and 3.0°F/100 ft. Salinity data from California Division of Oil and Gas (1973).

Field	Zone	Depth (ft)	Salinity (ppm)	Temperature (°F) range
Coalinga	Etch.–Tembl.	2,000	2,996	104–130
	Temblor	2,650	1,370	114–150
Cymric	Phacoides	500	25,680	78–85
	Etchegoin	650	18,318	81–90
	Tulare (Amn.)	1,000	4,965	87–100
	First McKitt	1,100	8,560	88–103
	Tulare (Amn.)	1,200	1,712	90–106
	2nd McKitt	1,230	8,560	91–107
	Carneros	1,950	15,322	103–129
	Phacoides	2,200	23,454	107–136
	Olig (Reef R.)	2,250	17,976	108–138
	Etchegoin	2,450	18,832	111–144
	Carneros	3,400	10,272	127–172
	Etchegoin	3,400	20,544	127–172
	Agua	3,400	21,400	127–172
	Carneros	4,150	21,914	140–195
	Phacoides	4,300	15,066	142–199
	Phacoides	4,600	22,256	147–208
	Oceanic	4,700	17,120	149–211
	Oceanic	4,900	18,832	152–217
	Point of Rocks	5,400	21,400	161–232
	Carneros	5,560	21,400	163–237
	Phacoides	7,870	11,984	202–306
	Oceanic	8,570	10,272	214–327
	Carneros	8,600	6,163	214–328
	Phacoides	10,145	9,587	240–374
Lost Hills	Tulare	200	2,568	73–76
	Etchegoin	1,000	23,968	87–100
	Cahn	4,900	29,104	152–217
	Carneros	6,020	18,832	171–251
McKittrick	Tulare	500	856	78–85
	Tulare	650	4,194	81–90
	Phacoides	790	9,758	83–94
	Olig	800	7,704	83–94
	Basal Reef R.	1,500	9,074	95–115
	Stevens	3,375	20,544	127–171

Field	Zone	Depth (ft)	Salinity (ppm)	Temperature (°F) range
McKittrick	Antelope	3,600	24,482	130–178
	Carneros	6,500	21,058	179–265
	Oceanic	8,300	11,642	209–319
	Point of Rocks	9,100	22,770	223–343
Midway–Sunset	Tulare	800	10,272	83–94
	Marvic	1,000	685	87–100
	Mya Tar	1,100	4,451	88–103
	Metson	1,250	13,525	91–108
	Monarch	1,300	11,556	92–109
	Potter	1,350	3,467	93–111
	Top Oil	1,500	31,244	95–115
	Sub–Lakeview	1,750	7,533	99–123
	Moco	2,150	16,778	106–135
	Wilhelm	2,500	32,528	112–145
	Gusher	2,500	25,851	112–145
	Kinsey	2,800	28,762	117–154
	Lakeview	2,950	28,590	119–159
	Calitroleum	3,000	31,330	120–160
	Republic	3,100	1,198	122–163
	Leutholtz	3,200	9,416	124–166
	Obispo	3,600	16,606	130–178
	Pacific	3,700	10,272	132–181

the literature. Some oil-field data, however, show salinity decreasing with depth (Weddle, 1968; Berry, 1973). Thus, average TDS values for deeper horizons is probably less than 30,000 ppm.

Production History

Production statistics are tabulated in table 2 for the heavy-oil reservoirs in selected fields within the San Joaquin Basin. Most of these fields are undergoing or have already undergone secondary production stimulation for heavy-oil recovery. The largest single producing reservoir is the lower Miocene Temblor Formation in Coalinga field (fig. 1). Production since discovery in 1900 through 1963 was 198 MMbbl of 15° API oil. Heavy-oil production at Coalinga field is augmented using cyclic steam flooding. Farther south, the Main (Upper) reservoirs of McKittrick field (fig. 1) produced about 111 MMbbl of 15° API oil from about 1896 through 1963. Various reservoir-stimulation methods have been employed in this field.

Typical Fields

Coalinga Field

In Coalinga field depths to the upper Temblor heavy-oil-producing zone range from about 500 ft in the Westside area to nearly 3,600 ft in the east part of the field. Most of the Tertiary-age producing formations crop out in the west (fig. 5). Potential geopressured geothermal reservoirs lie within Upper Cretaceous sandstones of the Panoche Formation at depths of 5,000 ft to more than 10,000 ft (Berry, 1973).

Table 2. Production statistics for selected significant heavy-oil fields in California (Dietzman and others, 1965; California Div. of Oil and Gas, 1989).

San Joaquin Basin

County	Field	Reservoir	API gravity	Cumulative production through 1-1-64 (Mbbl)
Fresno	Coalinga	Westside Area	15	197,984
Kern	Cymric	1-Y Area(1-Y gas sand)	14	31
		McKittr.Front(upper)	13	9,567
		McKittr.Front(lower)	18	6,702
		Salt Creek Main (Carneros unit)	20	18,741
		Salt Creek Main (Carneros West)	16	1,426
		Welport Area(Tulare)	13	17,906
	Lost Hills	Williamson	14	5,260
	McKittrick	Main(upper)	15	110,900
	Midway-Sunset	Others	16	785,206
		Olig	15	254
		Ethyl "D"	19	4,229
		Republic	19	20,678
		Quality	15	15,118
		Metson	11	888
		Leutholtz	19	16,321

Los Angeles Basin

County	Field	Reservoir	API gravity	Cumulative production through 1-1-64 (Mbbl)
Los Angeles	Inglewood	Vickers	19	345,879 *
	Whittier	Central Area (Main)	19	45,511 *
		Rideout Heights Area	20	4,981 *
Orange	Huntington Beach	Huntngton Ave(Temblor)	18	5,574
		Huntngton Ave(Others)	13	794
		North Area (Tar Bolsa)	20	324,812
		South Area, onshore (Tar Zone)	15	14,052
		(A-37)	19	15,396
		(Jones)	16	7,565
		South Area, offshore (Jones)	17	65,662

* Cumulative production through 1-1-89.

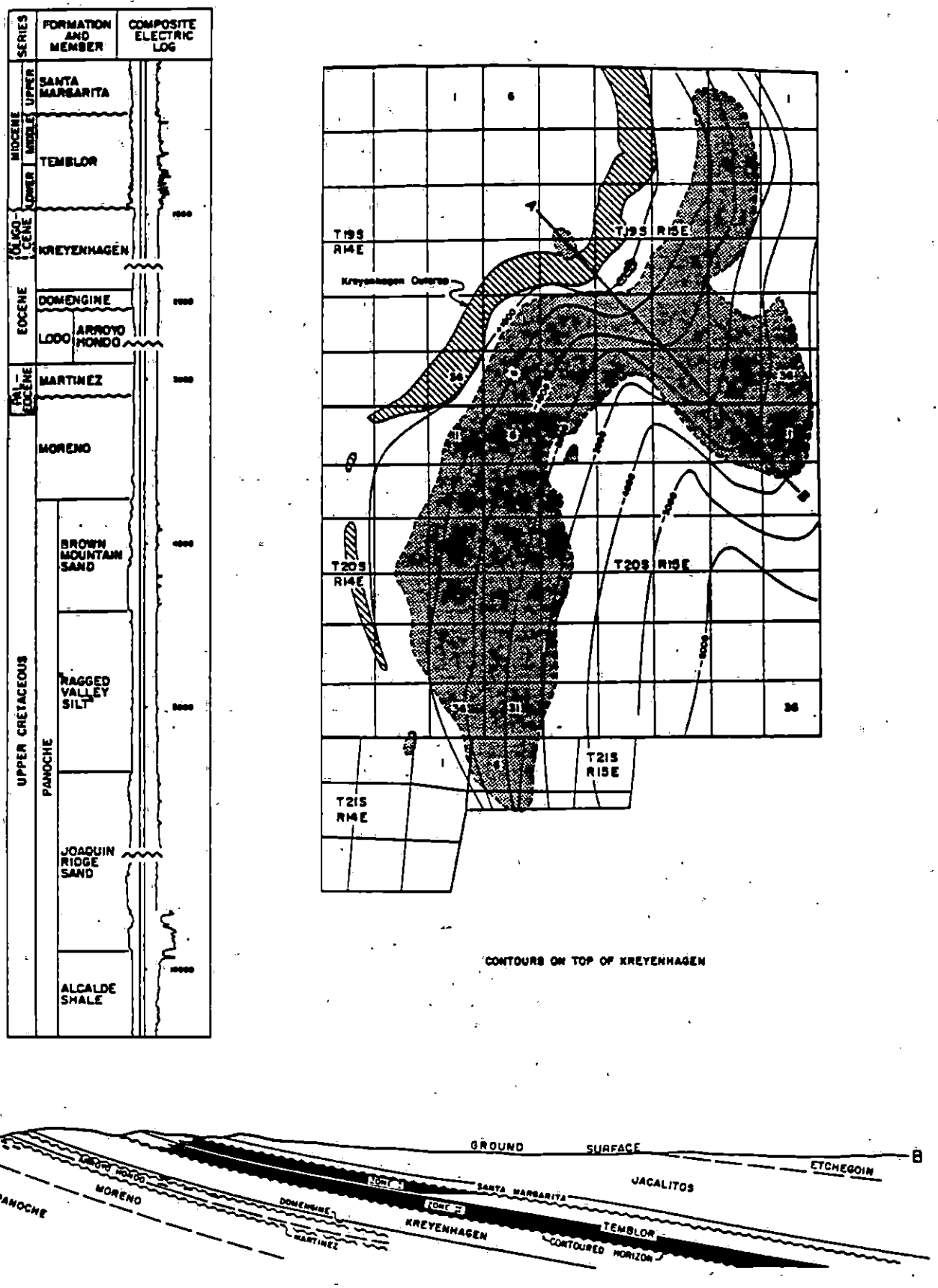

Figure 5. Stratigraphic column, structure map, and generalized cross section of Coalinga oil field. From California Division of Oil and Gas (1973). Heavy-oil producing zones shown in black.

Lost Hills Field

Most heavy-oil production at Lost Hills field is from the Williamson (W-4) zone in the lower Etchegoin Formation (table 2; fig. 6). Minor heavy-oil production has come from the basal Pleistocene Tulare Formation. Typical production depth for the W-4 zone averages about 1,200 ft; the Tulare Formation reservoirs are less than 500 ft deep.

Greater-than-hydrostatic pressures have been reported as shallow as 4,000 ft in the Miocene Antelope Shale at Lost Hills (McGuire and others, 1984) and at less than 1000 ft within the Etchegoin Formation (Berry, 1973)(fig. 4). The sandstones of the lower Miocene Temblor Formation are commonly overpressured and have high temperatures (California Division of Oil and Gas, 1973). Potential zones for geopressured geothermal water production include the Agua Sand and Phacoides Sands of the Temblor Formation and the Point-of-Rocks Sandstone within the Eocene Kreyenhagen Formation (fig. 6).

Cymric Field

Most heavy-oil production in Cymric field is from the Tulare reservoir in the Welport area of the field and from the Carneros Unit reservoir in the Salt Creek Main area. Production depths range from as shallow as 1,200 ft in the Welport area (fig. 7) to about 3,000 ft in the Salt Creek Main area (fig. 8). The Point-of-Rocks Sandstone of the Kreyenhagen Formation is a potential geopressured reservoir in the Salt Creek Main area at a depth of about 5,500 ft. The Point-of-Rocks Sandstone is a light-oil reservoir in the Welport area (California Division of Oil and Gas, 1973). Geopressured sandstones in the Wellport area lie in Cretaceous strata at about 10,000 ft.

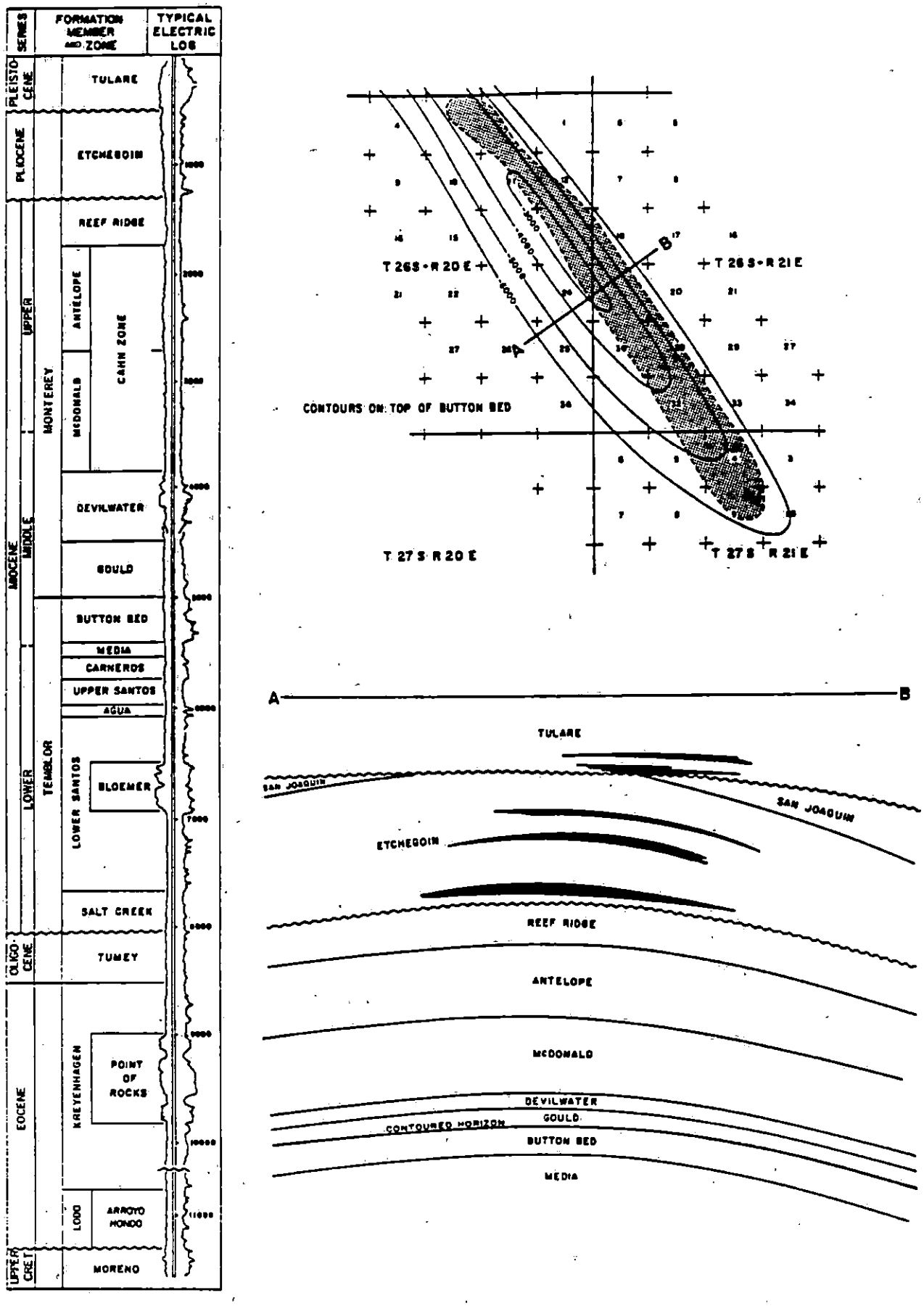

Figure 6. Stratigraphic column, structure map, and generalized cross section of Lost Hills oil field. From California Division of Oil and Gas (1973). Heavy-oil reservoirs in Tulare and Etchegoin Formations shown in black.

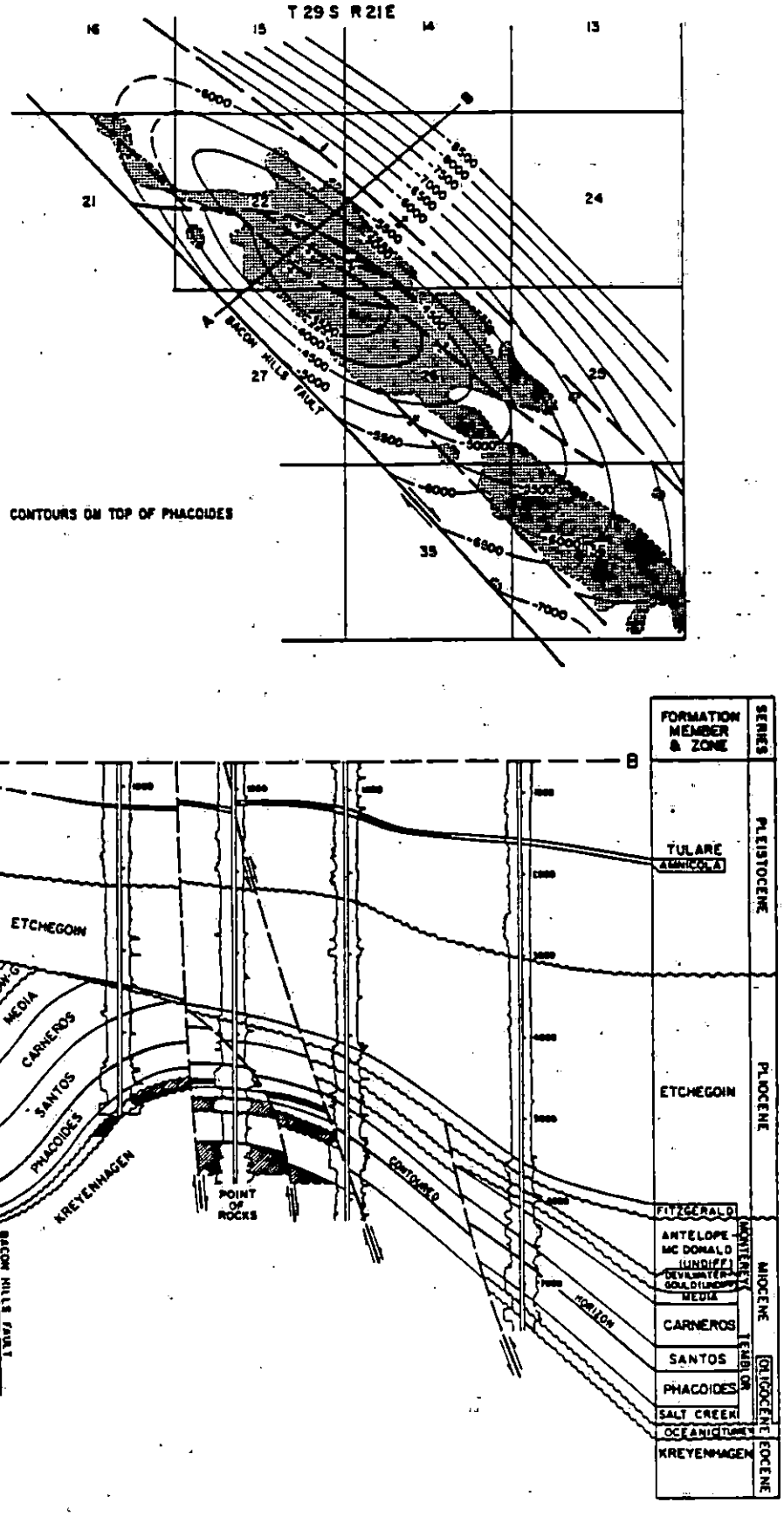

Figure 7. Structure map and cross section of Welport area of Cymric oil field. From California Division of Oil and Gas (1973). The cross section shows the Tulare Amnicola Sand heavy-oil reservoir at a depth of 1,200 to 1,500 ft.

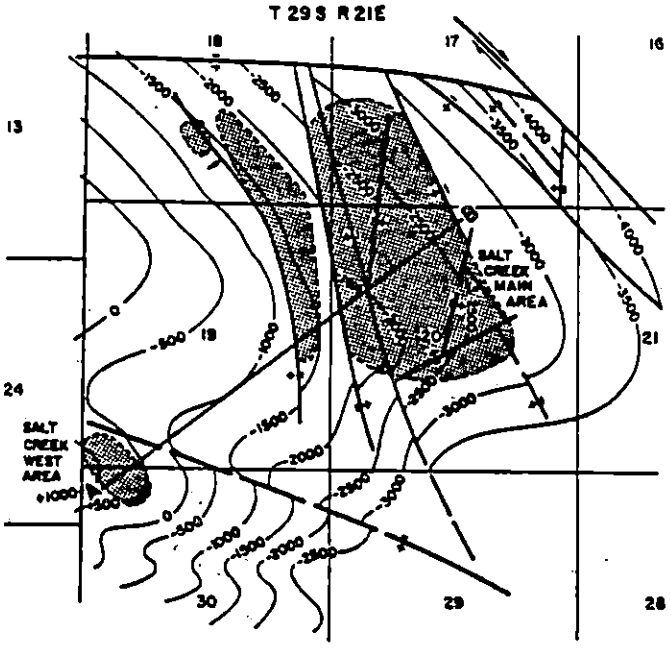

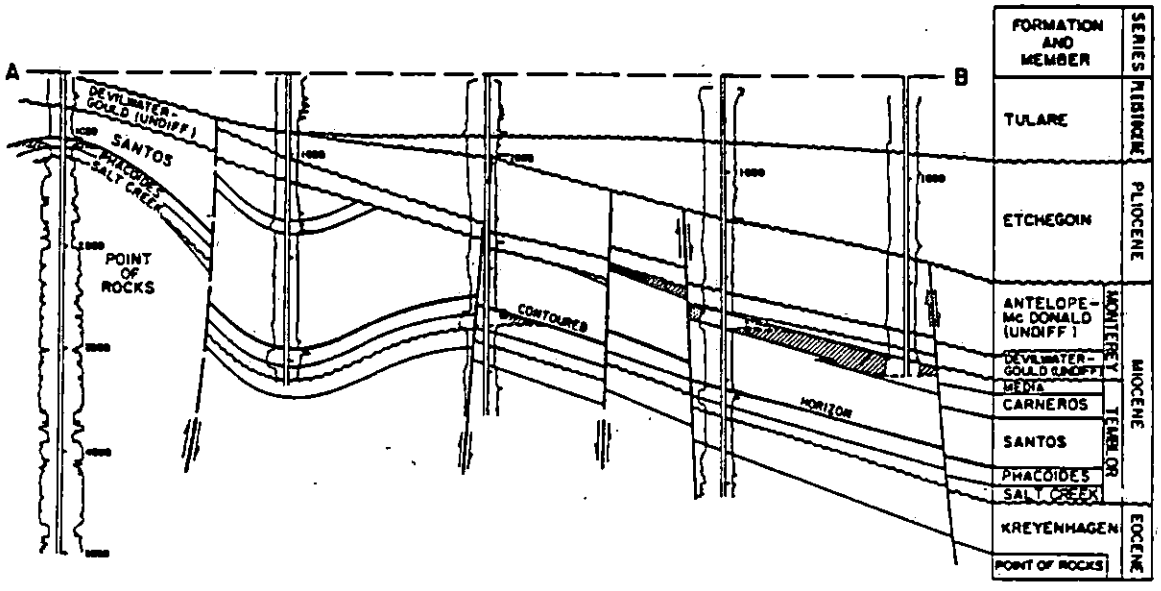

Figure 8. Structure map and cross section of Salt Creek Main area of Cymric field. From California Division of Oil and Gas (1973). Heavy-oil production is from the Carneros Sand of the Temblor Formation at a depth of 2,000 to 3,000 ft.

McKittrick Field

All producing zones at McKittrick field contain some heavy oils, but the Tulare, Olig, and basal Reef Ridge zones in the Main area are the largest heavy-oil-producing reservoirs (fig. 9). The Olig reservoir within the Reef Ridge member of the Monterey Formation lies at an average depth of 800 ft in the McKittrick Main area (fig. 9). Overpressured zones having the potential for production of geothermal waters probably occur below 9,000 ft in the Kreyenhagen Formation or in underlying strata (fig. 9).

Midway-Sunset Field

Numerous heavy-oil reservoirs occur in Midway-Sunset field in the upper 5,000 ft of strata. The largest producer, the upper Miocene Republic Sand in the basal Antelope Shale member of the Monterey Formation (fig. 10), occurs at an average depth of 1,300 ft in the central part of the field. Overpressured zones suitable for thermal water production probably occur below 10,000 ft in the Kreyenhagen Formation or within the underlying Cretaceous strata. Exact formation depths below the Antelope Shale (fig. 11) at Midway-Sunset have not been reported in the literature.

LOS ANGELES BASIN

A literature review of heavy-oil fields in the Los Angeles Basin, California, reveals potential co-location of heavy oil and geopressured geothermal reservoirs. Most of the heavy-oil accumulations are associated with the major fault trends (fig. 12). Fields reviewed here are Inglewood and Huntington Beach fields in the west part of the basin and Whittier field in the

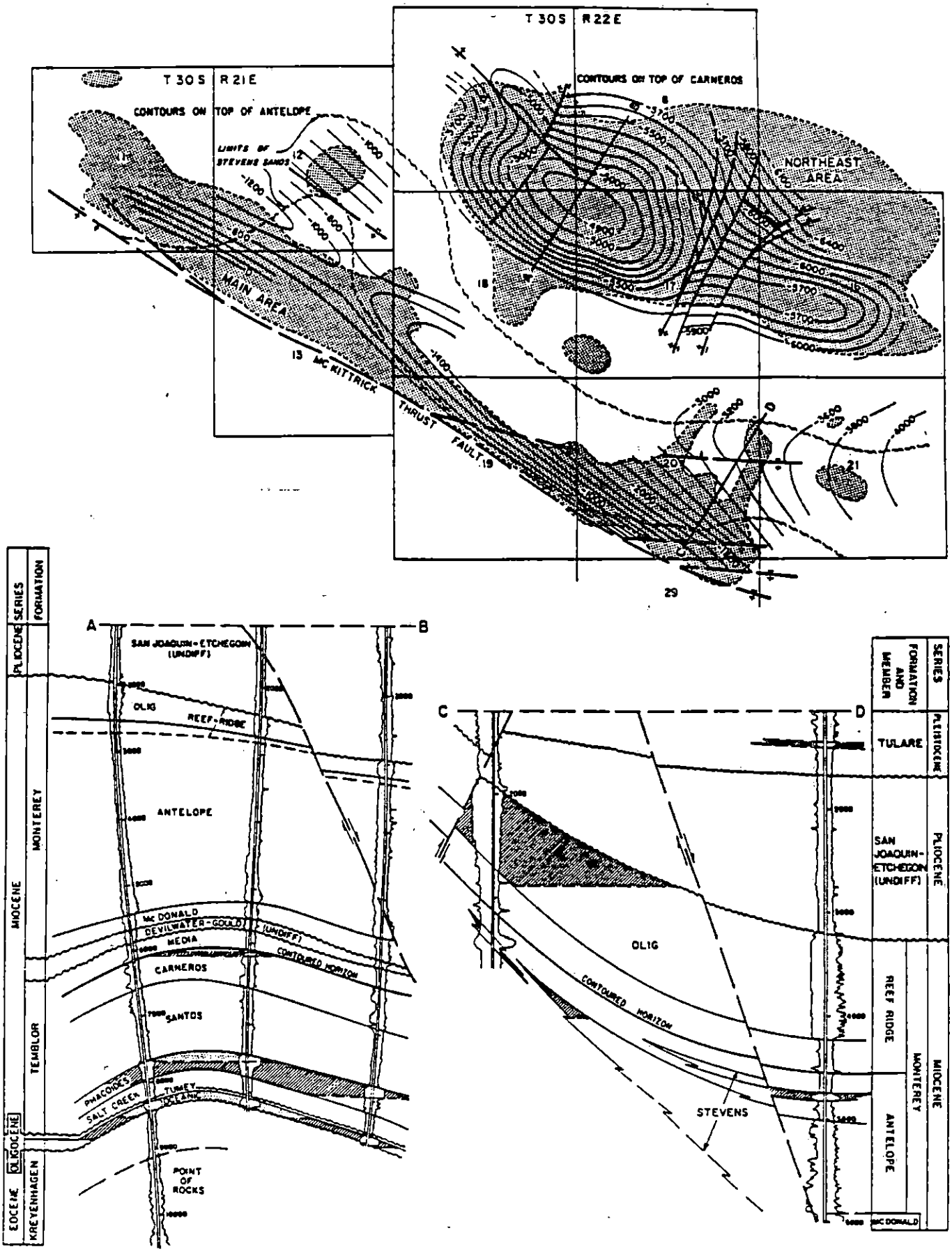

Figure 9. Structure map and cross sections of McKittrick oil field showing heavy-oil-bearing stratigraphic units. From California Division of Oil and Gas (1973). Most heavy-oil production comes from reservoirs in Tulare and Monterey Formations.

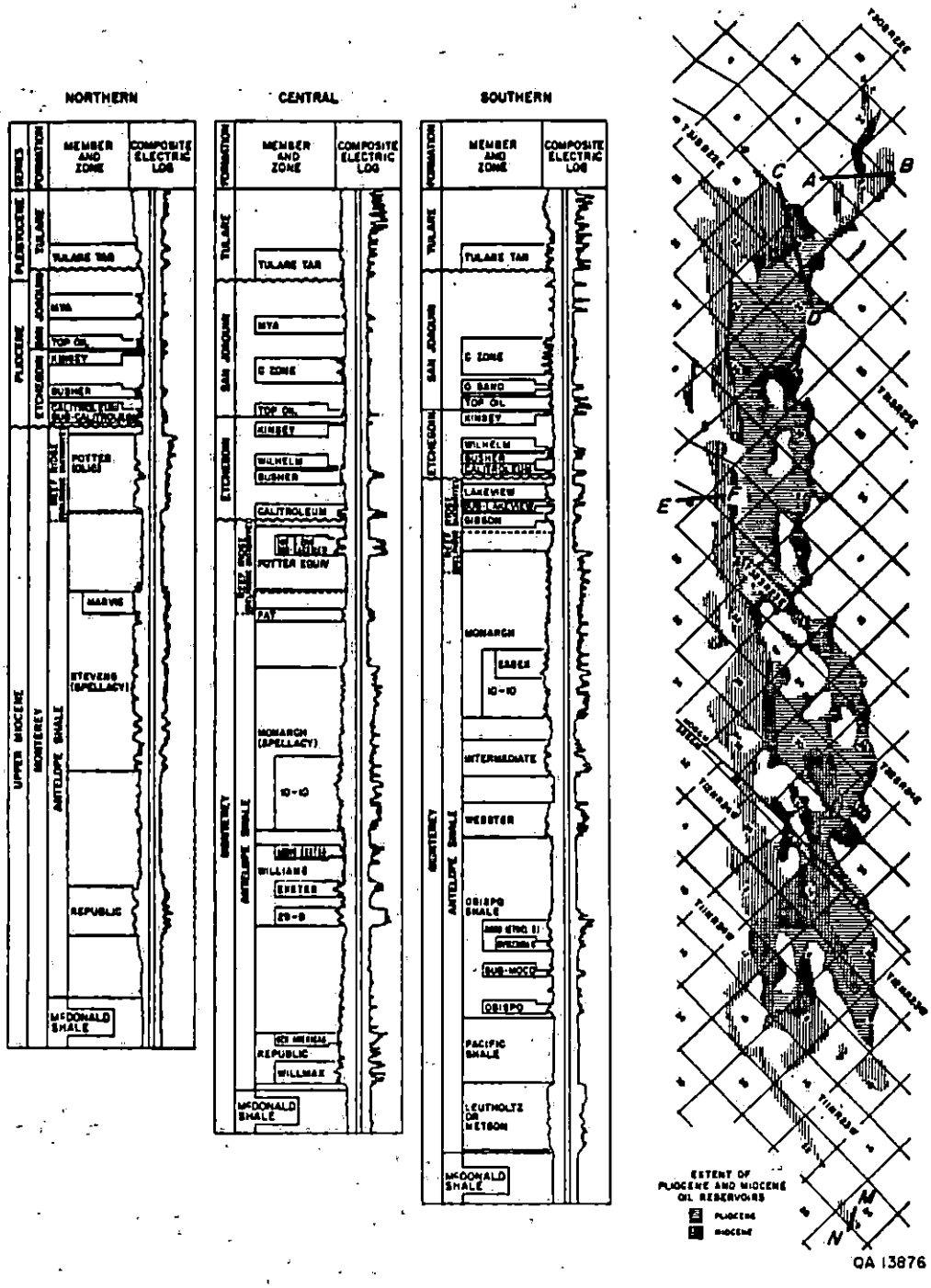

Figure 10. Stratigraphic columns and reservoir distribution map of Midway-Sunset oil field. From California Division of Oil and Gas (1973). Significant heavy-oil reservoirs lie in Potter, Republic, Leutholtz, and Metson zones. Cross sections A–B, C–D, E–F, and N–M shown in figure 11.

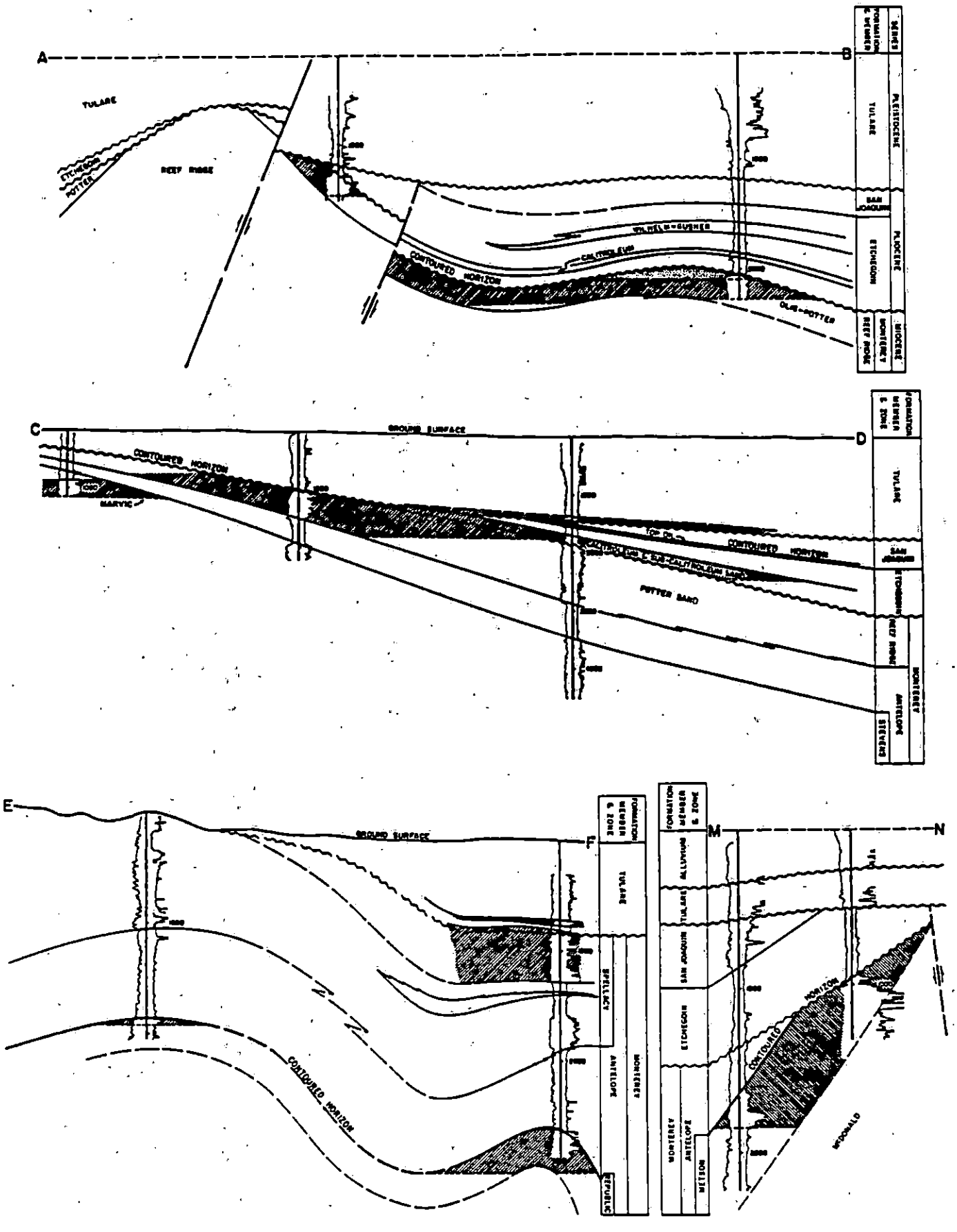

Figure 11. Cross sections of Midway-Sunset oil field. From California Division of Oil and Gas (1973). Line of sections shown in figure 10.

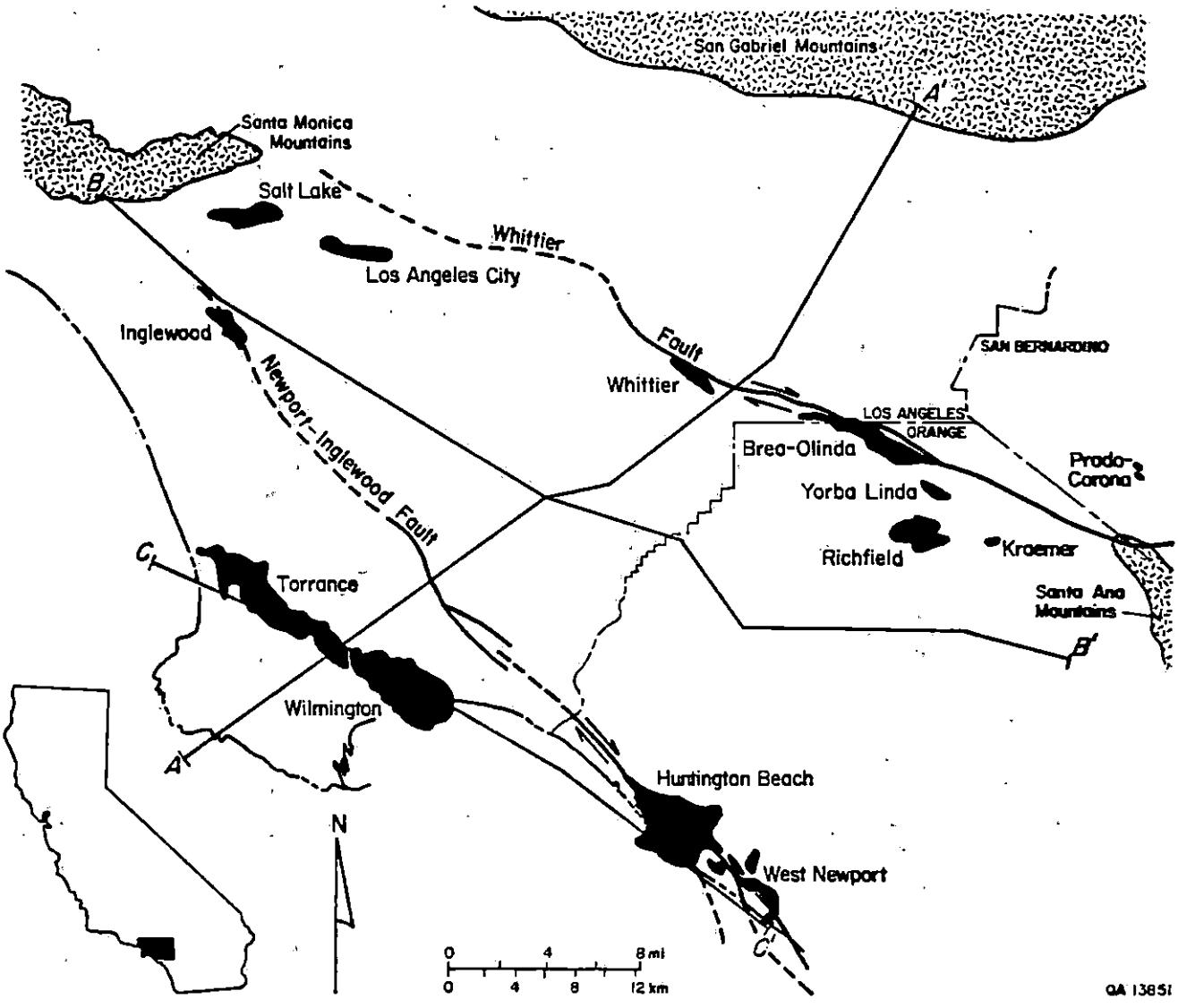

Figure 12. Location map of Los Angeles Basin, California, showing heavy-oil fields (Nehring and others, 1983) and major structural features. Modified from Yerkes and others (1965). Cross section A–A′ shown in figure 13, B–B′ in figure 14, and C–C′ in figure 15.

east-central portion. These fields are typical of those having the potential for overpressured sandstones at depth.

Geology

The Los Angeles Basin is largely comprised of middle Miocene-age sandstones and mudstones surrounded on three sides by outcropping Mesozoic-age crystalline basement rocks (Yerkes and others, 1965). Enclosed within a compressional tectonic regime, basin margins are generally delineated by normal and reverse faults (figs. 13 to 15). The basin interior is dissected by northwest-southeast-trending strike-slip faults (fig. 12), which subparallel the San Andreas Fault to the east of the Los Angeles Basin.

These strike-slip faults control the distribution of the oil fields (fig. 12). Inglewood field and Huntington Beach field are both intimately associated with the Newport-Inglewood Fault zone. In both of these fields most traps for oil occur as abrupt terminations against the main fault or against subparallel normal and reverse faults. Some heavy oil is also found in drag fold crests formed by lateral movement along the faults. Whittier field shows similar relationships with the Whittier Fault. Stratigraphic traps are important in some fields of the Los Angeles Basin.

Pressure

Strongin (1981) and Wallace and others (1979) indicated that geopressured geothermal zones occur in the Los Angeles Basin but did not cite specific examples. Berry (1973) suggested that little or no significant geopressure is present in California basins onshore farther south than the Ventura Basin. Berry (1973) did not exclude, however, the possibility of geopressure in the basin margin sediments of the offshore region of the Los Angeles Basin. Isolated well data indicate that geopressured geothermal conditions are present in Huntington Beach field at

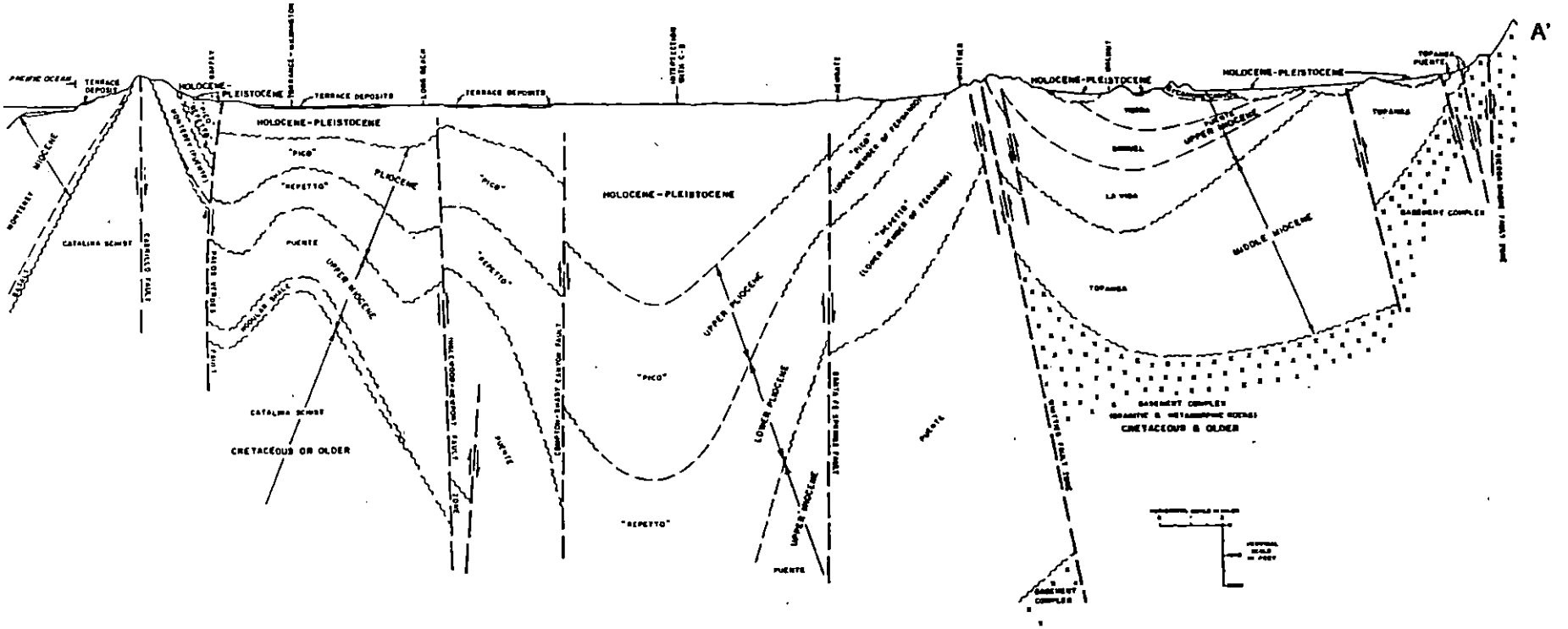

Figure 13. Southwest-northeast cross section A–A' of Los Angeles Basin. From California Division of Oil and Gas (1974). Line of section shown in figure 12.

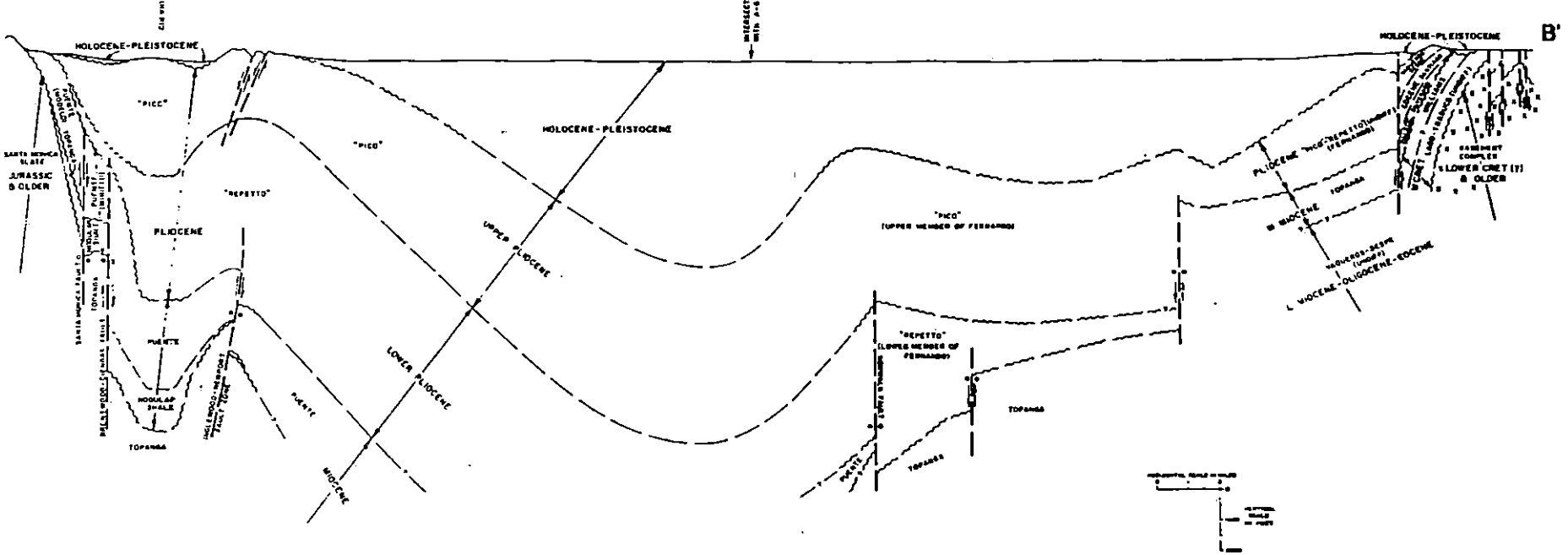

Figure 14. West-east cross section B–B′ of Los Angeles Basin. From California Division of Oil and Gas (1974). Line of section shown in figure 12.

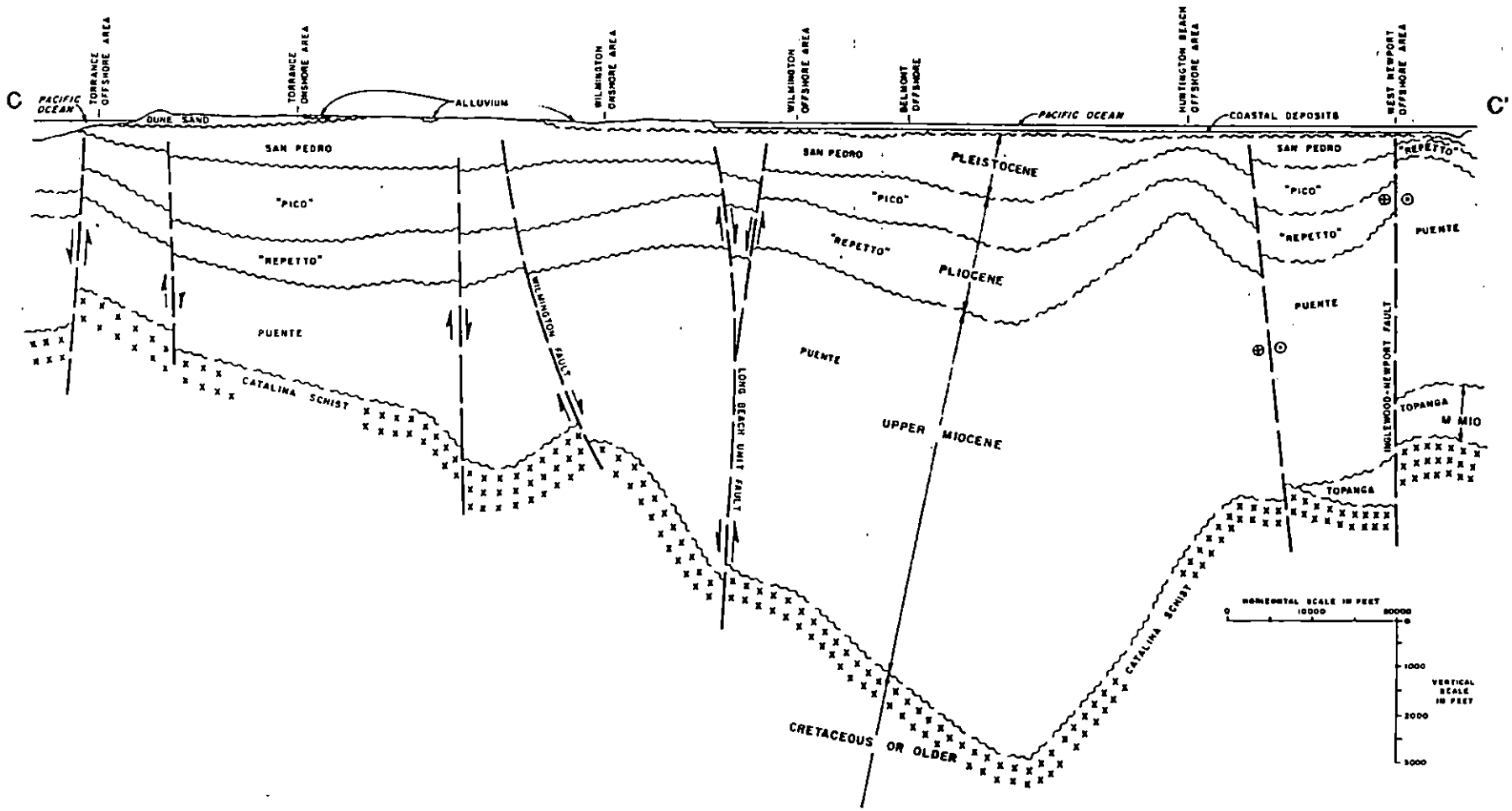

Figure 15. Northwest-southeast cross section C–C′ of Los Angeles Basin. From California Division of Oil and Gas (1974). Line of section shown in figure 12.

a depth of approximately 8,350 ft (Thomas, 1979) and are probably associated with the Newport-Inglewood Fault zone (figs. 12 to 15). Similarities are probably also present at depth in other fault-related fields under a similar compressional regime in the basin, such as those fields along the Whittier Fault (fig. 13 to 15).

Temperature

The Los Angeles Basin has temperature gradients similar to those of other California basins, ranging from 1.5°F to 3.5°F/100 ft (Wallace and others, 1979; Strongin, 1981). Wallace and others (1979) gave a statewide average gradient of 1.8°F/100 ft. Average gradients determined from field-specific data (Van Orstrand, 1934) indicate that Huntington Beach field and Wilmington field have temperature gradients of 2.62°F and 3.06°F/100 ft, respectively. Fields farther inland exhibit slightly lower temperature gradients. In Whittier field, for example, the average temperature gradient is 1.89°F/100 ft. An overall average for the basin calculated from the data of Van Orstrand (1934) is 2.22°F/100 ft.

Production History

Heavy-oil-producing zones in the Los Angeles Basin vary stratigraphically from field to field. Inglewood field, through 1963, produced more than 174.5 MMbbl of 19° API gravity oil from the uppermost horizons—the Upper Investment and Investment members of the Pico Formation (Pliocene), and the Vickers-Machado member of the Pico-Repetto Formation (Dietzman and others, 1966). Farther south, in Huntington Beach field, heavy oil is produced from numerous reservoir sandstones in the lower Pliocene Repetto Formation and from upper Miocene Puente Formation sandstones. The Tar Bolsa reservoir in the North Area of Huntington Beach field has greatly dominated basin production, having produced nearly 325 MMbbl of 20° API gravity oil (Dietzman and others, 1966). Heavy-oil production farther

inland at Whittier field comes mainly from the Repetto Formation, with some contribution from the Puente Formation.

Secondary stimulation techniques have been employed in most fields in the Los Angeles Basin. The most common methods have been water flooding and cyclic steam injection of the heavy-oil reservoirs (California Division of Oil and Gas, 1974).

Typical Fields

Inglewood Field

Heavy-oil production at Inglewood field is generally shallow; wells are typically less than 1,500 ft deep. Strata show a distinct drag-fold relationship to the Newport-Inglewood fault (fig. 16). Subsidiary faults paralleling the main fault zone compartmentalize reservoirs and locally produce traps for heavy oil in the shallow strata. Potential strata for geopressured geothermal water production are likely to occur below the Sentous zone reservoir of the Topanga Formation at depths below 9,000 ft (fig. 16).

Huntington Beach Field

Heavy-oil reservoirs in Huntington Beach field occur within a faulted anticline associated with the Newport-Inglewood fault (fig. 12). Producing horizons range from as shallow as 1,800 ft for the Upper Bolsa Sand to as deep as 4,300 ft for the Upper Jones Sand. Faults and angular unconformities form most of the traps in this field (fig. 17). Data for this field have indicated that geopressured geothermal waters occur at a depth of 8,350 ft in Topanga Formation sediments (fig. 15)(Thomas, 1979). Temperatures in excess of 424°F make this a reasonable prospect for geopressured geothermal water production.

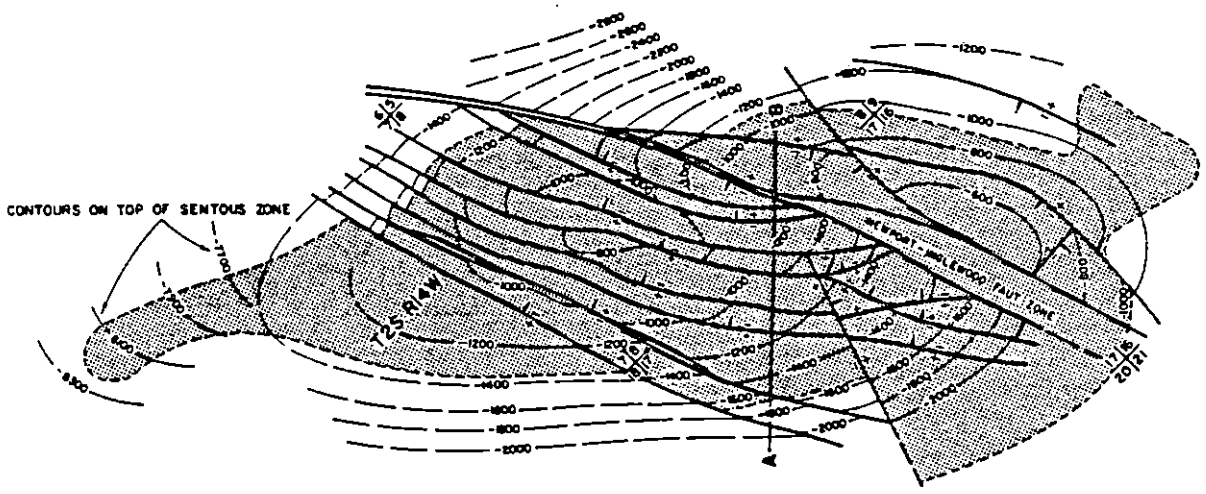

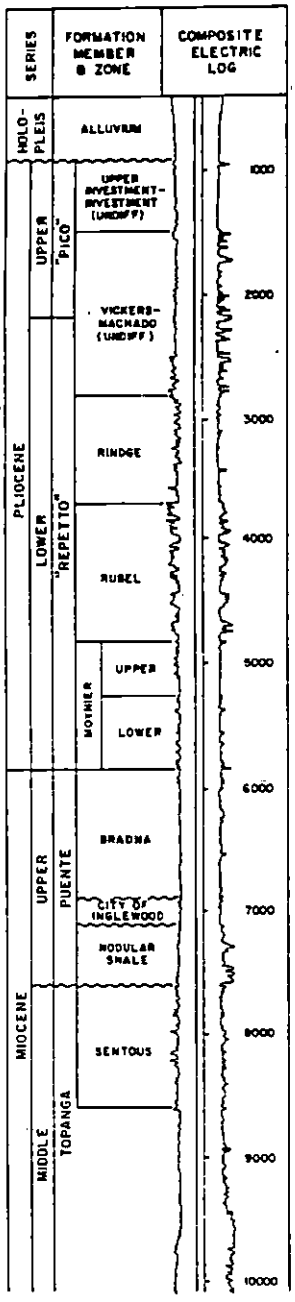

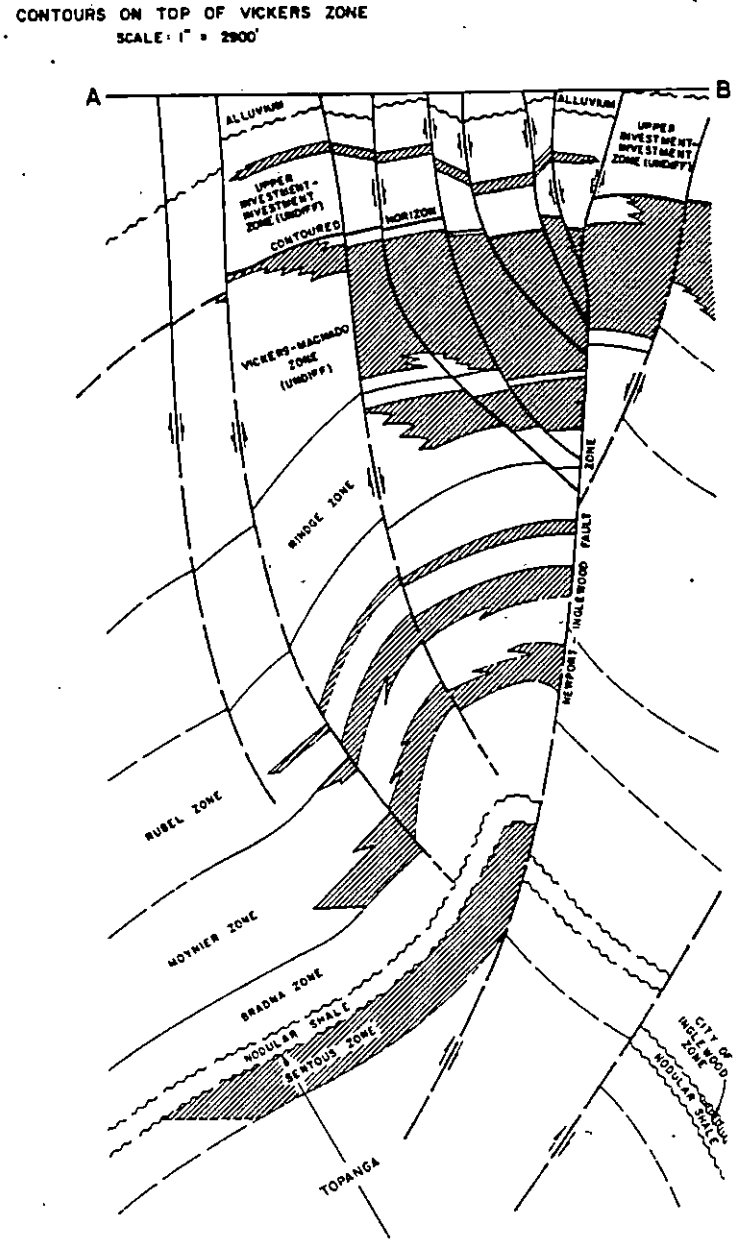

Figure 16. Structure map, stratigraphic column, and cross section of Inglewood oil field. From California Division of Oil and Gas (1974). Heavy-oil occurs in the Upper Investment and Investment zones. Geopressured geothermal reservoirs probably occur below the Sentous zone.

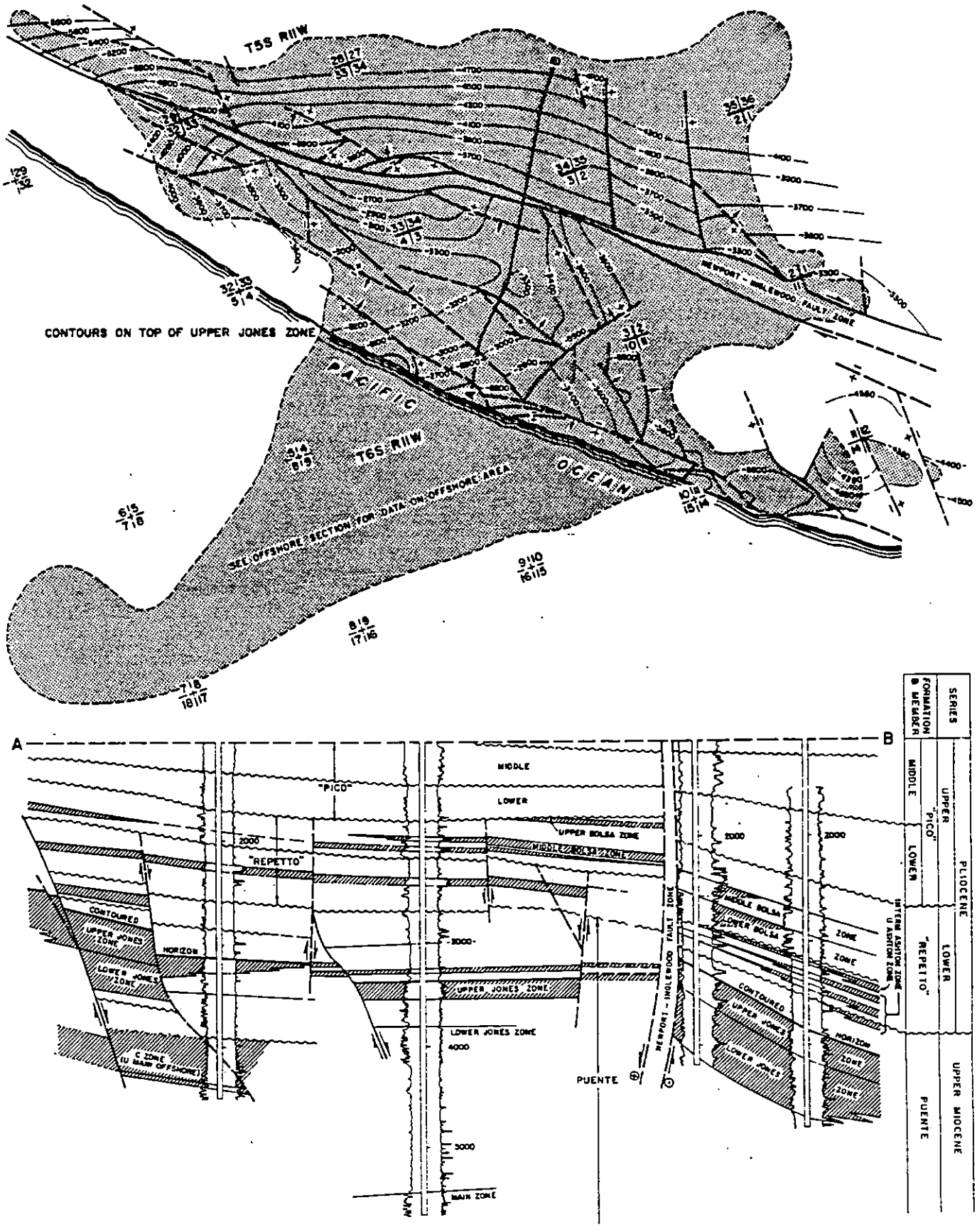

Figure 17. Structure map and cross section of Huntington Beach oil field. From California Division of Oil and Gas (1974). Heavy-oil occurs in the Bolsa and Jones reservoirs.

Whittier Field

Whittier field lies adjacent to the Whittier Fault (fig. 12). The upper four producing zones in the footwall strata are heavy-oil-bearing sands within the Repetto Formation. Zones 5 and 6 produce heavy oil from the upper Miocene Puente Formation (fig. 18). The hanging wall of the Whittier Fault in the area of Whittier field is comprised entirely of Puente Formation strata and has no heavy-oil production. Geopressured occurrences at depth are less likely at Whittier field than in other fields examined. If present, geopressure probably occurs at a depth in excess of 10,000 ft in lower Puente Formation strata (fig. 13).

SOUTH TEXAS

Previous studies at the Texas Bureau of Economic Geology have focused on the stratigraphy of the Mirando Trend (Fisher and others, 1970) and on the geopressured geothermal resources of the deep Wilcox Formation (Gregory and others, 1980; Bebout and others, 1982; Morton and others, 1983). During 1989 we re-evaluated findings from these studies in terms of potential for co-location of Mirando Trend heavy-oil reservoirs and Wilcox geopressured geothermal reservoirs.

Mirando Trend

The Mirando Trend includes heavy-oil sandstone reservoirs of the Eocene Jackson and Yegua Formations occurring at depths of between 100 ft and 5,000 ft. More than 60 MMbbl of heavy oil has been produced from these fields, which is about 30 percent of the more than 200 MMbbl of OHOIP (Nehring and others, 1983; Railroad Commission of Texas, 1989). Figure 19 shows the distribution of heavy-oil fields in South Texas that have produced more

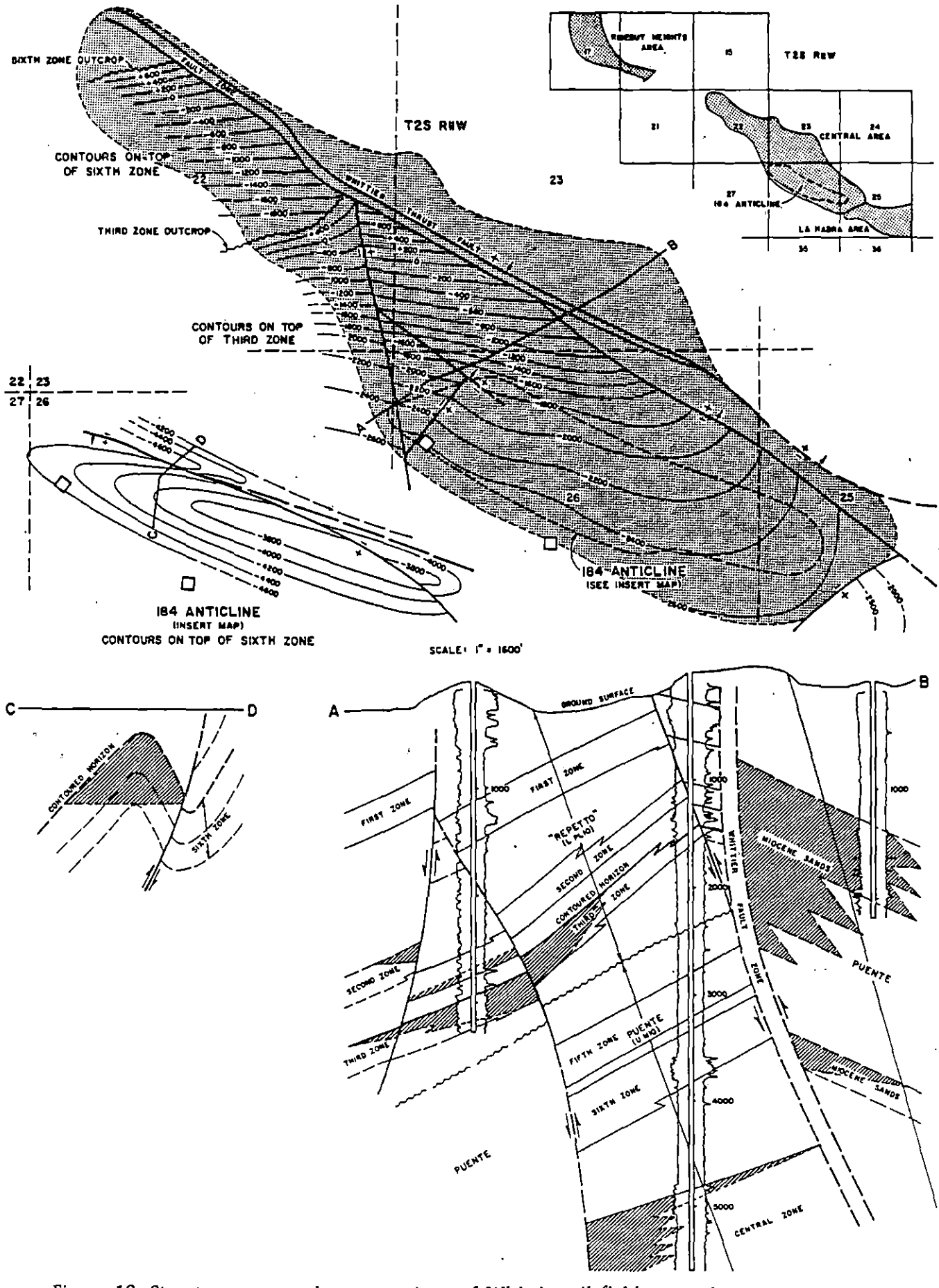

Figure 18. Structure map and cross sections of Whittier oil field, central area. From California Division of Oil and Gas (1974).

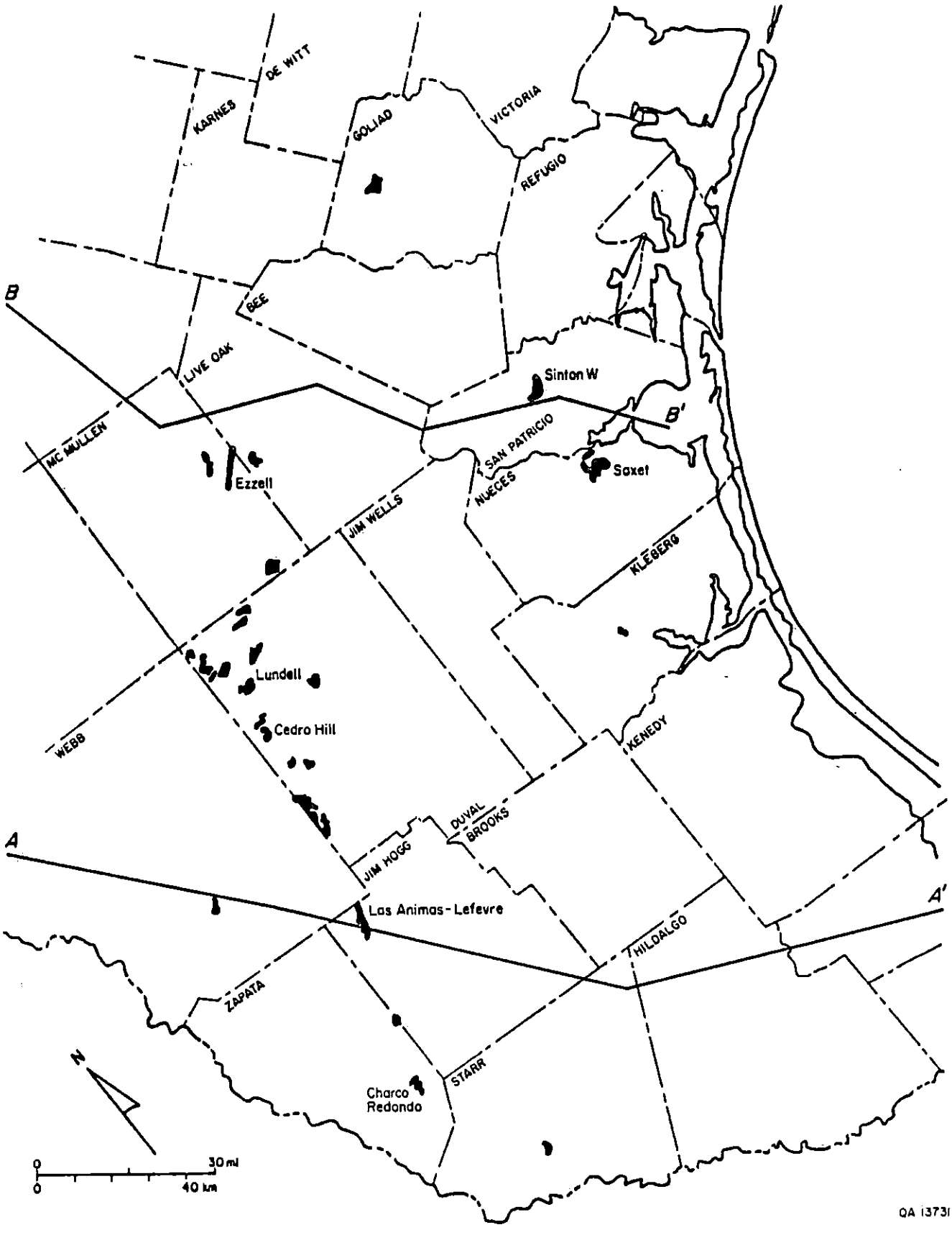

Figure 19. Location map of heavy-oil fields in South Texas that have cumulative production greater than 100 Mbbl (Railroad Commission of Texas, 1989). Fields that have greater than 25 MMbbl OHOIP (Nehring and others, 1983) are named. Cross sections A–A′ and B–B′ shown in figures 22 and 23, respectively.

than 100,000 barrels (Mbbl) of heavy oil. These fields are listed in table 3. The Mirando Trend lies in Duval, Goliad, Jim Hogg, McMullen, Starr, Webb, and Zapata Counties. Closer to the coast, a second group of heavy-oil fields lies in the Frio Formation producing trend (fig. 19).

Reservoir sandstones of the Mirando Trend are typically thin, strike-aligned barrier/strandplain deposits that partly overlap one another (Fisher and others, 1970; Ewing, 1983)(figs. 20 and 21). The producing sandstones are separated vertically by lagoonal and marine shelf mudstone facies. Within the sandstones continuous permeability barriers, such as carbonate-cemented zones, commonly compartmentalize Mirando Trend reservoirs (Schultz, 1982). Sandstone bodies pinch out updip into lagoonal facies. Mudstone-filled channels locally cut across the sandstones, creating lateral permeability barriers. Stratigraphic traps are associated with updip pinch-out margins and with lateral barriers within the sandstone bodies (Ewing, 1983).

Wilcox Group

Wilcox deltaic sandstone in the Rio Grande Embayment of South Texas is the largest Wilcox gas play in Texas and the fourth largest gas play in the onshore Texas Gulf Coast (Kosters and Hamlin, 1989). Deep Wilcox sandstones were the focus of studies at the Texas Bureau of Economic Geology in the 1970's and early 1980's to assess their geopressured geothermal brine and dissolved methane resource potential (Gregory and others, 1980; Bebout and others, 1982; Morton and others, 1983). These studies generated abundant regional temperature, pressure, salinity, and stratigraphic data.

The Wilcox Group (Paleocene to lower Eocene) is a coastward-thickening wedge of sandstone and shale that expands markedly across strike-trending growth faults (figs. 22 and 23). In South Texas only the upper part of the Wilcox has significant quantities of sandstone. The upper Wilcox consists primarily of wave-dominated delta systems having thick sequences of delta-front and barrier/strandplain sandstones (Fisher, 1969; Bebout and others, 1982). These

Table 3. Production statistics for South Texas heavy-oil fields. Fields that have had production >100 Mbbl are listed (Railroad Commission of Texas, 1989).

County	Field	Reservoir	API gravity	Cumulative production through 1-1-89 (Mbbl)
Duval	Casa Blanca		19.0	5,000
	Cedro Hill		19.2	6,569
	Charamousca		19.8	1,510
	Charamousca,S.		20.0	2,713
	Colmena		18.9	3,868
	DCR-79		20.0	1,485
	Dinn		19.0	319
	Eagle Hill		19.0	5,718
	Govt.Wells,N.	900 Sand	20.0	315
		1000 Sand	19.0	80
		1150 Sand	19.9	23
		1550 Sand	20.0	30
	Hagist Ranch	Purple Sand	19.8	210
	Hoffman,E.		20.0	1,387
	Kohler,N.E.	Mirando No. 2	18.7	1,217
	Lopez,N.	Lopez	20.0	2,225
	Lundell		19.3	10,358
	Neely,E.	1150	19.5	160
	Neely,W.	1150	20.0	111
	Orlee		20.0	266
	Rancho Solo		19.4	465
		Cole Second	20.0	30
		Extension	19.4	520
	Richardson		18.0	147
Goliad	Albrecht	Yegua	17.0	212
Jim Hogg	Alworth	Cole Sand	18.0	79
	Las Animas-Lefevre		18.5	3,402
Kleberg	Kingsville		20.0	1,130
		Oakville	19.6	114
		2500	19.0	101
McMullen	Campana,S.	Chernosky	20.0	1,684
		1870 Sand	20.0	160
	Dragoon Creek	Govt.Wells (Upper)	16.0	313
	Dragoon Crk,SW	Government Wells	18.0	112
	Ezzell		20.0	6,938
	Little Alamo		18.0	137
	Wheeler-Mag	1200	15.0	447
Nueces	Saxet		20.0	63,103
	Viola	4000	18.2	747

County	Field	Reservoir	API gravity	Cumulative production through 1-1-89 (Mbbl)
San Patr.	Sinton,W.		18.9	7,655
		Shallow	19.0	5,757
Starr	Los Olmos		20.0	984
Webb	Presa de Oro	Yegua-C-	20.0	152
		Yegua-G-	17.0	221
Zapata	Charco Redondo		17.0	659
	Joe Moss	500 Sand	20.0	557

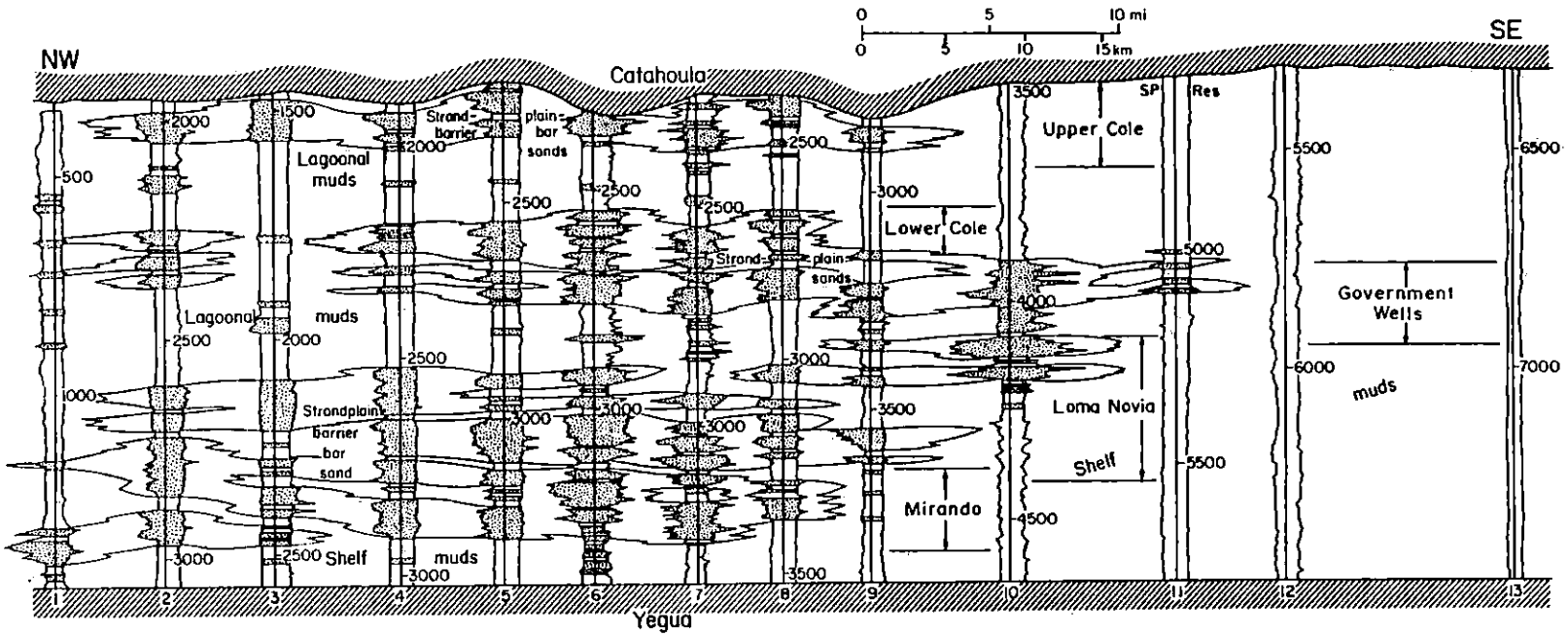

Figure 20. Dip-oriented northwest-southeast cross section of Jackson strandplain system. From Fisher and others (1970). Line of section shown in figure 21.

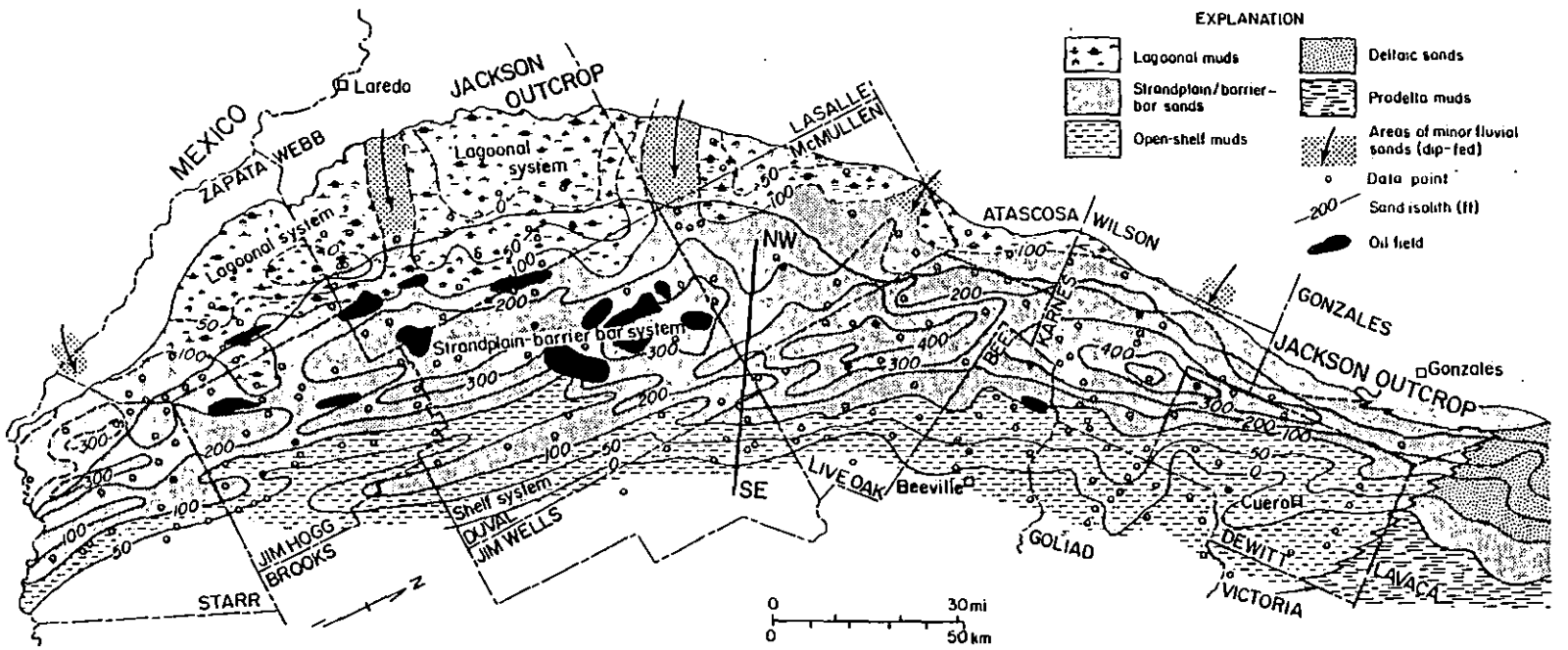

Figure 21. Map showing principal depositional systems and sandstone thicknesses of the Jackson Group in South Texas. From Fisher and others (1970). Yegua sandstone distribution is similar. Cross section NW–SE shown in figure 20.

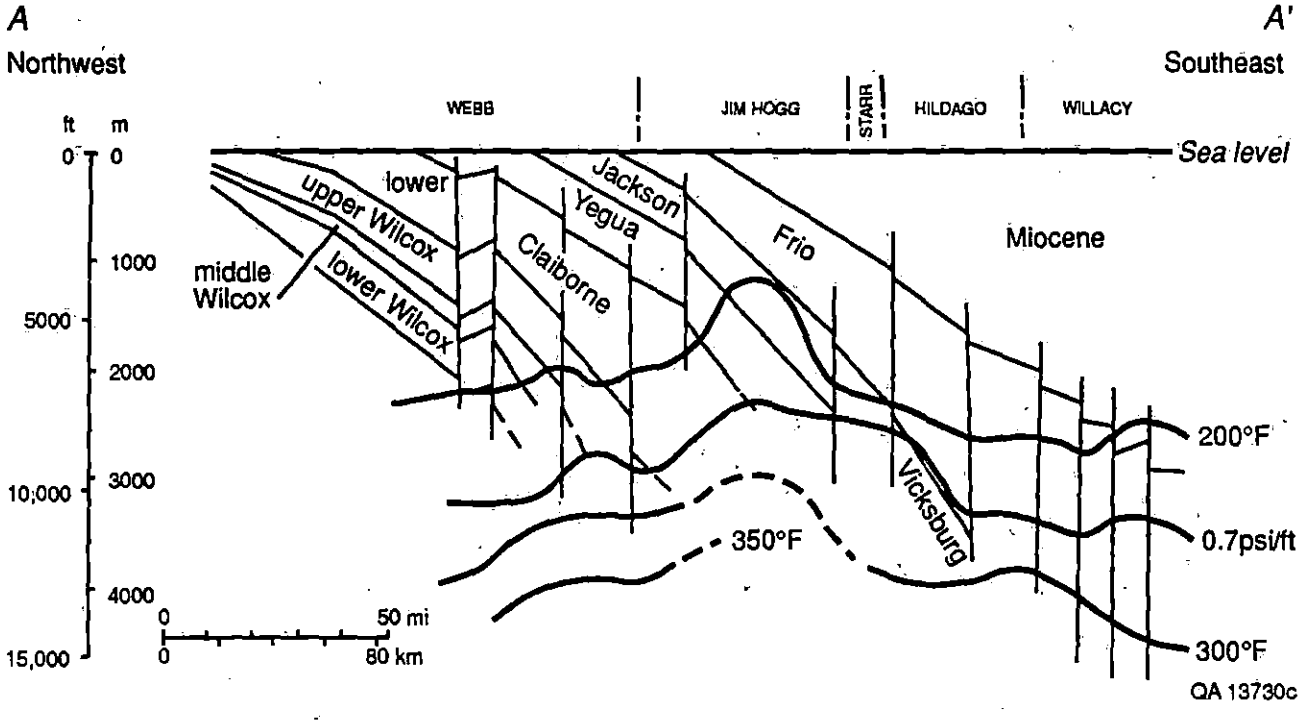

Figure 22. Generalized regional northwest-southeast cross section A–A' of South Texas. Modified from Dodge and Posey (1981). Pressure gradient isobar and fluid-temperature isotherms shown in their approximate position (data from Gregory and others, 1980). Line of section shown in figure 19.

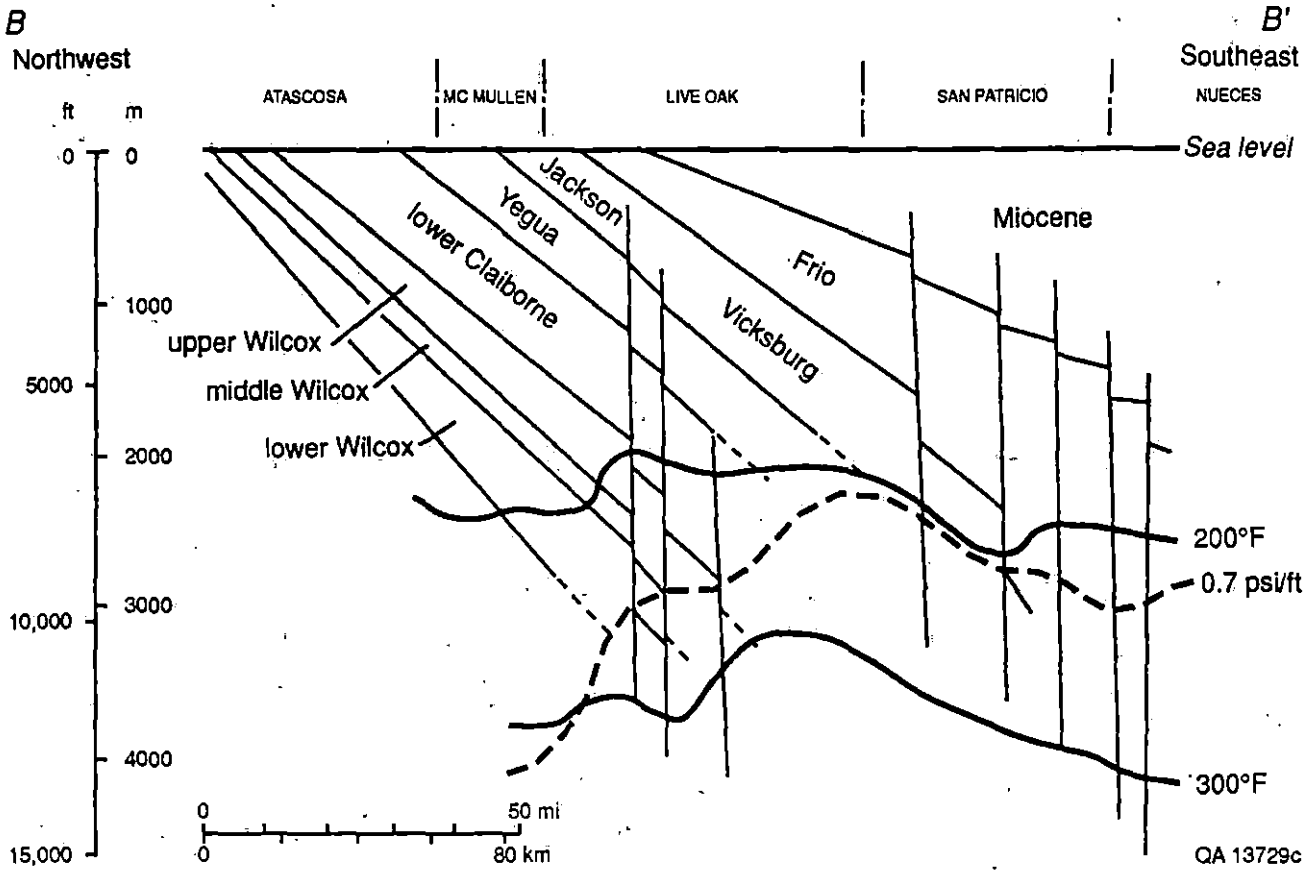

Figure 23. Generalized regional northwest-southeast cross section B–B′ of South Texas. Modified from Dodge and Posey (1981). Pressure gradient isobar and fluid-temperature isotherms shown in their approximate position (data from Gregory and others, 1980). Line of section shown in figure 19.

sandstones are generally continuous along strike, and reservoirs are primarily separated by the growth faults. At depths greater than 8,000 ft, formation fluids in the upper Wilcox Formation are at temperatures greater than 250°F, and fluid-pressure gradients are at least 0.7 psi/ft (figs. 22 and 23)(Gregory and others, 1980). Because many of the heavy-oil fields in the Mirando Trend directly overlie this deep Wilcox geopressured geothermal zone (figs. 24 and 25), we made it the focus of our investigation. Using data from Gregory and others (1980), we generated maps showing the distribution of temperature, pressure, net sandstone, porosity, and salinity in the deep upper Wilcox in relation to significant heavy-oil fields in the Mirando Trend (figs. 24 to 28).

By overlaying figures 24 through 28 we were able to outline and characterize various parts of the deep upper Wilcox geopressured geothermal zone (fig. 29). Areas with the highest temperatures and pressures occur downdip and in the northeast. These downdip areas have low salinities, but porosities are also low (fig. 29). Higher porosities and thicker sandstones generally coincide with lower temperatures and pressures. However, in general, the entire region outlined in figure 30 has fair to good geopressured geothermal potential.

Morton and others (1983) studied the Wilcox sandstones in Jim Hogg and Zapata Counties as part of the U.S. Department of Energy geopressured geothermal program. Data from their study is presented here as a field-scale example of a typical upper Wilcox sandstone reservoir. The uppermost Wilcox sandstone unit in this two-county area lies approximately 200 ft below the top of the Wilcox Formation and is referred to as the First Hinnant Sand (figs. 30 and 31). Test well data from eastern Zapata County indicate that the First Hinnant Sand is a geopressured geothermal reservoir, having a shut-in pressure of 6,627 psi at a depth of 9,120 ft (0.68 psi/ft gradient) and a temperature of 300°F at the same depth. The average porosity of the sandstone is 16 percent, the average permeability is 7 md, and the salinity of the reservoir fluid is 13,000 ppm. Porosity is relatively homogeneous within the Hinnant sandstone complex, but permeability varies in two upward-decreasing cycles. Pore-water volume estimated for the

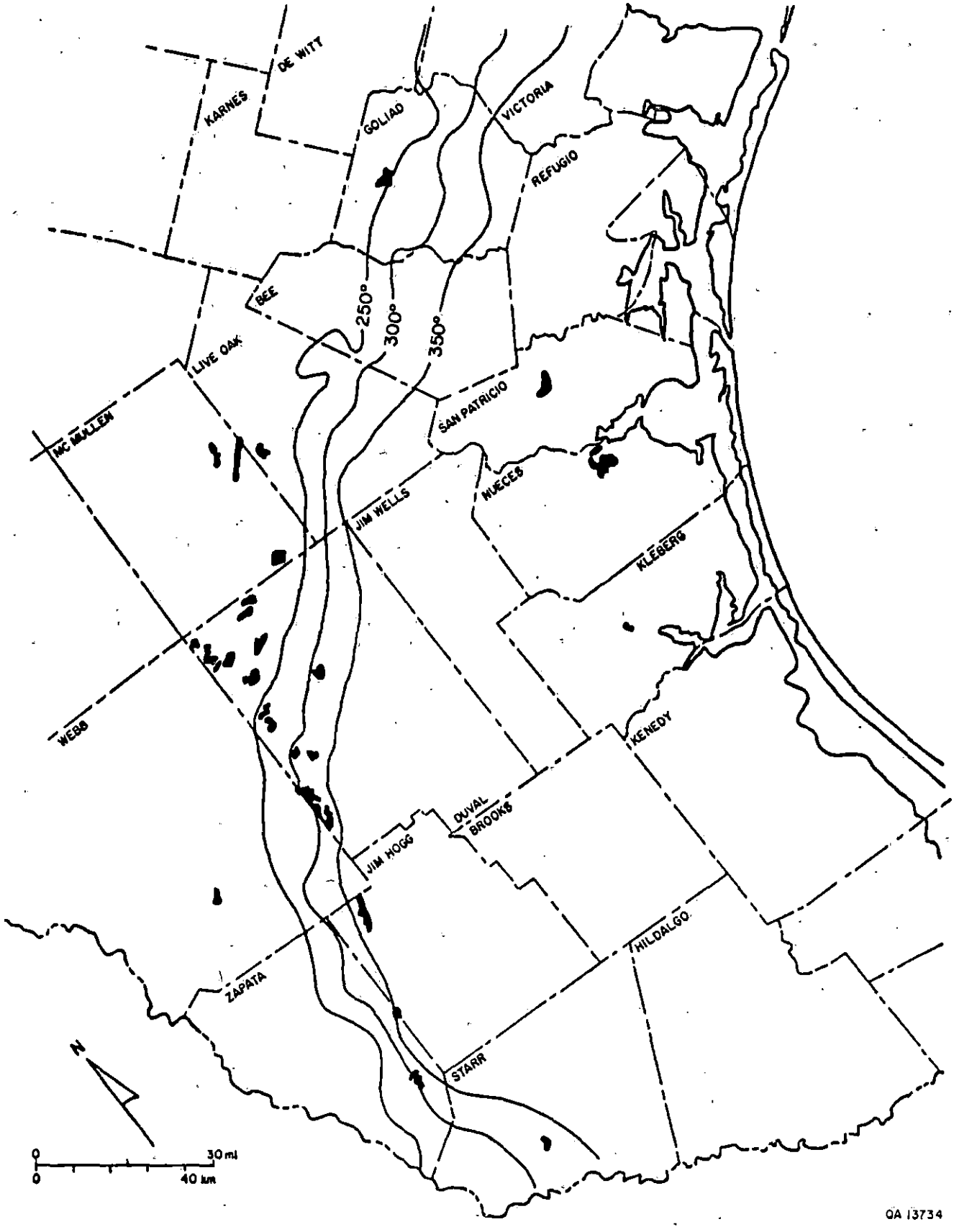

Figure 24. Map showing average fluid-temperature distribution for the deep upper Wilcox. Modified from Gregory and others (1980). The 250°F isotherm generally coincides with a depth of 8,000 ft.

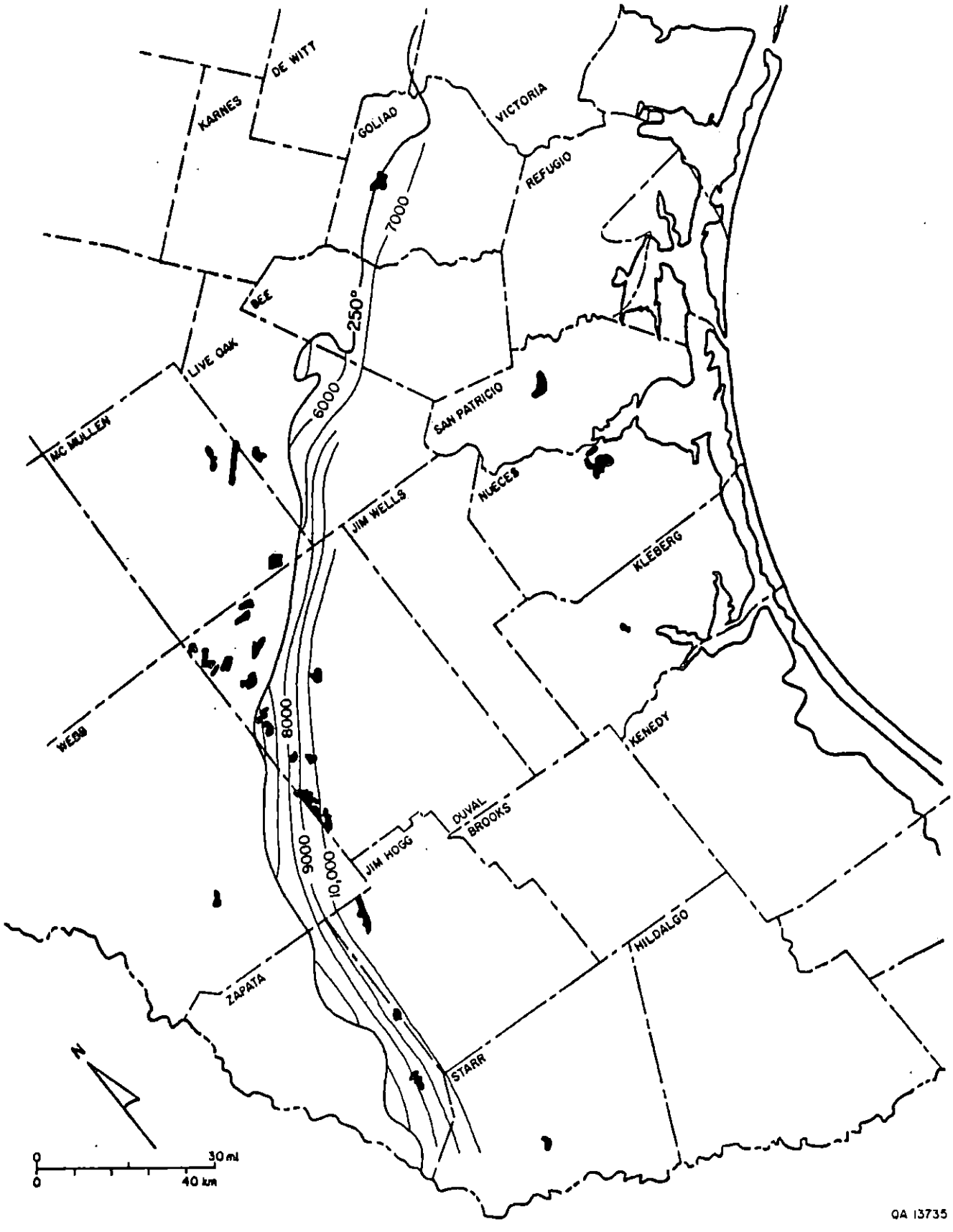

Figure 25. Map showing average fluid-pressure distribution of the deep upper Wilcox downdip from the 250°F isotherm. Modified from Gregory and others (1980). Depth to upper Wilcox in this area ranges from 8,000 ft to more than 12,000 ft, and corresponding pressure gradients generally exceed 0.7 psi/ft.

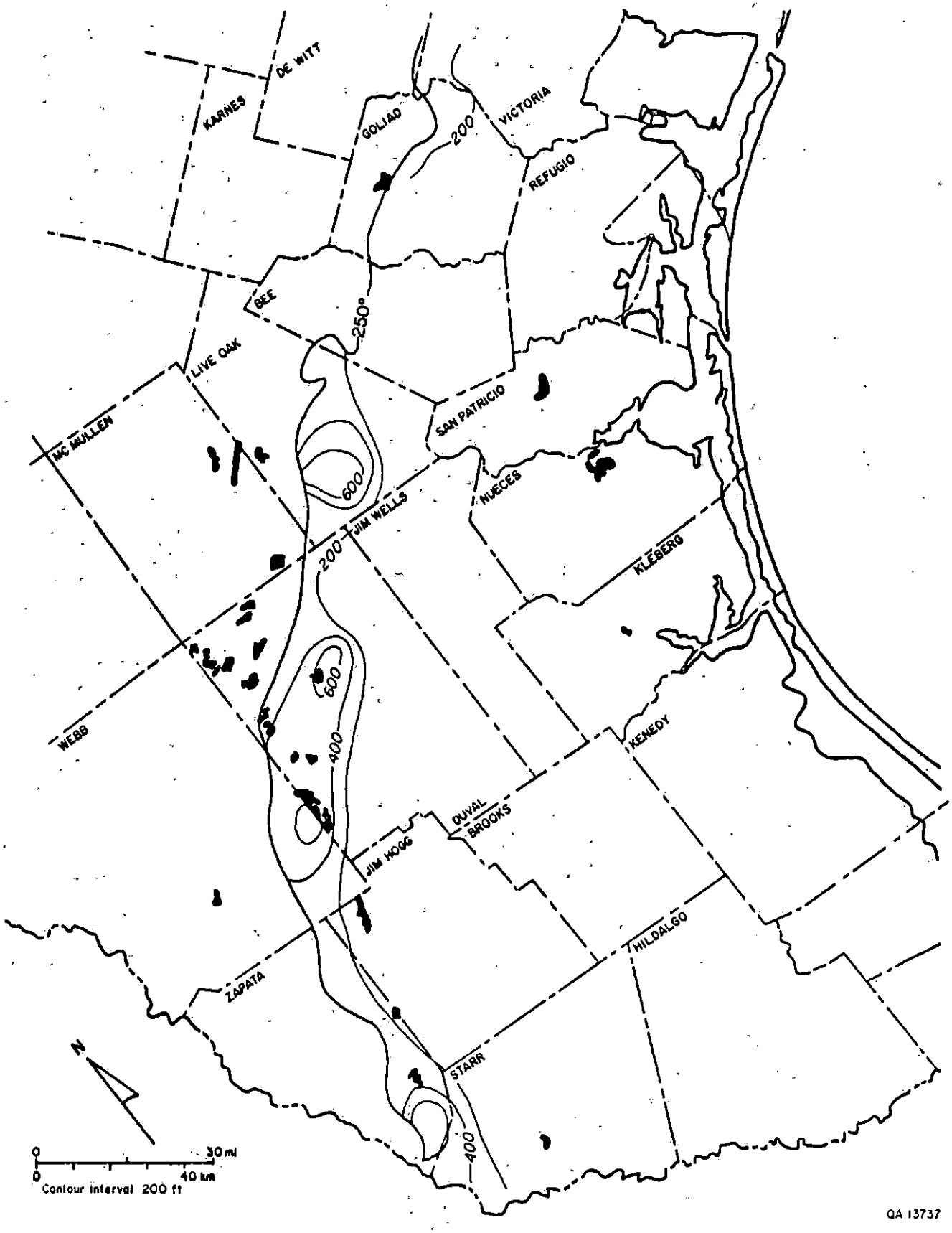

Figure 26. Map showing net sandstone thickness in the deep upper Wilcox downdip from the 250°F isotherm. Modified from Gregory and others (1980). Sandstone thickness and abundance generally decrease downdip to the southeast.

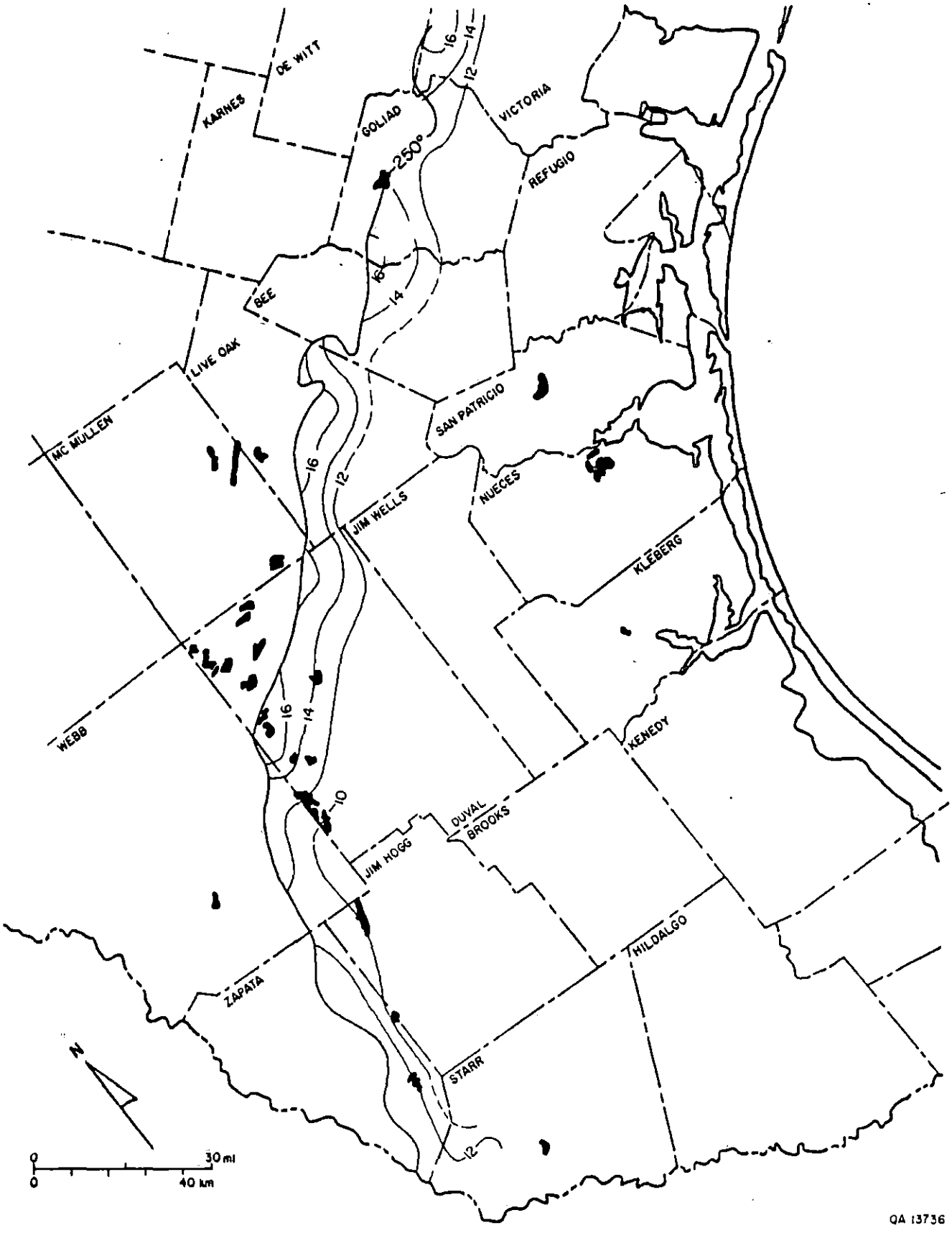

Figure 27. Map showing average porosity of the deep upper Wilcox downdip from the 250°F isotherm. Modified from Gregory and others (1980). Average porosity ranges from 17 per cent to 9 per cent and generally decreases with depth and from the northeast to southwest. Porosity was determined using whole core analysis and calculations from sonic and induction-SP logs (Archie, 1942).

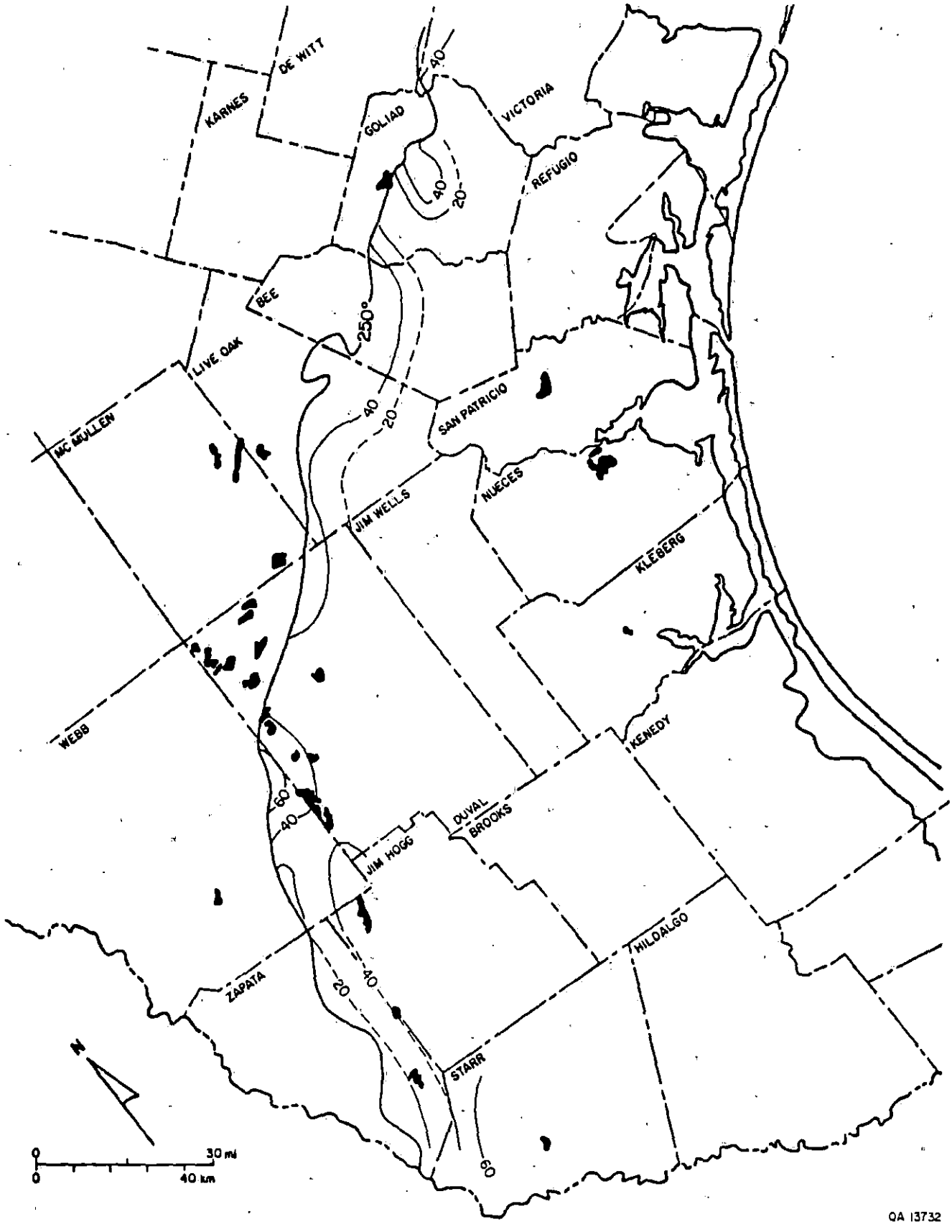

Figure 28. Map showing average pore-fluid salinity for the deep upper Wilcox downdip from the 250°F isotherm. Modified from Gregory and others (1980). Data were calculated using the SP-log method (Archie, 1942).

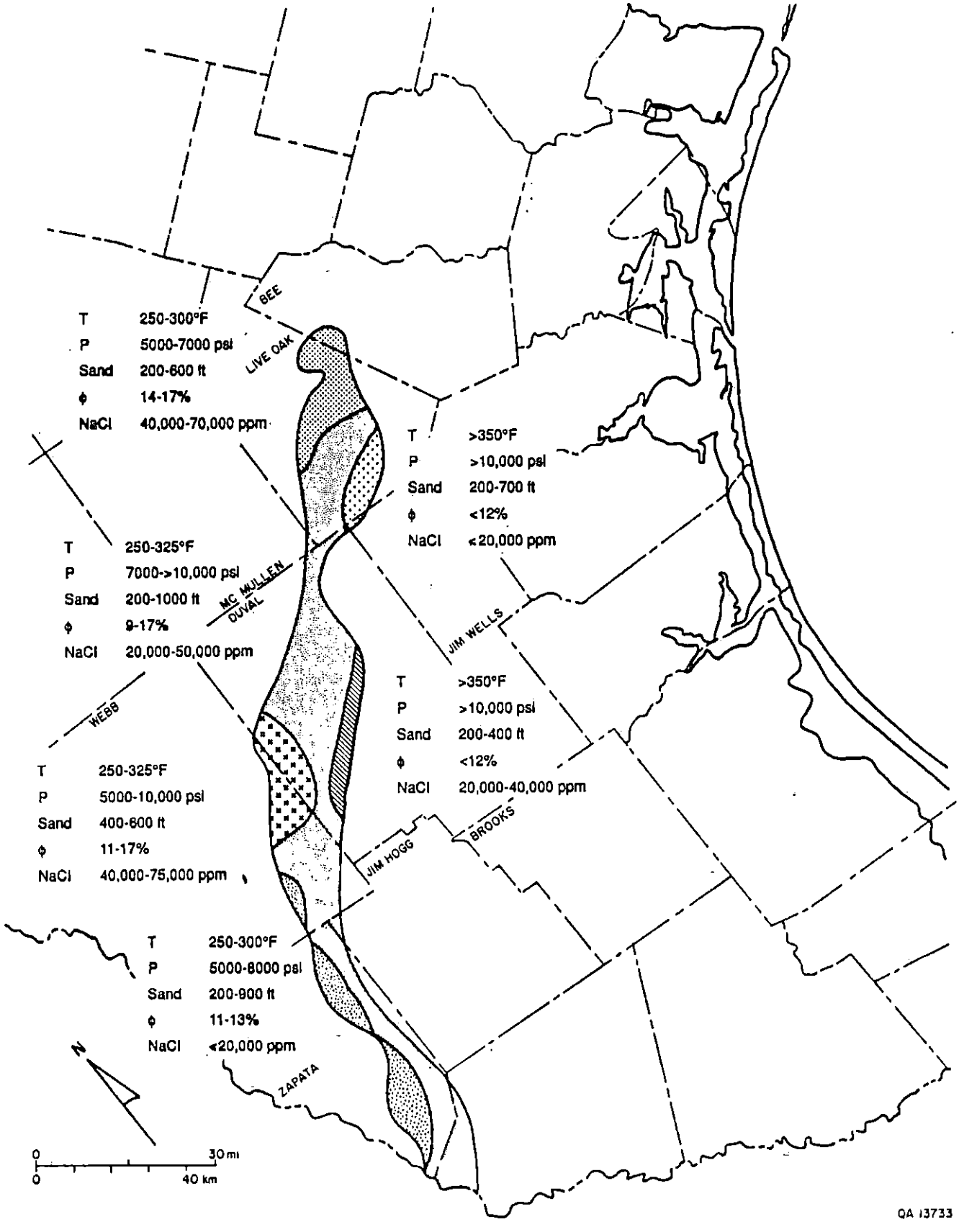

Figure 29. Map showing geothermal fairways in the deep upper Wilcox.

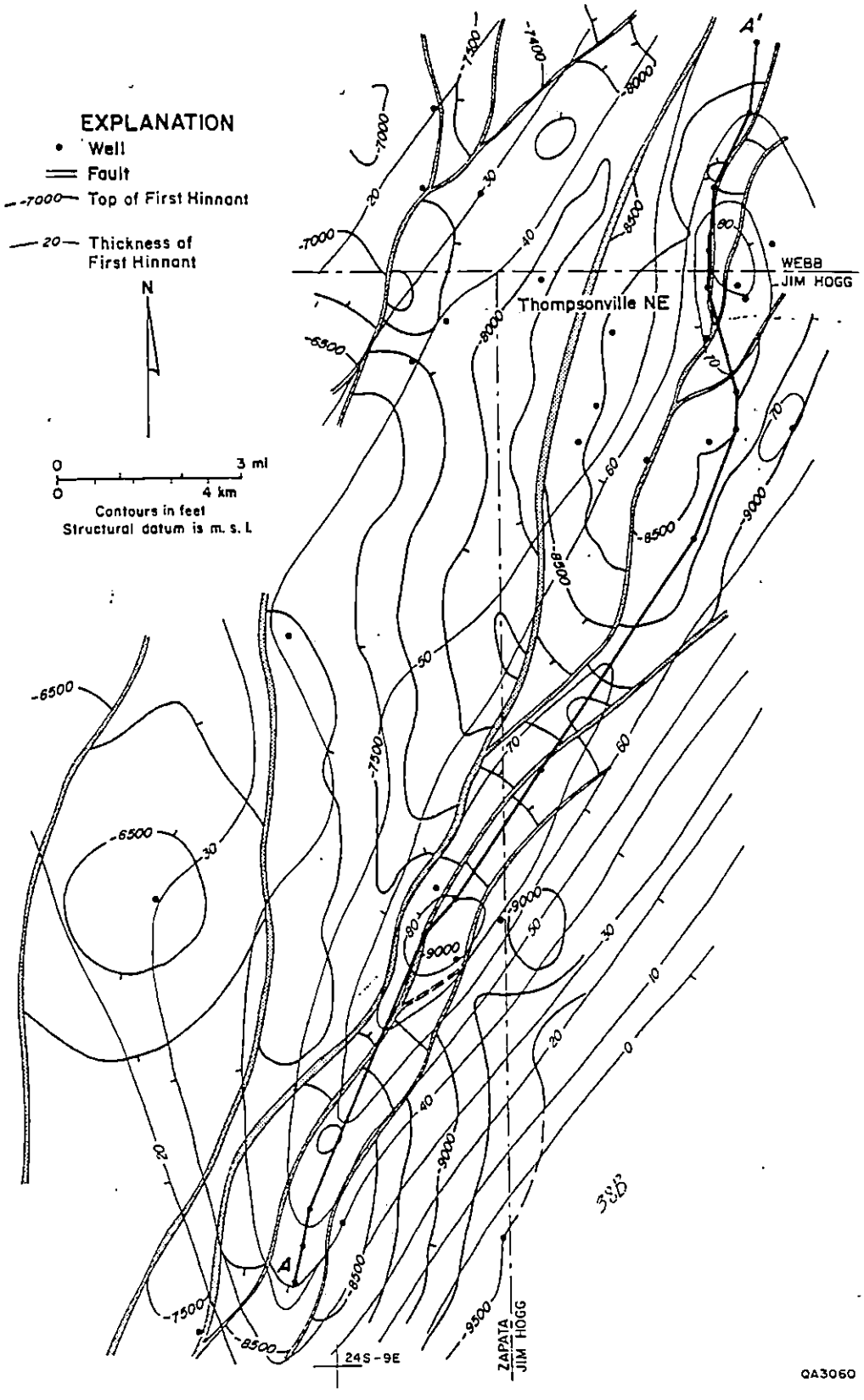

Figure 30. Structure map of Thompsonville Northeast and Martinez fields in Jim Hogg and Zapata Counties, Texas (from Morton and others, 1983). Cross section A–A' shown in figure 31.

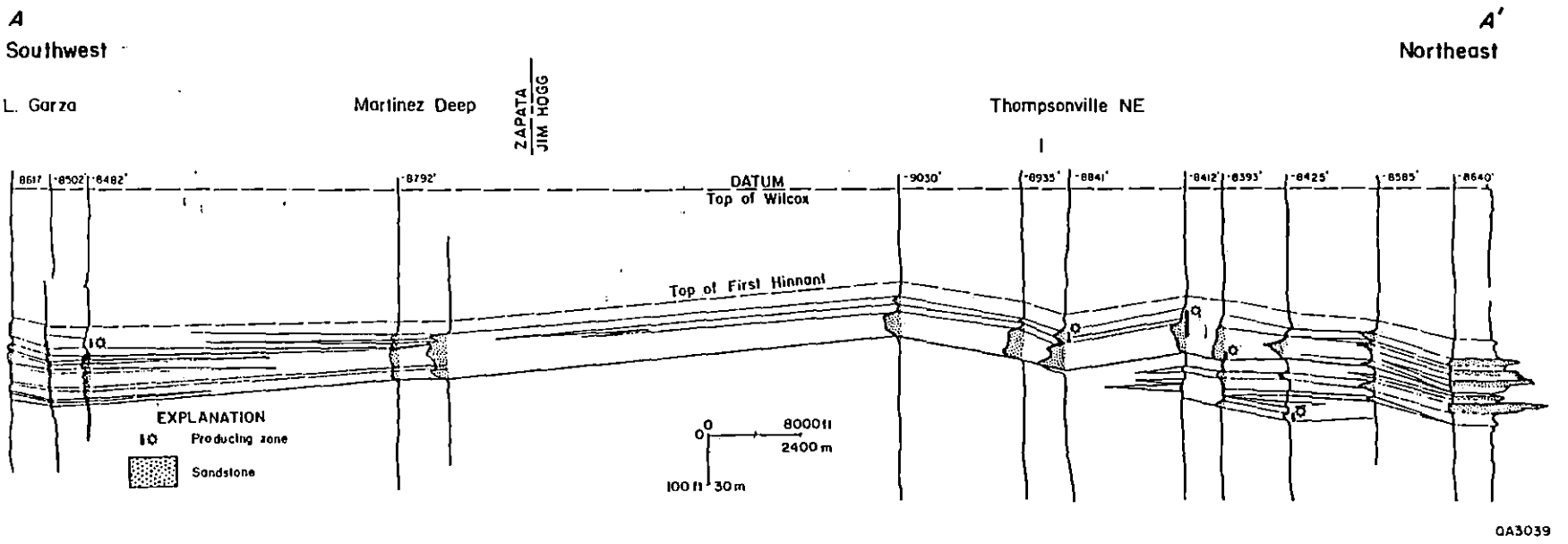

Figure 31. Southwest-northeast strike-aligned stratigraphic cross section A–A′ of Thompsonville Northeast and Martinez fields in Jim Hogg and Zapata Counties, Texas (from Morton and others, 1983). Line of section shown in figure 30.

First Hinnant Sand, for an area of about 3.6 mi^2 between Martinez field and the Jim Hogg county line, ranges from 100 to 800 MMbbl.

During the last decade many new deep wells have been drilled to the upper Wilcox, which is an actively explored deep gas play in South Texas. Data from these new wells can be used to revise and extend mapping based on earlier work (figs. 24 to 29). Regional geologic studies in the Mirando Trend (Fisher and others, 1970) also need updating. Further geologic evaluation of co-location potential will therefore entail (1) expansion of earlier Wilcox studies using a broader, updated data base and (2) stratigraphic investigations in the Jackson and Yegua of the Mirando Trend.

ACKNOWLEDGMENTS

This research was funded by the U.S. Department of Energy, Advanced Technologies Division, under Contract No. DE-FC07-NV10412. The manuscript was edited by Lana Dieterich. Word processing was by Melissa Snell. Illustrations were prepared by Maria Saenz under the direction of Richard L. Dillon. We extend our appreciation to all who contributed to the preparation of this report.

REFERENCES

Archie, G. E., 1942, The electrical resistivity log as an aid in determining some reservoir characteristics: American Institute of Mining Engineers Transactions, v. 146, p. 54–67.

Bebout, D. G., Weise, B. R., Gregory, A. R., and Edwards, M. B., 1982, Wilcox sandstone reservoirs in the deep subsurface along the Texas Gulf Coast—their potential for production of geopressured geothermal energy: The University of Texas at Austin, Bureau of Economic Geology, Report of Investigations No. 117, 125 p.

Berry, F. A. F., 1973, High fluid potentials in California coast ranges and their tectonic significance: American Association of Petroleum Geologists Bulletin, v. 57, no. 7, p. 1219–1249.

California Division of Oil and Gas, 1973, California oil and gas fields, vol. 1: Report TR11, unpaginated.

———— 1974, California oil and gas fields, vol. 2: Report TR12, unpaginated.

———— 1989, Seventy-fourth annual report, p. 61–82.

Callaway, D. C., 1968, Habitat of oil on the west side, San Joaquin Valley, California, *in* Karp, S. E., ed., Guidebook—geology and oilfields, west side southern San Joaquin Valley: Pacific Sections—American Association of Petroleum Geologists, Society of Exploration Geophysicists, and Society of Economic Paleontologists and Mineralogists, p. 21–25.

Dietzman, W. D., Carrales, M., Jr., and Jirik, C. J., 1966, Heavy crude oil reservoirs in the United States: U.S. Bureau of Mines, Information Circular 8263, 53 p.

Dodge, M. M., and Posey, J. S., 1981, Structural cross sections, Tertiary formations, Texas Gulf Coast: The University of Texas at Austin, Bureau of Economic Geology Cross Sections, 6 p.

Ewing, T. E., 1983, Jackson-Yegua barrier/strandplain sandstone, *in* Galloway, W. E., Ewing, T. E., Garrett, C. M., Tyler, Noel, and Bebout, D. G., Atlas of major Texas oil reservoirs: The University of Texas at Austin, Bureau of Economic Geology, Special Publication, p. 30–32.

Fisher, W. L., 1969, Facies characterization of Gulf Coast Basin delta systems, with some Holocene analogues: Gulf Coast Association of Geological Societies Transactions, v. 19, p. 239–261.

Fisher, W. L., Proctor, C. V., Jr., Galloway, W. E., and Nagle, J. S., 1970, Depositional systems in the Jackson Group of Texas—their relationship to oil, gas, and uranium: The University of Texas at Austin, Bureau of Economic Geology, Geological Circular 70-4, 28 p.

Foss, C. D., and Blaisdell, R., 1968, Stratigraphy of the west side southern San Joaquin Valley: *in* Karp, S. E., ed., Guidebook—geology and oilfields, west side southern San Joaquin Valley: Pacific sections—American Association of Petroleum Geologists, Society of Exploration Geophysicists, and Society of Economic Paleontologists and Mineralogists, p. 33–43.

Gregory, A. R., Dodge, M. M., Posey, J. S., and Morton, R. A., 1980, Volume and accessibility of entrained (solution) methane in deep geopressured reservoirs—Tertiary formations of the Texas Gulf Coast: The University of Texas at Austin, Bureau of Economic Geology, final

report prepared for the U.S. Department of Energy, Division of Geothermal Energy, under contract no. DE-AC08-78ET11397, 390 p.

Kosters, E. C., and Hamlin, H. S., 1989, WX-4. Wilcox deltaic sandstone in the Rio Grande Embayment, *in* Kosters, E. C., Bebout, D. G., Seni, S. J., Garrett, C. M., Jr., Brown, L. F., Jr., Hamlin, H. S., Dutton, S. P., Ruppel, S. C., Finley, R. J., and Tyler, Noel, Atlas of major Texas gas reservoirs: The University of Texas at Austin, Bureau of Economic Geology, Special Publication, p. 17–20.

McGuire, M. D., Bowersox, J. R., and Earnest, L. J., 1984, Diagenetically enhanced entrapment of hydrocarbons—southeastern Lost Hills fracture shale pool, Kern County, California: San Joaquin Geological Society Selected Papers, v. 6, p. 40–49.

Morton, R. A., Ewing, T. E., and Tyler, Noel, 1983, Continuity and internal properties of Gulf Coast sandstones and their implications for geopressured fluid production: The University of Texas at Austin, Bureau of Economic Geology, Report of Investigations No. 132, 70 p.

Nehring, Richard, Hess, R., and Kamionski, M., 1983, The heavy oil resources of the United States: Rand Corporation, contract report prepared for the U.S. Department of Energy, under contract no. R-2946-DOE, 143 p.

Railroad Commission of Texas, 1989, 1988 oil and gas annual report: v. 1, 428 p.

Schultz, A. L., 1982, Geology of the First Mirando sand, South Lopez unit, Lopez field, Webb and Duval Counties, Texas: South Texas Geological Society Bulletin, v. 22, no. 7, p. 11–24.

Strongin, O., 1981, Identification of geopressured occurrences outside of the Gulf Coast, *in* Proceedings, 16th Intersociety Energy Conversion Engineering Conference: New York, American Society of Mechanical Engineers, p. 1279–1284.

Thomas, D., 1979, Possible geopressured well at Huntington Beach, California: California Division of Oil and Gas, Geothermal Hot Line, v. 9, no. 3, p. 8–9.

Van Orstrand, C. E., 1934, Temperature gradients, *in* Wrather, W. E., and Lahee, F. H., eds., Problems of petroleum geology: American Association of Petroleum Geologists, Sidney Powers Memorial Volume, p. 989–1021.

Wallace, R. H., Kraemer, T. F., Taylor, R. E., and Wesselman, J. B., 1979, Assessment of geopressured-geothermal resources in the northern Gulf of Mexico basin, *in* Muffler, L. J. P., ed., Assessment of geothermal resources of the United States—1978: U.S. Geological Survey Circular 790, p. 132–155.

Weddle, J. R., 1968, Oilfield waters in southwestern San Joaquin Valley, Kern County, California, *in* Karp, S. E., ed., Guidebook—geology and oilfields, west side southern San Joaquin Valley: Pacific sections—American Association of Petroleum Geologists, Society of Exploration Geophysicists, and Society of Economic Paleontologists and Mineralogists, p. 25–32.

Yerkes, R. F., McCulloh, T. H., Schoellhamer, J. E., and Vedder, J. G., 1965, Geology of the Los Angeles Basin—an introduction: U.S. Geological Survey Professional Paper 420-A, 57 p.